

Department of Civil and Environmental Engineering

University of Strathclyde

**LABORATORY INSIGHTS INTO REACTIONS
BETWEEN GAS SHALES AND HYDRAULIC
FRACTURING FLUIDS AT RESERVOIR
TEMPERATURES AND PRESSURES:
A GLOBAL PERSPECTIVE.**

By

Izabella Otalega

Thesis submitted in fulfilment of the requirements for
the degree of Doctor of Philosophy.

May 2021

DECLARATION

This thesis is the result of the author's original research. It has been composed by the author and has not been previously submitted for examination which has led to the award of a degree.

The copyright of this thesis belongs to the author under the terms of the United Kingdom Copyright Acts as qualified by University of Strathclyde Regulation 3.50. Due acknowledgement must always be made of the use of any material contained in, or derived from, this thesis.

Signed:

Date:

ACKNOWLEDGEMENTS

Firstly, a massive thank you to my supervisors, Dr Jo Renshaw, Dr Kate Dobson, Prof. Zoe Shipton and Dr Simon Apte, for their continuous support and encouragement throughout this PhD. I would like to especially thank Simon and the rest of the CSIRO Land and Water team at Lucas Heights for making my time in Australia such a wonderful experience. In particular, I am incredibly grateful to Josh King for his incredible patience and immense help. I'm certain that without his kind support, the days in the labs would have been full of doom and gloom.

I am extremely grateful to Dr Katriona Edlmann and Dr Andreas Buch for providing me with the very needed shale samples. I would also like to thank Dr Paul Edwards for the EPMA and EDX analysis of the shale chips.

A big thank you to Cornelius, Tom, Alan, Ben, Christina, Jonathan, James and Mark – I am so very grateful for your incredible friendship throughout the years! A special thank you goes to Ghillie for being the best canine companion one could have during the write-up period and watching with me the 101 Dalmatians on repeat.

Most importantly, I would like to thank my mother and grandmother for all their encouragement. This work could not have been completed without their amazing support.

ABSTRACT

The large quantities of wastewater produced throughout the lifetime of a shale gas well can contain heavy metals and other regulated potentially toxic elements. Their release from the target formation can be enhanced by some of the additives (e.g. ammonium persulfate, EDTA) present in the hydraulic fracturing fluids. High levels of inorganic geogenic chemicals may pose a hazard to the environment through accidental releases such as spills of untreated wastewater. The concentration of mobilised elements and the hazard they pose is uncertain and is likely dependent on the chemical agents used in fracturing fluids, composition of formation waters and the trace element content of targeted shale gas formation.

This study aimed to investigate the release of potential inorganic contaminants of concern (e.g. As, Co, Cu, Ni) from shale gas formations from around the world. In systematic batch experiments at elevated temperature (80°C) and a range of pressures (1-200 bar), powdered samples were leached for up to 500 hours with synthetic hydraulic fracturing fluid (SHFF) and synthetic groundwater (SGW). Elemental concentrations released into solution were generally much higher in the SHFF leachates than in the SGW treatments, indicating that the chemical additives in the SHFF influenced element mobilisation.

Electron probe microanalyser (EPMA) and energy-dispersive X-ray (EDX) detector images showed mineral etching and precipitation of secondary phases on shale chips leached for 360 h with SHFF at 80°C and ~180 bar when compared to the SGW experiment. Time-series data also showed evidence of mineral dissolution and subsequent precipitation, which resulted in the sequestration of a number of trace elements that were initially mobilised into the solution. Additionally, carbonate content

of the unreacted shale sample was the primary control on the final pH of the SHFF leachates.

This study shows that additives can enhance the release of geogenic chemicals, but also that subsequent precipitation within the fracture system could limit ultimate release to surface. Monitoring during field-operations is recommended to understand the system-specific environmental implications and hazards.

TABLE OF CONTENTS

DECLARATION	i
ACKNOWLEDGEMENTS	ii
ABSTRACT	iii
TABLE OF CONTENTS	v
LIST OF FIGURES	viii
LIST OF TABLES	xii
CHAPTER 1 - RATIONALE	1
1.1. Introduction	1
1.1.1. Gas shales and hydraulic fracturing	2
1.2. Flowback and produced water	6
1.2.1. Chemical composition	6
1.2.2. Management practices: reuse, treatment and disposal	8
1.2.3. The efficacy of treatment	10
1.3. Environmental concerns associated with flowback and produced water	11
1.3.1. Surface and groundwater contamination pathways	11
1.3.2. Potential hazards to human health and the environment ..	16
1.4. Summary and gaps in knowledge	18
CHAPTER 2 - PREVIOUS LABORATORY STUDIES: A REVIEW	22
2.1. Introduction	22
2.2. Rock-fluid interactions during hydraulic fracturing	23
2.3. Differences in experimental parameters	29
2.4. Summary and further work	33
2.4.1. Scope of this study	35
CHAPTER 3 - SAMPLE CHARACTERISATION	36

3.1. Introduction	36
3.2. Shale samples	38
3.2.1. Mineralogy	39
3.2.2. Elemental content and its environmental significance	48
3.3. Implications for the experimental studies	58
CHAPTER 4 - MOBILISATION OF ELEMENTS FROM SHALES DURING HYDRAULIC FRACTURING: LABORATORY STUDIES	65
4.1. Introduction	65
4.2. Leaching fluids	67
4.2.1. Dilute hydrochloric acid (1M HCl)	67
4.2.2. Synthetic groundwater	67
4.2.3. Synthetic hydraulic fracturing fluid	68
4.3. Experimental approach	75
4.3.1. General procedures	75
4.3.2. Batch leach experiments	75
4.4. Results	81
4.4.1. Effect of fluid type on leachate element concentrations	81
4.4.2. Effect of leaching time on elemental release into solution	96
4.5. What about acid flush?	109
4.6. Summary	117
CHAPTER 5 - EXPERIMENTAL FACTORS AFFECTING ELEMENT MOBILISATION FROM SHALES	119
5.1. Introduction	119
5.2. Fluid additives and solid:fluid ratio	120
5.2.1. Solid:fluid ratio	120
5.2.2. EDTA and citric acid concentration	123
5.2.3. Ammonium persulfate concentration	124
5.3. The effect of temperature	130
5.4. The effect of pressure	134
5.4.1. Methods	136

5.4.2. Fluid chemistry	137
5.4.3. The effects of pressure on the fracture surface	142
5.4.4. SGW	143
5.4.5 SHFF	155
CHAPTER 6 - DISCUSSION	168
6.1. Rationale and main research questions	168
6.2. Not each shale is the same, and it matters.	172
6.2.1. Mineralogy and trace element content	172
6.2.2. Neutralisation capacity	175
6.3. Element mobilisation trends.	177
6.4. Factors affecting element mobilisation	180
6.4.1. Solid:fluid ratio and additives.	180
6.4.2. Temperature and pressure.	183
6.4.3. Powder to chip to fracture surface.	188
6.5. (Environmental) Implications for future practice	190
6.5.1. Approach and water quality guidelines used.	192
6.5.2. Environmental and human health implications	194
6.5.3. Implications for future practice	199
6.6. Applications to other systems	201
CHAPTER 7 - CONCLUSIONS AND FUTURE WORK	203
7.1. Conclusions	203
7.1. Future work	207
REFERENCES	208
Appendix A	224
Appendix B	225
Appendix C	226

LIST OF FIGURES

Figure 1.1	Schematic model of different wastewater management strategies. Grey lines – strategies involving injection (for reuse or disposal), blue line – other end points such as discharge, evaporation, landfills. POTW – public owned treatment works, CWT – centralised (industrial) waste treatment facilities. From US EPA (2016)..	8
Figure 1.2	Conceptual model (not to scale) of potential receptors and some of the possible contamination pathways associated with shale gas wastewater. Adapted from Vengosh et al. (2014) and Weltman-Fahs and Taylor (2013).	12
Figure 1.3	Conceptual model (not to scale) of potential pathways (white arrows) for fluid movement in a cemented well: (1) a casing and tubing leak into the surrounding rock; (2) an uncemented annulus (i.e., the space behind the casing); (3) microannuli between the casing and cement; (4) gaps in cement due to poor cement quality; and (5) microannuli between the cement and the surrounding rock. From US EPA (2016).	14
Figure 3.1	Location of the three Bowland Shale wells - Blacon East 1, Long Eaton 1 and Kirby Misperton 1, from which the core samples were obtained. Background GIS map taken from arcgis.com.	40
Figure 3.2	Location of the three Australian shale gas basins which were chosen by the Australian Government as the main prospects for shale gas exploitation. The basins were studied in a government-funded Geological and Bioregional Assessment Program (GBA), which examined potential impacts of shale and tight gas development on water and the environment. Listed on the map are well locations from which the core samples used in this study were obtained. Background map image and basin and GBA shapefiles were taken from csiro.au.	41
Figure 3.3	Whole-rock mineralogy of the non-Australian samples.	44
Figure 3.4	Whole-rock mineralogy of Mt Isa Superbasin samples: (a) mineralogy of a core section from which Termite Range sample was taken, where the sample depth is indicated by the yellow strip; (b) XRD results for the Lawn Hill sample	44
Figure 3.5	Approximate mineralogy of the Beetaloo sub-basin samples from the two wells: (a) Altree-2, and (b) Tanumbirini 1. The sample depths are indicated by the yellow strips	45
Figure 3.6	Approximate mineralogy of the Cooper Basin samples from the Encounter-1 well. The sample depths are indicated by the yellow strips.	46
Figure 3.7	Approximate mineralogy for (a) Roseneath-1, (b) Murteree-1, and (c) Patchawarra shales from the Holdfast-1 well, Cooper Basin. The sample depths are indicated by the yellow strips	47
Figure 3.8	Approximate mineralogy of the Cooper Basin samples from the Encounter-1 well. The sample depths are indicated by the yellow strips.	48
Figure 4.1	An example of a hydraulic fracturing fluid decision tree for gas wells (from US EPA, 2016). HPG - hydroxypropylguar, guar derivatized with propylene oxide; kf - fracture permeability; w - fracture width; and xf - fracture half-length.	69
Figure 4.2	Evolution of pH in the experiments with (a) SHFF and (b) SGW.	83
Figure 4.3	pH evolution with samples divided based on their acid neutralisation potential: (a) SHFF experiments, (b) SGW experiments.	84
Figure 4.4	Aqueous concentrations of Ca, Mg and Mn in SHFF and SGW experiments (all timepoints) plotted against the total available content of a given element in the solids. Note that graphs have different scales.	86

Figure 4.5	Aqueous concentrations of Al and Fe in SHFF and SGW experiments (all time-points) plotted against the total available content of a given element in the solids. Note that graphs have different scales.	87
Figure 4.6	Aqueous concentrations of S in SGW experiments (all timepoints) plotted against the total available S in the solids for: (a) non-acid producing samples; (b) acid producing samples; and (c) uncertain samples.	89
Figure 4.7	Aqueous concentrations of Cd, Co and Cr in SHFF and SGW experiments (all timepoints) plotted against the total available content of a given element in the solids. Note that graphs have different scales.	92
Figure 4.8	Aqueous concentrations of Cu, Li and Ni in SHFF and SGW experiments plotted against the total available content of a given element in the solids. Note that graphs have different scales.	93
Figure 4.9	Aqueous concentrations of Sr, Tl and Zn in SHFF and SGW experiments plotted against the total available content of a given element in the solids. Note that graphs have different scales.	94
Figure 4.10	Aqueous concentrations of Sb and Mo in SHFF and SGW experiments plotted against the total available content of a given element in the solids. Note that graphs have different scales.	95
Figure 4.11	Aqueous concentrations of As, V and U in SHFF and SGW experiments plotted against the total available content of a given element in the solids. Note that graphs have different scales.	97
Figure 4.12	Amount of total available element content mobilised over time in the SGW experiments for Ca, Mg, Mn, Fe, Cd, Co, Cu, Ni, U and Zn. Note that y axis has different scales among the graphs.	99
Figure 4.13	Amount of total available element content mobilised over time in the SGW experiments for S, Li and Sr. Shales are grouped by their acid neutralisation potential. Note that y axis has different scales among the graphs.	100
Figure 4.14	Amount of total available element content mobilised over time in the SGW experiments for As and V. Shales are grouped by their acid neutralisation potential. Note that y axis has different scales among the graphs.	101
Figure 4.15	Amount of total available element content mobilised over time in the SGW experiments for Ba, Mo and Sb. Shales are grouped by their acid neutralisation potential. Note that y axis has different scales among the graphs.	102
Figure 4.16	Amount of total available element content mobilised over time in the SHFF experiments for Ca, Mg, Mn and Sr. Shales are grouped by their acid neutralisation potential. Note that y axis has different scales among the graphs.	103
Figure 4.17	Amount of total available element content mobilised over time in the SHFF experiments for Ba, Mo and Sb. Shales are grouped by their acid neutralisation potential. Note that y axis has different scales among the graphs.	104
Figure 4.18	Amount of total available element content mobilised over time in the SHFF experiments for Al and Fe. Shales are grouped by their acid neutralisation potential; non-acid producing shales mobilised little to no Al and Fe into solution. Note that y axis has different scales among the graphs.	105
Figure 4.19	Graphs on the left show the amount of total available Ca, Mn, Mg, Fe and Al mobilised over time in the HCl experiments. Graphs on the right show aqueous concentrations of Ca, Mn, Mg, Fe and Al in HCl experiments plotted against the total available content of a given element in the solids.	111
Figure 4.20	Top graphs show the amount of total available S mobilised over time in the (a) HCl and (b) SGW experiments. Bottom graphs show aqueous S concentrations in the (c) HCl and (d) SGW experiments plotted against the total available S content.	112
Figure 4.21	Graphs on the left show the amount of total available As, Ba and Cd mobilised over time in the HCl experiments. Graphs on the right show aqueous concentrations of As, Ba and Cd in HCl experiments plotted against the total available content of a given element in the solids.	113

Figure 4.22	Graphs on the left show the amount of total available Co, Cr and Cu mobilised over time in the HCl experiments. Graphs on the right show aqueous concentrations of Co, Cr and Cu in HCl experiments plotted against the total available content of a given element.	114
Figure 4.23	Graphs on the left show the amount of total available Li, Mo and Ni mobilised over time in the HCl experiments. Graphs on the right show aqueous concentrations of Li, Mo and Ni in HCl experiments plotted against the total available content of a given element.	115
Figure 4.24	Graphs on the left show the amount of total available Pb, Sr, V and Zn mobilised over time in the HCl experiments. Graphs on the right show aqueous concentrations of Pb, Sr, V and Zn in HCl experiments plotted against the total available content of a given element.	116
Figure 5.1	Aqueous element concentrations after 5h leaching of KC-1 sample with 1M HCl for different solid:fluid ratios. Data are shown as the averages of duplicates.	121
Figure 5.2	Aqueous element concentrations after 5h leaching of KC-1 sample SGW for different solid:fluid ratios. Data are shown as the averages of duplicates. Sulphate concentration for 1:10 ratio exceeded the upper limits of detection on ICP-AES.	122
Figure 5.3	Aqueous element concentrations after 3h leaching of KC-4 sample with three fluids: (1) EDTA and citric acid solution; (2) synthetic hydraulic fracturing fluid (SHFF#1 recipe); and (3) SHFF#4 with EDTA and citric acid. Data are shown as the averages of duplicates.	125
Figure 5.4	Aqueous element concentrations after 3h leaching of Murteree-2 sample with three fluids: (1) EDTA and citric acid solution; (2) synthetic hydraulic fracturing fluid (SHFF#1 recipe); and (3) SHFF#4 with EDTA and citric acid. Data are shown as the average of duplicates.	126
Figure 5.5	pH changes observed during heating of SHFF with and without ammonium persulfate (APS) to 80°C. The initial pH of the SHFF with APS was 5.1 and 5.6 for SHFF without APS. The fluids reached the targeted temperature of 80°C after 47 min of heating.	127
Figure 5.6	Amount of total available element Ca and Mg content mobilised over time in the SGW and SHFF temperature experiments. Note that y axis has different scales among the graphs.	132
Figure 5.7	Aqueous concentrations of Ca and Mg leached at different temperatures by SHFF and SGW plotted against the total available content of a given element in the solids. Note that graphs have different scales.	133
Figure 5.8	Evolution of pH in the temperature experiments with SHFF and SGW.	135
Figure 5.9	EPMA backscatter (BS) image and EDX maps for selected elements of the unreacted B4 chip. Red arrows in the BS image indicate features serving as markers between before and after leaching images. Band 1 - a silicate-rich zone, approximately 2.5 mm thick, with scattered framboidal pyrite, and dispersed carbonate clusters and discontinuous wispy carbonate ~0.1 mm laminae; Band 2 - a gradational transition into a carbonate-dominated 2.5 mm thick layer, with little to no pyrite present; Band 3 - a relatively sharp transition into another silicate-rich 0.5 mm lamina with dispersed carbonate clusters and more abundant pyrite; Band 4 - a carbonate-rich ~0.5 mm lamina; and Band 5 - a silicate-rich 0.5 m lamina with less abundant carbonates dispersed in a clay matrix with abundant pyrite.	145
Figure 5.10	EPMA backscatter (BS) image of B4 chip after leaching with SGW at 80°C for 360h and EDX maps for selected elements. No S was detected by EDX after the experiment. The post-leaching images are offset 0.14 mm vertically and 0.12 mm horizontally from the unreacted ones and slightly rotated left. Red arrows in the BS image indicates a feature serving as a marker between before and after leaching images.	146

Figure 5.11	EPMA backscatter image of B4 chip zoom in, taken in the middle of the transect, before and after leaching with SGW at 80°C for 360h. Yellow arrows indicate pyrite framboids. Before and after images and maps do not coincide, as the post-leaching transect images are offset 0.14 mm vertically and 0.12 mm horizontally from the unreacted ones.	148
Figure 5.12	EPMA backscatter (BS) image and EDX maps for selected elements of the unreacted B2 chip. Red arrows in the BS image indicate features serving as markers between before and after leaching images.	151
Figure 5.13	EPMA backscatter (BS) image of B2 chip after leaching with SGW at 80°C and 140 bar for 360h and EDX maps for selected elements. The post-leaching images are offset by 0.03 mm both vertically and horizontally from the unreacted ones. Red arrows in the BS image indicate features serving as markers between before and after leaching images.	152
Figure 5.14	EPMA backscatter (BS) image and EDX maps for selected elements of the unreacted B3 chip. Red arrows in the BS image indicate features serving as markers between before and after leaching images.	153
Figure 5.15	EPMA backscatter (BS) image of B3 chip after leaching with SHFF at 80°C for 360h and EDX maps for selected elements. The post-leaching images are offset by 0.01mm vertically and 0.1 mm horizontally from the unreacted ones. Red arrows in the BS image indicate features serving as markers between before and after leaching images.	154
Figure 5.16	EPMA backscatter image of B3 chip zoom in, taken in the middle of the transect, before and after leaching with SHFF at 80°C for 360h. Yellow arrows indicate examples of pyrite framboids. Before and after images and maps do not coincide, as the post-leaching transect images are offset by 0.01 mm vertically and 0.1 mm horizontally from the unreacted ones.	156
Figure 5.17	LVSEM backscatter (BS) image and EDX maps for selected elements of the unreacted B1 chip. Red arrow in the BS image indicates a feature serving as a marker between before and after leaching images.	159
Figure 5.18	LVSEM backscatter (BS) image and EDX maps for selected elements of the unreacted B1 chip. Red arrow in the BS image indicates a feature serving as a marker between before and after leaching images.	160
Figure 5.19	Relative abundance of Fe, S and Ca across the length of B1 chip (a) before and (b) after leaching with SHFF at HPHT. Data represent EDX measurements and do not represent actual concentrations.	161
Figure 5.20	LVSEM backscatter image of B1 chip zoom in, taken on the lower left side of the transect, before and after leaching with SHFF at 80°C and 183 bar for 360h. Yellow arrows indicate examples of pyrite framboids. Before and after images and maps do not coincide, as the post-leaching transect images are offset by 0.2 mm vertically and 0.15 mm horizontally from the unreacted ones.	163
Figure 5.21	LVSEM backscatter image of precipitates formed during cooling of B1 leachate, following a 360h experiment with SHFF at 80°C and 183 bar.	164
Figure 6.1	Ternary plot of bulk mineralogy of shale samples used in this study, superimposed on the Shlumberger's sCore classification scheme for organic mudstones. sCore scheme layout adapted from Gamero-Diaz et al. (2012), and Linder (2016).	174
Figure 6.2	Conceptual model of the main rock-fluid interactions observed in the laboratory experiments; (d) adapted from Jew et al. (2017).	187

LIST OF TABLES

Table 1.1	Typical chemical additives in hydraulic fracturing fluid (adapted from Vidic et al., 2013 and fracfocus.org).	4
Table 1.2	Summary descriptive statistics for the concentrations of PTEs in Marcellus shale gas wastewater. n/a – statistics not applicable due to no detections; blank – element not analysed; % <DL– percent of samples below the detection limit; n detects/ n total – number of detects versus number of samples analysed for a given element.	20
Table 2.1	Summary of experimental parameters used by the different studies discussed in section 2.2	24
Table 3.1	Background information for the shale samples used in this study.	42
Table 3.2	Summary of XRD data sources for Australian samples.	43
Table 3.3	TRE concentrations for the shale samples - major elements (µg/g). Values highlighted in green exceed >10x average upper crustal abundances (Rudnick and Gao, 2003), values in yellow exceed >10x the average shale values (Turekian and Wedepohl, 196), and in orange both values are exceeded >10x. "-" value not available (above the upper detection limit).	50
Table 3.4	TRE concentrations for the shale samples - minor elements (µg/g). Values highlighted in green exceed >10x average upper crustal abundances (Rudnick and Gao, 2003), values in yellow exceed >10x the average shale values (Turekian and Wedepohl, 196), and in orange both values are exceeded >10x. "-" value not available (above the upper detection limit).	51
Table 3.5	AEE concentrations for the shale samples - major elements (µg/g).	53
Table 3.6	AEE concentrations for the shale samples - minor elements (µg/g).	54
Table 3.7	Ratio (%) of AEE to TRE for selected major elements in the shale samples, colour coded using traffic light system (high values are in red, low - in green).	55
Table 3.8	Ratio (%) of TRE values for UK samples and selected UK soil guideline values, colour coded using traffic light system (high values are in red, low - in green). SGV- Soil Guideline Values (for residential purposes), SSV - Soil Screening Values (for assessing ecological risks).	57
Table 3.9	Ratio (%) of TRE values for Australian samples an Australian soil guideline values for residential purposes with garden (NEPM HILs A), colour coded using traffic light system (high values are in red, low - in green).	58
Table 3.10	Results of the mineralogical ABA for selected shale samples. NPR and NNP values are coloured accordingly: dark grey – potentially acid producing, light grey – non-acid generating, and uncertainty zone is white cells.	64
Table 4.1	Prud'home's recipe for a titanate cross linked HPG 40 lb/bbl gel.	72
Table 4.2	Composition of the final formulation of the synthetic fracturing fluid (SHFF) used in this study.	74
Table 4.3	Range and median values for the recovery ranges of the reference material (ERM-CC018-2) for 9 available elements with certified values.	78
Table 4.4	Range, mean and median values for spike recoveries, expressed as percentage. Spike recoveries were performed on 47 elements out of 54 included in the full dataset.	79
Table 4.5	Range and median values for calculated limits of detection for all analysed elements. Elements reported as µg/l were analysed by ICP MS, whereas those reported in mg/l by ICP AES.	80
Table 4.6	Classification of shale samples based on mineralogical Acid-Base Accounting (ABA).	82

Table 5.1	Details on composition of three fluids used in the EDTA and citric acid experiments.	123
Table 5.2	Details on composition of fluids used in the ammonium persulfate experiments.	128
Table 5.3	Results of the ammonium persulfate experiments for the KC-4 sample. All concentrations are in mg/l.	129
Table 5.4	Results of the ammonium persulfate experiments for the Murteree-2 sample. All concentrations are in mg/l.	130
Table 5.5	Effect of pressure on dissolved element concentrations in SHFF leachates from Eagle Ford powdered samples. HPHT – high pressure and high temperature; HT – high temperature and atmospheric pressure.	138
Table 5.6	Effect of pressure on dissolved element concentrations in SGW leachates from Eagle Ford powdered samples. HPHT – high pressure and high temperature; HT – high temperature and atmospheric pressure.	139
Table 5.7	Effect of pressure on dissolved element concentrations in SGW leachates from Bowland-BE chips. Results from powdered Bowland-BE leachates given for comparison. HPHT – high pressure and high temperature; HT – high temperature and atmospheric pressure.	141
Table 5.8	Effect of pressure on dissolved element concentrations in SHFF leachates from Bowland-BE chips. Results from powdered Bowland-BE leachates given for comparison. HPHT – high pressure and high temperature; HT – high temperature and atmospheric pressure. Zn, Cr and Pb were excluded from this table due to high blank values.	142
Table 6.1	Trace element content of several gas-producing shales from US(Eagle Ford, Marcellus, New Albany, Utica and Woodford) and Canada (Duvernay and Montoney).	173
Table 6.2	Ratio of maximum aqueous element concentration mobilised by SHFF from Australian shale samples versus Australian Water Quality Criteria (WQC) for freshwater aquatic toxicants.	195
Table 6.3	Ratio of maximum aqueous element concentration mobilised by SHFF from Australian shale samples versus Australian Water Quality Criteria (WQC) for irrigation water.	195
Table 6.4	Ratio of maximum aqueous element concentration mobilised by SHFF from Australian shale samples versus Australian Water Quality Criteria (WQC) for livestock drinking water.	196
Table 6.5	Ratio of maximum aqueous element concentration mobilised by SGW from Australian shale samples versus Australian Water Quality Criteria (WQC) for freshwater aquatic toxicants.	197
Table 6.6	Ratio of maximum aqueous element concentration mobilised by SGW from Australian shale samples versus Australian Water Quality Criteria (WQC) for irrigation water.	197
Table 6.7	Ratio of maximum aqueous element concentration mobilised by SGW from Australian shale samples versus Australian Water Quality Criteria (WQC) for livestock drinking water.	198
Table 6.8	Ratio of maximum aqueous element concentration mobilised by SHFF and SGW from powdered Bowland shale samples versus UK Environmental Quality Standards (EQS) for freshwater.	199

Chapter 1

RATIONALE

1.1. Introduction

Hydraulic fracturing and horizontal drilling were first developed in the late 1940s and 1930s, respectively (EIA, 1993; US EPA, 2016). However, only the relatively recent advancements and simultaneous application of both technologies over the last few decades have facilitated the economic extraction of hydrocarbons from previously inaccessible low-permeability strata (Boyer et al., 2006; Charaig, 2007; Holditch et al., 2007; King, 2012; US EPA, 2016 Vidic et al., 2013). This has resulted in an acceleration of natural gas production, especially shale gas, in the USA (Vidic et al., 2013) and subsequently transformed the global energy markets. Natural gas production in the US increased from less than 20 Trillion cubic feet (Tcf) in 2000 to approximately 40 Tcf in 2019, where shale gas production accounted for ~7.3 Tcf and 27.8 Tcf, respectively (EIA, 2020). The most productive shale gas plays in the USA include Marcellus and Utica shales in the Appalachian Basin, Wolfcamp in the Permian Basin, and Eagle Ford and Haynesville shales in the Gulf Coast (EIA, 2021a). The number of horizontally drilled and hydraulically fractured natural gas wells in the US has grown from approximately 26,000 in 2000 to an estimated 300,000 by 2015 (EIA Today in Energy, 2016). Consequently, the USA has reduced its reliance on energy imports and experienced a shift in the primary source of the USA electricity generation from coal to natural gas (EIA, 2020; EIA, 2021b), significantly reshaping the American energy and power sectors.

Given the current technical and economic feasibility of extraction from shale gas systems, natural gas offers a range of benefits to the countries rich in this resource. It can provide

an indigenous energy supply and therefore decrease reliance on energy imports (EIA 2021a). Due to its more efficient and cleaner combustion than other fossil fuels, natural gas can also contribute to the reduction of greenhouse gas emissions (Moniz et al., 2011). It has also been recognised as a potential transition fuel into renewable energy sources (Jenner and Lamadrid, 2013; Moniz et al., 2011). Unsurprisingly, commercial shale gas extraction expanded to Canada, Argentina and China, while many other countries, including Australia and UK, began evaluating their own shale gas resource potential (UNCTAD, 2018).

Significant concerns, however, have been raised about the potential negative environmental, social and human health impacts of shale gas development (Bazilian et al., 2014; Jackson et al., 2014; Sovacool, 2014), which culminated in several countries or regions imposing a ban on shale gas extraction (Thomas et al., 2017). One of the key concerns regards the composition of the fluids produced from shale gas extraction activities, and their potential to contaminate water resources (e.g. Entrekin et al., 2011; Rahm and Riha, 2012; Vengosh et al., 2014).

This chapter first provides an overview of the hydraulic fracturing process and shale gas wastewater composition and fate. Subsequently, it focuses on environmental concerns associated with the inorganic geogenic chemicals present in the wastewater and explores their potential hazards to human health and the environment. Lastly, it identifies current gaps in knowledge before laying out the structure of this thesis.

1.1.1. Gas shales and hydraulic fracturing

Gas-bearing shales are classified as unconventional hydrocarbon systems, where the shale simultaneously functions as the source rock, the reservoir and the seal (Cole et al., 1987 in USGS, 2013; Holditch et al., 2007). The gas is generated *in situ* and trapped within the shale, either interstitially within the natural fractures and pores, or sorbed

onto organic matter and clay particles (Boyer et al., 2006). Although gas shales are typically regionally extensive formations with pervasive gas saturation, the gas recovery is hindered by the extremely low matrix (primary) permeability of the shales. Economic production is only possible by increasing both the reservoir exposure to the wellbore and the secondary permeability of the formation (Boyer et al., 2006; Holditch et al., 2007).

Increased reservoir contact is accomplished through horizontal drilling. The initially vertical or inclined wellbore is steered into horizontal or sub-horizontal position within the target zone to conform to the shale formation; once parallel with the reservoir, it is drilled until the intended length is achieved. Horizontal drilling provides greater contact with the reservoir than a typical vertical well, which is needed to compensate for the low permeability of shales (Charaig, 2007; EIA, 1993; Vidic et al., 2013).

Reservoir permeability is improved by hydraulic fracturing, which involves high-pressure injection (typically at 2000-12000 psi; US EPA, 2016) of large volumes of fracturing fluid (approximately $14\text{-}24 \times 10^6$ L per well; Kondash and Vengosh, 2015) to induce new fractures or enhance the existing ones (Boyer et al., 2006). The fracturing process tends to last less than two weeks per well and is commonly performed in stages. One of the initial sub-stages often involves an acid pre-flush to clean well perforations (US EPA, 2016; Morsy et al., 2015). Subsequently, a series of fracturing fluid mixtures are injected for each fracturing stage; their composition depends on each stage's particular needs (US EPA, 2016).

Typically, fracturing fluids are 90-97% water (freshwater or minimally treated recycled shale gas wastewater; US EPA, 2011), 2-10% proppant such as sand, to keep the fractures open, and less than 2% by mass a mixture of chemical additives that serve specific engineering purposes (Morsy et al., 2015; US EPA, 2016; Wang et al., 2016). The most common additives include friction reducers, pH adjusting agents, iron stabilising agents, biocides and breakers, such as polyacrylamide, potassium hydroxide, citric acid,

glutaraldehyde, and ammonium persulfate, respectively (Gregory et al., 2011; Vidic et al., 2013) (Table 1.1). The mixture is often site-specific, depending on the geology, the well development stage, and the operator (Gregory et al., 2011; Ferrer and Thurman, 2015).

Following fracture stimulation, the well may be temporarily shut-in (soaking period). Although a common field practice to potentially improve the initial hydrocarbon production, the would-be benefits of prolonged fluid contact with the formation are subject to a debate (e.g. Bertonecello et al., 2014; Crafton and Noe, 2013; Li et al., 2019a; Yan et al., 2015). A large volume of the injected fracturing fluid is lost to the shale formation (a process known as leak-off), saturating the near-fracture matrix and severely reducing near-fracture permeability due to clay swelling, solid precipitation and fine

Table 1.1 Typical chemical additives in hydraulic fracturing fluid (adapted from Vidic et al., 2013 and fracfocus.org).

Additive	Example compounds	Purpose
<i>Acid</i>	Hydrochloric or muriatic acid	Clean out wellbore, dissolve minerals and initiate cracks in rock
<i>Biocide</i>	Glutaraldehyde, 2,2-dibromo-3-nitrilopropionamide (DBNPA)	Bacterial control
<i>Corrosion inhibitor</i>	Isopropanol, acetaldehyde	Prevent corrosion of pipe by diluted acid
<i>Crosslinker</i>	Borate salts, titanate	Maximise fluid viscosity at high temperatures
<i>Friction reducer</i>	Polyacrylamide, petroleum distillate	Reduce friction between fluid and the pipe
<i>Gelling agent</i>	Guar, hydroxyethyl cellulose	Thicken water to suspend proppant
<i>Iron control</i>	Citric acid, thioglycolic acid	Prevent precipitation of metal oxides
<i>Breaker</i>	Ammonium persulfate, magnesium peroxide	Promote breakdown of gel polymers
<i>Scale inhibitor</i>	Ethylene glycol	Reduce deposition on pipes
<i>Surfactant</i>	Lauryl Sulfate, ethanol, 2-Butoxyethanol	Decrease surface tension to allow water recovery

migration. It can also result in the formation of a water-block area near the fracture face, which severely impairs hydrocarbon flow channels (e.g. Sinha and Marfurt, 2017; Yan et al., 2015). Shutting-in the well for a period of time following hydraulic fracturing is thought to help regain the permeability lost to the leak-off (Li et al., 2019a; Yan et al., 2015). Shut-in allows the injected fluids to permeate further into the formation, evolving the imbibition process driven by the capillary pressure (Bertoncello et al., 2014; Yan et al., 2015). Experimental studies have shown that shut-in enables aqueous phases to redistribute and migrate into smaller pores deeper into the formation, lowering the near-fracture water saturation and eventually dissipating the initial near-fracture water-block. This results in increased relative permeability of hydrocarbon phases and improved initial hydrocarbon production (Bertoncello et al., 2014; Li et al., 2019a; Yan et al., 2015). The shut-in period can last days to months, however, the relationship between the length of the shut-in and the amount of regained permeability or improved well productivity is still questioned (e.g. Crafton and Noe, 2013; Li et al., 2019; Yan et al., 2015).

The shut-in period is followed by a clean-up stage, also known as the flowback period, where the fracturing fluid is flowed back to the surface leaving behind the proppant to keep the fractures open (Crafton and Gunderson, 2007). This process is designed to prepare the well for the production stage as the unrecovered fracturing fluid can impair hydrocarbon flow paths by forming a concentrated polymer layer on the fracture surfaces (Tayong et al., 2019). The fluids that return to the surface during the clean-up stage are commonly referred to as flowback (US EPA, 2016; Vidic et al., 2013). Typically it can take from 2 to 20 days before the first gas is produced; this is dependent on the local geological conditions (Cook et al., 2013). For example, the typical clean-up period for wells accessing the Marcellus Shale in the US lasts between 3-10 days (Eshlman and Elmore, 2013). Most of the injected fracturing fluid remains in the subsurface, likely due to spontaneous imbibition into the shale formation; in some gas plays, fluid recovery during the post hydraulic fracturing clean-up, and prior to gas production, ranges from

~4 to 20% (Engelder et al., 2014; Li et al., 2019a). Overall fracturing fluid recovery over the lifetime of a well is often <30% (Engelder et al., 2014; US EPA, 2016).

Following clean-up, the well moves on to the production stage, when the gas flows to the surface together with formation water (i.e. water naturally occurring within the shale and any other rock formations that the fractures might intersect). The water that occurs as a by-product of the gas production, and is generated at much lower flow rates than flowback, is typically known as the produced water (Barbot et al., 2013; Vidic et al., 2013). Produced water typically flows from the wellhead through a separator, where the gas is separated from the water and any liquid hydrocarbons (US EPA, 2016). Some of the most water-productive formations (e.g. Barnett Shale, Permian Basin gas shales) can generate as high a 19,000 L of produced water per million cubic feet (MMCF) of gas. Relatively dry formations such as Eagle Ford or Haynesville can generate between 1900 and 7600 L of produced water per MMCF of gas (US EPA, 2016 and references therein).

1.2. Flowback and produced water

1.2.1. Chemical composition

Flowback and produced water composition is thought to be partially dependent on local geology, the composition of hydraulic fracturing fluids, varying spatially both between and within geological basins, but also exhibiting temporal changes during the lifetime of a single well (Barbot et al., 2013; Kim et al., 2016; US EPA, 2016). It is crucial to emphasise that the compositions of flowback and produced water are not identical to the injected hydraulic fracturing fluids. Flowback water contains mainly chemicals used in the hydraulic fracturing fluids, plus any geogenic chemicals mobilised during the fracturing process, which generate slightly to moderately elevated concentrations of the total dissolved solids (TDS) (Rowan et al., 2011; Barbot et al., 2013). Produced water

is thought to have a similar composition to that of naturally occurring formation water – it contains minor levels of fracturing fluid compounds, their degradation products, and is characterised by highly elevated total TDS, often 5-10 times the concentration in seawater (Bibby, 2013; Haluszczak et al., 2013; Rowan et al., 2011). For example, produced water from the Marcellus Shale has a median TDS value of 200, 000 mg/l (Hayes, 2009). The high levels of TDS are of geogenic origin, arising from: (1) mixing of formation brines (with naturally high TDS) with fracturing fluids; and (2) rock-fluid interactions, such as the dissolution of shale minerals caused by the injection of fracturing fluids into the target formation (Chapman et al., 2012; Haluszczak et al., 2013; Phan et al., 2015; Renock et al., 2016). Both processes are not mutually exclusive and likely contribute to the high TDS content (Chapman et al., 2012; Phan et al., 2015). Generally, the concentration of geogenic chemicals in the produced waters increases with time (Barbot et al., 2013; Chapman et al., 2012; Haluszczak et al., 2013).

A number of the geogenic constituents found in shale gas wastewater may be potentially hazardous to human health and the environment. These include organic compounds (e.g. Butkovskiy et al., 2017) and inorganics such as naturally occurring radioactive materials (NORMs) (e.g. Rowan et al., 2011), most commonly radium isotopes, as well as salts (e.g. bromide, chloride) and potentially toxic elements (PTEs), including barium, arsenic and lead (e.g. Chapman et al., 2012; Haluszczak et al., 2013; Jackson et al., 2013; Warner et al., 2013a). Consequently, the toxicity, potential environmental hazards and possible human and animal health effects of shale gas wastewater as well as the fracturing fluids have been the topic of numerous studies (e.g. Colborn et al., 2011; Gordalla et al., 2013; Kassotis et al., 2013; Wattenberg et al., 2015; Weltman-Fahs and Taylor, 2013; Wollin et al., 2020; Yost et al., 2016).

1.2.2. Management practices: reuse, treatment and disposal

Flowback and produced water (FPW) represent the largest volume waste stream from shale gas operations ($\sim 10^7$ L; Kondash and Vengosh, 2015) and require management strategies in place before hydraulic fracturing commences (Priestley, 2020; Tawonezvi, 2017; US EPA, 2016). The highest volumes of water return to the surface during the first few months, primarily during the flowback, before the flow rates decrease by order of magnitude. Typically, the amount of flowback is roughly equal to the total volume of produced water generated over a lifetime of the well. Initially, FPW is captured and stored onsite in storage tanks and/or impoundments for subsequent reuse, treatment or disposal (US EPA, 2016) (Figure 1.1).

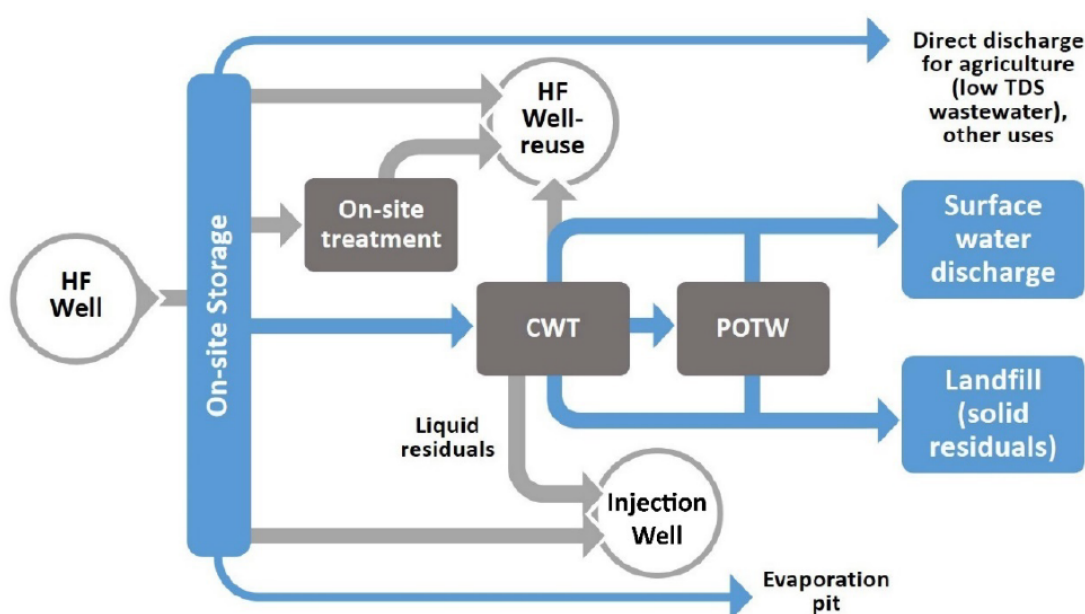


Figure 1.1 Schematic model of different wastewater management strategies. Grey lines – strategies involving injection (for reuse or disposal), blue line – other end points such as discharge, evaporation, landfills. POTW – public owned treatment works, CWT – centralised (industrial) waste treatment facilities. From US EPA (2016).

The most common management practice in the US is disposal through deep underground injection (Class II disposal wells). The available number of disposal wells is often the limit to this method. Their construction is costly and time-consuming, and tends to be constrained by the lack of suitable geology (suitable permeability and depth of geologic formations) (Gregory et al., 2011; Lutz et al., 2013; Vidic et al., 2013). Where injection wells are scarce, alternative FPW management approaches have to be employed, including reuse or treatment followed by surface water discharge (Wilson and VanBriesen, 2012). Management choices can evolve over time, driven by, e.g. decrease or increase in hydrocarbon production, changes in regulations, changes in costs, or the advancements in treatment technologies (US EPA, 2016). The changing temporal trends in wastewater management are best illustrated by the experience in Pennsylvania, where in 2011 the development of Marcellus shale generated ~570% more wastewater than conventional oil and gas wells, overwhelming the existing local wastewater treatment and disposal infrastructure (Lutz et al., 2013).

Due to the lack of deep underground injection facilities in the state, FPW in Pennsylvania was initially treated primarily at municipal wastewater treatment plants (i.e. public owned treatment works, POWT) followed by a discharge to local surface waters under permit. Centralised (industrial) waste treatment facilities (CWT) were also used but to a lesser extent. POWTs were not designed to handle high salinities and so were unable to successfully remove the TDS from the shale gas wastewater. Consequently, the effluent discharges had been linked to elevated levels of TDS and salts (bromide) in Pennsylvania's surface waters (Lutz et al., 2013; Vidic et al., 2013 and references therein; Wilson and VanBrissen, 2012). As a result, in 2010, Pennsylvania's Department of Environmental Protection imposed a more stringent standard for treated discharges of 500 mg/l TDS, and in 2011 asked the operators to voluntarily cease delivering FPW to POWTs. The industry complied, shifting the FPW treatment from POTWs to CWTs, which are better equipped to remove TDS and significantly increasing the reuse of Marcellus shale gas wastewater (Lutz et al., 2013; Schmidt, 2013). The reuse of FPW in

Pennsylvania, mainly of flowback, rose by 43% to a total of 56% by volume in 2011 (Lutz et al., 2013).

Flowback reuse can be direct, where untreated flowback is blended with fresh water to lower the TDS content and form the base hydraulic fracturing fluid for subsequent fracturing jobs or can involve some on- or off-site treatment before the reuse. The latter two options are more costly than direct reuse but decrease the potential for scaling and well plugging, which can arise from high concentrations of some TDS constituents (e.g. sulphate and barium) (US EPA, 2016 and references therein). Reuse reduces the total amounts of freshwater needed for subsequent fracturing operations, decreasing the costs associated with water acquisition, and is mainly in demand in areas where shale gas development is still active with new wells being drilled (Boschee, 2014; US EPA, 2016). Reuse is only a temporary solution; once the well construction rates decline, opportunities for flowback reuse likewise decrease, and the wastewater will require management through other means (Lutz et al., 2013; Vidic et al., 2013).

Other disposal options include storage in evaporation ponds in arid and semi-arid regions (e.g. Colorado, Utah, Texas) (Sun et al., 2019; US EPA, 2016), and some states in the US allow reuse outside of hydraulic fracturing operations, such as de-icing of roads, dust suppression or irrigation (Clark and Veil, 2009; Tasker et al., 2018; US EPA, 2016). However, the latter have been associated with concerns related to accumulation of metals or radionuclides in roads treated with FPW or increased salinity in freshwater resources (Skalak et al., 2014; Tasker et al., 2018).

1.2.3. The efficacy of treatment

The high levels of TDS, including salts, PTES and radionuclides, in the FPW can make effective treatment challenging as well as expensive (Entrekin et al., 2011; Soeder and Kappel, 2009). When Pennsylvania was still sending its shale gas wastewater through

CWTs and POTWs, ineffective shale gas wastewater treatment and disposal, were recognised in the Marcellus region as the most probable contamination pathway (Rozell and Reaven, 2012). It was estimated to be several orders of magnitude more likely to occur than any other pathways (e.g. transportation spills or leaks through well casing and fractured rocks (Rozell and Reaven, 2012).

Ferrar et al. (2013) sampled effluents from two publicly owned treatment works and one commercial industrial brine treatment plant in Pennsylvania, showing that neither could successfully lower TDS concentrations, chlorides and bromides, and metals such as barium and strontium, below US EPA water quality criteria. Brine treatments were also documented to be unable to successfully remove halides and ammonium (Harkness et al., 2015). The treatment facilities that can handle FPW more effectively, for example by removing TDS through reverse osmosis, thermal distillation or chemical precipitation, tend to have high capital and operating costs, and are not always widely available (Boschee et al., 2014; Entekin et al., 2011; Gregory et al., 2011).

1.3. Environmental concerns associated with flowback and produced water

1.3.1. Surface and groundwater contamination pathways

One of the primary concerns associated with the development of shale gas resources is the potential for environmental and human health impacts, particularly due to contamination of water resources (e.g. Entekin et al., 2011; Vengosh et al., 2014). In their report assessing the relationship between hydraulic fracturing and drinking water quality, US EPA (2016) reviewed 1,200 cited sources of data and information, identifying above and below ground mechanisms that have the highest likelihood to result in more frequent or more severe impacts on water resources. These were mostly

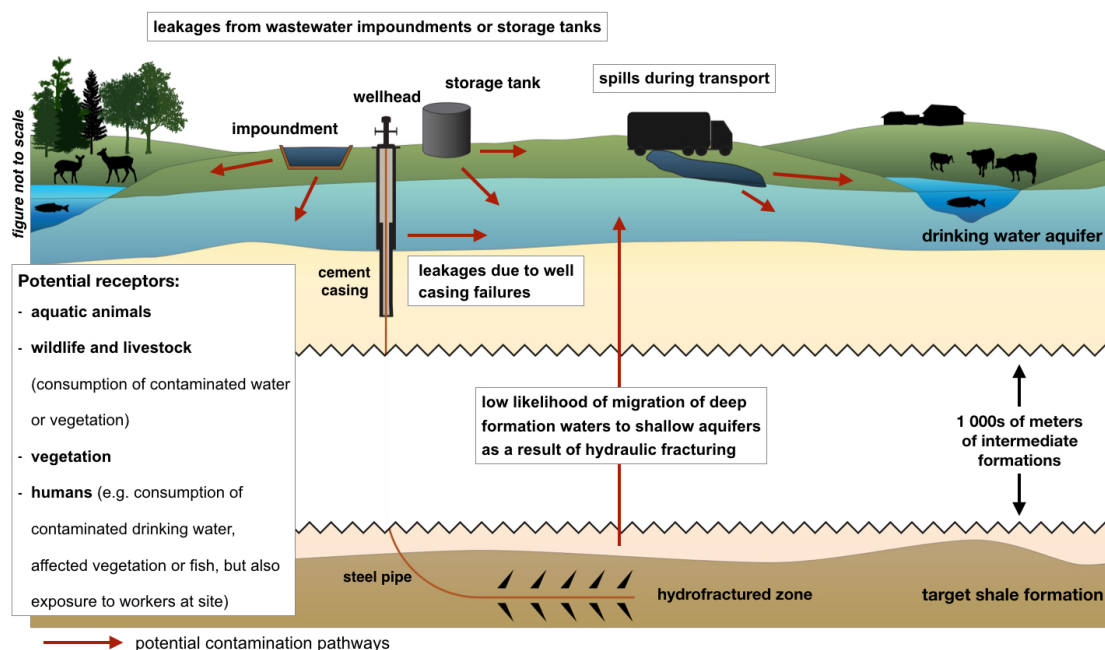


Figure 1.2 Conceptual model (not to scale) of potential receptors and some of the possible contamination pathways associated with shale gas wastewater. Adapted from Vengosh et al. (2014) and Weltman-Fahs and Taylor (2013).

associated with leaks and spills of FPW, both as an outcome of accidents and routine activities.

Flowback and produced water could potentially contaminate water resources (shallow aquifers and surface waters) through several underground and overground pathways (Figure 1.2):

(1) Underground pathways

Plausible subsurface modes of contamination include leakage of flowback or produced water from the well due to well integrity failures or inadequate well design and construction (Llewellyn et al., 2015; US EPA, 2016; Vidic et al., 2013). Hydraulic fracturing repeatedly exposes a well to much higher pressure and temperature changes than during any other phase in the lifetime of the well. These could cause degradation of well casing and cement over time, and so well components should be designed to withstand these stresses to preserve

the mechanical integrity of the well (US EPA, 2016). Inadequate or degraded casing or cement can create several pathways for fluid migration via or adjacent to the production well, such as gaps in cement due to poor cement quality or casing (Fig 1.3).

Another possibility for hydraulic fracturing fluids or FPW to contaminate shallow groundwater sources is through upward migration of fluids from deep formations along natural pathways (e.g. faults) and via the fracture networks created during hydraulic fracturing (e.g. Myers, 2012; US EPA, 2016; Warner et al., 2012; Rozell and Reaven 2012). However, multiple studies indicate that such a contamination mechanism has a low likelihood of occurrence (Engelder et al., 2014; Flewelling et al., 2013; Jackson et al., 2013; Llewellyn et al., 2015). Fluid migration directly from the production zone is unlikely due to high capillary and osmotic forces as well as imbibition processes sequestering hydraulic fracturing fluid lost to the leak-off (Engelder et al., 2016; US EPA, 2016). In fact, production of hydrocarbons will reduce the gas and brine pressures below local hydrostatic levels, creating an underpressured zone, and drawing fluids toward the shale rather than away from it (Flewelling and Sharma, 2014; Thorogood and Younger, 2014). The likelihood of upward fluid flow from the shale target zone to a shallow drinking water aquifer is additionally limited by the large separation difference between the two formations. This distance varies across the plays in the US, but it is often equal to or exceeds 1.6 km (US EPA, 2016).

However, it is worth noting that any impacts that might occur due to the underground pathways are challenging to manage as the interplay between the well and the geological environment is intricate and cannot be observed directly. There is also limited information available on the well performance or subsurface fluid movement related to hydraulic fracturing operations, which further complicates the prediction and assessment of when shallow aquifers

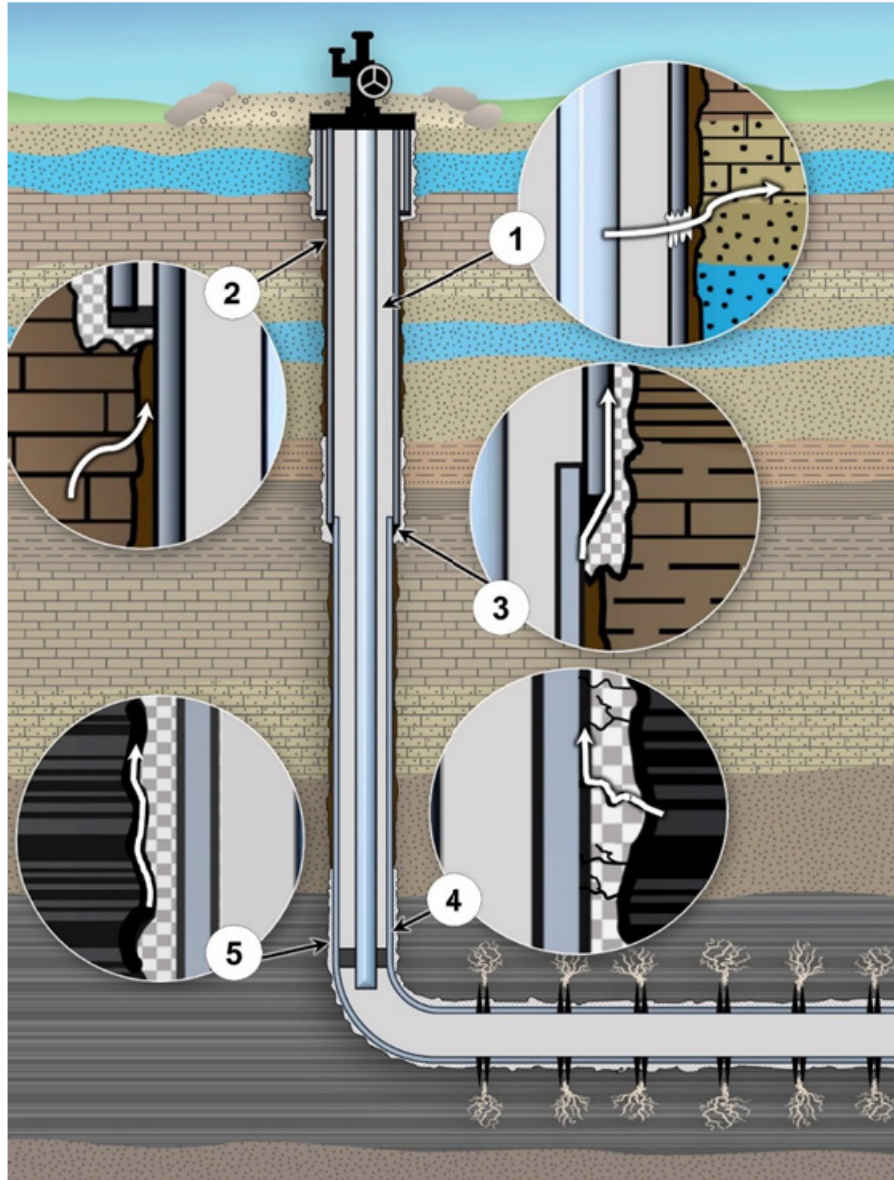


Figure 1.3 Conceptual model (not to scale) of potential pathways (white arrows) for fluid movement in a cemented well: (1) a casing and tubing leak into the surrounding rock; (2) an uncemented annulus (i.e., the space behind the casing); (3) microannuli between the casing and cement; (4) gaps in cement due to poor cement quality; and (5) microannuli between the cement and the surrounding rock. From US EPA (2016).

are impacted or identification of the primary cause (US EPA, 2016).

(2) Above ground pathways

The most significant surface pathways that could lead to degradation of shallow groundwater and surface waters are: (1) spills and leakages from surface storage or during transportation of FPW to treatment facilities; and (2) stream discharges of inadequately treated FPW (Jackson et al., 2014; Lauer et al., 2016). Beyond the immediate impact, these can also cause a long-term risk to the environment by accumulating radionuclides and toxic elements in stream sediments and soil near to disposal sites and spill locations (Burgos et al., 2017; Harkness et al., 2015; Lauer et al., 2016; Vengosh et al., 2014).

Certain PTEs (e.g. Br, V, Se) have the potential to persist in the impacted water environment for a long-time (months to 4 years) following a contamination incident (Lauer et al., 2016). Increased total Ra activity in soils has also documented, particularly downstream from the spill location (Lauer et al., 2016). Discharges of treated unconventional oil and gas wastewater by centralised waste treatment (CWT) plants to Pennsylvania surface waters, have also led to elevated radium levels and other alkaline earth metals in sediments downstream from the CWT plant (Burgos et al., 2016).

The rapid expansion of shale gas operations could also increase the cumulative risk of surface spills or leaks (Entrekin et al., 2011; Vengosh et al., 2014). Maloney et al. (2017) analysed wastewater spill data for unconventional oil and gas wells in Colorado, New Mexico, North Dakota and Pennsylvania from 2005 to 2014. The highest number of spills (1,538) and the largest reported spill volumes (2,702,784 L) occurred in North Dakota, which is potentially attributable to the significant increase in the number of new horizontal wells installed between 2012 and 2014 (Maloney et al., 2017).

As such, incidences of contamination from shale gas wastewater are more likely

to be episodic (short-lived incidences such as spills) rather than systematic (Fontenot et al., 2013) but might have a long-term effect on the environment (Lauer et al., 2016).

1.3.2. Potential hazards to human health and the environment

A few studies examined the quality of water bodies where shale gas wastewater has entered the environment, and the effects on the aquatic life and other affected species, including the impacts caused by PTEs (Bamberger and Oswald, 2012; Cozzarelli et al., 2017; Lauer et al., 2016; Papoulias and Velasco, 2013). One study demonstrated that an accidental release of flowback water into a creek in Kentucky decreased the pH and increased Al and Fe levels in the creek water, causing widespread distress or death of fish and aquatic invertebrates (Papoulias and Velasco, 2013). Gill lesions observed in these fish have been previously documented in many fish species exposed to low pH, heavy metals or both (Papoulias and Velasco, 2013). It is worth noting that produced waters are highly saline and their salt content will be a major toxicant (Frag and Harper, 2014). Spills of FPW can increase freshwater salinity - a parameter many freshwater species are often sensitive to, and thus lead to adverse effects on aquatic biota (Brittingham et al., 2014 and references therein).

Another study catalogued cases of reported exposure of livestock and domestic animals to shale gas wastewater. In most cases, death or severe health effects were observed (Bamberger and Oswald, 2012). Based on the symptoms, heavy metal poisoning was suspected (but not confirmed) in a few horses. Later, arsenic poisoning was diagnosed in a child living in a house located within a mile from a wastewater impoundment, where several instances of spills and leakages were noted. No elevated levels of arsenic were detected in the well water used for drinking by the child and their family;

however, the tests were conducted a year after the child initially fell sick. Screening for other toxicants revealed that the child and their family also suffered chronic exposure to benzene in the air, which is a common volatile organic toxicant detected in shale gas wastewater (Akob et al., 2015). After ceasing to drink the water from the well, the child gradually recovered from the arsenic poisoning. Phenol levels and the symptoms caused by exposure to benzene decreased in the family members who eventually moved away from the house (Bamberger and Oswald, 2012). A direct link to shale gas operations could not be established for this case due to incomplete testing and nondisclosure agreements. However, the multiple lines of evidence presented in the study indicated that the adverse health effects in humans and animals were connected to shale gas operations, particularly wastewater mismanagement.

Vegetation could also be adversely impacted by flowback and produced water spills. An experimental release of ~303 000 litres of shale gas wastewater onto 0.2 ha of mixed hardwood forest instantaneously caused severe damage and near 100% mortality in ground vegetation within a few days. The overstory trees displayed premature leaf drop within ten days, and within two years following the release of the fluids, 56% of trees within the test area were dead (Adams, 2011). Consequently, even though a contamination events are likely to be transitory, the adverse environmental effects might persist in the long-term.

Only a few epidemiological studies have so far focused on the direct impacts of hydraulic fracturing on human health; often, the consequences for human health are indirectly deduced from the environmental impacts and the focus tends to be on acute rather than chronic toxicity (Werner et al., 2015; Wollin et al., 2020). Although the studies have demonstrated associations between hydraulic fracturing processes and the observed human health effects, establishing a clear casualty is challenging. The most hindering factors in the assessment of environmental and human health impact have been the lack of baseline data prior to the shale gas operations as well as knowledge of the contaminants present in FPW, and their concentrations, which is often only known

approximately (Wollin et al., 2020).

1.4. Summary and gaps in knowledge

Hydraulic fracturing of gas shales generates large quantities of flowback and produced water that provide a challenge for safe management and effective treatment due to their composition. They typically contain high levels of TDS, including NORM (particularly in the Marcellus region) and PTEs, which are likely derived from the rock-fluid interactions with the shale formation due to the injection of fracturing fluids. High levels of these inorganic geogenic chemicals may pose a hazard to the environment, for example, through accidental releases or spills of untreated wastewater. Neither municipal nor commercial brine treatment plants have been able to successfully treat shale gas flowback and produced water in the USA. In other areas, facilities that can treat FPW, removing TDS e.g. through reverse osmosis, might not be easily available and involve high operation and capital costs (Boschee, 2014; Entekin et al., 2011; Estrada and Bhamidimarri, 2016). The release of insufficiently treated effluent to surface waters has been recognised as a contamination risk several magnitudes higher than that of the other pathways (e.g. transportation spills, and leaks through well casing and fractured rocks) (Rozell and Reaven, 2012).

Limited data available on the concentrations of some of the geogenic contaminants that might be present in FPW creates uncertainty around the potential hazard posed by them (e.g. Annevelink et al., 2016; Shrestha et al., 2017; Tasker et al., 2018). A number of studies investigated the salinity (major elements) or NORM present in the shale gas wastewater (e.g. Haluszczak et al., 2013; Rowan et al., 2011); however, PTEs have so far received limited attention (Abualfaraj et al., 2014; Hayes, 2009; Ziemkiewicz and He, 2015). Despite often being identified as the hazardous constituents, little information on the actual concentrations of PTEs in flowback and produced water is available in the

peer-reviewed literature or other publicly available sources (Alley et al., 2011; Rowan et al., 2015; Ziemkiewicz and He, 2015).

A literature review for this PhD done mainly in 2017, based on convenience sampling data-mining, yielded only 12 different data sources for PTEs, and six of them were for shale gas wastewater from the Marcellus Shale (Pennsylvania, US) (BOGM, no date; Hayes, 2009; PA DEP (2009-2010) in Blondes et al., 2016; Phan et al., 2015; Rowan et al., 2015; Strong et al., 2014). Three sources gave details on the flowback composition from Bakken play (US) (Lauer et al., 2016; Stepan et al., 2010; Strong et al., 2014). Three studies provided one data point each (each representing a different well) for flowback from Duvernay Formation in Alberta, Canada (Blewett, et al., 2017; Flynn et al., 2019; He et al., 2017). Lastly, one report provided data for one well in the Bowland Shale in the UK (EA, 2011). For all other produced shales around the globe, there were either no publicly available data sources or the data did not pass the screening criteria. Sources were excluded if they reported major elements or TDS, but no information on PTEs, or provided only descriptive statistics, rather than individual measurements of PTEs concentrations. Within this limited dataset, the frequency of detection for individual PTEs is variable and PTEs typically show a wide range of concentrations, even within one shale play (Table. 1.2).

The majority of the publicly available data on PTE concentrations in shale gas wastewater, which meet the screening criteria, were for the Marcellus Shale – a single shale gas play out of the eight major plays that have been developed in the US (Stephenson, 2015), and others that are being explored globally. Indeed, two of the Marcellus sources - the Hayes (2009) and BOGM (no date) datasets - underlie the vast majority of the peer-reviewed analyses of wastewaters from shale gas activities to date (e.g. Abualfaraj et al., 2014; Barbot et al., 2013; Engle and Rowan, 2013; Haluszczak et al., 2013; Kondash et al., 2017).

The lack of water quality data impedes extrapolation of findings to regions where shale gas development is still under consideration and hinders the comprehensive evaluation

Table 1.2 Summary descriptive statistics for the concentrations of PTEs in Marcellus shale gas wastewater. n/a – statistics not applicable due to no detections; blank – element not analysed; % <DL– percent of samples below the detection limit; n detects/ n total – number of detects versus number of samples analysed for a given element.

		Regulated Potentially Toxic Elements (mg/L)											
Data source		As	Cd	Co	Cr	Cu	Hg	Mn	Ni	Pb	Se	Tl	Zn
BOGM (no date)	<i>n detects/ n total</i>	1/20	0/22		0/22	4/22		22/22	1/4	1/4	1/7	0/8	1/2
	Minimum	0.05	n/a		n/a	0.02		0.01	0.1	0.02	0.1	n/a	0.02
	Median	0.05	n/a		n/a	0.1		2	0.2	0.04	0.1	n/a	0.2
	Maximum	0.05	n/a		n/a	0.2		29	0.5	0.1	0.1	n/a	1
PA DEP (2009 - 2010)	<i>n detects/ n total</i>	3/14	3/14	4/14	4/14	3/14	1/14	14/14	3/14	2/14	0/15	1/2	5/14
	Minimum	0.01	0.001	0.04	0.01	0.01	0.001	0.6	0.03	0.004	n/a	0.03	0.04
	Median	0.01	0.002	0.1	0.03	0.02	0.001	1	0.05	0.01	n/a	0.03	0.04
	Maximum	0.03	0.002	0.5	156	0.2	0.001	14	0.2	0.02	n/a	0.03	0.3
Rowan et al. (2015)	<i>n detects/ n total</i>			11/20		21/22		57/57	13/22	4/22			22/22
	Minimum			0.001		0.03		0.1	0.01	0.001			0.1
	Median			0.02		0.3		3	0.3	0.002			0.9
	Maximum			0.03		1.6		24	19	0.003			2
Hayes (2009)	<i>n detects/ n total</i>	44/44	44/44	44/44	44/44	44/44	44/44	44/44	44/44	44/44	44/44	44/44	44/44
	Minimum	0.01	0.001	0.001	0.01	0.03	0.00002	0.004	0.004	0.003	0.01	0.01	0.04
	Median	0.1	0.03	1	0.03	0.3	0.0002	0.4	0.4	0.03	0.1	0.1	0.1
	Maximum	0.2	0.1	25	0.1	0.5	0.0003	11	4	0.6	0.1	1	1.8
Strong et al. (2014)	<i>n samples</i>	1/1	1/1	1/1	1/1	1/1		1/1	1/1	1/1	1/1	1/1	1/1
		0.04	0.001	0.001	0.005	0.2		2	0.01	0.01	0.01	0.002	1
Phan et al. (2015)	<i>n samples</i>							33/43					
	Minimum							0.5					
	Median							3					
	Maximum							11					

of potential impacts arising from shale gas wastewater mismanagement.

Experimental studies could provide means to fill this gap in knowledge until more publicly available field data is available. Although replicating the exact field-conditions in an experimental setting is unlikely, laboratory studies could still provide useful insights into geochemical reactions that may occur upon injection of fracturing fluids into the targeted shale formation, and help to evaluate the potential for PTE mobilisation during the hydraulic fracturing process.

The main focus of this thesis is to: (1) characterise PTE mobilisation from a range of gas shales, with different mineralogical characteristics, due to contact with synthetic hydraulic fracturing fluids; and (2) investigate key factors that may affect element mobilisation into solution.

CHAPTER 2

PREVIOUS LABORATORY STUDIES: A REVIEW

2.1. Introduction

Environmental risks associated with shale gas production, especially those related to water resource contamination with flowback and produced water, are the focus of much public and academic attention (e.g. Haluszczak et al., 2013; Vengosh et al., 2014; Warner et al., 2013; Wollin et al., 2020). The large quantities of wastewater produced throughout the lifetime of a well ($\sim 10^7$ L; Kondash and Vengosh, 2015) can contain regulated potentially toxic elements (PTEs) that are mobilised from the targeted shale formations by the hydraulic fracturing fluids or derive from mixing with the formation brines (Harrison et al., 2017; Renock et al., 2016).

The injection of oxygenated and potentially acidic fluids into a reducing reservoir environment results in chemical disequilibrium and thus should induce a range of geochemical reactions while the system re-equilibrates, such as mineral dissolution-precipitation, cation exchange or surface complexation (Harrison et al., 2017). These reactions have the potential not only to mobilise PTEs and other elements from the formation into the wastewater but also affect the efficiency of the production due to changes in the reservoir's permeability and mechanical properties (e.g. Al-Bazali et al., 2008; Jew et al., 2017; Li et al., 2019b; Paukert Vankeuren et al., 2017; Zolfaghari et al., 2016). Changes in pH and the introduction of complexing agents, such as citric acid, which serves as an iron control measure, can result in the desorption of metals from their host minerals and the formation of strong complexes. This can lead to increased

mobility of several regulated elements (Kourgiantakis et al., 2000; Wang et al., 2016). Oxidation of pyrite and other Fe and/or S²⁻-bearing minerals could result in the release of PTEs into the wastewater as well as precipitation of secondary minerals that may negatively impact hydrocarbon recovery. Conversely, dissolution of calcite induced by the presence of acids could increase the near-fracture matrix porosity (e.g. Harrison et al., 2017; Jew et al., 2017; Li et al., 2019b; Wang et al., 2016) and affect the strength of the rock mass.

The changes in the chemical composition of flowback and produced waters have received significant attention, especially concerning the mixing of injected fluids with formation brines (e.g. Haluszczak et al., 2013; Rowan et al., 2015; Stewart et al., 2015). However, the extent to which the rock-fluid interactions during hydraulic fracturing is still not fully known, nor how the local geochemical/mineralogical environment contribute to the observed temporal changes in the wastewater geochemistry or impact the shale formation properties (e.g. Harrison et al., 2017; Li et al., 2019b; Phan et al., 2020).

2.2. Rock-fluid interactions during hydraulic fracturing

Ten recent studies, designed mostly as benchtop or batch reactor experiments, investigated the rock-fluid interactions during hydraulic fracturing operations (Table 2.1). The majority of them show evidence for calcite dissolution and pyrite oxidation, as well as precipitation of secondary iron and sulfate phases. These processes appear to control the amount of PTEs mobilised into solution (Harrison et al., 2017; Jew et al., 2017; Wang et al., 2015; Wang et al., 2016; Wilke et al., 2015). Most studies were performed under atmospheric pressures and ambient or elevated temperatures and utilised primarily powdered shale samples exposed to distilled water or water mixed with common hydraulic fracturing additives (e.g. citrate, HCl) for varying lengths

Table 2.1 Summary of experimental parameters used by the different studies discussed in section 2.2

Reference	Shale	Sample type	Reaction time	T and P used	Fluids	solid:fluid ratio	General aims
Dieterich et al., 2016	Marcellus (US) and Huntersville Chert (US)	solid core samples	Marcellus - 6 days, Huntersville - 89 days	Marcellus - 77°C, 275 bar; Huntersville Chert - 50°C, 103 bar	synthetic fracturing fluid for Marcellus, field collected recycled frac fluid for the chert	about 1:14 or 1:30	aimed to investigate chemical and physical changes to the shale after interaction with frac fluid; looked at short-term reactions for Marcellus
Harrison et al., 2017	Barnett, Marcellus, Green River, Eagle Ford (all US)	150-250 µm powders	3 weeks, 3 months and 6 months	circum-atmospheric P and 80°C	synthetic frac fluid with typical additives used in Marcellus wells	1:200	batch reactor experiments investigating shale-fluid reactions, effect of mineralogy, potential release of metals and alterations to shale porosity
Jew et al., 2017	Barnett, Marcellus, Green River, Eagle Ford (all US)	150-250 µm powders and cm-scale chips	3 weeks, 3 months and 6 months	circum-atmospheric P and 80°C	synthetic fracturing fluid with and without HCL, only DDI water, and only HCl	approximately 1:200	designed to examine Fe-centred reactions that occur in the pore spaces during the initial fluid-shale reactions prior to and during acid neutralisation, not representative of flowback water conditions
Li et al., 2019b	Marcellus and Eagle Ford (US)	1 cm diameter, 1.5 cm length cores - not fractured	3 weeks	80°C, 77 bar	synthetic fracturing fluids with and without barium chloride and sodium sulfate	n/a	aimed to characterize the thickness of the alteration zone in the shale matrix after shale-fracturing fluid interactions
Marcon et al., 2017	Marcellus (US)	powders (147 µm) and chips (1-3 mm) used at 3:1 ratio	approximately 14 and 15 days	130°C, 275 bar	synthetic brine with and without synthetic fracturing fluid	aimed to be 1:20	designed to simulate the conditions during the shut-in phase
Paukert Vankeuren et al., 2017	Marcellus (US)	artificially fractured cores	7 days	65.5°C, pore pressure - 200 bar, confining pressure - 214 bar	spring water with and without additives, synthetic reused produced water with and without additives	100:1	core flooding experiments designed to closely approximate field conditions, looking at mineral reactions during the shut-in phase

Table 2.1. Continued.

Reference	Shale	Sample type	Reaction time	T and P used	Fluids	solid:fluid ratio	General aims
Pearce et al., 2018	Roseneath and Murteree Shales (Australia)	1 cm ³ cubes	1 week (168 h)	75°C, 200 bar	MilliQ water	approx. 1:23 and 1:22	aimed to investigate reactions between shales and water at HPHT and measure metal mobilisation
Tasker et al., 2016	Marcellus (US)	297 µm - 2 mm powders	36 h	80°C, 82.7 bar and atmospheric (22°C, 1 bar)	synthetic fracturing fluids	1:40 for HPHT	looked at how the organics in the fracturing fluid affect metal mobilisation from the shale samples, and how reactions with the shale alter the fracturing fluids under HPHT
Wang et al., 2015	Eagle Ford (US)	powders (finest of 53-106 µm)	96 and 120 h	room T, ambient P	water with additives (acids and oxidants)	1:100, 1:1000 or 1:500	series of batch experiments with varying pH, oxidant conditions, and solid:water ratios
Wang et al., 2016	Bakken (US)	powdered to a 53-106 µm size fraction	120h	22, 50 and 80°C, ambient P	water with and without common additives	1:1000 (typically), 1:100	series of batch experiments examining element mobilisation during shale-fluid interactions as a function of aqueous chemistry (pH, redox conditions, temperature, chemical additives, and solid:water ratios)
Wilke et al., 2015	Alum Shale (Denmark), Posidonia Shale (Germany)	<2mm powders	short term - 24h, long term - 2 and 6 months	short term - 1 bar and 100°C, long term - 100 bar and 100°C	water with and without common additives (4 different fluid compositions)	1:12.5 for all experiments	long term studies done in an autoclave, short term ones in reaction vessels
Xiong et al., 2020	Marcellus (US)	artificially fractured cores	4 days at 0.3 ml/min flow rate, 21 days at 0.01 ml/min or no flow	66°C, 125 bar core pressure, ~138 bar confining pressure,	synthetic fracturing fluids	n/a	aimed to investigate the influence of flow rate and fluid composition on barite scale formation during hydraulic stimulation and the shut-in phase

of time (24 h to 6 months). Most of these studies have been undertaken at elevated temperatures and atmospheric pressures or both elevated temperatures and pressures.

Although the mineral dissolution and oxidation observed during these experiments were dependent on the pH and oxidant levels of the hydraulic fracturing fluids (Harrison et al., 2017; Wang et al., 2015; Wang et al., 2016), the solution pH and the concentration of dissolved elements in the solution appeared to be chiefly controlled by the shale mineralogy, particularly the amount of pyrite versus the amount of carbonates (Wilke et al., 2015).

In experiments where dissolved oxygen was present, if the shale contained little to no carbonate minerals, oxidation of pyrite was the driving force for element mobilisation and controlled the solution pH through the generation of sulfuric acid (Wilke et al., 2015). PTEs would have then be released directly from pyrite as well as from other host phases as the sulfuric acid would also react with silicate minerals and Fe-Mn oxides (Jeng et al., 1991; Jeng et al., 1992; Matamoros-Veloza et al., 2011). On the other hand, in shales with higher carbonate content, the dissolution of carbonates neutralised the acidity produced by pyrite oxidation and resulted in a much lower element load in the solution (Chermak and Schreiber, 2014; Harrison et al., 2017; Wang et al., 2015; Wilke et al., 2015).

At higher pH conditions, and in the presence of oxidants, most of the heavy metals tend to be removed from the solution by adsorption or coprecipitation with secondary minerals, for example, Fe-(oxy)hydroxides. The latter forms in greater abundance at higher pH due to faster rates of aqueous Fe(II) oxidation (Harrison et al., 2017; Jew et al., 2017). Furthermore, under neutral to alkaline pH, new precipitates are likely to cover pyrite surfaces, leading to their passivation, and consequently impeding pyrite oxidation (Chandra and Gerson et al., 2010; Harrison et al., 2017; Jeng et al., 1992). However, secondary phases could also precipitate as coatings on carbonate minerals, inhibiting further neutralisation (Salomons, 1995).

In the long-term experiments (2-6 months) conducted by Wilke et al. (2015) at elevated pressure and high-temperature conditions, PTEs such as Co, Ni and Th reached their highest concentrations within four days, before showing an overall decreasing trend - most likely caused by their coprecipitation or adsorption by secondary minerals. Harrison et al. (2017) also observed that mineral dissolution at elevated temperature (80°C) released potential contaminants (e.g. Pb, U and Ni), which were subsequently sequestered from the solution by the precipitation of Fe(III)(oxy)hydroxide phases. Precipitation of oxidised Fe-bearing secondary minerals was facilitated by higher pH and thus was highly dependent on the relative abundances of calcite and pyrite in the shale as well as the acidity and dissolved oxygen levels in the injected fluids (Harrison et al., 2017; Jew et al., 2017).

Upon injection of oxygenated and acidic fluids, abundant carbonates are likely to maintain the solution pH at near-neutral levels, leading to the rapid oxidation of Fe(II) and subsequent precipitation of large Fe(III)-(oxy)hydroxide grains or grain clusters near the source of the Fe(II) (typically pyrite). This could block oxidant diffusion into the mineral and thus inhibit further oxidation and release of Fe(II), as well as occlude porosity and impede gas flow into the fractures.

In carbonate-poor shales, where the buffering capacity is low, and consequently, the pH is more acidic, oxidation of released Fe(II) into Fe(III) is slower, and any secondary Fe(III)-bearing minerals formed would be highly dispersed (Jew et al., 2017; Morgan and Lahav, 2007). However, Jew et al. (2017) noted that bitumen, which may be mobilised from the shale by the organic additives in the fracturing fluids, could facilitate Fe(II) oxidation at low pH. Similarly, organic additives such as EDTA and citric acid, which may be used as scale inhibitors/iron complexing agents in the fracturing fluid (Elsner and Heolzer, 2016; Ferrer and Thurman, 2015), were observed to enhance Fe(II) oxidation rate under acidic pH by complexing the Fe(II) in the solution (Jones et al., 2015). This may result in a slow formation of small Fe(III)-bearing phases, distributed in a diffuse manner at significant distances from the Fe(II) source. These precipitates could

also lead to the blocking of pores, fractures and wellbore piping, negatively impacting gas production (Jew et al., 2017).

Similar trends of coupled dissolution and precipitation were also observed in the few experiments that exposed shale material to synthetic fracturing fluids or ultrapure water under more reservoir-representative high pressures and high temperatures (HPHT) (65.5-130°C, 82.7-275 bar). Dieterich et al.'s (2016) study on the Marcellus Shale observed dissolution and etching of carbonate minerals, precipitation of gypsum on the core surface and in several fractures, but no alteration of pyrite or the clay matrix. Another set of laboratory experiments by Marcon et al. (2017), also on Marcellus Shale chips and powders, showed evidence for calcite and pyrite dissolution, and precipitation of anhydrite on carbonate substrates. Additionally, certain PTEs (e.g. Co, Cr, Cu, Ni), mobilised from the shale sample by the synthetic fracturing fluid, showed an initial enrichment (~24 h) in the solution before subsequently decreasing in concentration (Marcon et al., 2017). A similar trend was observed by Wilke et al. (2015) and Pearce et al. (2018) under elevated P and high T experimental conditions.

Pearce et al. (2018) exposed 1cm³ cubes of Australian shales to MilliQ water with no additives at HPHT and under mildly oxic conditions. At the outset, elements such as Fe, Cr, Ni and Hg substantially increased in concentration in the solution but later decreased (typically after 24 or 72 h). Minerals such as pyrite and sphalerite, as well as carbonates (ankerite and/or siderite), showed evidence of dissolution, with the latter creating secondary porosity that was subsequently occluded by the precipitation of Fe-oxides (Pearce et al., 2018) (see Chapter 3.3. where these reactions are discussed in more detail). Metal release from Marcellus Shale under HPHT conditions was also studied by Tasker et al. (2016), who concluded that the initial mineralogy and pH of the fracturing fluids would exert a strong control on metal dissolution.

Lastly, in a Marcellus core flooding experiment (Paukert Vankeuren et al. (2017) observed calcite dissolution and gypsum precipitation on the fracture surface after

contact with natural spring water or spring water with common fracturing additives, and after contact with synthetic reused produced water with and without common fracturing additives. Furthermore, oxidation of pyrite by ammonium persulfate increased dissolved sulfate concentrations and resulted in barite scale precipitation in all experiments with the synthetic reused produced water (Paukert Vankeuren et al., 2017). However, a complementary study by Phan et al. (2018) concluded that the fluid-rock interactions would not exert a strong influence on the evolution of produced water from Marcellus shale. Instead, mixing of formation waters with injected fluids was suggested to be the most likely primary control.

2.3. Differences in experimental parameters

Any experimental study will be designed to test a specific hypothesis or recreate certain set of in-operando conditions, and so use a specific, tailored set of parameters. Fluid composition, length of experiment, solid:fluid ratio and the pressure and temperature conditions therefore vary widely among the reviewed studies. Although some general trends on the possible rock-fluid interactions during hydraulic fracturing emerge from the laboratory studies, the differences in the key experimental parameters - especially if their exact control on the observed interactions is not always known – hinders meaningful cross-study comparisons as well as the extrapolation of the results to field conditions. Table 2.1 summarises the differences in the experimental framework of all the studies discussed in section 2.2, with key parameters discussed in more detail below:

Pressure and temperature – Temperatures and pressures used in the experiments vary from atmospheric and ambient to reservoir-representative (up to 130°C and 275 bar). Frequently, T and P represented downhole conditions for a given well, often from Marcellus Shale. Different temperature conditions were commonly explored, with pressures often remaining circum-atmospheric,

whereas elevated pressures were only ever applied simultaneously with elevated temperatures. At atmospheric pressures, an increase in temperature from 22 to 80°C increased pyrite oxidation rates, mobilising more sulphate into the solution, but did not affect the release of most of the other elements (Wang et al., 2016). However, higher pressures could increase element mobilisation rates (Wilke et al., 2015) and promote greater secondary mineral precipitation (Pearce et al., 2018). Furthermore, widening of pre-existing fractures and their further propagation along the bedding plane was recorded after contact with synthetic fracturing fluids, possibly owing to in-situ pressure and temperature in the autoclave (Dieterich et al., 2016). This could potentially enable greater exposure of shale surface area to the fluids and consequently allow for more rock-fluid interactions and increased element mobilisation. Conversely, another study concluded that elevated pressures and temperatures did not impact metal dissolution from their Marcellus sample, as the metal concentrations released into solution in the experiments under atmospheric and HPHT conditions were comparable (Tasker et al., 2016).

Fluid composition - Fluid composition varied from just ultrapure water to water with common fracturing additives. Two studies examined the impact of certain additives (acids and oxidants) on the release of metals from shales, showing that they have a strong influence on mineral dissolution and oxidation, and consequently element mobilisation (Wang et al., 2015; Wang et al., 2016). Other studies designed their simulated fracturing fluid to mimic the actual fluids used in shale gas operations, based on information provided by FracFocus (a US-centric hydraulic fracturing chemical disclosure registry) or previously published fracturing fluid analyses (Dieterich et al., 2016; Harrison et al., 2018; Jew et al., 2017; Marcon et al., 2017; Tasker et al., 2016; Paukert Vankeuren et al., 2017). Tasker et al. (2016) developed two fluids, one with high and one with low organic content, which comprised water, pH adjustors, citric acid, ammonium

persulfate and seven other additives, including corrosion inhibitors and clay stabilisers. Metal dissolution during shale-fluid interactions appeared not to be particularly influenced by the organic content of the fluids (Tasker et al., 2016).

All of the studies that used water-based fluids with common additives mixed the chemicals into one solution before exposing shale samples to it. However, in an actual hydraulic fracturing operation, the chemicals are injected individually at different times, following a specific order (Harrison et al., 2018; Jew et al., 2017). Furthermore, most of the experiments utilised low salinity fluids. Hydraulic fracturing fluids are typically made up with fresh water and, where possible, with a recycled (treated) flowback and produced water from previous shale gas operations or a mix of both (e.g. Capo et al., 2014; Hayes, 2009). Where recycled wastewater is used, the TDS levels of the injected fluids are expected to be elevated (Jew et al., 2017; Rowan et al., 2015). The commonly applied upper limit of TDS concentrations in fracturing fluids is ~ 25 000 mg/l (Lester et al., 2015); however, fluids with values over 50 000 mg/l have also been successfully used (Rowan et al., 2015; US EPA, 2011). One study designed a high TDS fluid representing synthetic reused produced water for the core-flooding experiments (Paukert Vankeurren et al., 2017), whereas another used a mixture of ultra-pure water and different salts yielding a total TDS of ~26,000 mg/l that replicated TDS levels observed in a recycled fracturing fluid from a Marcellus shale gas well (Dieterich et al., 2016). Nevertheless, the impact of high salinity fluids on the possible shale-hydraulic fracturing fluid reactions has not yet been investigated.

Experiment timescale - The length of the experiments varied depending on the study's objectives but were not always justified in the reported experimental method (Wilke et al., 2015; Pearce et al., 2018). Three studies aimed to investigate the initial effects of fracturing fluids on the Marcellus Shale during the shut-in period, designing their experiments to last between six days and two weeks

(Dieterich et al., 2016; Macron et al., 2017; Paukert Vankeuren et al., 2017). The initial shut-in period is when most the rock-fluid interactions and shale alterations are thought to occur (Jew et al., 2017; Macron et al., 2017). Both Harrison et al. (2017) and Jew et al. (2017) focus on different data from the same set of experiments, which lasted three weeks, 3- and 6-months. Jew et al. (2017) aimed to investigate the chemical reactions and shale alteration that occur in the first ten days following the fluid injection, whereas Harrison et al. (2018) intended to look at both the interactions during fluid injection and those that may occur between the shale and unrecovered fracturing fluid.

A few studies used preliminary experiments to guide their choice of appropriate reaction time. Tasker et al. (2016) chose 36 h reaction time, based on the conductivity of distilled water reaching a constant value following its interaction with powdered Marcellus Shale, whereas two studies on Eagle Ford and Bakken shales used 96 and/or 120 h as this timeframe would allow for most elements to achieve stable concentrations in the solution (Wang et al., 2015; Wang et al., 2016).

Solid:fluid ratio - All of the studies, except for Paukert Vankeuren et al. (2017), used very small solid:fluid ratios, ranging from 1:12.5 up to 1:1000, with no justification for their choice of the parameter value. The estimated solid:fluid ratio during hydraulic fracturing is about five orders of magnitude higher (100:1) (Renock et al., 2016). Therefore, laboratory experiments may be potentially observing more dilute solutions than what could occur during actual hydraulic fracturing operations, as there is less rock exposed to the fluids (Harrison et al., 2017; Paukert Vankeuren et al., 2017). Furthermore, the ratio could also affect calcite dissolution, where lower ratios would be expected to facilitate a greater dissolution (Paukert Vankeuren, 2017).

Two studies investigated the effect of solid:fluid ratio on element mobilisation

using 1:100, 1:500 or 1:1000 ratios. The impact of varying ratios varied widely among the different elements, with some increasing in concentrations with higher ratios (U, Ba, S²⁻), but overall other parameters – such as solution pH and redox conditions – had a stronger influence on element mobilisation (Wang et al., 2015; Wang et al., 2016).

It is also worth noting that some studies used powdered samples, whereas others exposed shale chips or cubes to leaching solutions, which results in different surface areas. Using powdered samples during laboratory experiments increases available surface area and hence produces faster reaction rates. Powdering samples could also eliminate any inherent heterogeneities that may be present along a fracture surface or within a rock chip. This allows the leaching agent a concurrent contact with all minerals present within a shale sample, and consequently, is likely to result in a more significant element mobilisation within a given time compared to realistic field conditions. Thus, the results from the batch leaching experiments on powder samples should be treated as upper bound estimates of geogenic element release.

2.4. Summary and further work

Flowback and produced water contain progressively higher TDS levels with time, potentially including heavy metals and other PTEs, which can be sourced from the formation waters trapped within the shale or arise from fluid-rock interactions induced by the injection of fracturing fluids. However, the exact extent to which the rock-fluid interactions during hydraulic fracturing contribute to the observed temporal changes in the wastewater geochemistry or impact the shale formation properties is not yet fully understood (Harrison et al., 2017). In recent years, several laboratory studies have tried to fill in this gap, reporting evidence of reactions such as pyrite oxidation and

calcite dissolution (e.g. Harrison et al., 2017; Pearce et al., 2018; Wilke et al., 2015). These reactions resulted in the mobilisation of PTEs into the solution, which could be then subsequently sequestered through precipitation of secondary minerals due to changes in and pH and redox conditions at later stages of the experiments (e.g. Jew et al., 2018; Pearce et al., 2018; Wilke et al., 2015).

Even though some common trends emerge from the laboratory studies summarised in sections 2.2 and 2.3, the differences in the experimental parameters impede cross-study comparison or extrapolation of the results to other shale samples or field setting, particularly if their exact influence on the observed interactions is not fully understood.

The majority of studies discussed in this chapter did not aim to fully replicate in-situ conditions during hydraulic fracturing. Limited attention has been paid to how different parameters, beyond broad differences in the mineralogies, influence the shale-fluid interactions, especially at reservoir-representative conditions. Additionally, the suite of shale samples used in the studies is often limited to a few American shales, predominantly Marcellus Shale. Furthermore, synthetic fracturing fluids used in the experiments have so far been designed to mimic a recipe for fluids used in the field at a well not always from the same shale gas play as the samples used in the experiment. Therefore, it would be desirable to systematically examine how different parameters (e.g. temperature, pressure, solid:fluid ratio) during batch experiments influence the observed rock-fluid interactions and investigate the role different additives may have on element mobilisation from a range of shale samples.

Determining how rock-fluid interactions impact the evolution of shale gas wastewater chemistry and assessing the potential for geogenic contaminant mobilisation is important for developing effective strategies for managing flowback and produced waters and the assessment of potential environmental impacts that may arise from their mismanagement.

2.4.1. Scope of this study

This study aims to systematically investigate the potential for inorganic geogenic contaminant mobilisation from a range of shale samples from around the world, and determine the main controls on their mobilisation under hydraulic fracturing conditions. The experiments are designed as leaching tests attempting to simulate upper bound estimates of geogenic element release under reservoir representative temperature and pressure conditions, generating data for a reaction-series of up to 360h. Therefore, the experiments will use powdered shale samples to document what reactions can occur if all of the shale is available to react with the injected fluids, hence serving as a worst-case assessment for the contaminant release. That is, if the contaminants are not detected under the purposefully harsh conditions in the laboratory experiments, then they are unlikely to cause concern in the field.

The leaching agents used in this study will primarily include representative synthetic groundwater and synthetic hydraulic fracturing fluid; additionally, several samples will be short-term leached with dilute hydrochloric acid to investigate the effects of acid pre-flush.

The key research questions the laboratory work aims to answer are:

Q1. What are the trace element concentrations of the selected gas shales, and how much do they vary? Which metals and metalloids may be amenable to mobilisation under environmental conditions?

Q2. Do hydraulic fracturing fluids mobilise elements from the shale? Do the considered chemical additives affect element mobilisation? Are the trace element mobilisation patterns consistent among the different shales? If not, why?

Q3. How do experimental conditions (T, P, pH and solid:fluid ratio) affect element mobilisation?

CHAPTER 3

SAMPLE CHARACTERISATION

3.1. Introduction

Shales are traditionally defined as fissile or laminated fine-grained sedimentary rocks formed through the consolidation of mud, silt or clay. They are typically composed of at least 50% silt-size or finer particles, dominated by clay minerals, followed by fine-sized quartz and often feldspars. Other minerals, in various subordinate amounts, can also be present, including carbonates and sulphides (usually pyrite), as well as organic matter (Boggs, 2006; Leventhal, 1993).

Shales that are particularly enriched in organic matter are commonly referred to as black shales. They commonly contain 2-10 wt% of total organic carbon (TOC), which gives them their characteristic dark colour. In many instances, black shales also contain minor amounts of authigenic carbonate minerals (Tourtelot, 1979). Black shales are especially economically important as they are the best and main source rocks for conventional petroleum systems; it has been suggested that black shales generated about 90% of world's recoverable oil and gas reserves (Schieber 1978 and references therein). Apart from the elevated TOC content, black shales are often enriched in trace elements, such as As, Cu, Mo, V and Zn, relative to average shales or even average crustal abundances (Armstrong et al., 2019; Leventhal, 1993; Tourtelot, 1979).

Due to their generally high TOC content, gas shales tend to be broadly categorised as black shales. Although they often contain black shale facies, gas shale formations are typically heterogeneous, with multiple lithologies and lithofacies often occurring

in cyclical sequences (e.g. Dawson, 2000; Harris et al., 2011; Hemmesch et al., 2014). For example, Bowland Shale, the principal UK shale gas prospect, comprises fine-grained turbidites, detrital siliciclastics and hemipelagic clay-rich facies (Clarke et al., 2014), whereas the upper member of the Eagle Ford Formation, one of the most productive shale gas plays in the US, is dominated by thin, high-frequency cycles of shales, limestones and siltstones (Dawson, 2000). Such lithological heterogeneity, and associated mineralogical variations, will have implications for mechanical properties of the shale as well as its chemical composition, particularly trace element distribution (Harris et al., 2011; Harris et al., 2013; Sano et al., 2013; Totten and Hanan, 2007).

One study collated both published mineralogical and trace element data from nine producing US gas shales, highlighting a wide intergroup and intragroup variance in mineralogy, and wide ranges of trace metal concentrations among and within the examined shales (Chermak and Schreiber, 2014). At the time of publication, Chermak and Schreiber (2014) also noted a lack of (published) studies on how potentially toxic elements, especially those regulated in soils, sediment and water, might be mobilised from gas shales during hydraulic fracturing.

As discussed in Chapter 2, several experimental studies have started to fill in that knowledge gap. However, their focus has been mostly regionally narrow: with a few exceptions, the samples used in the experiments were US gas shales, specifically Marcellus Shale. Only two of the studies (performed on the same set of samples) referenced in Chapter 2 have examined how hydraulic fluids interact with various shales of different mineralogies (Harrison et al., 2017; Jew et al., 2017). Furthermore, the differences in the experimental parameters, such as leaching time and fluid composition, impede cross-study comparisons and extrapolation of the results to other gas shales.

Therefore, to systematically investigate the potential for trace element release from gas shales, and determine the main controls on their mobilisation under hydraulic fracturing conditions, samples from 15 shale formations from around the world have

been obtained for this study.

This chapter will first characterise these samples, highlighting any differences or similarities in their mineral and elemental content, before discussing any environmental and experimental implications that may arise from their potentially toxic element content.

3.2. Shale samples

The sample-set comprised twenty-six shale samples from 15 shale formations around the world. The formations include two producing US gas shales (Eagle Ford and Haynesville), and nine prospective shale gas targets: two from Europe (Posidonia and Bowland shales) and seven from Australian (Roseneath, Epsilon, Patchawarra and Murteree shales from Cooper Basin; Termite Range and Lawn Hill shales from Mt Isa Superbasin; and Velkerri Formation from Beetaloo sub-basin). Additionally, samples from two other mudrocks, Kimmeridge Clay and Callovo-Oxfordian Claystone were included. Callovo-Oxfordian Claystone (COx) is a possible host rock for radioactive waste disposal in France (Seeman et al., 2017). Kimmeridge Clay is a major petroleum source rock for many conventional hydrocarbon accumulations in the North Sea (Myers and Wignall, 1987)

Eagle Ford, Callovo-Oxfordian Claystone and Haynesville samples were provided courtesy of Prof. Andreas Busch from Herriot-Watt University. Kimmeridge Clay samples, provided by Dr Katriona Edelmann from the University of Edinburgh, came from a 0.4-m long core section from the East Brae Field. Bowland Shale samples were obtained from BGS National Geological Repository and each represents a different well and basin. Australian samples were provided by CSIRO and mostly came powdered. The Cooper Basin samples were obtained from two wells, both passing through the

Roseneath, Epsilon and Murteree formations. Beetaloo Sub-basin samples represent two wells which intersect Amungee member of the Velkerri Formation.

Figure 3.1. and 3.2. show locations of the wells from which the Bowland Shale and Australian shale samples were taken, respectively. These samples represent prospective shale gas targets for the UK and Australia, with only a few exploratory wells drilled and hydraulically fractured (e.g. Preese Hall-1 for Bowland Shale; EA, 2011). Including these shale samples, representing different geographical locations, in a laboratory study of element mobilisation due to exposure to hydraulic fracturing fluids will therefore provide further insights into their potential flowback and produced water composition and its spatial variability. These insights could then be used to guide future field-based monitoring or assess appropriate wastewater management and treatment options ahead of any potential larger-scale field operations.

Further sample details, including the sample IDs that will be used henceforth throughout the study are summarised in Table 3.1.

3.2.1. Mineralogy

The bulk (whole-rock) and clay-fraction mineralogy for Kimmeridge Clay and Bowland Shale samples was determined by an external laboratory (by X-ray Mineral Services Ltd.), prior to any leaching experiments. Mineralogy of Eagle Ford, Haynesville, Posidonia and CO_x samples used in this study have already been established and published by Seemann et al. (2017). Information on mineralogy for most Australian samples was obtained from previously published or confidential sources (Table 3.2) that analysed the core intervals from which the samples studied here were taken. If no data were provided specifically for the sample depths, data from the closest depth is presented here as an approximation, taking into account any vertical heterogeneity (for example, Figure 3.5 and 3.7). Lastly, the Lawn Hill sample from Mt Isa Superbasin has



Figure 3.1 Location of the three Bowland Shale wells - Blacon East 1, Long Eaton 1 and Kirby Misperton 1, from which the core samples were obtained. Background GIS map taken from arcgis.com.

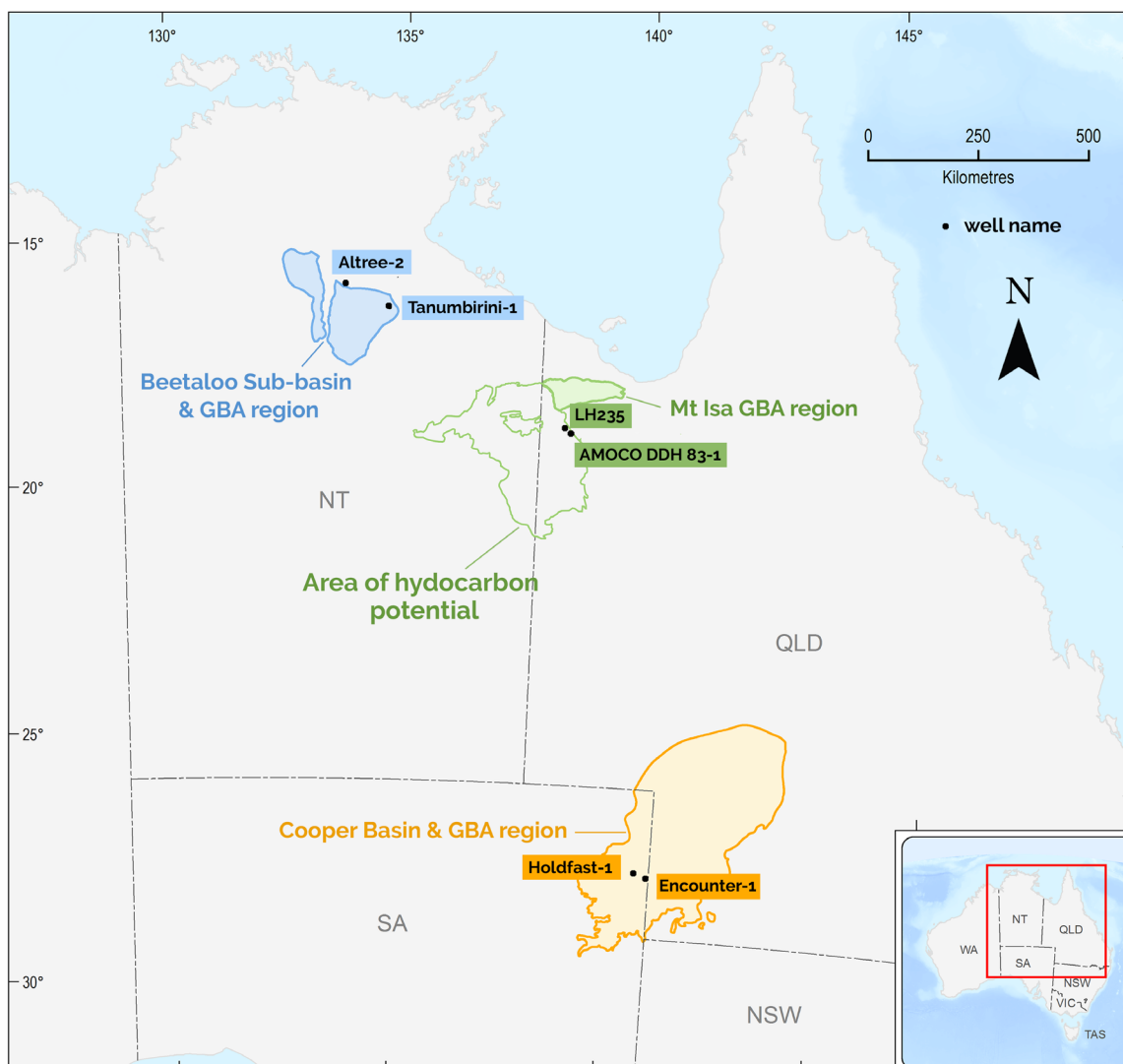


Figure 3.2 Location of the three Australian shale gas basins which were chosen by the Australian Government as the main prospects for shale gas exploitation. The basins were studied in a government-funded Geological and Bioregional Assessment Program (GBA), which examined potential impacts of shale and tight gas development on water and the environment. Listed on the map are well locations from which the core samples used in this study were obtained. Background map image and basin and GBA shapefiles were taken from csiro.au.

Table 3.1 Background information for the shale samples used in this study.

Sample ID	Shale Formation	Geography	Basin	Depositional environment	Use	Sample origin and depth
KC1 to KC5	Kimmeridge Clay	UK sector of Northern North Sea	East Brae sub-basin	Marine	Petroleum source rock for conventional hydrocarbon systems	Core, East Brae field, well 16/3a-E5, 5296 m depth
Bowland (KM)	Bowland shale (Upper Bowland-Hodder member)	North Yorkshire, England	Cleveland Basin	Marine	Prospective shale gas play	Core, Kirby Misperton 1 well, 2321m depth
Bowland (BE)		Cheshire, England	Blacon Basin			Core, Blacon East 1 well, 2142 m depth
Bowland (LE)		East Midlands, England	Widmerpool Trough			Core, Long Eaton 1 well, 1798 m depth
COx	Callovo-Oxfordian Claystone	Bure, France	Paris Basin	Marine	Prospective host for radioactive waste disposal	Core, ANDRA Meuse-Haute Marne site, depth unknown
Posidonia	Posidonia	Harderode, Germany	Lower Saxony Basin	Shallow marine	Prospective shale gas play	Core, depth unknown
Eagle Ford	Eagle Ford	Texas, USA	East Texas Basin	Marine	Producing gas shale	Outcrop
Haynesville	Haynesville			Deep marine		Core, depth unknown
Amungee-1	Velkerri Formation, Amungee member	Northern Territory, Australia	Beetaloo sub-basin	Shallow to distal marine shelf	Prospective shale gas play	Core, Tanumbirini 1 well, 3235 m depth
Amungee-2						Core, Tanumbirini 1 well, 3272.8 m depth
Amungee-3						Core, Altree-2 well, 709 m depth
Wyworrie						Core, Altree-2 well, 671 m depth
Termite Range	Termite Range	Queensland, Australia	Mt Isa Superbasin	Marine shelf to deep marine	Prospective shale gas play	Core, AMOCO DDH 83-1 well, from 33.7 depth
Lawn Hill	Lawn Hill			Shoreface to deep marine		Core, LH235 well, from 44.7 m depth
Roseneath-1	Roseneath	Queensland, Australia	Cooper Basin	Lacustrine, fluviodeltaic	Prospective shale gas play	Core, Holdfast-1 well, 3110.5 m depth
Roseneath-2						Core, Encounter-1 well, 3285 m depth
Epsilon-1	Epsilon			Fluviodeltaic, lacustrine with peat swamp		Core, Holdfast-1 well, 3171.2 m depth
Epsilon-2						Core, Holdfast-1 well, 3336.75 m depth
Epsilon-3				Core, Encounter-1 well, 3396 m depth		
Murteree-1	Murteree			Lacustrine		Core, Holdfast-1 well, 3384.5 m depth
Murteree-2						Core, Encounter-1 well, 3519 m depth
Patchawarra	Patchawarra			Fluviolacustrine, floodplain		Core Holdfast-1 well, 3430.85 m depth

Sources for the depositional environment : Seemann et al., 2017; Gross et al., 2015 ; Hall et al., 2020; Orr et al., 2020; Owens et al., 2020;

Table 3.2 Summary of XRD data sources for Australian samples.

Basin	Sample ID	Well	Data source
Cooper	Roseneath-1 Epsilon-1 Epsilon-2 Murteree-1 Patchawarra	Holdfast-1	Hill and Mauger, 2016
	Roseneath-2 Epsilon-3 Murteree-2	Encounter-1	Dewhurst et al. 2015
Beetaloo	Amungee-1 Amungee-2	Tanumbirini 1	Revie et al., 2021
	Amungee-3 Wyworrie	Altree-2	
Mt Isa	Termite Range	AMOCO DDH 83-1	Jarrett et al., 2019

been analysed externally by CSIRO using quantitative X-ray diffraction.

The shale samples have variable mineral composition, with silica vs carbonate abundance being the most visible trend in the non-Australian samples (Figure 3.3). All Kimmeridge Clay samples are consistently silica-dominated, with ubiquitous pyrite (~5-12 wt%), but contain no carbonates. On the other end of the spectrum are Eagle Ford and Bowland (BE), which are carbonate-rich (predominantly calcite) with a comparably small fraction of quartz (~19 wt%), clay-minerals (6-7 wt%) and accessory quantities of pyrite (~1 wt%). The other two Bowland Shale samples, Bowland(KM) and Bowland(LE), have a more quartz and clay-dominated composition, with little carbonates (<10 wt%) and variable quantities of pyrite (1 and 9 wt%, respectively).

Haynesville and COx are dominated by clays (>50 wt%), whereas Posidonia is predominantly composed of clays and carbonates, with the highest amount of pyrite (6 wt%) among the calcareous samples (Fig 3.3.). Gypsum is only present in the Eagle Ford and in trace quantity in the Haynesville shale. Seemann et al. (2017) note that gypsum

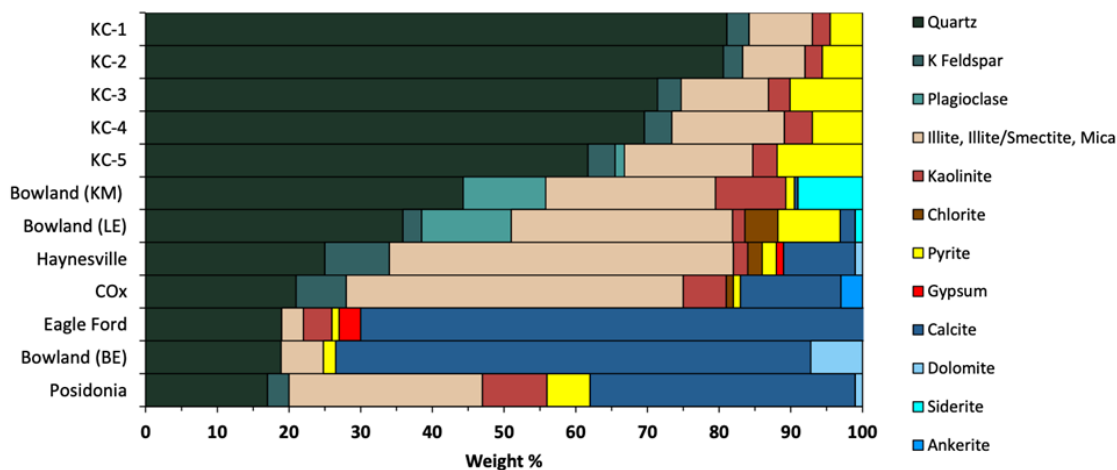


Figure 3.3 Whole-rock mineralogy of the non-Australian samples.

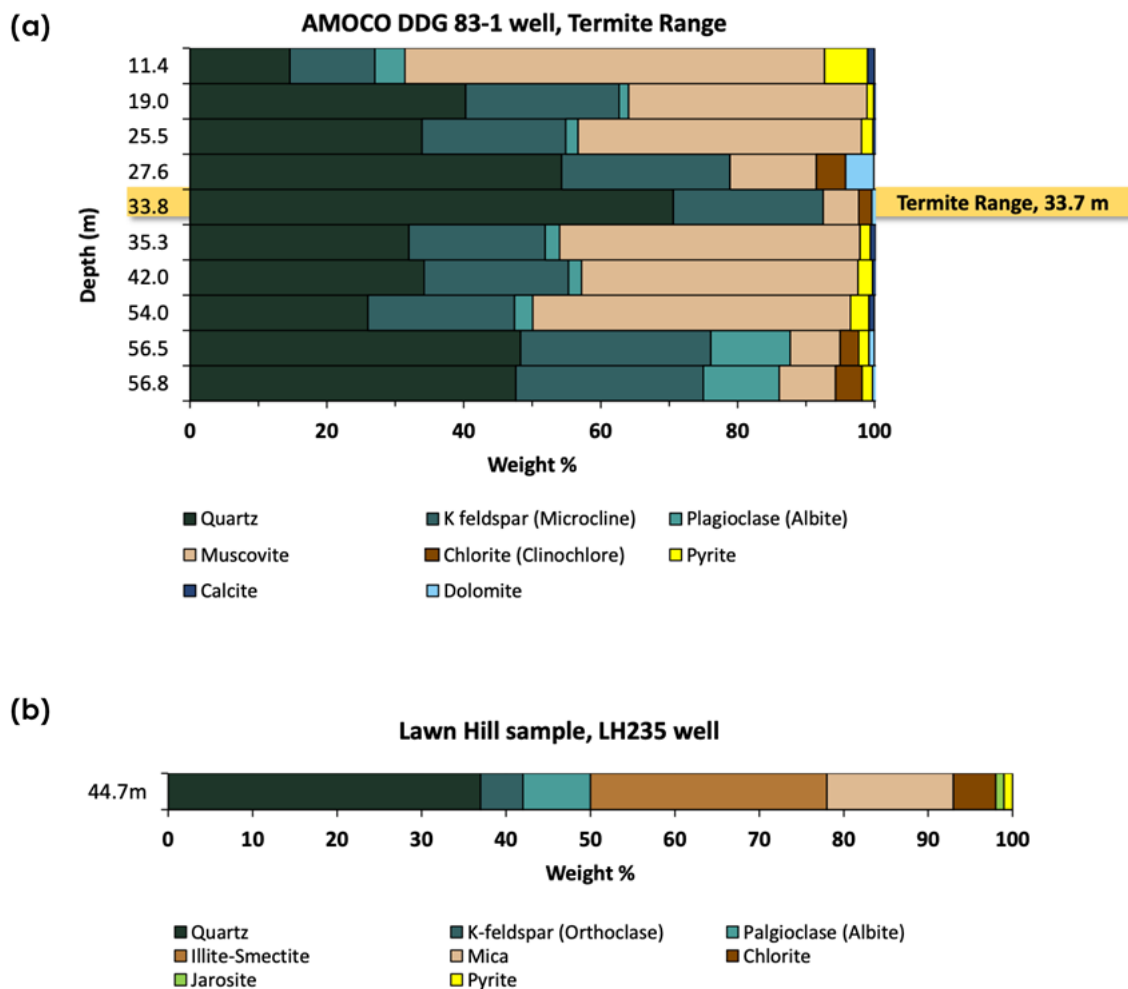


Figure 3.4 Whole-rock mineralogy of Mt Isa Superbasin samples: (a) mineralogy of a core section from which Termite Range sample was taken, where the sample depth is indicated by the yellow strip; (b) XRD results for the Lawn Hill sample

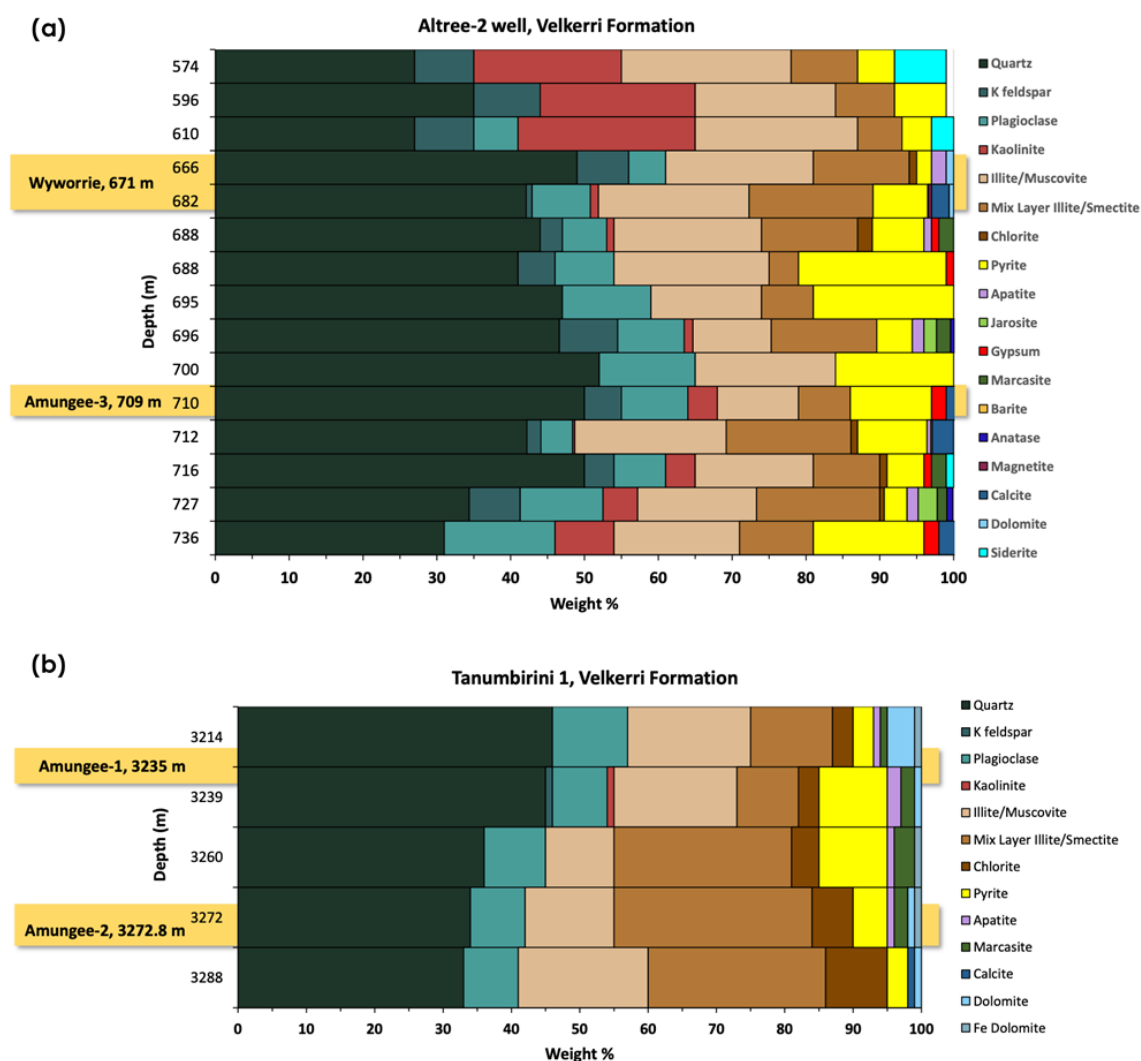


Figure 3.5 Approximate mineralogy of the Beetaloo sub-basin samples from the two wells: (a) Atree-2, and (b) Tanumbirini 1. The sample depths are indicated by the yellow strips

may be a product of pyrite oxidation during sample preparation or core storage.

The samples from Australian shale gas prospects are distinctly carbonate-poor. The Termite Range sample from Mt Isa Superbasin is predominantly composed of quartz and K-feldspar, with small amounts of muscovite and chlorite (Figure 3.4a). In the Lawn Hill sample, quartz is codominant with clay minerals (predominantly illite-smectite), followed by mica, minor feldspar component (orthoclase and albite), and trace amounts (1 wt%) of pyrite and jarosite (Fig 3.4b). Mineralogy of the Amungee and

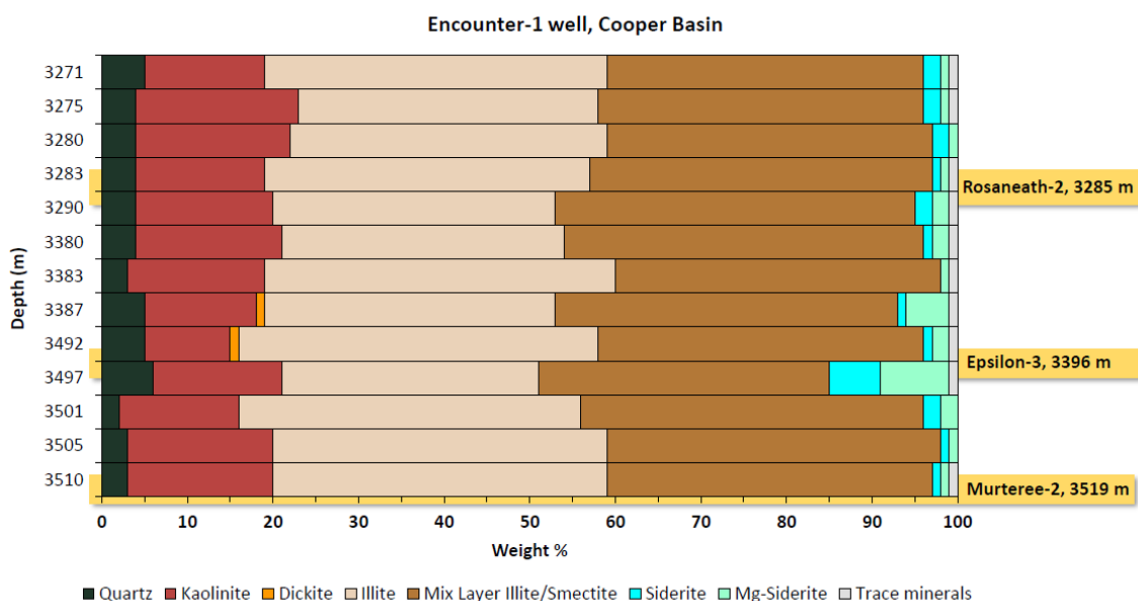


Figure 3.6 Approximate mineralogy of the Cooper Basin samples from the Encounter-1 well. The sample depths are indicated by the yellow strips.

Wyworrie members of the Velkerri Formation in Beetaloo sub-basin are dominated by quartz and clay minerals, followed by feldspars and pyrite (Fig 3.5). All of the Amungee and Wyworrie samples likely contain a considerable amount of pyrite, based on their total recoverable element values for sulphur (see 3.2.2.1). Notably, they are also the only Australian shale samples to contain sulphide minerals beyond 1 wt%.

For Cooper Basin shales, mineralogy of the samples from the same formations varies between the two wells. The three shale formations present in the Encounter-1 well have comparable mineralogy: Roseneath-2, Epsilon-3 and Murteree-2 samples were all expected to be extremely clay-rich (likely >80% clay content), with subsidiary amounts of quartz and siderite (Figure 3.6). Samples from the Holdfast-1 well are more varied, but equally dominated by clay minerals and quartz. The Patchawarra, Epsilon-1 and Epsilon-2 samples are likely to have a high quartz concentration, with subordinate amounts of clays (Figure 3.7c and 3.8). Roseneath-1 and Murteree-1 are more clay-rich,

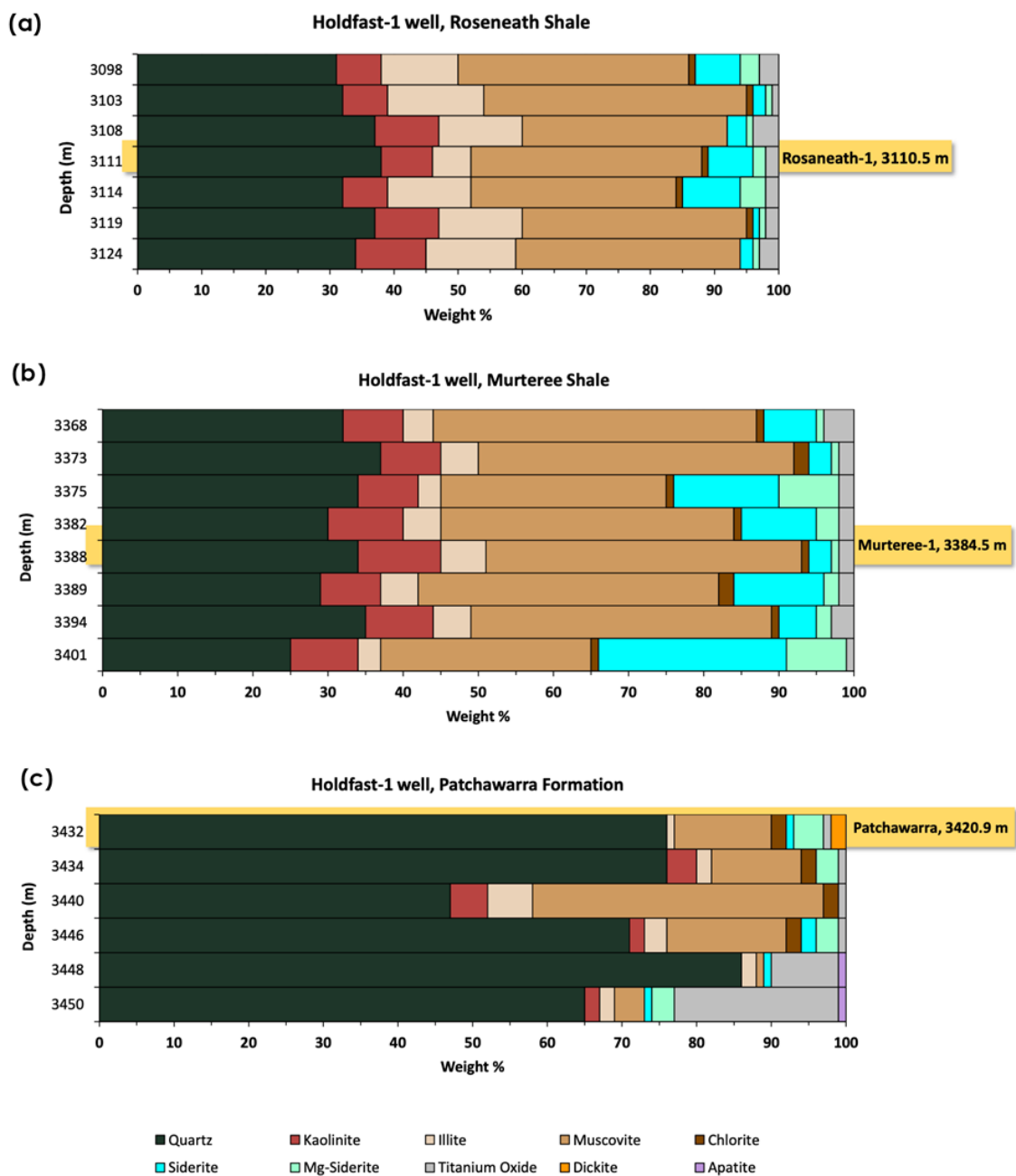


Figure 3.7 Approximate mineralogy for (a) Roseneath-1, (b) Murteree-1, and (c) Patchawarra shales from the Holdfast-1 well, Cooper Basin. The sample depths are indicated by the yellow strips

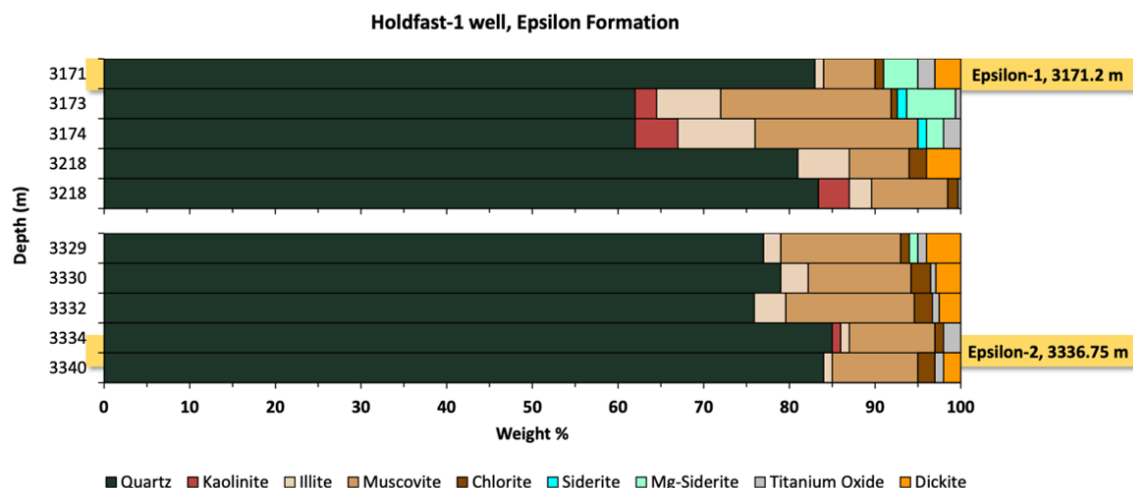


Figure 3.8 Approximate mineralogy of the Cooper Basin samples from the Encounter-1 well. The sample depths are indicated by the yellow strips.

with approximately 30-40 wt% quartz content (Figure 3.7a and b). Most samples from the Cooper Basin are likely to contain small to moderate amounts of siderite or Mg-siderite (approx. 3-10 wt%).

3.2.2. Elemental content and its environmental significance

All samples were analysed for their total recoverable concentrations, as well as the acid extractable concentrations, for approximately 55 elements (Appendix A):

Total recoverable elements (TRE) were obtained using microwave-assisted reverse aqua regia digestion (based on USEPA method 3051A). Acid washed plastic digest tubes containing 0.5 g of shale sample, which was powdered and sieved to <125 μm , mixed with 9 mL of concentrated HNO_3 , and 3 mL of concentrated HCl were heated in a commercial microwave (MARS Xpress 6, CEM) to 175°C for 16.5 minutes. Sample digests were then syringe-filtered through 0.45 μm SFCA filter cartridges (Sartorius Minisart) and diluted with ultrapure deionised water (18 $\text{M}\Omega\cdot\text{cm}$ conductivity, Millipore, Australia),

then analysed by a combination of ICP-MS and ICP-AES. Samples for ICP-MS and ICP-AES were diluted at least 10 fold into diluent containing 2.25% v/v HNO₃ and 0.75% HCl prior to analysis. Calibration standards were prepared in high purity water and the same acid matrix from certified stock solutions (High Purity Standards and Accutrace). The extractions were performed in duplicate, and the average results are reported here on a dry weight basis. Spike recoveries were carried out on selected samples. Certified reference materials were included in each digestion batch, and spike recoveries were carried out on selected samples (see Chapter 4.3.2.2 for more details on reference materials and spike recoveries).

Acid extractable trace element (AEE) concentrations were determined on 0.5 g of shale samples, which were powdered and sieved to <125 µm, weighed into acid-washed 70 ml plastic vials. After adding 30 mL of 1 M HCl, the vials were shaken and left to sit for 1 hour at room temperature, before being syringe-filtered through 0.45 µm SFCA filter cartridges (Sartorius Minisart). Ten-fold dilutions of the acid extracts were then analysed by ICP-MS and ICP-AES. The extractions were performed in duplicate, and the average results are reported here on a dry weight basis. Spike recoveries were carried out on selected samples.

As 1M HCl will not target silicate minerals at all, AEE concentrations indicate the fraction of particulate metals that may be susceptible to mobilisation under environmental conditions and hence yield results that may be more representative of the bioavailable fraction (ANZECC/ARMCANZ, 2000; McCready et al., 2003). Trace elements associated with the silicate minerals are assumed to be biologically inert owing to the insolubility of the host mineral.

Table 3.3 TRE concentrations for the shale samples - major elements ($\mu\text{g/g}$). Values highlighted in green exceed $>10\times$ average upper crustal abundances (Rudnick and Gao, 2003), values in yellow exceed $>10\times$ the average shale values (Turekian and Wedepohl, 196), and in orange both values are exceeded $>10\times$. "-" value not available (above the upper detection limit).

Sample ID	Al	Ca	Fe	K	Mg	Na	P	S
KC-1	4174.2	2643.06	16825	2293	1159.2	615.4	272.0	18919
KC-2	3336.6	2293.15	17434	1981	1016.1	547.8	237.5	19638
KC-3	3053.7	3630.64	20149	1827	1420.1	421.4	317.9	22874
KC-4	5304.4	2926.47	22413	2907	1364.9	715.0	285.8	25363
KC-5	3278.2	2808.49	14762	1875	1170.7	450.5	240.7	16662
COx	3042.8	196016.8	10765	2531	7432.6	479.3	166.1	7198.7
Eagle Ford	1776.3	317337	9520.7	832.9	1518.9	587.0	166.5	15779
Haynesville	13019	61674.8	21331	5463	4854.4	995.3	831.2	12890
Posidonia	3475.6	148943	22340	1885	2149.5	311.7	1290	24921
<i>Bowland Shale</i>								
Bowland (KM)	3784.5	5061.94	29066	2374	4697.1	1256	569.4	1396.2
Bowland (BE)	453.15	348039	2807.9	460.3	6423.9	472.1	56.42	2538.1
Bowland (LE)	10306	11565.2	32286	2461	4333.4	1197	113.1	23825
<i>Beetaloo Sub-basin</i>								
Amungee-1	10500	10800.0	41200	4200	3860.0	950.0	2710	38700
Amungee-2	20600	6070.00	45300	6500	4220.0	1600	1580	33400
Amungee-3	14100	5450.00	41400	5800	3210.0	790.0	1500	34600
Wyworrie	17700	9190.00	35300	7500	4340.0	900.0	3170	31400
<i>Mt Isa Superbasin</i>								
Termite Range	2400.0	2400.00	6600.0	840.0	2000.0	—	140.0	1000.0
Lawn Hill	12000	1600.00	23000	4100	5000.0	—	470.0	11000
<i>Cooper Basin</i>								
Roseneath-1	9542.0	972.682	54890	3624	4679.6	250.1	207.3	348.12
Roseneath-2	11906	2088.01	49915	4777	5243.1	467.1	793.9	334.13
Epsilon-1	3086.6	527.556	56145	909.2	13078	62.6	71.24	78.803
Epsilon-2	10573	234.813	18112	1898	3299.6	150.6	45.68	69.240
Epsilon-3	3971.7	1462.77	60887	2754	8283.0	242.0	204.9	86.573
Murteree-1	21483	1389.26	50948	6314	5286.6	282.5	648.5	323.27
Murteree-2	6833.5	815.210	25667	3499	4394.7	506.9	246.1	182.30
Patchawarra	7805.1	297.829	16162	2119	2944.2	128.4	100.7	114.43
<i>Average shale</i>	80000	22100	47200	26600	15000	9600	700	2400
<i>Upper Crustal Average*</i>	84151	45812	52158	15026	28101	22775	567	621

Table 3.4 TRE concentrations for the shale samples - minor elements ($\mu\text{g/g}$). Values highlighted in green exceed $>10\times$ average upper crustal abundances (Rudnick and Gao, 2003), values in yellow exceed $>10\times$ the average shale values (Turekian and Wedepohl, 196), and in orange both values are exceeded $>10\times$. "-" value not available (above the upper detection limit).

Sample ID	As	B	Ba	Cd	Co	Cr	Cu	Hg	Li	Mn	Mo	Ni	Pb	Sb	Sr	Tl	U	V	Zn
KC-1	36	27	222	4.8	11	8.8	44.0	<0.1	3.1	70.65	50	105	15	6.4	18.5	1.76	7.4	69.9	278
KC-2	37	20	123	3.6	12	7.0	47.4	<0.1	2.8	68.76	53	114	15	7.5	15.6	1.97	5.0	56.7	195
KC-3	44	21	69.2	2.6	11	7.5	37.0	<0.1	2.2	67.98	45	112	13	7.1	16.3	1.83	6.7	62.7	134
KC-4	41	25	109	4.9	13	8.2	44.9	<0.1	3.7	73.72	57	139	18	8.3	20.7	2.09	6.2	76.6	242
KC-5	31	17	85.3	2.4	9.2	5.6	33.3	<0.1	2.3	64.62	39	88.1	14	6.0	15.2	1.50	4.9	55.1	119
COx	7.9	30	17.8	0.3	2.4	13.5	4.04	<0.1	5.1	94.28	1.2	15.6	13	0.1	508	0.10	0.4	11.5	81.7
Eagle Ford	20	11	33.7	3.2	6.7	19.7	45.2	<0.1	2.2	98.10	55	94.2	6.4	3.8	666	4.17	6.9	348	96.8
Haynesville	13	40	710	0.6	11	25.3	25.0	<0.1	24	154.9	18	67.0	19	0.8	254	1.52	1.5	28.3	105
Posidonia	13	31	213	1.3	8.5	13.4	46.9	<0.1	2.8	234.5	24	54.6	14	0.3	541	1.11	1.7	23.8	83.4
<i>Bowland Shale</i>																			
Bowland (KM)	3.4	35	168	0.1	18	11.1	21.9	<0.1	4.5	485.4	0.4	29.0	18	0.1	55.2	0.15	0.5	15.4	87.8
Bowland (BE)	3.1	9.3	2.92	0.1	1.8	4.46	4.79	<0.1	1.4	479.1	0.7	13.6	5.2	0.2	405	0.04	1.3	3.99	<5.48
Bowland (LE)	20	39	79.7	1.5	18	12.7	38.3	0.2	27	198.1	3.8	37.0	23	2.0	102	0.23	0.2	17.1	97.0
<i>Beetaloo Sub-basin</i>																			
Amungee-1	42	43	157	3.6	26	28.2	116	0.7	8.7	102.8	92	318	37	4.5	54.5	8.60	3.0	128	362
Amungee-2	33	57	238	3.6	22	21.3	114	0.5	22	112.1	60	124	39	6.1	47.9	2.90	4.9	81.0	218
Amungee-3	51	48	212	8.8	18	15.4	95.1	0.7	14	81.98	74	163	26	5.1	28.9	8.80	4.3	124	751
Wyworrie	39	53	93.6	13.0	18	25.6	206	0.7	13	68.21	55	233	45	7.6	27.9	9.00	4.0	259	763
<i>Mt Isa Superbasin</i>																			
Termite Range	2.4	1.0	11.3	<0.04	2.4	260	4.61	<0.1	3.3	300.0	0.6	7.76	3.9	0.3	2.34	0.07	0.3	2.80	6.70
Lawn Hill	21	17	28.4	1.1	22	67.7	67.9	<0.1	20	110.0	20	45.5	40	2.1	5.47	0.74	4.6	30.0	150
<i>Cooper Basin</i>																			
Roseneath-1	5.0	2.8	140	0.3	18	60.2	67.5	<0.1	18	1019	0.8	33.6	35	0.6	3.15	0.27	0.51	13.8	110
Roseneath-2	4.8	4.2	250	0.3	17	37.5	47.6	<0.1	18	1158	1.0	45.4	39	0.5	9.13	0.32	2.03	18.4	106
Epsilon-1	8.0	0.6	26.0	0.1	11	264	32.9	<0.1	5.7	1527	0.5	35.0	8.4	0.2	1.10	0.05	0.12	5.61	62.6
Epsilon-2	8.3	1.1	57.8	0.0	4.9	116	16.3	<0.1	20	299.0	0.5	16.9	8.2	0.2	1.50	0.10	0.03	4.25	65.1
Epsilon-3	3.0	1.3	102	0.1	15	96.7	14.0	<0.1	3.2	1036	0.9	25.1	16	0.2	3.89	0.12	0.69	10.4	66.3
Murteree-1	5.4	5.5	264	0.2	18	70.6	54.9	<0.1	33	761.2	1.0	36.2	41	0.8	20.5	0.40	1.44	28.0	122
Murteree-2	2.8	1.9	177	0.2	16	32.7	37.2	<0.1	12	254.8	0.8	28.5	31	0.6	9.93	0.22	0.89	11.6	102
Patchawarra	19	1.2	60.8	0.2	13	116	101	<0.1	12	151.3	0.4	28.3	13	0.4	2.70	0.12	0.29	4.92	97.1
Average shale	13	100	580	0.3	19	90	45	0.4	66	850	2.6	68	20	1.5	300	1.4	4	130	95
Upper Crustal	4.8	17	624	0.1	17	92	28	0.05	21	774	1.1	47	17	0.4	320	0.9	3	97	67

3.2.2.1. Total Recoverable Elements

The total recoverable concentrations (TRE) of the major and trace elements of interest in this study are summarised in Table 3.3 and Table 3.4, respectively.

The TRE concentrations for many elements were quite variable and typically ranged over one to two orders of magnitude across the shales. Comparisons of the elemental data with the average upper crustal abundance (Rudnick and Gao, 2003) and the average shale values (Turekian and Wedepohl, 1961) indicated that approximately half of the samples are consistently enriched in Cd, Mo, Sb and S relative to these benchmarks.

Among the Bowland Shale samples, only the Long Eaton (Bowland-LE) sample contains higher amounts of Cd and S than the average shale concentrations or upper crustal element abundances. The Blacon East (Bowland-BE) notably contains the highest amount of Ca found among the samples used in this study, followed by the Eagle Ford, which corresponds to their highest carbonate mineral content among the sample suite.

By comparison, Cooper Basin samples contain considerably more Fe, and often Mn than other shales. Beetaloo Basin shales are the only samples with detectable Hg levels, which exceed the average upper crustal abundance 10-15 times, and, compared to other shales, have higher levels of Ni and Zn.

3.2.2.2. Acid Extractable Elements

The acid extractable element (AEE) concentrations of commonly occurring major and trace elements are summarised in Tables 3.5 and 3.6.

A useful indication of the extent to which trace elements could be easily mobilized under environmental as well as experimental conditions is the ratio of AEE to TRE, expressed as a percentage (Table 3.7). This ratio shows that almost all available Ca,

Table 3.5 AEE concentrations for the shale samples - major elements ($\mu\text{g/g}$).

Sample ID	Al	Ca	Fe	K	Mg	Na	P	S
KC-1	504.8	2563.05	878.82	445.9	810.1	466.2	247.9	1010
KC-2	456.0	2350.38	699.32	455.1	763.2	580.0	231.4	853.1
KC-3	318.4	3376.94	1008.1	325.6	1110	364.9	275.5	1107
KC-4	477.2	2471.09	836.61	466.5	813.9	629.9	225.4	1216
KC-5	349.8	2725.47	872.13	358.6	892.6	408.2	214.3	1075
COx	369.0	174994	3683.6	686.1	6191	447.5	154.0	2075
Eagle Ford	150.9	313038	752.47	173.1	1403	603.3	127.4	8515
Haynesville	386.7	71735.8	2217.7	665.7	1399	876.6	824.7	1178
Posidonia	275.4	184186	621.97	359.5	1975	318.7	1369	723.4
<i>Bowland Shale</i>								
Bowland-KM	558.2	4639.57	13716	713.9	2408	1406	573.9	56.22
Bowland-BE	73.75	439413	1354.3	153.4	6647	499.1	67.92	957.8
Bowland-LE	514.2	12805.2	1140.2	558.9	570.2	1174	122.8	1785
<i>Beetaloo Sub-basin</i>								
Amungee-1	1720	11000.0	3560.0	1300	1810	740.0	2860	2680
Amungee-2	1820	5840.00	2450.0	1600	925.4	1300	1570	1460
Amungee-3	2210	5240.00	2450.0	1200	1250	99.43	1340	4340
Wyworrie	2160	8880.00	2460.0	1500	1530	330.0	3070	3060
<i>Mt Isa Superbasin</i>								
Termite Range	320.0	2400.00	2400.0	350.0	1000	20.00	130.0	220.0
Lawn Hill	1400	1700.00	1800.0	680.0	1200	20.00	440.0	2500
<i>Cooper Basin</i>								
Roseneath-1	834.6	576.120	11492	691.3	859.3	187.8	117.2	38.49
Roseneath-2	1138	1893.85	9753.1	816.9	1002	364.8	750.1	94.33
Epsilon-1	351.7	345.352	18037	312.9	3790	70.31	68.01	23.25
Epsilon-2	614.1	218.585	2478.1	364.0	343.4	133.2	47.57	27.03
Epsilon-3	962.8	1023.88	29844	699.5	3911	217.1	224.3	27.71
Murteree-1	1666	1220.07	11291	976.0	843.3	175.6	479.0	32.23
Murteree-2	896.7	626.597	6414.0	656.3	1145	418.9	193.1	40.79
Patchawarra	718.3	292.888	3088.4	492.2	402.5	116.6	76.82	21.27

Table 3.6 AEE concentrations for the shale samples - minor elements ($\mu\text{g/g}$).

Sample ID	As	B	Ba	Cd	Co	Cr	Cu	Hg	Li	Mn	Mo	Ni	Pb	Sb	Sr	Tl	U	V	Zn
KC-1	10	<15	133	0.38	4.30	1.52	9.2	0.029	0.7	30.0	11	45	4.8	2.1	13.4	0.09	4.55	11	24.5
KC-2	10	<15	72.5	0.34	3.70	2.36	7.9	<0.01	0.8	28.7	9.2	41	4.2	2.1	12.7	0.08	3.68	8.6	16.6
KC-3	11	<15	42.1	0.25	4.10	2.05	7.7	<0.01	0.6	34.9	9.7	51	3.6	2.1	11.7	0.10	4.96	17	14.2
KC-4	12	<15	59.8	0.40	4.40	1.24	8.6	<0.01	0.8	25.9	11	57	5.1	2.7	13.2	0.12	4.15	9.7	17.5
KC-5	11	<15	54.9	0.31	4.20	1.22	8.1	<0.01	0.6	30.9	10	47	4.4	2.0	11.3	0.10	3.78	12	14.0
COx	3.3	<15	12.9	0.03	1.00	1.71	1.4	0.066	1.1	82.7	0.4	6.4	10	<0.1	479	0.04	0.29	2.4	11.8
Eagle Ford	3.4	<15	22.9	1.98	1.20	7.73	11	<0.01	0.4	57.7	6.4	26	2.0	0.8	644	0.84	6.38	83	27.2
Haynesville	2.4	<15	355	0.09	2.20	1.17	3.6	<0.01	2.0	84.2	8.0	14	4.6	0.3	253	0.11	1.31	1.9	19.6
Posidonia	4.2	<15	161	0.06	3.50	5.51	1.6	<0.01	0.3	178	6.6	19	2.0	0.1	599	0.08	1.61	5.7	6.40
<i>Bowland Shale</i>																			
Bowland-KM	0.2	<15	132	<0.05	0.99	1.00	1.6	<0.01	0.3	247	<0.04	2.6	3.5	<0.1	48.8	<0.01	0.04	1.6	4.60
Bowland-BE	0.2	<15	2.24	<0.05	1.05	1.10	<0.02	<0.01	0.3	482	<0.04	<0.2	0.7	<0.1	434	<0.01	0.36	1.1	0.50
Bowland-LE	1.1	<15	43.7	0.08	1.70	<0.1	2.5	<0.01	0.3	35.0	0.2	2.5	1.9	0.1	91.3	<0.01	0.02	0.2	3.70
<i>Beetaloo Sub-basin</i>																			
Amungee-1	14	<10	106	1.4	4.80	1.89	77	0.041	1.2	73.7	62	165	20	2.1	51.5	0.22	2.10	21	173
Amungee-2	11	<10	137	1.3	3.20	1.21	88	0.037	2.3	67.7	45	27.0	26	3.0	42.3	0.09	2.60	7.1	93.0
Amungee-3	18	<10	76.0	3.7	6.30	1.63	38	<0.02	3.6	47.0	10	80.1	3.5	1.1	14.1	0.15	1.80	13	463
Wyworrie	13	<10	34.0	7.9	6.50	2.21	89	0.036	2.7	29.1	12	119	8.2	1.8	18.6	0.27	2.30	23	497
<i>Mt Isa Superbasin</i>																			
Termite Range	0.6	<1	7.10	0.00	1.40	200	2.2	0.080	0.2	270	0.2	2.37	2.1	0.1	1.80	0.04	0.11	0.6	3.40
Lawn Hill	13	4.0	2.90	0.72	8.90	27.2	36	0.110	2.8	54.6	4.1	16.9	14	0.6	0.74	0.01	2.10	2.1	57.0
<i>Cooper Basin</i>																			
Roseneath-1	0.9	<1	84.7	<0.05	4.08	35.1	27	<0.004	2.5	242	0.4	5.12	20	0.3	1.57	0.01	0.12	1.8	8.45
Roseneath-2	1.9	<1	147	<0.05	12.5	20.8	31	<0.004	3.4	226	0.7	19.5	26	0.4	2.93	0.02	1.46	2.2	24.1
Epsilon-1	3.5	<1	18.7	<0.05	3.32	184	16	<0.004	0.4	560	<0.3	10.8	6.1	0.1	0.75	0.01	0.06	1.6	9.84
Epsilon-2	5.4	<1	32.1	<0.05	1.46	83.9	9.1	<0.004	1.1	104	<0.3	5.91	5.7	0.1	0.77	0.01	0.02	0.6	15.0
Epsilon-3	1.8	<1	63.1	<0.05	7.03	81.2	4.2	<0.004	1.5	488	0.5	9.15	11	0.1	2.22	0.02	0.28	4.2	20.0
Murteree-1	0.7	<1	72.6	<0.05	3.59	39.2	20	<0.004	4.1	186	0.3	4.75	29	0.3	1.63	0.02	0.43	2.6	13.7
Murteree-2	1.4	<1	82.9	<0.05	5.64	22.5	11	<0.004	3.4	67.4	0.3	6.14	20	0.4	2.05	0.01	0.34	2.0	17.9
Patchawarra	8.1	<1	29.5	<0.05	3.39	84.4	91	0.004	1.5	48.4	<0.3	7.33	6.4	0.2	0.74	0.01	0.07	0.8	22.1

Table 3.7 Ratio (%) of AEE to TRE for selected major elements in the shale samples, colour coded using traffic light system (high values are in red, low - in green).

Sample ID	Al	Ca	Fe	K	Mg	Na	P	S	As	B	Ba	Cd	Co	Cr	Cu	Hg	Li	Mn	Mo	Ni	Pb	Sb	Sr	Tl	U	V	Zn
KC-1	12	97	5	19	70	76	91	5	28	n/a	60	8	38	17	21	n/a	24	42	22	43	33	33	72	5	62	16	10
KC-2	14	103	4	23	75	106	98	4	28	n/a	59	9	31	34	17	n/a	29	42	18	36	27	28	82	4	74	15	10
KC-3	10	93	5	18	78	87	87	5	24	n/a	61	10	38	28	21	n/a	26	51	21	46	28	30	71	5	74	27	11
KC-4	9	84	4	16	60	88	79	5	29	n/a	55	8	34	15	19	n/a	23	35	20	41	29	33	64	6	67	13	8
KC-5	11	97	6	19	76	91	89	6	34	n/a	65	13	46	21	24	n/a	27	48	27	53	33	33	74	7	77	22	12
COx	12	89	34	27	83	93	93	29	41	n/a	72	10	42	13	35	n/a	22	88	35	41	75	n/a	94	46	73	20	14
Eagle Ford	9	99	8	21	92	103	77	54	17	n/a	67	62	18	39	25	n/a	17	59	12	27	31	21	97	20	92	29	28
Haynesville	3	116	10	12	29	88	99	9	18	n/a	50	15	21	5	14	n/a	9	54	46	21	25	37	100	7	85	7	19
Posidonia	8	124	3	19	92	102	106	3	32	n/a	76	5	41	41	3	n/a	9	76	28	35	15	34	111	7	93	24	8
<i>Bowland Shale</i>																											
Bowland-KM	15	92	47	30	51	112	101	4	7	n/a	79	n/a	9	9	7	n/a	8	51	n/a	9	20	n/a	88	n/a	8	11	5
Bowland-BE	16	126	48	33	103	106	121	38	7	n/a	77	n/a	1	24	n/a	n/a	21	101	n/a	n/a	13	n/a	107	n/a	29	28	n/a
Bowland-LE	5	111	4	23	13	98	109	7	6	n/a	55	5	10	n/a	7	n/a	1	18	6	7	8	5	90	n/a	11	1	4
<i>Beetaloo Sub-basin</i>																											
Amungee-1	16	102	9	31	47	78	106	7	33	n/a	68	39	18	7	66	5	14	72	67	52	54	47	94	3	70	16	48
Amungee-2	9	96	5	25	22	81	99	4	33	n/a	58	36	15	6	77	8	11	61	75	22	67	49	88	3	53	9	43
Amungee-3	16	96	6	21	39	13	89	13	35	n/a	36	42	35	11	40	n/a	25	57	13	49	13	22	49	2	42	10	62
Wyworrie	12	97	7	20	35	37	97	10	33	n/a	36	61	36	8	43	6	21	43	22	51	18	24	67	3	58	9	65
<i>Mt Isa</i>																											
Termite Range	13	100	36	42	50	n/a	93	22	26	n/a	65	n/a	58	77	48	n/a	5	90	35	31	54	42	78	53	38	20	51
Lawn Hill	12	106	8	17	24	n/a	94	23	62	24	10	65	40	40	53	n/a	14	50	21	38	35	30	13	2	46	7	38
<i>Cooper Basin</i>																											
Roseneath-1	9	59	21	19	18	75	56	11	17	n/a	60	n/a	23	58	40	n/a	14	24	43	15	59	54	50	6	25	13	8
Roseneath-2	10	91	20	17	19	78	94	28	40	n/a	59	n/a	72	56	66	n/a	18	20	75	43	68	69	32	6	72	12	23
Epsilon-1	11	65	32	34	29	112	95	29	44	n/a	72	n/a	30	70	50	n/a	8	37	n/a	31	73	56	68	24	56	28	16
Epsilon-2	6	93	14	19	10	88	105	39	65	n/a	56	n/a	30	72	56	n/a	6	35	n/a	35	70	53	51	10	76	14	23
Epsilon-3	24	70	49	25	47	90	109	32	58	n/a	62	n/a	47	84	30	n/a	46	47	61	36	65	54	57	13	41	40	30
Murree-1	8	88	22	15	16	62	74	10	14	n/a	27	n/a	20	56	36	n/a	12	24	33	13	69	41	8	6	30	9	11
Murree-2	13	77	25	19	26	83	78	22	50	n/a	47	n/a	36	69	29	n/a	27	26	39	22	64	61	21	6	38	17	18
Patchawarra	9	98	19	23	14	91	76	18	43	n/a	49	n/a	27	73	90	n/a	12	32	n/a	26	48	56	27	5	24	16	23

Na and P are present in an easily mobilised form in the majority of analysed samples. Other elements showing consistently high mean AEE/TRE ratios across the sample suite include Ba, Mg, Mn and U, the latter especially for the Kimmeridge Clay, CO_x, Eagle Ford, Haynesville and Posidonia shales (77% on average). Cooper Basin shales had relatively high amounts of Cr, Pb and Sb present in a mobilizable form (all greater than 50% mean AEE/TRE percentage). Additionally, almost all of the Cu present is available for mobilisation in the Patchawarra sample (90%). Conversely, for most shale samples, the AEE fraction of As and V comprised a small proportion of these elements' total recoverable concentrations.

3.2.2.3. Environmental significance

The weathering of metal(loid)-enriched shales is a known natural source of soil and water contamination (Paikaray, 2012; Parviainen and Loukola-Ruskeeniemi, 2019). Organic matter and sulphide minerals tend to be the main host sites for potentially toxic elements (PTEs) in black shales (Paikaray, 2012). These phases are easily altered during weathering processes, releasing contaminants associated with them into the environment (Gu et al., 2020; Tuttle et al., 2014a). Natural soils derived from black shale bedrock have been shown to contain elevated concentrations of PTEs and serve as a non-point source of pollution to nearby watersheds (e.g. Cappuyns et al., 2019; Tuttle et al., 2014a; Tuttle et al., 2014b). PTEs from black shale-derived soils can be translocated into plants, often hindering their growth, and accumulating within agricultural products (Parviainen and Loukola-Ruskeeniemi, 2019 and references therein). Trace levels of PTEs in soils might contribute to the aetiology of some types of cancer (Nunez et al., 2017). In particular, chronic exposure even to low levels of As and Cd from topsoil or drinking water may substantially increase cancer risk (Nunez et al., 2016; Roh et al., 2017).

Table 3.8 Ratio (%) of TRE values for UK samples and selected UK soil guideline values, colour coded using traffic light system (high values are in red, low - in green). SGV- Soil Guideline Values (for residential purposes), SSV - Soil Screening Values (for assessing ecological risks).

	As	Cd	Cd	Co	Cu	Mo	Ni	Sb	V	Zn
<i>guideline</i>	SGV	SGV	SSV	SSV	SSV	SSV	SSV	SSV	SSV	SSV
<i>value (ug/g)</i>	32	10	0.6	4.2	35.1	5.1	28.2	37	2	35.6
TRE vs guideline values enrichment factor:										
KC-1	1	<1	8	3	1	10	4	<1	35	7
KC-2	1	<1	6	3	1	10	4	<1	28	5
KC-3	1	<1	4	3	1	9	4	<1	31	4
KC-4	1	<1	8	3	1	11	5	<1	38	6
KC-5	1	<1	4	2	1	8	3	<1	28	3
Bowland-KM	<1	<1	<1	4	<1	<1	1	<1	8	2
Bowland-BE	<1	<1	<1	<1	<1	<1	<1	<1	2	<1
Bowland-LE	<1	<1	3	4	1	<1	1	<1	9	3

Shale samples collected for this study contain concentrations of potentially toxic elements (PTEs), such as As (average reference material recovery 102%; see Chapter 4.3.2.2) and Mo, at levels exceeding average shale or average upper crustal abundances. As a tentative assessment of potential environmental hazards posed by these concentrations, the TRE values of UK and Australian shales were examined against soil contaminant regulations and guideline values for the host country.

The TRE values of Kimmeridge Clay and Bowland Shale samples were compared against the UK's Soil Guideline Values (SGVs) for residential purposes and the Soil Screening Values (SSVs) for assessing ecological risks (Table 3.8). These regulations exist only for few elements and, apart from Cr, the elements have either an SGV or SSV set. Only concentrations of V and Mo in Kimmeridge Clay samples were, on average, 32 and 10 times higher than the SSV. Other elements were either below the guidelines (e.g. Cd and Sb) or slightly above them (e.g. As, Co, Ni) for both shales.

Table 3.9 Ratio (%) of TRE values for Australian samples an Australian soil guideline values for residential purposes with garden (NEPM HILs A), colour coded using traffic light system (high values are in red, low - in green).

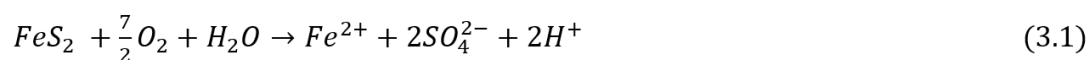
	As	Cd	Co	Cr	Cu	Hg	Mn	Ni	Pb	Zn
<i>value (ug/g)</i>	100	20	100	100	7000	200	3000	400	300	8000
TRE vs guideline values enrichment factor:										
Amungee-1	<1	<1	<1	<1	<1	<1	<1	<1	<1	<1
Amungee-2	<1	<1	<1	<1	<1	<1	<1	<1	<1	<1
Amungee-3	<1	<1	<1	<1	<1	<1	<1	<1	<1	<1
Wyworrie	<1	<1	<1	<1	<1	<1	<1	<1	<1	<1
Termite Range	<1	n/a	<1	3	<1	n/a	<1	<1	<1	<1
Lawn Hill	<1	<1	<1	<1	<1	n/a	<1	<1	<1	<1
Roseneath-1	<1	<1	<1	<1	<1	n/a	<1	<1	<1	<1
Roseneath-2	<1	<1	<1	<1	<1	n/a	<1	<1	<1	<1
Epsilon-1	<1	<1	<1	3	<1	n/a	<1	<1	<1	<1
Epsilon-2	<1	<1	<1	1	<1	n/a	<1	<1	<1	<1
Epsilon-3	<1	<1	<1	1	<1	n/a	<1	<1	<1	<1
Murteree-1	<1	<1	<1	<1	<1	n/a	<1	<1	<1	<1
Murteree-2	<1	<1	<1	<1	<1	n/a	<1	<1	<1	<1
Patchawarra	<1	<1	<1	1	<1	n/a	<1	<1	<1	<1

Comparison of the TRE values in the Australian samples to Australian soil guideline values for residential purposes with garden (NEPM HILs A; National Environment Protection (Assessment of Site Contamination) Measure 1999) indicated that the samples are generally not enriched in the regulated metal(oids) (Table 3.9).

3.3. Implications for the experimental studies

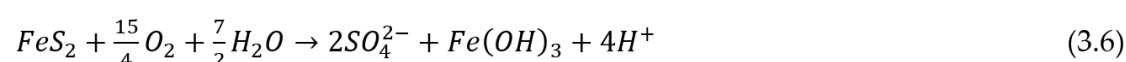
Previous studies, discussed in detail in Chapter 2, highlighted the role of relative abundances of carbonate minerals versus sulfides (particularly pyrite) in the mobilisation

of PTEs from shales during hydraulic fracturing (e.g. Harrison et al., 2017; Jew et al., 2017).



The injection of oxygenated hydraulic fracturing fluids can cause pyrite oxidation, which causes acidification and releases pyrite-hosted PTEs into solution (see 2.2). Aqueous oxidation of pyrite (FeS_2) in the presence of atmospheric oxygen can generally be described by the following five reactions, each with different kinetics:

The initial step involves oxidation of sulfur to sulfate by oxygen, and the release of ferrous iron (Fe^{2+}) (Eq. 1), which can be subsequently oxidised to ferric iron (Fe^{3+}) (Eq. 3.2). The rate of oxidation of Fe^{2+} to Fe^{3+} (Eq. 3.2) is pH-dependent: it occurs automatically at pH >4 but proceeds slowly under acidic conditions unless accelerated by bacterial activity (e.g. *Acidithiobacillus* spp. or *Leptospirillum* spp.) (Dold et al., 2017; Evangelou and Zhang, 1995). Ferric iron can also oxidise pyrite (Eq. 3). In fact, under acidic conditions, Fe^{3+} is the dominant oxidant, oxidising pyrite significantly faster than O_2 can oxidise Fe^{2+} . Consequently, the oxidation of Fe^{2+} to Fe^{3+} (Eq. 3.2) is the rate-limiting step in abiotic pyrite oxidation (Evangelou and Zhang, 1995). Ferric iron can also be an effective oxidant at circumneutral pH in the presence of dissolved O_2 ; however, as the pH increases, the solubility of Fe^{3+} is limited by the precipitation of ferric hydroxides



(Fe(OH)₃) (Eq. 3.4) and oxyhydroxides (FeOOH) (Eq. 3.5) (Evangelou and Zhang, 1995; Lottermoser, 2010; Moses and Herman, 1991).

It is generally accepted that during oxidation and the associated precipitation of Fe(III)-(oxy)hydroxides, one mole of pyrite produces 4 mol of H⁺ (acidity) (Eq. 3.6)

The acidity produced by pyrite oxidation can be neutralised by the dissolution of acid-neutralising minerals, chiefly Ca-Mg carbonates, and, much slower reacting, aluminosilicates such as chlorite (Dold, et al., 2017; Karlsson et al., 2018).

It is possible to predict whether a rock sample will generate acid, neutral or alkaline environment through Acid-Base Accounting (ABA), an industry-wide method employed in acid mine drainage studies (e.g. Dold, 2017; Evangelou and Zhang, 1995). ABA relies on establishing: (1) the Acid Potential (AP) of the sample, by quantifying acid-producing minerals and the number of moles of protons that they can potentially liberate; and (2) the Neutralisation Potential (NP), by quantifying acid-neutralising minerals and the moles of protons they can neutralise. The difference between the two potentials indicates if enough acid-neutralising minerals are present to counteract all protons that will be produced, and can be expressed as the Neutralization Potential Ratio (NPR=NP/AP) or as the Net Neutralisation Potential (NNP=NP-AP). If NNP <-20 or NPR <1, the sample will be potentially acid-generating, and if NNP >20 or NPR >3, it will have no acidification potential. Values between these ranges are considered to have an uncertain acid generation potential. However, this can be ascertained with good knowledge of the sample's mineralogy (Dold, 2017; Karlsson et al., 2018).

There are many variants of the ABA tests, but at its simplest, ABA employs a range of static laboratory tests to measure the total sulphur and carbon content, expressed as pyrite and calcite equivalent, respectively. These are then used to calculate AP and NP (e.g. Bouzahzah et al., 2014; Dold, 2010; Skousen, 2017). Traditional geochemical ABA tests have known limitations associated with the simplification of the sample's mineralogy, which may result in over- or underestimation of either potential (e.g. Dold,

2017; Parbhakar-Fox and Lottermoser, 2015). For example, traditional ABA methods do not distinguish between different carbonate minerals, however, siderite (FeCO_3) can act as a neutraliser under acidic conditions but at pH of about 5, the overall siderite dissolution-oxidation reaction will be a net acid producer, and consequently may lead to falsely high NP values (Dold, 2017; Haney et al., 2006). To address this and other limitations, some mineralogical approaches to ABA have been proposed (Dold, 2017; Karlsson et al., 2018).

Following the findings from the previous studies on shale-hydraulic fracturing fluid interactions, a simplified mineralogical ABA approach was used to characterise the shale samples used in this study to predict their potential behaviour during leaching experiments.

$$AP = (\text{mass\% } S \text{ in mineral} / 100) \times \text{wt\% of the mineral} \times 31.25 \text{ or } 62.5$$

The mineralogical ABA, based on Dold (2017) and Karlsson et al. (2018), was performed only for samples that contain any of the most relevant sulphide minerals (after Dold, 2017). Consequently, only pyrite and marcasite were considered (polymorphs of FeS_2)



and hence, all of the Cooper Basin samples were excluded from the calculations.

The AP value was calculated as follows:

The choice of factor for multiplication relates to the amount of protons that can be neutralised by calcite. Calcite (CaCO_3) solubility and carbonate speciation is pH dependent:

Traditionally, a factor of 31.25 has been used based on the assumption that 1 mol of

calcite can neutralise 2 mol of protons (Eq. 3.7); however, this is only applicable under acidic conditions. At circumneutral pH, bicarbonate will be the dominant species and 1 mol of calcite will only neutralise 1 mol of protons (Eq. 3.8), necessitating a factor of 62.5 (Dold, 2010; Dold, 2017). Therefore, two AP values were calculated to account for any pH conditions.

$$NP \text{ carbonates} = (\% \text{ mole mass C in the mineral}/100) \times \text{mineral wt\%} \times 83.3$$

To simplify NP calculations, only carbonate minerals (apart from siderite) and intermediate to fast weathering non-carbonate silicate minerals were considered (Dold,

$$\begin{aligned} NP \text{ non-carbonate} & \\ &= (\text{mineral wt\%}/100) \times 1000 \text{ kg/t} \\ &\times (\text{mole mass calcite}/\text{mole mass mineral}) \times \text{reactivity factor} \end{aligned}$$

2017). Thus, the total NP values were based on contributions from calcite, dolomite and chlorite.

NP values for carbonate minerals, converted to calcite equivalent, were calculated as follows:

For non-carbonate minerals, NP contribution in kg CaCO₃ was obtained using the following equation:

The reactivity factor, in terms of acid neutralisation capacity, depends on the total percentages of different mineral groups in the sample (Sverdrup, 1990 in Karlsson et al., 2018); carbonate minerals always have a reactivity factor of 1, whereas a factor of 0.3 was assumed for chlorite based on the mineral's abundance.

The results of the mineralogical ABA calculations are presented in Table 3.10.

Majority of the shale samples used in this study are potentially acid-producing,

regardless of the AP factor applied, especially the Kimmeridge Clay samples which contain no carbonates or other minerals with any acid neutralisation capacity. Bowland Shale (KM) and Lawn Hill samples appear to be overall acid-producing, however, NNP values for AP1 for both are in the uncertain range. Bowland Shale (KM) contains 9wt% siderite, which excluded from calculations, is likely to contribute to the generated acidity (Dold, 2017). With no buffering capacity present in the shale to counteract the acidity generated from pyrite dissolution, particularly if the fracturing fluid is well-oxygenated and acidic, leaching of these samples is likely to generate an environment that favours contaminant mobility (e.g. Harrison et al., 2017; Langmuir et al., 2014).

Conversely, Bowland (BE), Haynesville, COx, Eagle Ford and Posidonia samples are overall non-acid generating. It is likely they will buffer the pH during leaching with fracturing fluids, creating circumneutral to alkaline conditions, which will promote precipitation of Fe(III)-(oxy)hydroxides and sorption of metals, limiting contaminant concentrations in the solution (e.g. Harrison et al., 2017; Langmuir et al., 2014).

Table 3.10 Results of the mineralogical ABA for selected shale samples. NPR and NNP values are coloured accordingly: dark grey – potentially acid producing, light grey – non-acid generating, and uncertainty zone is white cells.

Sample ID	Intermediate weathering Chlorite (wt%)	Carbonates		Sulphides	Acid Potential (AP): Pyrite		Neutralisation Potential (NP):				NPR:		NNP:	
		Calcite (wt%)	Dolomite (wt%)	Pyrite (wt%)	AP1 (31.25)	AP2 (62.5)	Calcite	Dolomite	Chlorite	Total NP	NP/AP1	NP/AP2	NP-AP1	NP-AP2
Amungee-1	3.0		1.0	12.0	200	400		11	0.15	11	0.05	0.03	-189	-389
Amungee-2	6.0		2.0	7.0	117	233		22	0.30	22	0.19	0.09	-95	-211
Amungee-3		2.0		11.0	183	366	20			20	0.11	0.05	-163	-346
Wyworrie	1.0		1.0	2.0	33	67		11	0.05	11	0.33	0.16	-22	-56
Termite Range	1.9		0.8		0	0		8	0.10	8			8	8
Lawn Hill	5.0			1.0	17	33			0.25	0	0.02	0.01	-16	-33
KC-1				4.5	75	150				0			-75	-150
KC-2				5.6	93	187				0			-93	-187
KC-3				10.1	168	336				0			-168	-336
KC-4				7.0	117	233				0			-117	-233
KC-5				11.9	198	396				0			-198	-396
Bowland (KM)		0.5		1.2	20	40	5			5	0.25	0.13	-15	-35
Bowland (BE)		66.3	7.2	1.7	28	57	663	78		741	26.2	13.1	712	684
Bowland (LE)	4.6	2.1		8.7	145	290	21		0.23	21	0.15	0.07	-124	-269
Haynesville	2.0	10.0	1.0	2.0	33	67	100	11	0.10	111	3.33	1.66	78	44
COx	1.0	14.0		1.0	17	33	140		0.05	140	8.40	4.20	123	107
Eagle Ford		71.0		1.0	17	33	710			710	42.6	21.3	693	676
Posidonia		37.0	1.0	6.0	100	200	370	11		381	3.81	1.90	281	181

CHAPTER 4

MOBILISATION OF ELEMENTS FROM SHALES DURING HYDRAULIC FRACTURING: LABORATORY STUDIES

4.1. Introduction

As discussed in Chapters 1 and 2, the large quantities of wastewater produced throughout the lifetime of a shale gas well can contain heavy metals and other regulated potentially toxic elements (PTEs). These can be mobilised from the target formation by hydraulic fracturing fluids or derive from mixing with the formation brines (Harrison et al., 2017; Renock et al., 2016). The concentration of mobilised elements and the hazard they pose is uncertain and is likely dependant on the chemical agents used in hydraulic fracturing fluids, composition of formation water and the trace element content of targeted shale gas formation.

Previous experimental studies, which investigated rock-fluid interactions during hydraulic fracturing, were performed at a wide range of *in-operando* conditions. Temperatures and pressures used in the experiments ranged from atmospheric to reservoir-representative; frequently, they represented downhole conditions from a Marcellus Shale well. Fluid composition varied from just ultrapure water to water containing common fracturing additives. Previous studies showed that certain hydraulic fracturing fluid additives (acids and oxidants) have a strong influence on

mineral dissolution and oxidation, and consequently element mobilisation (Wang et al., 2015; Wang et al., 2016; Xiong et al., 2018). Lastly, the suite of shale samples used in the studies was often limited to a few American shales, predominantly Marcellus Shale. These differences limit meaningful cross-study comparisons and extrapolation of results to other gas shales or field setting, which highlights the need for a systematic study on element mobilisation by hydraulic fracturing fluids from a wider range of shale samples.

This chapter describes laboratory work designed to systematically investigate the release of potential inorganic contaminants of concern from selected shale samples and to determine the main controls on their mobilisation. The experiments were designed as leaching tests attempting to simulate ‘worst case’ conditions during hydraulic fracturing operations, particularly the shut-in phase when most of the rock-fluid interactions and shale alterations are thought to take place (Jew et al., 2017; Marcon et al., 2017). The leach tests have been adapted from the experimental methods developed by Apte et al. (2017) to investigate the release of geogenic contaminants during coal seam gas operations.

The leaching agents used in this study included diluted hydrochloric acid (1M HCl), synthetic groundwater (SGW) and synthetic hydraulic fracturing fluid (SHFF). The main tests were performed at a reservoir-representative temperature and atmospheric pressure, generating data for a reaction time-series up to 550 h for Kimmeridge Clay samples, and up to 360 h for the remaining shales. The 550h leaching was performed to explore the effects of a lengthier shut-in period on element mobilisation, and only Kimmeridge Clay samples were selected for this due to their large quantities. A few exploratory tests on selected shale samples were also performed at elevated pressures as well as temperatures (see 5.4).

This chapter will first describe the composition of each leaching fluid, particularly SHFF, before outlining the experimental approach. Subsequently, the results of the leaching

tests with SGW and SHFF will be presented and discussed. Lastly, the smaller-scale experiments with 1M HCl will be summarised.

4.2. Leaching fluids

4.2.1. Dilute hydrochloric acid (1M HCl)

A dilute acid flush is primarily used to clean well perforations, prior to the commencement of hydraulic fracturing. Typically 15% HCl (5M HCl) is used, but concentrations may range from 3% to 28% (Arthur et al., 2009; McCurdy, 2011). This treatment can also interact with the matrix near the wellbore by removing any acid-soluble minerals in the shale, and thus increasing the exposed surface area of the rock (Arthur et al., 2009; Ferrer and Thurman, 2015; Grieser et al., 2007). Acid flush can also be applied during later stages of hydraulic fracturing jobs as a pad acid, which can decrease the initiation fracture pressure during high-rate water fracturing as well as remove any further obstructions from the well perforations or near the wellbore (Grieser et al., 2007; Li NY et al., 2016).

The experiments with dilute hydrochloric acid (1M HCl, equivalent to 3% HCl) aimed to replicate the effects of a low concentration HCl acid flush, with a maximum leaching time of 17 h.

4.2.2. Synthetic groundwater

Synthetic groundwater (SGW) was composed of 750 mg/l sodium chloride (NaCl) and 750 mg/l of sodium bicarbonate (NaHCO_3) (total dissolved solids of 1500 mg/l), buffered to a pH of approximately 7.5 with 1M HCl. This recipe followed a typical groundwater composition associated with the unconventional gas extraction in Australia and was selected as most of the experimental work was conducted in Australia on the prospective

Australian gas shales (Apte et al. 2017; Worley Parsons, 2010).

SGW tests helped to assess which elements were most readily leached under reservoir conditions and also acted as control for the SHFF leaching experiments. SGW was used as a background matrix for the synthetic hydraulic fracturing fluids and thus served as a benchmark to establish how the chosen chemical additives impacted element mobilisation.

4.2.3. Synthetic hydraulic fracturing fluid

4.2.3.1. Types of hydraulic fracturing fluids used in the industry

The design of fracturing fluid for a given well is based on the operator's empirical knowledge, the geology and geochemistry of the targeted formation, economics, aims of the fracturing process, individual preferences of the operator, and the availability of chemical additives (US EPA, 2016). The number of additives used during any given fracture treatment is well-specific, depending on the characteristics of the water used and the shale formation; however, usually between 3 and 12 additives are employed (GWPC and ALL Consulting, 2009).

The selection of a fracturing fluid type is typically based on the temperature, pressure, water sensitivity and permeability of the target zone (Figure 4.1). The crucial design choice is the viscosity of the fluid because it governs successful transport and emplacement of proppant as well as the initiation of new fractures (US EPA, 2016).

Different types of fracturing fluids have been developed over time to accommodate the variability in reservoir properties, starting with oil-based and water-based fluids in the late 1940s and late 1950s, respectively. Since their introduction, water-based fluids have become the most widely used type of fracturing fluids due to their low cost, high

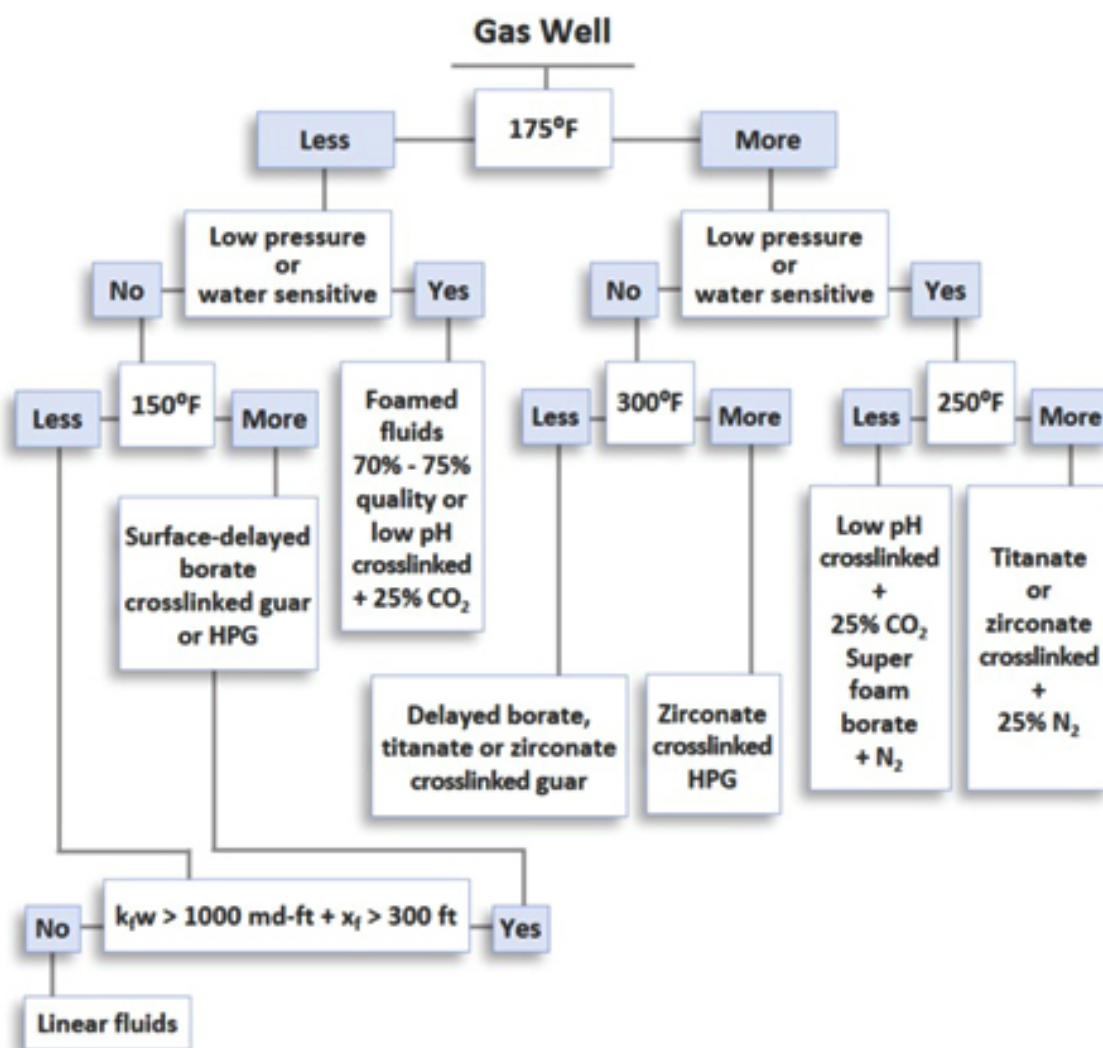


Figure 4.1 An example of a hydraulic fracturing fluid decision tree for gas wells (from US EPA, 2016). HPG - hydroxypropylguar, guar derivatized with propylene oxide; k_f - fracture permeability; w - fracture width; and x_f - fracture half-length.

performance and ease of handling (Gulbis and Hodge, 2000; Palisch et al., 2010).

Three types of water-based fluids are classically used - linear gels, crosslinked gels, and slickwater. Linear gels are primarily composed of water and a gelling agent, typically a natural water-soluble polymer such as guar gum, which is added to increase the solution's viscosity so that it is capable of suspending proppants (Barati and Liang, 2014; Gulbis and Hodge, 2000). However, linear gels thin with increasing temperatures,

limiting their suitability for subsurface operations. To compensate for the thermal effect, crosslinking agents can be added to the solution to increase the polymer's effective molecular weight considerably and thus enhance the fluid viscosity without the addition of more gel (Gulbis and Hodge, 2000). Frequently used crosslinkers include borate, and transition metals such as Ti(IV) and Zr(IV) compounds, and the choice of a crosslinking agent depends on the fluid pH, reservoir temperatures and polymer type (Barati and Liang, 2014; Gulbis and Hodge, 2000).

Conversely, slickwater fluids consist mainly of large quantities of water with a very low concentration of linear gel (~10 pounds per thousand gallons, equivalent to 1.2 kg/L) or a polyacrylamide friction reducer that lowers the fluid friction while it is pumped downhole. The primary advantage of slickwater treatment is reduced gel damage to the fracture: linear and crosslinked gels can leave residue along the fracture, reducing porosity, permeability and fracture length. Slickwater treatment is also potentially cheaper due to its simpler chemical composition, making fluid treatment and recycling easier. However, the low viscosity of slickwater fluids results in a poor proppant transport, which is typically counteracted by higher pumping rates and larger volumes of water required, making such fracturing treatments unfeasible in areas with limited water availability (Barati and Liang, 2014; Palisch et al., 2010).

4.2.3.2. Development of the synthetic hydraulic fracturing fluid recipe

As mentioned before, the fracturing fluid composition is site-specific and may vary depending on the fracturing job stage, often including vendor's proprietary mixes (e.g. WFR-61LA, a friction reducer). Numerous fluid make-ups might be applicable at a given well stimulation, and one fluid composition might be appropriate for multiple wells. Consequently, there is no standard set of chemicals used at every site or a single representative composition of a hydraulic fracturing fluid used in the industry (US

EPA, 2016).

Furthermore, a large variety of unique chemicals can be used as additives, and the initial reticence of operators to disclose them to the public led to concerns from a range of stakeholders around their potential environmental and human health impacts (Adgate et al., 2014; Bamberger and Oswald, 2012; King et al., 2012; Stringfellow et al., 2014). In the USA and Canada, the industry's response was to set up FracFocus (<https://fracfocus.org>), an online portal managed by the US Ground Water Protection Council and Interstate Oil and Gas Compact Commission, where shale gas operators disclose all chemical additives used in their operations as well as their quantities. Some of the most common additives disclosed to the database include biocides, gelling agents, clay stabilisers, pH adjusting agents and iron control agents (US EPA, 2015). However, the exact details of how the additives are mixed to form a working fracturing fluid are typically considered a trade secret (Maule et al., 2013; US EPA, 2016).

In the mid-1980s, the American Petroleum Institute funded a project researching rheological properties of the transition metal crosslinked guar-based gels, where the fluid recipe was provided in detail (Prud'homme et al., 1984; Kramer et al., 1987). The fluid preparation was clearly outlined in a number of subsequent publications by Prud'homme and others (e.g. Kesavan and Prud'homme, 1992; Prud'homme et al., 1988). The formulation of the synthetic hydraulic fracturing fluid (SHFF) was subsequently based mainly on Prud'homme's recipe for a titanate crosslinked hydroxypropyl guar 40 lb/bbl gels as it is easily reproducible (e.g. no proprietary additives, detailed instruction on fluid mixing) and readily accepted by the operators (Mike Williams, Principal Reservoir Engineer – Research, Schlumberger, personal communication, 30 July 2018). Moreover, despite the rise in popularity of the slickwater treatments, linear and crosslinked guar-based gels are still widely used (Barati et al., 2014; Palisch et al., 2010).

Prud'homme's formulation includes a gelling agent (guar), pH buffer (sodium

Table 4.1 Prud'home's recipe for a titanate cross linked HPG 40 lb/bbl gel.

Ingredient	Purpose	Comments
500 ml distilled water	base fluid	
2.4 g hydroxypropyl guar (HPG)	gelling agent	More stable at higher T, better suited to be used in wells where T>150°C than just guar gum.
0.6 g sodium diacetate	pH control	
10 g analytical grade potassium chloride (KCL)	clay stabiliser	Solutions containing 1% to 3% KCL are commonly used as the base liquid in fracturing fluids to stabilise clays and prevent swelling.
0.125 ml 25% glutaraldehyde in water	biocide	Prevents viscosity loss caused by bacterial degradation of the polymer.
2 ml of (9:1) solution by vol. isopropyl alcohol and Tyzor AA titanate	crosslinker	In HF applications, titanate and zirconate cross linked gels form as the fluid is pumped down the well (i.e. during highest shear rates). Transition metal cross linkers were developed for HT applications and/or low-pH environments, with Ti and Zr used most often. Upper T limit for such gels is 150-200°C.

diacetate), biocide (glutaraldehyde), crosslinker (titanate), and a clay stabiliser (potassium chloride) (Table 4.1).

Two more types of additives were added to the base recipe for this study – two iron control agents and a breaker:

Iron control - Citric acid and EDTA are the most common scavenging agents used to prevent dissolved iron precipitation in the wellbore through the formation of soluble complexes (Ferrer and Thurman, 2015). They can also result in the desorption of metals from host minerals, forming strong complexes with them and increasing their mobility (Kourgiantakis et al., 2000; Wang et al., 2016). A review of disclosures within FracFocus database showed that if EDTA was used as the main iron control compound, its concentration typically ranged from 0.0022 - 0.0034% by mass of the total fluid, and it was accompanied by citric acid as an iron control additive (0.0007-0.0012% by mass). McCurdy

(2011) reported usage for all the iron control acids as 5000 ppm of the total acid volume (0.004 - 0.011% total fluid volume). Both additives were included in the fluid formulation used in this study at 0.0012 and 0.0034% by mass for citric acid and EDTA, respectively.

Breaker - Following fracturing, the gel fluid needs to be broken down into a low-viscosity liquid to ensure high conductivity in the proppant pack. The most commonly used breakers include oxidisers, primarily the ammonium, potassium and sodium persulfate salts (Gulbis and Hodge, 2000; Montgomery, 2013). Above 51°C, the persulfates will thermally decompose and form highly reactive sulphate radicals that reduce the polymer's molecular weight by breaking it down into its constitutive sugars. The oxidiser reactivity increases with temperature, and at higher temperatures, the breaker may degrade the polymer during pumping stages, rather than after proppant emplacement. Nowadays, persulfate breakers can be encapsulated to improve their performance in high-temperature reservoirs (Barati and Liang, 2014; Gulbis and Hodge, 2000; Montgomery, 2013).

Due to their popularity, ammonium persulfate salts (APS) were included as a breaker for the SHFF. Based on the disclosures submitted to FracFocus, the median maximum concentration of APS in hydraulic fracturing fluids is 0.0069 with the 95th percentile being 0.064% m/v. One peer-reviewed study, also using FracFocus data, utilised 0.02% v/m of APS in their synthetic recipe (Paukert Vankeuren et al., 2017).

The initial amount of APS included in the formulation for this study was 0.03% m/v. However, it was ultimately increased to 0.4% m/v following initial testing due to the issues with reducing the gel's viscosity following the leaching experiment.

Following a preliminary test of the recipe, the guar gum was excluded from the final formulation of the SHFF to facilitate leachate extraction and alleviate potential analytical problems that may have arisen from elevated carbon concentrations. It was

Table 4.2 Composition of the final formulation of the synthetic fracturing fluid (SHFF) used in this study.

Chemical name	Purpose	Amount added per litre of fluid		Concentration
		g	ml	Mass %
Sodium diacetate	pH control	1.2		0.12%
Potassium chloride (analytical grade)	Clay stabiliser	20		2%
Glutaraldehyde solution (25%)	Biocide		0.25	0.03%
EDTA	Iron control	0.034		0.0034%
Citric acid	Iron control	0.012		0.0012%
Isopropyl alcohol/Tyzor AA titanate solution 9:1 (v/v)	Crosslinker		4	0.40%
Ammonium persulfate solution (6% m/v)	Breaker		67	0.40%
Synthetic groundwater (750 mg/L NaCl, 750 mg/L NaHCO ₃)	Base solution		Remaining volume to total 1 litre	97.05%

assumed that guar constituents would not mobilise geogenic chemicals from solids (see 5.2.3). APS was retained in the final (non-gelled) version of the SHFF at the elevated concentration (0.4% m/v) given it is a common component of field-based hydraulic fracturing fluids, and as it was proven to influence the release of elements into solution (see 5.2.3).

4.2.3.3. Synthetic fracturing fluid recipe

The final formulation of the SHFF used in this study is given in Table 4.2. All of the components were mixed in together by hand. Synthetic groundwater (SGW) with TDS of 1500 mg/l was used as the base fluid instead of distilled water to make the recipe more field-representative. Water used in the hydraulic fracturing fluids is typically acquired from surface water or groundwater sources, depending on the local availability, or minimally treated recycled flowback. Water from these sources will vary in its initial quality, but freshwater (i.e. low TDS) is often preferable to maximise the performance of the hydraulic fracturing fluid (US EPA, 2016).

The final pH of the unreacted fluid was tested each time a batch was prepared. The pH ranged between 2.3 and 5.4, with an average of 4.7 and a median value of 5.25. The degradation of ammonium persulfate due to storage or age is likely responsible for this variation, where the fluid pH decreases with increased degradation of the reagent. The resulting initial fluid pH was shown to have little influence during leaching experiments, as the blank fluid samples degrade to a pH of approximately 2 regardless of the initial pH due to ammonium persulfate breakdown (see 5.2.3).

4.3. Experimental approach

4.3.1. General procedures

The study utilised high purity deionised water obtained from a Milli-Q system (18 M Ω .cm conductivity, Millipore, Australia). Prior to use, all plasticware used for elemental analyses was acid-washed by soaking in 10% (v/v) analytical reagent nitric acid (Merck Tracepur) for at least 24 h and subsequently rinsing with large amounts of deionised water.

4.3.2. Batch leach experiments

The batch leach experiments were performed on powdered samples to increase surface area (to produce faster reaction rates than would be expected on natural fracture surfaces) and eliminate any inherent heterogeneities that may be present along a fracture surface or within a rock chip. This allowed the leaching agent to have a concurrent contact with all minerals present within a shale sample, which is likely to result in a more significant element mobilisation within a given time compared to realistic field conditions. Results from the batch leaching experiments on powder samples should be treated as upper

bound estimates of geogenic element release.

Cooper Basin and Mt Isa samples were already provided powdered and sieved to less than 74 μm . The remaining samples were powdered using a zirconium ball mill and sieved to <125 μm .

Batch leaching experiments were undertaken by weighing a known mass of a powdered shale sample (typically 0.3 g) into a 50 mL polypropylene centrifuge tubes, followed by the required volume of leach solution to achieve 1:50 (m/v) solids to fluid ratio.

This solid to fluid ratio was chosen based on sample availability and preliminary tests (see 5.2.1). The chosen ratio results in a more diluted solution than would be expected during actual hydraulic fracturing operations, which Renock et al., (2016) estimated to be 100:1 solid:fluid, about five orders of magnitude higher than the one used in this study (Harrison et al., 2017; Paukert Vankeuren et al., 2017); this is typical of lab-based studies.

The solutions were shaken and placed in an oven set to 80°C for 5, 24, 48, 120, 260 or 360 hours. The Kimmeridge Clay samples were also left for 550 h (greater amount of sample available). The solutions were mixed again after heating, then syringe filtered through 0.45 μm filter cartridges (Minisart, Sartorius Stedim, Germany).

The leach tests could only be performed in duplicate due to the limited sample availability. All experiments also included a blank control treatment - comprising three tubes with the leaching solution but without any solids added.

4.3.2.1. Analytical procedures

Major and trace element analysis was carried out at a CSIRO laboratory using a combination of inductively coupled plasma-atomic emission spectrometry (ICP-AES) (Varian 730-ES, Australia) and inductively coupled plasma-mass spectrometry (ICP-

MS) (8800, Agilent Technologies, Japan).

The filtered leachates were analysed as tenfold dilutions into 2.25% v/v nitric acid and 0.75% v/v hydrochloric acid. Calibration standards for ICP-MS were prepared by serial dilution of a 68 element certified standard mix (Choice Analytical) into 2.25% v/v nitric acid and 0.75% v/v hydrochloric acid. ICP-AES standards were prepared from certified stocks (Accustandard, USA) into a final acid concentration of 2% v/v nitric acid. Quality control procedures included analysis of certified reference materials (where feasible), replicate analyses and spike recoveries. Limits of detection were calculated as three times the standard deviation (3 Sigma) of the experimental blank control measurements.

The pH was measured on unfiltered samples using an Orion Versa Star Pro meter, with Orion Ross Ultra pH probe. The pH meter was calibrated using three pH buffer solutions (pH 4.01, pH 7.00, and pH 10.01) daily on use.

4.3.2.2. Errors and uncertainty

Due to the limited availability of majority of the shale samples, the experiments were primarily performed in duplicate using small sample volumes (typically 0.3 g). This is likely to be the main origin of uncertainty in the reported results.

However, care was taken to ensure quality control for the inorganic analyses. The CSIRO laboratory at Lucas Heights, Sydney, is a NATA accredited facility and uses validated methods for the analysis of various water quality parameters, including the determination of trace metals in waters and soils. Stringent quality control procedures (spike recovery tests, experimental duplicates, analysis of reference materials) were used throughout and the laboratory is subject to regular external audits.

The analysis of reference material (ERM-CC018-2) during the TRE analysis indicated

Table 4.3 Range and median values for the recovery ranges of the reference material (ERM-CC018-2) for 9 available elements with certified values.

	<i>As</i>	<i>Cd</i>	<i>Co</i>	<i>Cr</i>	<i>Cu</i>	<i>Ni</i>	<i>Pb</i>	<i>V</i>	<i>Zn</i>
unit	%	%	%	%	%	%	%	%	%
Min	92	96	84	89	91	91	99	79	93
Max	114	124	107	123	108	118	121	108	109
Mean	102	107	93	104	100	103	110	95	101

a recovery range between 84 to 124% across 9 elements that the reference material provided certified values for (Table 4.3).

The average spike recoveries for 47 elements ranged from 91 to 110%; the minimum, maximum, average and median values are given in Table 4.4.

The limits of detection for the element analyses were calculated based on the experimental (method) blank measurements made during the analyses (three times the standard deviation of the blank measurements). This provides a more realistic assessment of actual detection limits rather than the generalised detection limits based on historical data that are quoted by many commercial laboratories.

The range and median value of the limits of detection for all analyzed elements are listed in Table 4.5.

Table 4.4 Range, mean and median values for spike recoveries, expressed as percentage. Spike recoveries were performed on 47 elements out of 54 included in the full dataset.

	unit	Min	Max	Mean	Median		unit	Min	Max	Mean	Median	
<i>Al</i>	%	31	142	93	91		<i>Mn</i>	%	84	111	96	93
<i>As</i>	%	92	124	106	106		<i>Mo</i>	%	98	114	106	107
<i>B</i>	%	97	110	102	101		<i>Nb</i>	%	98	120	106	106
<i>Ba</i>	%	77	112	95	95		<i>Nd</i>	%	95	110	103	104
<i>Be</i>	%	85	113	101	102		<i>Ni</i>	%	94	153	107	103
<i>Bi</i>	%	84	111	98	96		<i>Pb</i>	%	85	107	97	96
<i>Ca</i>	%	62	139	102	101		<i>Pd</i>	%	87	110	99	101
<i>Cd</i>	%	92	112	102	102		<i>Pr</i>	%	94	112	102	103
<i>Ce</i>	%	93	115	102	102		<i>Rb</i>	%	95	117	107	107
<i>Co</i>	%	91	112	104	106		<i>Rh</i>	%	89	111	99	101
<i>Cr</i>	%	94	160	107	106		<i>Ru</i>	%	91	112	100	101
<i>Cs</i>	%	92	113	102	102		<i>S</i>	%	84	158	103	99
<i>Cu</i>	%	81	113	100	101		<i>Sb</i>	%	92	118	105	103
<i>Dy</i>	%	94	112	103	104		<i>Sc</i>	%	93	118	105	105
<i>Er</i>	%	94	113	102	104		<i>Si</i>	%	83	149	101	100
<i>Eu</i>	%	95	112	103	105		<i>Sm</i>	%	97	112	104	105
<i>Fe</i>	%	86	149	102	101		<i>Sn</i>	%	95	113	105	106
<i>Ga</i>	%	91	113	103	103		<i>Sr</i>	%	78	115	98	99
<i>Gd</i>	%	92	111	103	105		<i>Tb</i>	%	93	113	103	104
<i>Ge</i>	%	92	119	105	105		<i>Th</i>	%	91	109	101	103
<i>Hg</i>	%	95	120	104	100		<i>Tl</i>	%	85	113	99	101
<i>Ho</i>	%	94	112	102	103		<i>Tm</i>	%	93	113	103	104
<i>In</i>	%	91	125	103	104		<i>U</i>	%	89	113	101	103
<i>La</i>	%	94	111	102	102		<i>V</i>	%	99	122	109	110
<i>Li</i>	%	95	123	104	104		<i>Yb</i>	%	91	112	101	103
<i>Lu</i>	%	92	113	102	103		<i>Zn</i>	%	12	166	103	105
<i>Mg</i>	%	71	122	96	97		<i>Zr</i>	%	96	111	103	103

Table 4.5 Range and median values for calculated limits of detection for all analysed elements. Elements reported as $\mu\text{g/l}$ were analysed by ICP MS, whereas those reported in mg/l by ICP AES.

	Min	Max	Median		Min	Max	Median
<i>Ag</i>	0.005	0.59	0.02	<i>Nb</i>	0.006	0.40	0.02
<i>As</i>	0.001	0.77	0.23	<i>Nd</i>	0.003	0.07	0.01
<i>Ba</i>	0.11	0.86	0.50	<i>Ni</i>	0.15	37	0.84
<i>Be</i>	0.001	0.06	0.01	<i>Pb</i>	0.02	2.3	0.19
<i>Bi</i>	0.004	0.13	0.02	<i>Pd</i>	0.02	0.64	0.04
<i>Cd</i>	0.001	0.53	0.09	<i>Pr</i>	0.002	0.15	0.01
<i>Ce</i>	0.007	12	0.04	<i>Rb</i>	0.001	24	7.5
<i>Co</i>	0.017	0.50	0.07	<i>Rh</i>	0.004	18	0.02
<i>Cr</i>	0.13	2.1	0.45	<i>Ru</i>	0.01	31	0.06
<i>Cs</i>	0.010	0.5	0.04	<i>Sb</i>	0.01	0.31	0.12
<i>Cu</i>	0.06	15	0.50	<i>Sc</i>	0.001	0.64	0.001
<i>Dy</i>	0.003	0.14	0.01	<i>Sm</i>	0.005	0.21	0.02
<i>Er</i>	0.001	0.03	0.004	<i>Sn</i>	0.01	0.90	0.19
<i>Eu</i>	0.001	0.44	0.004	<i>Sr</i>	0.11	2.8	0.95
<i>Ga</i>	0.005	0.06	0.02	<i>Tb</i>	0.001	1.3	0.003
<i>Gd</i>	0.002	0.25	0.02	<i>Th</i>	0.001	0.54	0.01
<i>Ge</i>	0.04	7	0.21	<i>Tl</i>	0.02	2.1	0.08
<i>Hg</i>	0.02	0.47	0.07	<i>Tm</i>	0.001	0.12	0.001
<i>Ho</i>	0.001	0.02	0.003	<i>U</i>	0.001	0.01	0.002
<i>In</i>	0.006	23	0.04	<i>V</i>	0.02	2.75	0.12
<i>La</i>	0.003	0.10	0.01	<i>Yb</i>	0.001	0.41	0.01
<i>Li</i>	0.02	4.3	0.12	<i>Zn</i>	1.3	17	4.2
<i>Lu</i>	0.001	0.15	0.002	<i>Zr</i>	0.004	0.67	0.02
<i>Mo</i>	0.001	0.22	0.07				

4.4. Results

4.4.1. Effect of fluid type on leachate element concentrations

The concentrations of relevant elements (Chapter 3.2.2) leached into solution by SGW and SHFF are summarised in Appendix B (Tables B1 and B2). The full dataset (54 elements) is presented in Appendix C. The results are the mean of duplicate determinations. For elements with detectable concentrations, the average relative percent difference between duplicates ranged from 0.002 to 161% with an 12.2% average for ICP-AES measurement, a range of 0.01-194% and a 15% average for measurements obtained by ICP-MS. All reported element concentrations were method blank corrected.

For most shale samples, the concentrations of the majority of the elements in solution are relatively low throughout the time-series for the SGW tests. Many measurements were below the detection limit (<DL), particularly for Cr (65% <DL), Zn (63%), Fe (58%), Hg (53%), Pb (51%), Co (45%) and Cd (43%) across all samples. In comparison, the concentrations of elements mobilised into solution by SHFF were generally 33-57% higher, especially for the trace elements such as Cd, Co, Ni, Zn as well as Ca, Mg and Mn. Over half of Hg measurements remained below the detection limit (52%), with B at 45% below DL, Mo 31% and Al 22%.

For data points above the detection limit, the observed element concentrations mobilised into either solution typically vary to three orders of magnitude among the shale samples. This reflects the variability of total recoverable element (TRE) concentrations among the shales, which also vary up to several orders of magnitude, and the mineralogical differences (see 3.2). Therefore to facilitate comparison among the samples, the leaching test data were normalised to TRE content of each sample (3.2.2) and expressed as *element % TRE* (Appendix B, Tables B3 and B4). The element % TRE was then compared to

Table 4.6 Classification of shale samples based on mineralogical Acid-Base Accounting (ABA).

Potentially acid producing	Uncertain	Non-acid producing
KC1 to KC5	Termite Range	Bowland-BE
Bowland-KM	Roseneath-1 and -2	Eagle Ford
Bowland-LE	Epsilon-1 to -3	Posidonia
Amunsee-1	Murteree-1 and -2	Haynesville
Amunsee-2	Patchawarra	COx
Amunsee-3		
Wyworrie		
Lawn Hill		

the element's concentration in solution to examine both the extent of mobilisation and the absolute concentrations to assess the impact of the leaching solutions.

4.4.1.1. pH

The sample's ability to neutralise acid appeared to control the pH during the experiments with SHFF (Figure 4.2). The neutralisation potential was established using the mineral ABA calculations in Chapter 3.3 and used to classify samples into three groups: *non-acid producing*, *potentially acid producing*, and *uncertain* (Table 4.6).

The pH of unreacted SHFF ranged between 2.3 and 5.4, with an average of 4.7 and a median value of 5.2. Two distinct trends in fluid pH were evident in the SHFF experiments (Figure 4.3a): (1) *non-acid producing* shales saw an immediate increase to circumneutral pH within the first 5-24h, and then a slower rise to pH ~ 8.5; and (2) a rapid decrease to pH 2-3 among the *potentially acid producing* and *uncertain* shales, which maintained acidic conditions throughout the experiment. Samples in the *uncertain* category and the Bowland (KM) show a slight pH increase at 24h before plateauing at pH 2-4.

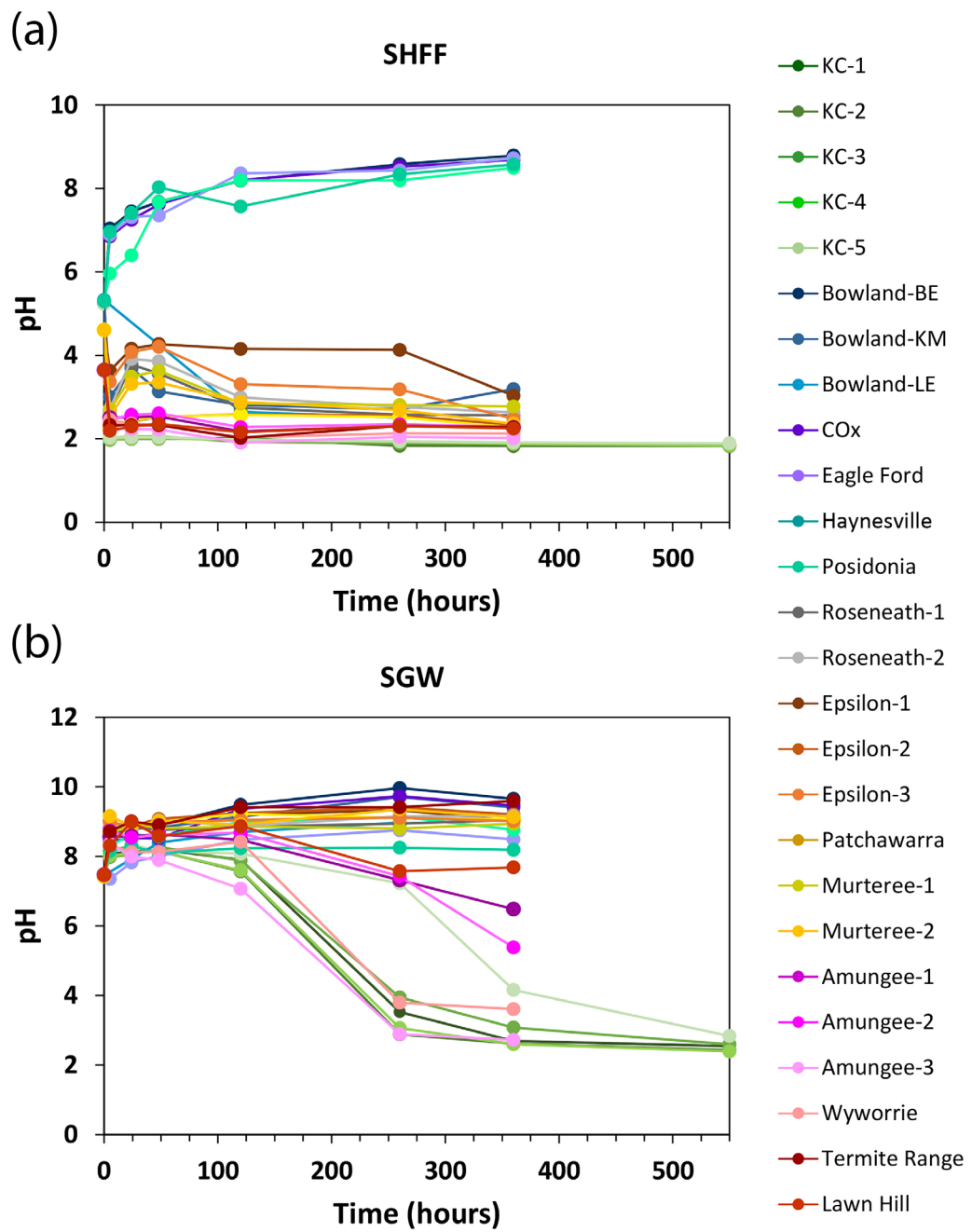


Figure 4.2 Evolution of pH in the experiments with (a) SHFF and (b) SGW.

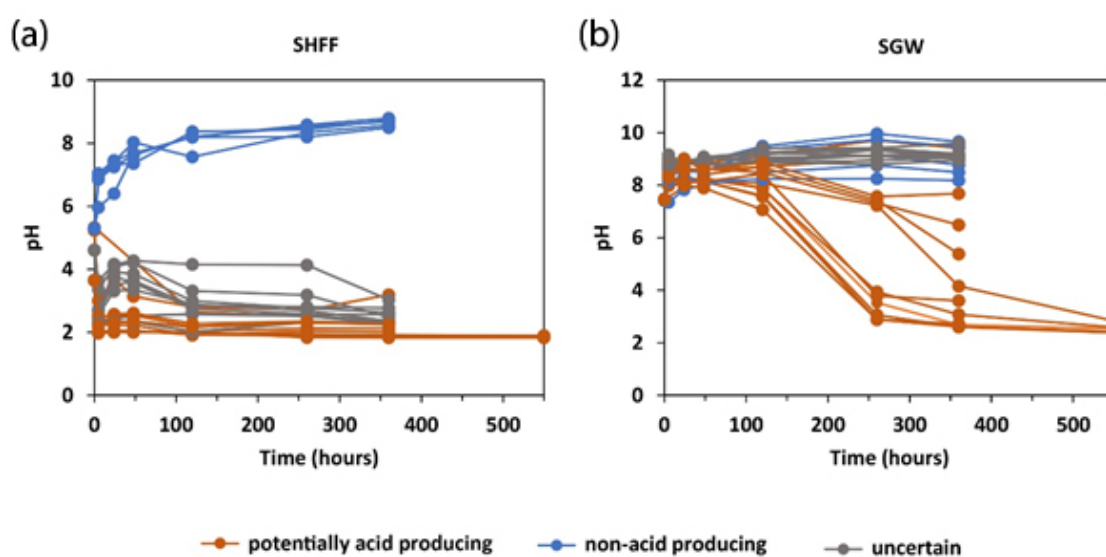


Figure 4.3 pH evolution with samples divided based on their acid neutralisation potential: (a) SHFF experiments, (b) SGW experiments.

The influence of acid neutralisation potential is also apparent in the experiments with SGW (Figure 4.3b). The *non-acid neutralising* as well as *uncertain* samples typically increase the initial pH (~7.5) within the first 5h to pH 8-9 and subsequently maintain it for the remainder of the experiment. Most of the *potentially acid producing* shales deviate from that trend at the 120h time point, when the first drop in pH was recorded. The pH proceeds to further decrease for the remainder of the experiment, although the rate of decrease varies among the samples.

Bowland-KM is the only *potentially acid producing* sample that does not follow this trend, maintaining pH 9-10 throughout the leaching. Bowland-KM divergence in pH behaviour from the other *potentially acid producing* shales in both SGW and SHFF experiments is likely caused by the considerable siderite content (9 wt%). Siderite was not accounted for in the simplified mineral ABA calculations as it may either contribute to the generated acidity or offer some buffering capacity depending on the solution pH (Dold, 2017).

4.4.1.2. Major elements

Generally, the experiments with SHFF tend to yield the highest observed maximum aqueous concentrations (Appendix B) as well as the highest degree of mobilisation for all of the major elements examined (Figure 4.4, Figure 4.5 and Figure 4.6).

Almost all available Ca was released into the SHFF solution at some point during the experiments for all *potentially acid producing* or *uncertain* samples (Figure 4.4). In some instances, the maximum Ca % TRE values exceeded 100%, likely due to heterogeneities among the starting solids.

The *non-acid producing* samples released the highest aqueous Ca concentrations (reflecting the higher concentrations present in these samples), although SHFF generally mobilised less than half of their available Ca content: Bowland (BE) 15% TRE; Eagle Ford 20% TRE; COx 29% TRE; Posidonia 43% TRE; and Haynesville 91% TRE. Haynesville has both the lowest TRE Ca content and the lowest NNP value among non-acid producing shales, which would explain the high maximum degree of Ca mobilisation needed to buffer the acidic SHFF to neutral pH (Figure 4.2a).

Most of the *potentially acid producing* and *uncertain* shales also released nearly all available Mn and Mg into SHFF solution, particularly the Kimmeridge Clay, Bowland (KM), Epsilon-1 to -3, Roseneath-1 and -2, Murteree-2 and Termite Range samples. The main exception was Bowland (LE), where the only maximum of 39 and 35% of available Mg and Mn was released into solution. Note that due to sample availability, this shale was only analysed for two timepoints: 120 and 240h.

The *non-acid producing shales* tended to release the lowest percentage of available Mg and Mn among the sample suite and yielded a correspondingly low element load into solution. Epsilon-1 and -3 released the highest Mg aqueous concentrations, and Epsilon-1 and Roseneath-2 the highest Mn.

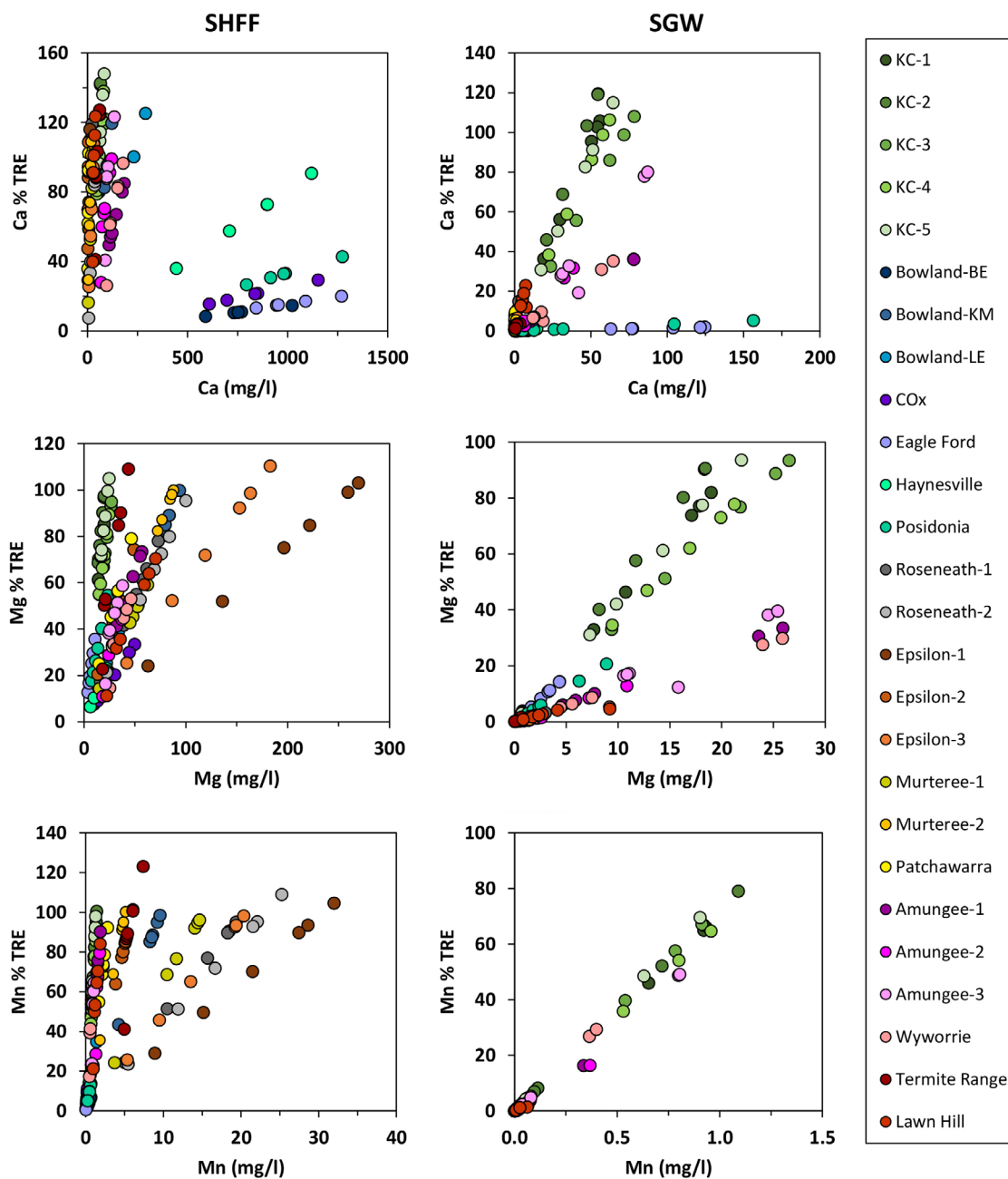


Figure 4.4 Aqueous concentrations of Ca, Mg and Mn in SHFF and SGW experiments (all timepoints) plotted against the total available content of a given element in the solids. Note that graphs have different scales.

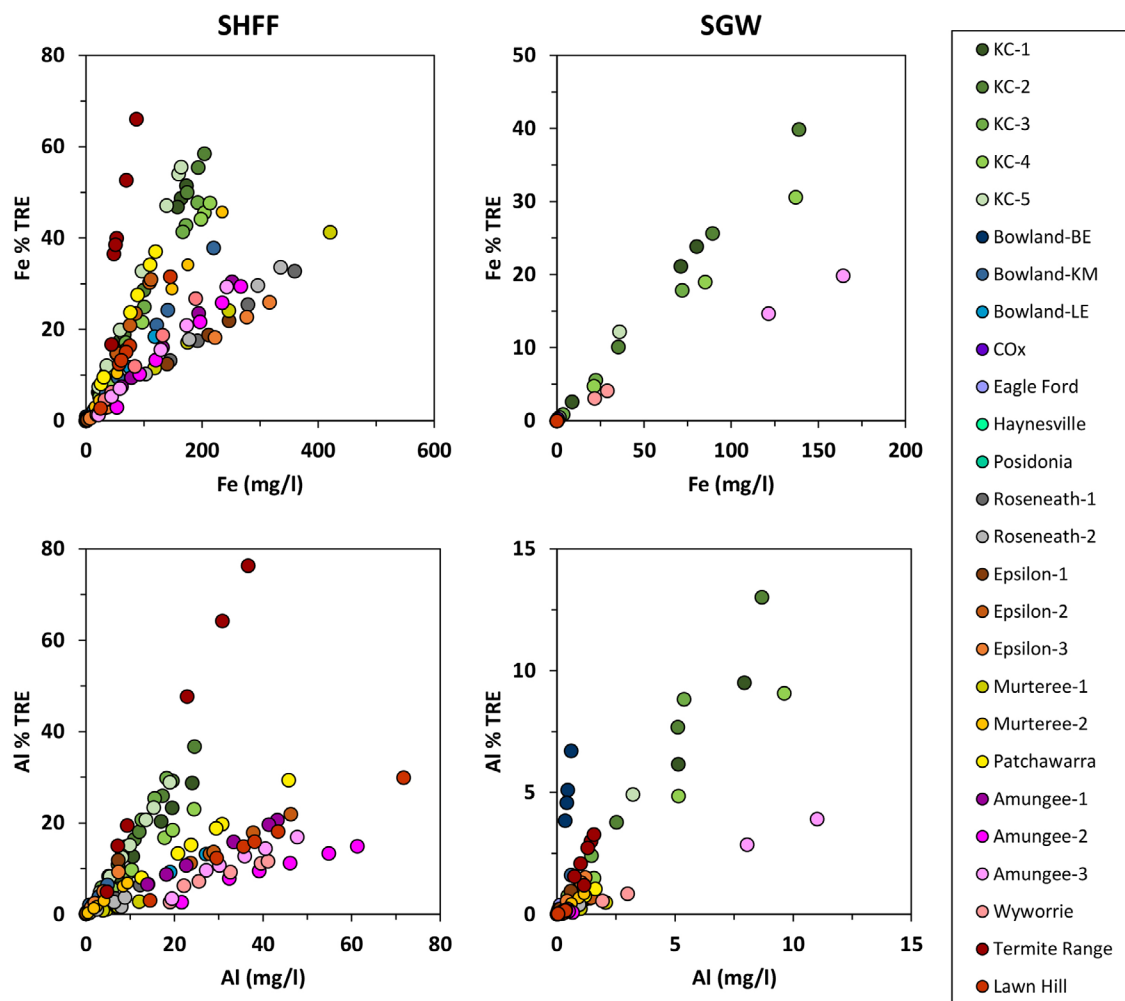


Figure 4.5 Aqueous concentrations of Al and Fe in SHFF and SGW experiments (all time-points) plotted against the total available content of a given element in the solids. Note that graphs have different scales.

Leaching with SHFF generally caused considerable mobilisation of Al and Fe into solution for all but the *non-acid producing* shales (Fig 4.5). The greatest extent of release for both Al and Fe was documented for the Termite Range sample (up to 76% and 66% TRE, respectively) but the highest aqueous concentrations were observed in Lawn Hill sample for Al (72 mg/l, 30% TRE) and Murteree-1 for Fe (420 mg/l, 41% TRE).

For the experiments with SGW, two trends in major element mobilisation are visible. Firstly, for most shales, SGW tests yield much lower aqueous Ca, Mg, Mn, Al and Fe concentrations than SHFF ones (Figure 4.4 and 4.5).

In contrast, Kimmeridge Clay (KC-1 to KC-5), Amungee-1 to -3 and Wyworrie samples consistently show a much higher degree of major element mobilisation in the SGW tests than other samples. In particular, almost all available Ca, Mg and ~70% of Mn in the Kimmeridge Clay samples is released into solution. These are also the only samples where Fe is present in the SGW leachate. The highest aqueous concentration was documented for Amungee-3 sample, reaching 164 mg/l (20% TRE), followed by 139 mg/l released from the KC-2 sample (40% TRE).

Little to no Fe was detectable into the solution for *non-acid producing* shales for both SHFF and SGW tests as well as for all other samples maintaining an alkaline pH during leaching with SGW. This indicates that either no Fe was mobilised from these shales or, due to the presence of O₂ in the system and the alkaline pH maintained during the experiment, the released Fe was quickly oxidised and precipitated as ferric(oxy) hydroxides (see 3.3). The high aqueous concentrations and the extent of release of S for all shales in the SGW leachates suggest the latter to be the more likely explanation (Figure 4.6). Sulfur was detectable in the solution for all shales throughout the time series, with only 3% of data points <DL, all within 48 h from the start of the leaching. Shales in the *uncertain* group mobilised at least half of their available S content, ranging from up to 49% TRE for Murteree-1 (3 mg/l) to 102% TRE for the Termite Range (20 mg/l), but their maximum S concentrations in solution were the lowest observed. This is consistent with their mineralogy, which lacks sulfide minerals in quantities detectable by XRD.

A similar percentage of the available S content was also mobilised from the *non-acid producing* and *potentially acid producing* shales but the released aqueous S concentrations were substantially higher. The *potentially acid producing* shales released the highest observed aqueous S, reaching 453 mg/l from KC-4 sample (89% TRE). Aqueous S concentrations were lower for the *non-acid producing* samples, with Posidonia recording the most at 298 mg/l (60% TRE). Pyrite and marcasite are the only sulfides present in the *non-acid producing* and *potentially acid producing* samples, and therefore the high release

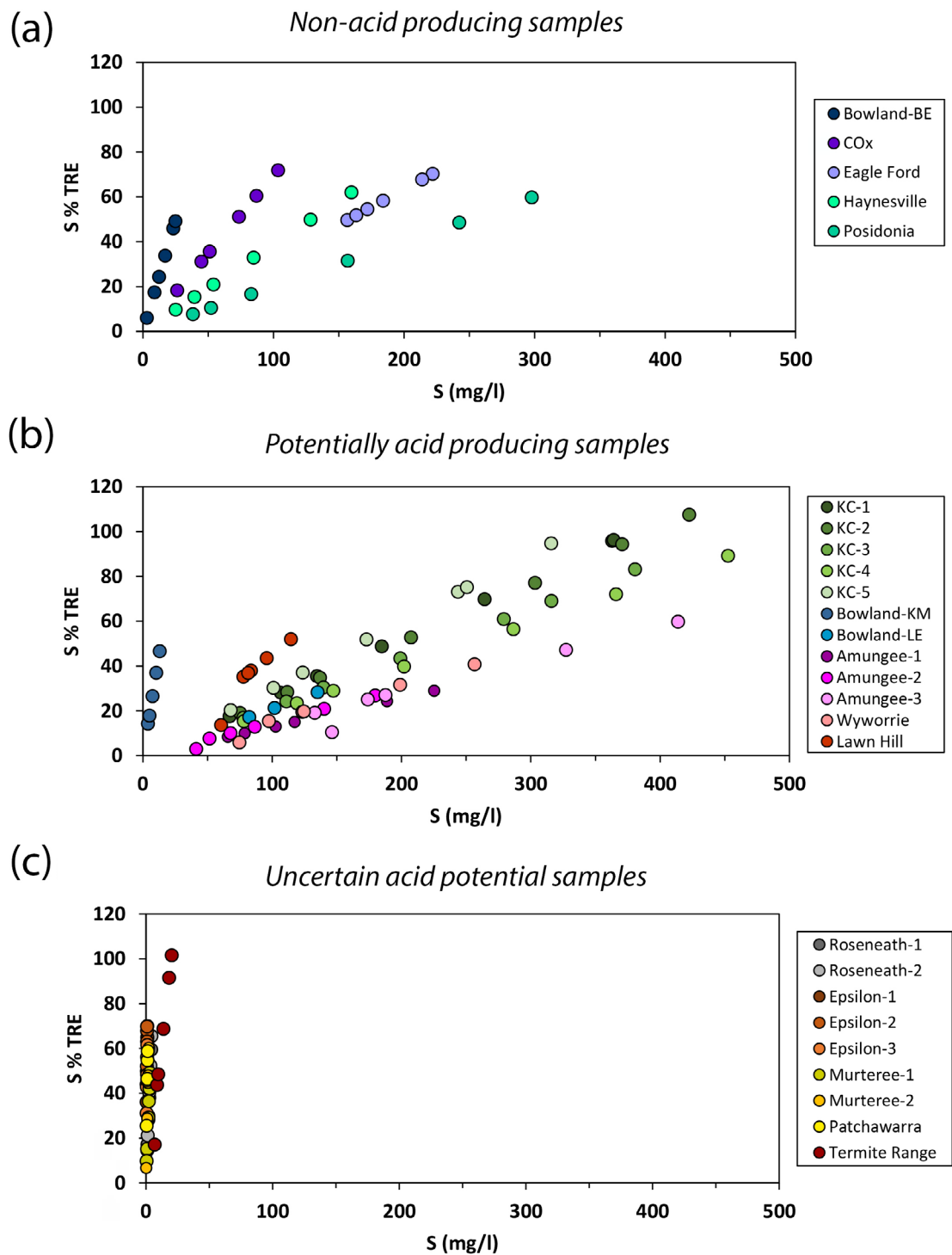


Figure 4.6 Aqueous concentrations of S in SGW experiments (all timepoints) plotted against the total available S in the solids for: (a) non-acid producing samples; (b) acid producing samples; and (c) uncertain samples.

of S into the solution can be attributed to the dissolution of these minerals.

Iron was likely continuously mobilised from all the pyrite-bearing shales throughout the SGW experiments due to pyrite oxidation and from siderite dissolution where the mineral was present. However, when the pH of the system was alkaline, it rapidly oxidised and precipitated as secondary Fe minerals. Conversely, the drop in pH observed in most *acid-producing* samples decreased the rate of Fe²⁺ to Fe³⁺ oxidation, which allowed the released Fe to remain in solution.

Sulphur concentrations could not be measured for the experiments with SHFF, due to ammonium persulfate; however, it is likely that the contact with SHFF has also induced oxidative dissolution of pyrite. It is also likely that pyrite oxidation is greater in the SHFF experiments with samples that could not buffer the pH to circum-neutral given that at lower pH values dissolved Fe(III) will act as an additional oxidant (see 3.3).

4.4.1.3. Trace elements

Some of the trends visible for major elements also present for trace elements, but they tend to be less clear and more varied among the samples regardless of their ABA group. This is likely because trace elements in shales can be hosted as impurities in numerous minerals as well as the organic matter, and where they are hosted depends on the conditions and processes prevailing during the sediment deposition and diagenesis (Abanda and Hanigan, 2006). For example, U, Mo, Co and Ni are generally associated with organic matter (e.g. Tribovillard et al., 2006; Vine and Tourtelot, 1970), but As, Co, Ni and Mo can also be incorporated into authigenic sulphides, e.g. pyrite and arsenopyrite (Gregory et al., 2015; Parnell et al., 2016; Tribovillard et al., 2006). Uranium can be hosted in silicate minerals, phosphates, carbonates and adsorbed to clay particles in shales (Jew et al., 2020; Phan et al., 2016). A sequential extraction study on Marcellus shale samples showed that up 20% of the total U was associated with carbonates (Phan

et al., 2016). Arsenic and V are redox-sensitive elements typically linked to deposition in oxygen-depleted waters, and hosted in organic matter or sulphides (Bodin et al., 2007; Tribovillard et al., 2006); however, they can also be sorbed onto clays in offshore marine environments (Tourtelot, 1965). Furthermore, heavy minerals, such as apatite or Fe-oxides, which typically occur at concentrations below the resolution of XRD analysis (<1 wt%), can be sources of trace elements in shales, such as U, V, Cr or Th (Totten and Hanan, 1998; Totten and Hannan, 2007). Consequently, more than one mineral can contribute to trace element release into the solution and a given trace element may be hosted in different minerals irrespective of the sample's ABA classification.

In general, SHFF yielded higher aqueous concentrations in solution than SGW for the majority of trace elements for most of the shales (Figure 4.7 to 4.9). High degrees of mobilisation in the SHFF leaching, with averages ranging from 36 to 57% of the total element content, were observed especially for Cd, Co, Cr, Cu, Li, Ni, Sr, Tl and Zn. In particular, all or nearly all available Co, Li, Ni and Zn was released into solution by Kimmeridge Clay samples and most of the shales from the *uncertain* ABA group. Approximately all of the available Cd was mobilised from Kimmeridge Clay KC-1 to KC-5 samples, Lawn Hill, Amungee-1 to -3, Wyworrie and Cooper Basin samples, apart from Epsilon-1. The maximum aqueous concentrations for Cd, Cu, Ni, Tl and Zn were recorded for the Beetaloo Sub-basin samples, Wyworrie in particular, often significantly surpassing concentrations released by the other shales. For example, the highest maximum Cu concentration was 2790 ug/l for Wyworrie, followed by 1678 ug/l from Patchawarra. Similarly, Termite Range released the most Cr into the solution – up to 58% TRE and 3039 ug/l, more than other samples.

Non-acid generating shales released the lowest percentage of their total Co, Cr, Cu, Li, Ni, and Zn content among the samples, and often recorded some of the lowest maximum aqueous concentrations of these elements. However, they mobilised significantly higher Sr concentrations into solution than other shales, particularly COx (up to 9105 ug/l, 90 %TRE).

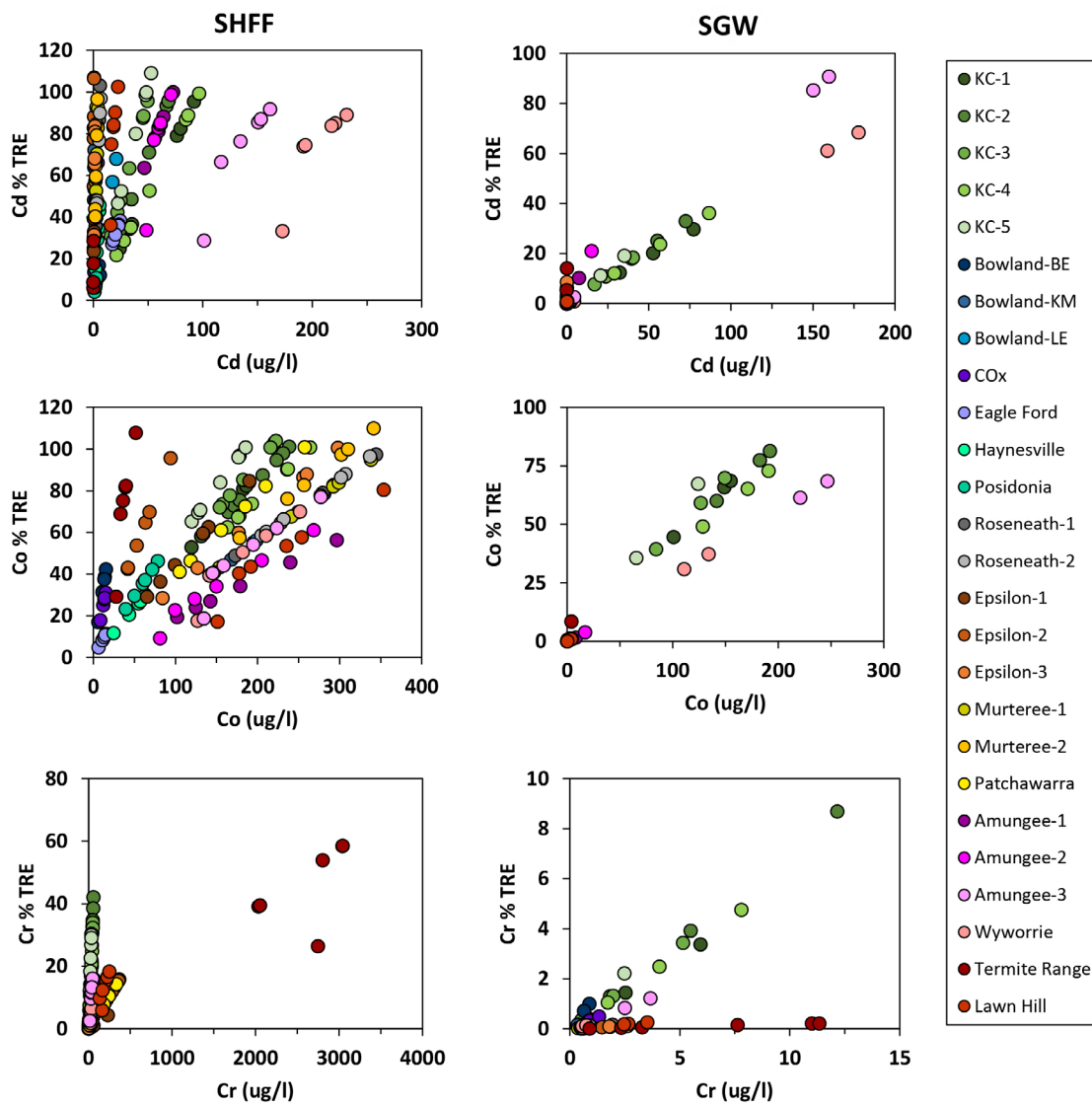


Figure 4.7 Aqueous concentrations of Cd, Co and Cr in SHFF and SGW experiments (all timepoints) plotted against the total available content of a given element in the solids. Note that graphs have different scales.

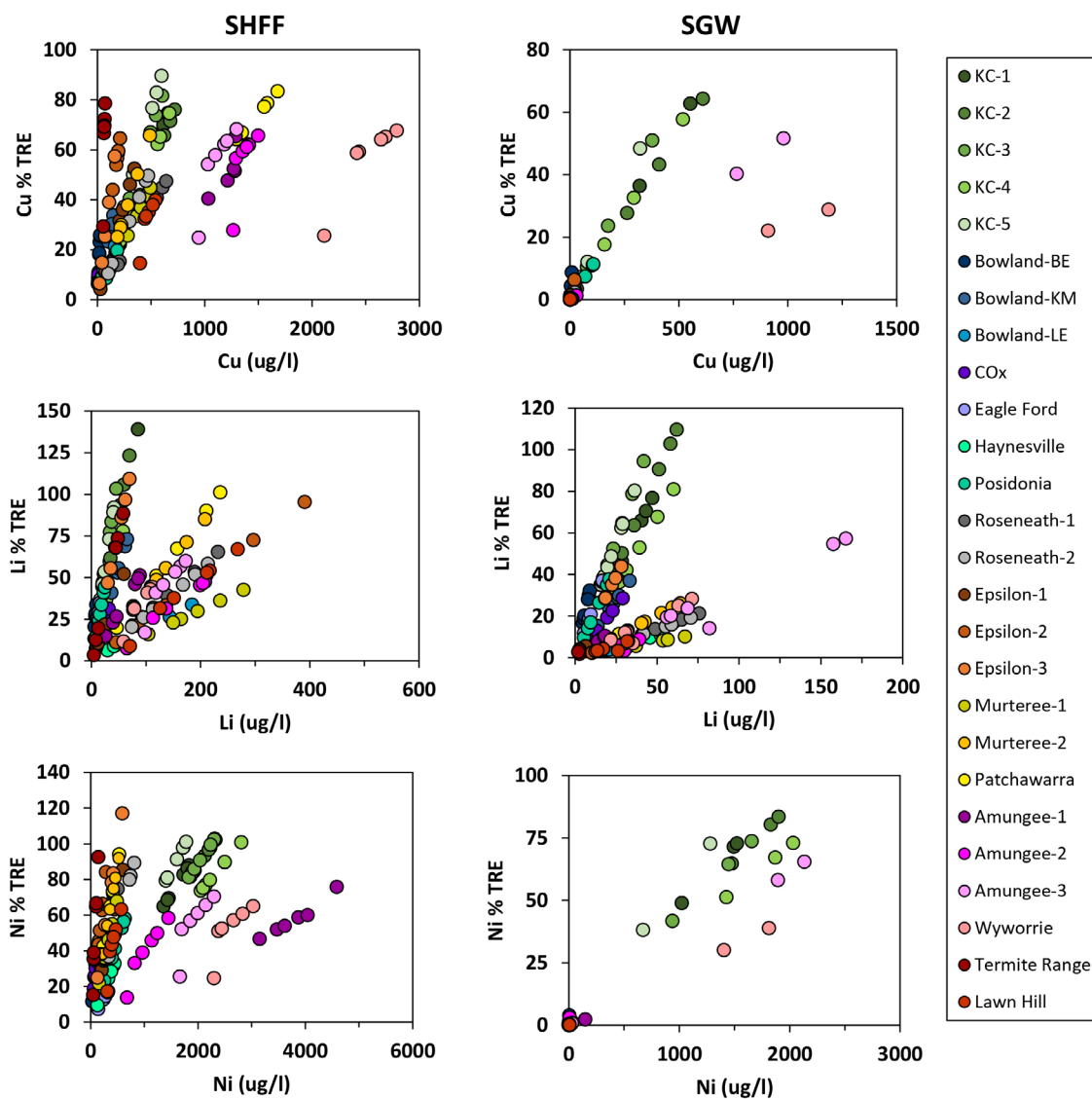


Figure 4.8 Aqueous concentrations of Cu, Li and Ni in SHFF and SGW experiments plotted against the total available content of a given element in the solids. Note that graphs have different scales.

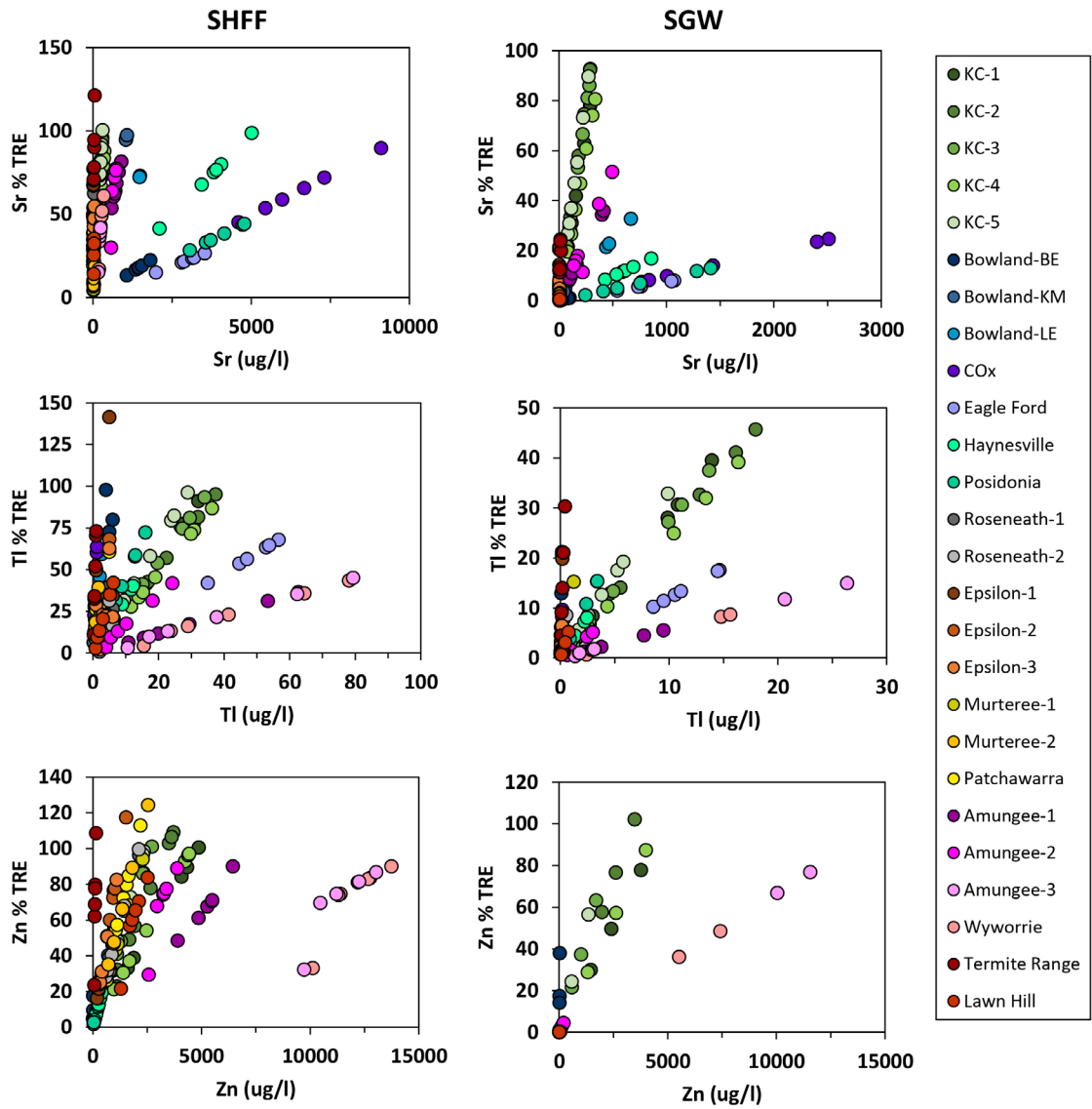


Figure 4.9 Aqueous concentrations of Sr, Tl and Zn in SHFF and SGW experiments plotted against the total available content of a given element in the solids. Note that graphs have different scales.

In the SGW tests, *non-acid generating* samples also released little to no Cd Co, Cr, Ni and Zn, on average <4% of the total element content in the samples. Both leaching fluids mobilised approximately the same amounts of Cr, Li and U from these shales.

Kimmeridge Clay and Beetaloo Sub-basin samples consistently showed higher release (% TRE) of major elements for SGW than other shales, and the same trend can be observed for the following trace elements: Cd, Co, Cr, Cu, Li, Ni, Sr and Tl. SGW released almost the same maximum amounts of Cd and Li from Kimmeridge Clay samples as SHFF.

Lastly, a few elements displayed distinct mobilisation trends (Figure 4.10 and Figure 4.11). Molybdenum was more impacted by SGW, which mobilised more of the total Mo and Sb content and yielded higher aqueous concentrations of each element (Figure 4.10). Cooper Basin shales released up to 1% of total Mo into SHFF, but between 23% and 80%

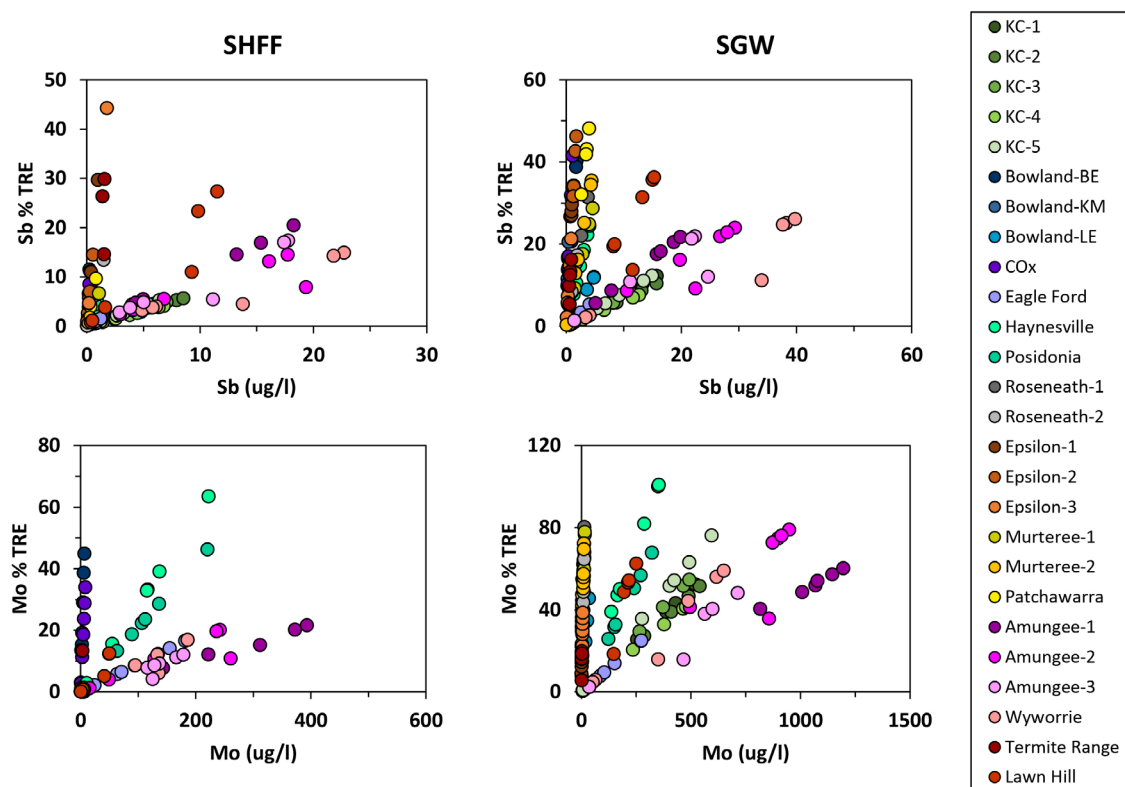


Figure 4.10 Aqueous concentrations of Sb and Mo in SHFF and SGW experiments plotted against the total available content of a given element in the solids. Note that graphs have different scales.

for SGW depending on the sample. The highest total Mo for both fluids was released by Haynesville shale: 64% TRE and 222 ug/l for SHFF, and 100 %TRE and 350 ug/l for SGW. However, the highest aqueous concentrations were recorded for Amungee-1: 393 ug/l (22% TRE) for SHFF, and 1196 ug/l (60% TRE) for SGW.

For As, overall greater mobilisation was observed for SGW (Figure 4.11): SGW leached up to 36% more As from COx, Epsilon-2 and Patchawarra samples, with the latter releasing the highest recorded aqueous concentration and % TRE of As into the SGW solution (146 ug/l, 39% TRE). SHFF had more impact on Kimmeridge Clay samples, mobilising up to 30% more As than SGW from them; the highest aqueous As concentration in the SHFF leachates was recorded for KC-4 at 252 ug/l (31% TRE).

Uranium was generally more susceptible to mobilisation in the experiments with SHFF; however, even leaching with SGW mobilised almost all available U from the Kimmeridge Clay samples.

SHFF mobilised much more V from Kimmeridge Clay samples than SGW (up to 34% more), and the highest V concentrations were recorded for Amungee-1 and Wyworrie samples (608 ug/l and 589 ug/l, respectively). Conversely, SGW released more of the total V from Bowland (KM), followed by Cooper Basin and Eagle Ford samples.

4.4.2. Effect of leaching time on elemental release into solution

These results demonstrate that the choice of leaching fluid will impact total element release into solution, with SHFF typically causing greater element mobilisation from the shale samples, but not for all elements. However, the time point at which the elements became present in solution during the experiments and how their concentrations evolved is a crucial factor for assessing contaminant release. The results of previous laboratory studies indicate that some geogenic contaminants may be initially released

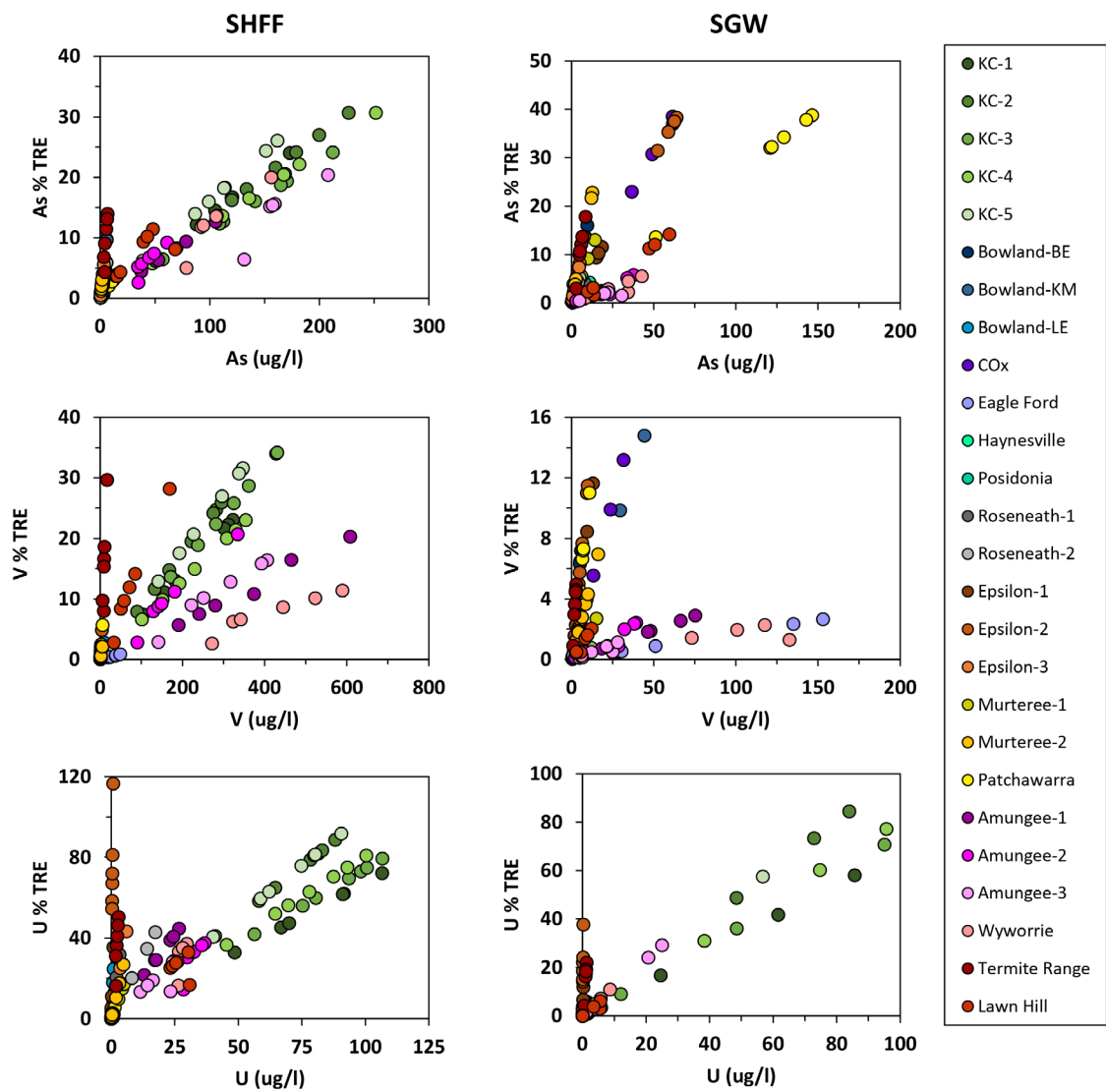


Figure 4.11 Aqueous concentrations of As, V and U in SHFF and SGW experiments plotted against the total available content of a given element in the solids. Note that graphs have different scales.

into solution before being sequestered during precipitation of secondary phases (see section 2.2).

The temporal evolution of element concentrations over the 300-500 hour duration of the leaching tests with SHFF and SGW will be discussed based on how much of a given sample's total element content was released into the solution to facilitate comparison among the different samples.

4.4.2.1. SGW

During the SGW experiments, the Kimmeridge Clay and Beetaloo Sub-basin samples displayed a markedly different temporal release behaviour compared to the remaining samples for most elements.

In all shales, little to no Mn, Fe, Cd, Co, Cu, Ni, U and Zn were initially mobilised (Figure 4.12) At the 120h timepoint, however, concentrations of these elements started rapidly increasing for the Kimmeridge Clay and Beetaloo samples, while for the other shales concentrations of these elements remained low and plateaued. A similar trend can be observed for Ca and Mg, however, Kimmeridge Clay samples experience a high initial release of 31 to 46% of their total Ca and Mg content, before decreasing to approximately 3% at 24h, and then increasing again to 48-65% TRE at 120h.

The increased mobilisation of elements in solution coincided with a decrease in solution pH (Figure 4.2). Continuously rising S concentrations, up to 100% of the total S content in the shales for Kimmeridge Clay, indicate that pyrite dissolution must have occurred throughout the SGW experiments for all pyrite-bearing samples (Figure 4.13). Even *non-acid producing* shales show a rising S release trend, and the only S-minerals they contain are pyrite or gypsum, the latter only present in Eagle Ford and Haynesville samples. As Kimmeridge Clay and Beetaloo samples are *potentially acid producing*, it

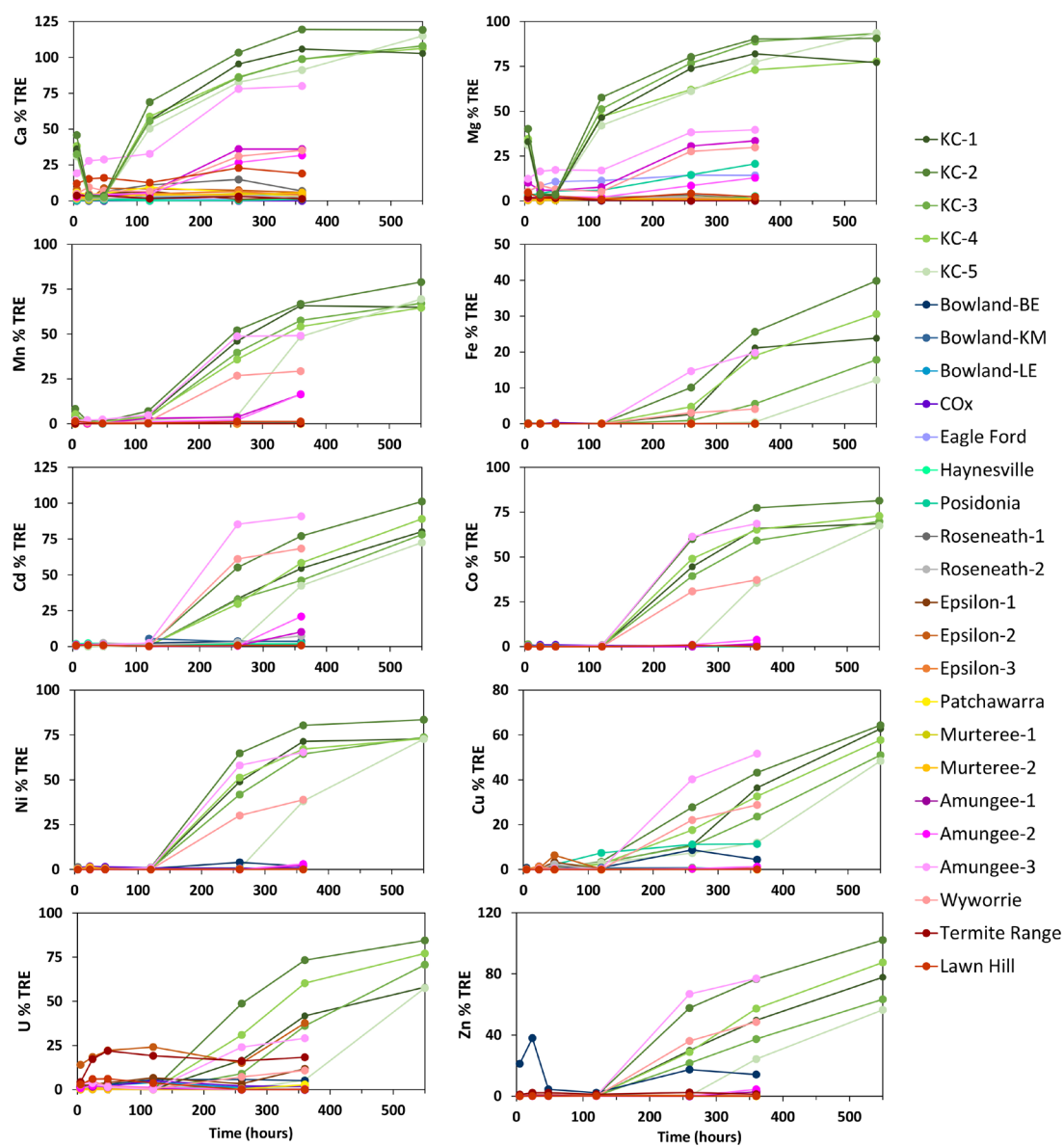


Figure 4.12 Amount of total available element content mobilised over time in the SGW experiments for Ca, Mg, Mn, Fe, Cd, Co, Cu, Ni, U and Zn. Note that y axis has different scales among the graphs.

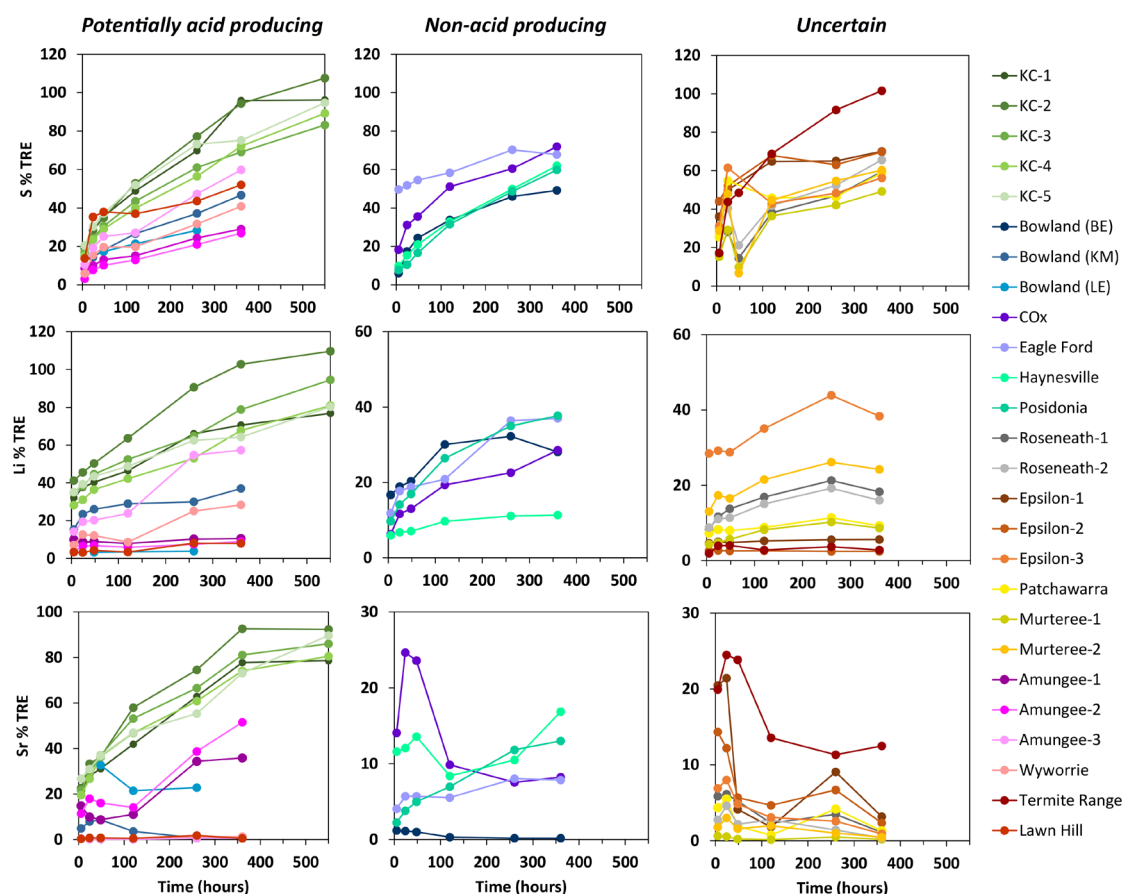


Figure 4.13 Amount of total available element content mobilised over time in the SGW experiments for S, Li and Sr. Shales are grouped by their acid neutralisation potential. Note that y axis has different scales among the graphs.

is likely that the drop in pH observed at 48-120h experiment time was caused when acid generation by pyrite oxidation surpassing the buffering capacity of the SGW. The acidification of the solution, in turn, allowed several trace metals such as Cd, Co, Cu and Ni, which could have been mobilised directly from pyrite, to remain in solution.

Several other trace elements were mobilised from all samples during the experiments, and not just the *potentially acid producing* ones that display a drop in pH.

Lithium and Sr were continuously mobilised into solution over the duration of the leaching experiment not only from the Kimmeridge Clay and Beetaloo samples, but

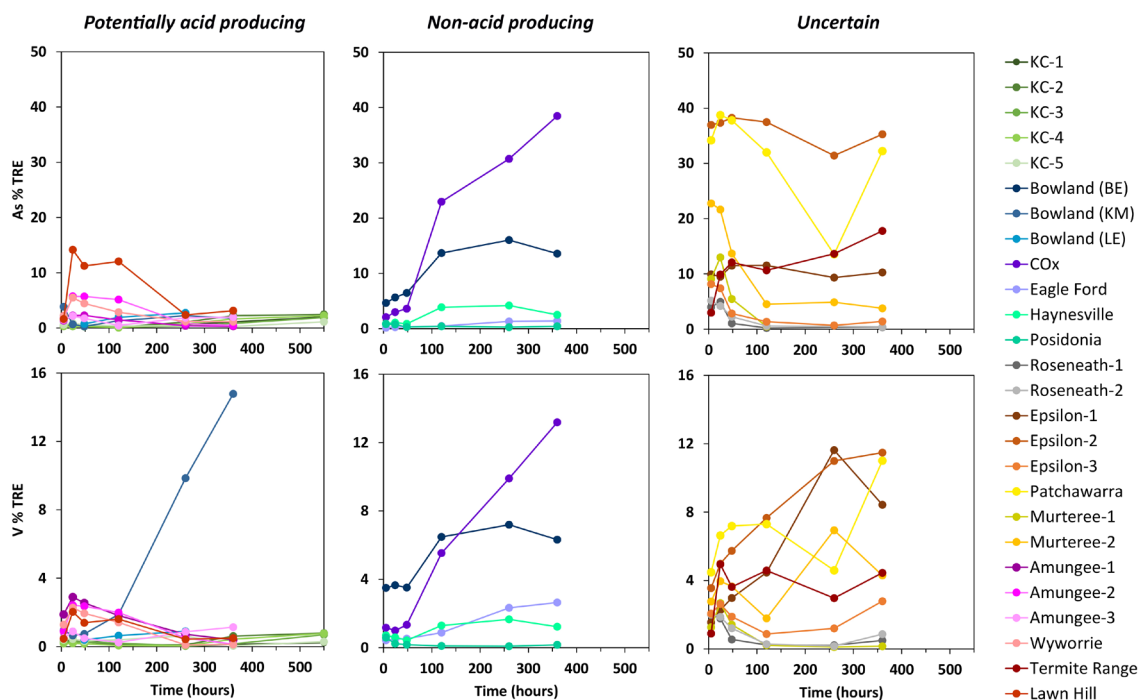


Figure 4.14 Amount of total available element content mobilised over time in the SGW experiments for As and V. Shales are grouped by their acid neutralisation potential. Note that y axis has different scales among the graphs.

also from the remaining shales (Figure 4.13). In particular, Kimmeridge Clay showed an increasing trend, releasing between 80-100% of available Li and Sr by 550h. Less than half of the available Li and Sr were released by the non-acid producing and uncertain shales. After the initial release within the first 48h, Li concentrations appear to either plateau or show a gentle increase. Strontium, on the other hand, fluctuated in solution, with some samples exhibiting a decreasing trend after the initial release within 48 h, e.g. COx, Epsilon-1, Termite Range.

Conversely, the release of As and V did not appear to be directly related to the ABA groups, although the *potentially acid generating* samples generally show the lowest release of both elements, except for V in Bowland (KM) (Figure 4.14). Dissolved concentrations of both elements fluctuated during the experiments, but several samples showed an overall decreasing, e.g. Lawn Hill or Epsilon-3.

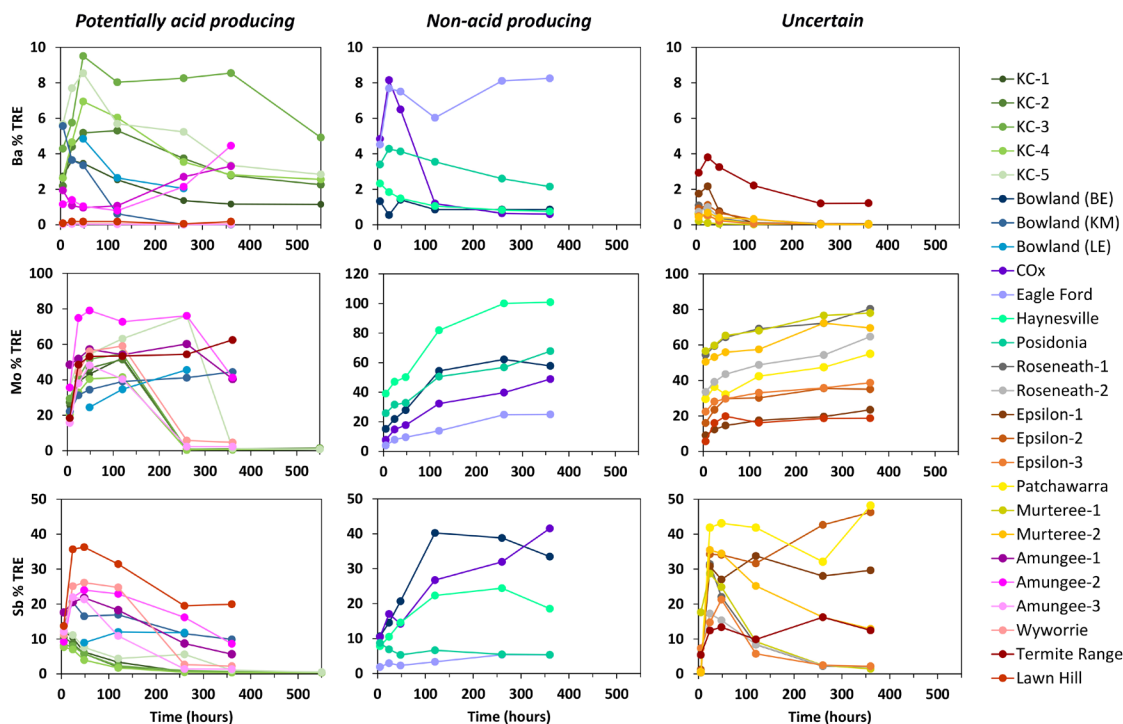


Figure 4.15 Amount of total available element content mobilised over time in the SGW experiments for Ba, Mo and Sb. Shales are grouped by their acid neutralisation potential. Note that y axis has different scales among the graphs.

After an initial release, a clear decreasing trend was evident for the majority of the shales for Ba, and for Mo and Sb for the *potentially acid producing* samples (Figure 4.15). A large portion of total Mo released from the *non-acid producing* and *uncertain* shales usually occurs within the first 5h from the start of the leaching, and subsequently either plateaus or rises in small increments. The reduction in dissolved Mo concentrations for Kimmeridge and Beetaloo samples once again coincided with the drop in pH, whereas the decrease in mobilised Sb happens immediately following the first measurement time point (5h).

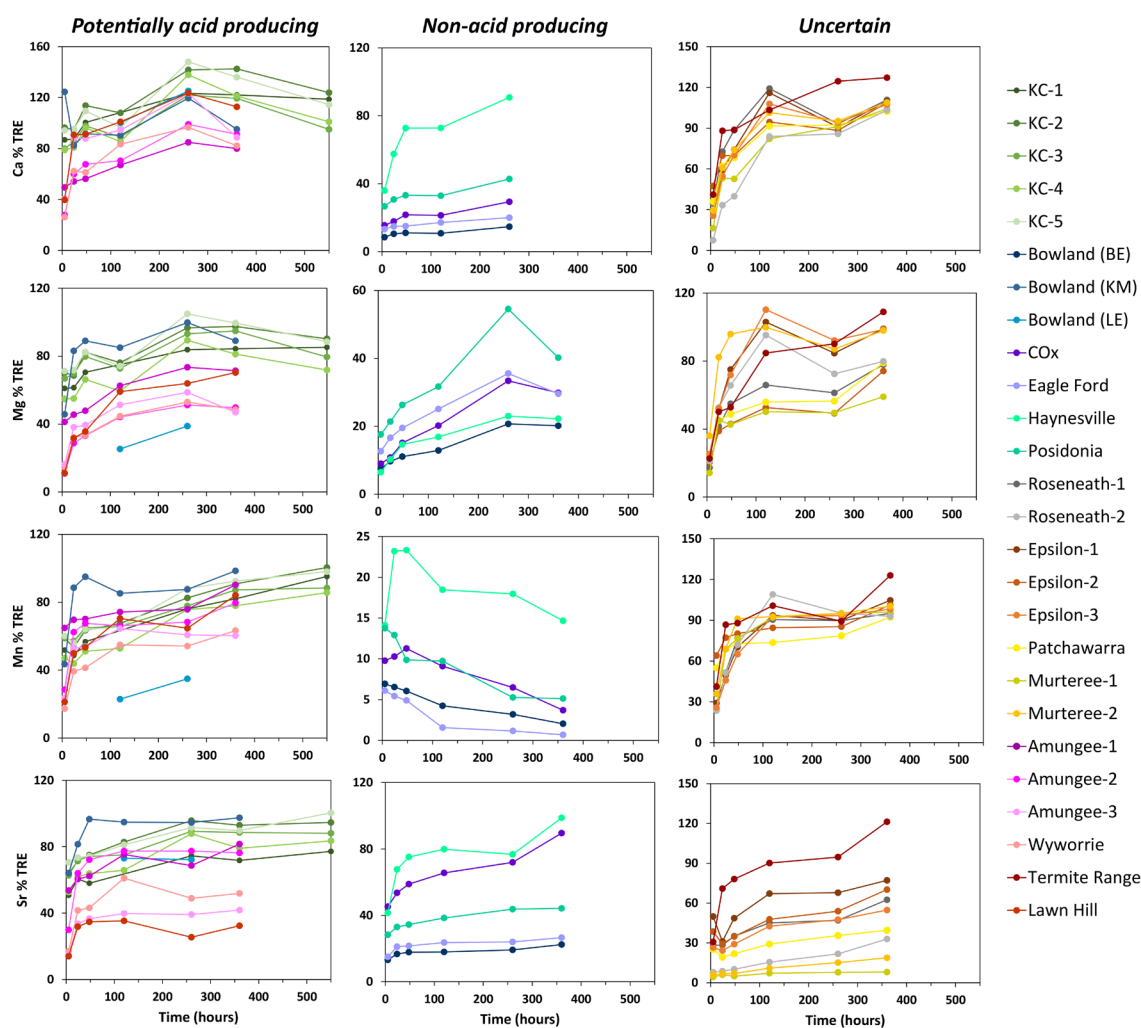


Figure 4.16 Amount of total available element content mobilised over time in the SHFF experiments for Ca, Mg, Mn and Sr. Shales are grouped by their acid neutralisation potential. Note that y axis has different scales among the graphs.

4.4.2.2. SHFF

Dissolved concentrations of Ca, Mg, Mn, Cd, Co, Cu, Li, Ni, Sr, U, V and Zn generally showed a rapid release into solution often leading to a plateau for the *potentially acid generating* and *uncertain* shales. Several samples released all of their total available content for some of these elements (Figure 4.16), e.g. all Kimmeridge Clay, Cooper Basin and Mt Isa samples, and Bowland-KM, Bowland-LE samples released all their total available Ca. In contrast, following the initial mobilisation within the 48h, the dissolved concentration of Ba, Mo and Sb decrease over time at various rates for all of

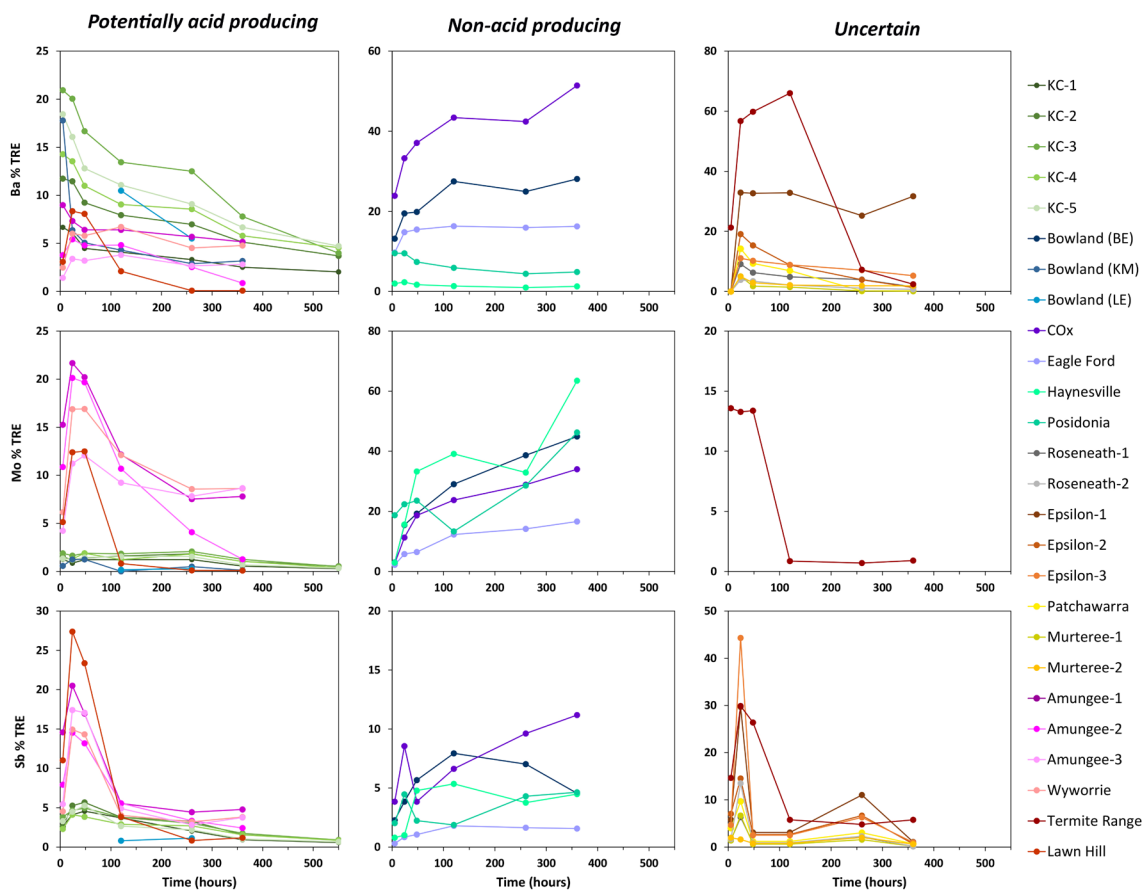


Figure 4.17 Amount of total available element content mobilised over time in the SHFF experiments for Ba, Mo and Sb. Shales are grouped by their acid neutralisation potential. Note that y axis has different scales among the graphs.

the *potentially acid producing* and *uncertain shales* (Figure 4.17).

Concentrations of other elements tend to show varying trends among the shales from *potentially acid producing* and *uncertain* groups. Aluminium generally increases over time, but its levels fluctuated sporadically among some shales. Iron showed an increasing mobilisation with time for Kimmeridge Clay, Bowland (LE) and Beetaloo samples, but decreased after a fast initial release for Bowland (KM) and the *uncertain* shales (Figure 4.18). This quick initial Fe mobilisation is likely due to the dissolution of siderite, an iron carbonate which would dissolve rapidly upon exposure to oxygenated and acidic SHFF.

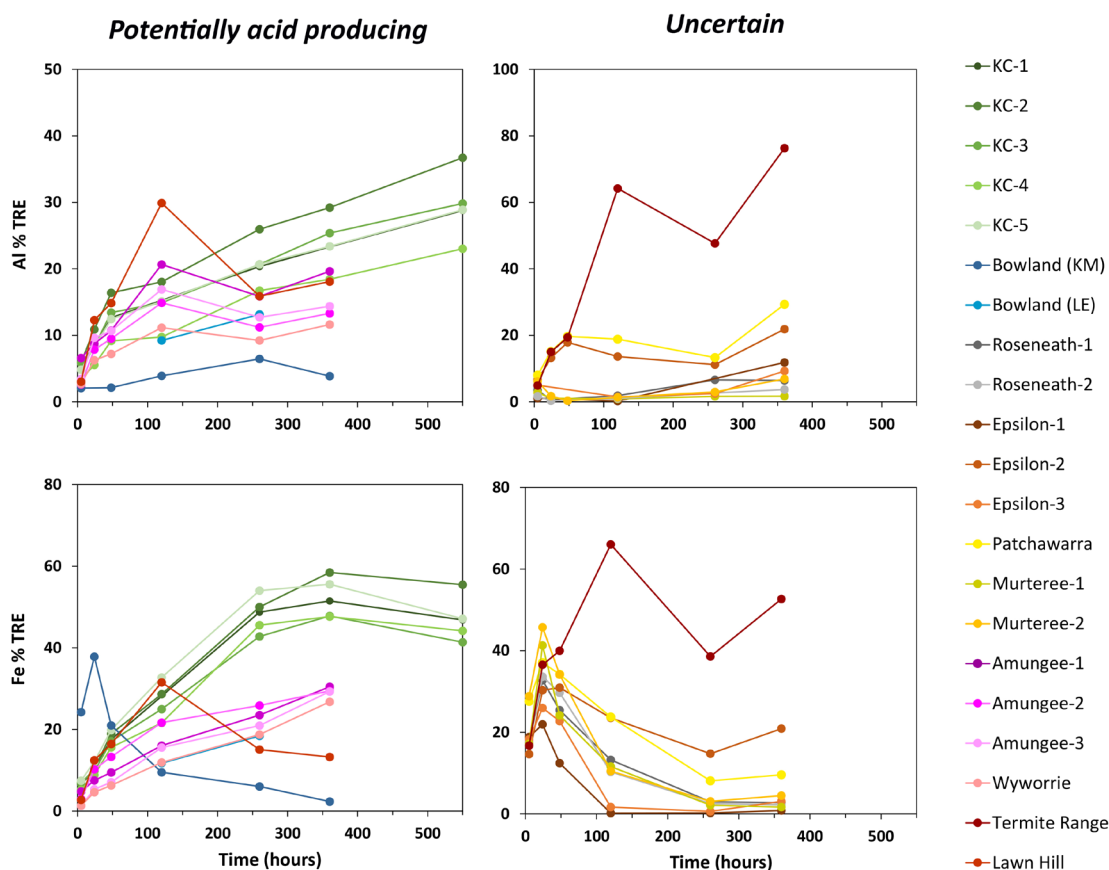


Figure 4.18 Amount of total available element content mobilised over time in the SHFF experiments for Al and Fe. Shales are grouped by their acid neutralisation potential; non-acid producing shales mobilised little to no Al and Fe into solution. Note that y axis has different scales among the graphs.

Several of the Cooper Basin samples showed a temporary decrease in dissolved concentrations of As, Cd, Cr, Cu and Zn at 24-48h, before increasing again.

The *non-acid producing* shales generally behaved differently than the *potentially acid producing* and *uncertain* shales. Mobilisation of Ca and Sr from non-acid producing shales was at first rapid, before more or less plateauing within 48 h. The only exception was Haynesville shale, which released 73% of its total Ca content within 48 h, rising to 91% at 260 h. The Haynesville sample has both the lowest TRE Ca content and the lowest NNP value among the *non-acid producing* shales, and likely required a higher degree of Ca mobilisation to buffer the acidic SHFF to neutral pH (Figure 4.2a). The dissolved Ca concentrations at 360 h surpassed the maximum DL, indicating that Ca

continued to increase incrementally. Magnesium increased gradually until 260 h and subsequently slightly decreased. Conversely, Mn showed an overall decreasing trend after the initial release.

The amount of total available Co, Cd, Cu, Li, Ni and Zn mobilised from *non-acid producing* shales was generally much lower than from the other samples. The elements often displayed a fast release within the first 48 h, before plateauing at more or less stable values. Cobalt and Cu showed a decrease towards the end of the leaching.

Lastly, while Ba, Mo and Sb showed a strong decreasing trend for the *potentially acid producing* and *uncertain* shales, their concentrations were generally increasing over time for the *non-acid producing* ones.

4.4.2.3. Trace element sources and mobility in solution

While both SGW and SHFF can mobilise elements into solution, the latter often mobilises elements to a much greater extent. However, attributing aqueous solute concentrations, especially for trace elements, to specific mineral dissolution-precipitation reactions is problematic. Shales have complex mineralogy, and many elements may be hosted in multiple minerals, likely with different reactivities, which might contribute to the observed element release at different times and conditions. Mineral dissolution might be incongruent, and elements might be concurrently released and removed from the solution due to precipitation of secondary phases. Multiple lines of evidence, for example, chemical modelling, multivariate statistical analysis and high-resolution characterisation of minerals hosting trace metals in shales, would be needed to infer any relationship between aqueous trace element concentrations and minerals that might have caused their release. These are beyond the scope of this project.

Some of the dissolved trace elements were likely released during the dissolution of pyrite and carbonate minerals. Dissolution of pyrite was inferred from the continuously rising

aqueous S concentrations in the SGW experiments among the *potentially acid producing* and *non-acid producing* shales, up to 100% S content in Kimmeridge Clay samples. Pyrite and marcasite (polymorphs of FeS_2) are generally the only sulfides present in the *non-acid producing* and *potentially acid-producing* samples, and therefore the high release of S into the solution can be primarily attributed to dissolution of these minerals. Due to the addition of ammonium persulfate, S concentrations could not be measured easily in the experiments with SHFF; however, it is likely that oxidative dissolution of pyrite also occurred during SHFF leaching.

Pyrite dissolution eventually surpassed the buffering capacity of the SGW, causing acidification of the solution among the Kimmeridge Clay and Beetaloo samples, which lack any neutralisation potential themselves. Aqueous concentrations of several elements, such as Cd, Co, Cu and Ni, increased concurrently with the observed pH drop (see Figures 4.2, 4.4 and 4.12).

Mobility of trace elements is usually strongly affected by the pH of the surrounding environment (as well as the redox potential). The solubility of most metals that occur as cations (e.g. Ni, Cu, Zn, Cd, Al, Fe) is greatest under acidic conditions, although some metals (e.g. Zn and Fe) display amphoteric behaviour and can become mobile again at alkaline pH. Conversely, the solubility of anion-forming elements (e.g. As, Mo, S, Sb, Cr) tends to increase with higher pH values (Langmuir et al., 2004). This pH dependence likely played a factor in the observed differences in element mobilisation trends between *potentially acid producing*, *uncertain* and *non-acid producing* shales. For example, Mo and Sb were mobilized by SHFF to a much greater extent from the *non-acid producing* shales, which buffered the SHFF pH to alkaline. On the other hand, SHFF generally caused a greater release of cationic metals from *potentially acid producing* and *uncertain* shales, where the leachate pH was acidic.

Several of the experimental studies reviewed in Chapter 2 reported an initial release and subsequent decrease in solution of some PTEs such as Co, Cr, Cu, Ni, attributing it

to adsorption at the surface/coprecipitation with secondary minerals, particularly (oxy) hydroxides (e.g. Harrison et al., 2018; Marcon et al., 2017; Wilke et al., 2015). All of the studies used their own synthetic fracturing fluids.

This pattern of element mobilization was also observed in this research. In the SHFF experiments, dissolved concentrations of Mn, Co and Cu decreased over time for the *non-acid producing* leachates, and Ba, Mo and Sb for the *uncertain* and *potentially acid producing* ones. Aqueous Fe concentrations also decreased among the *uncertain* shales as well as Bowland-LE and Lawn Hill ones from the *potentially acid producing* group.

Molybdenum and Sb are relatively mobile in oxidizing environments, but tend to be immobilized through sorption to Mn and Fe-oxides under acidic to neutral conditions (Langmuir et al., 2004), which would explain lower release into solution and decreasing aqueous concentrations for both elements among the *potentially acid producing* and *uncertain* shales.

Reduction of aqueous Mn concentrations after the initial release in the *non-acid producing* leachates is consistent with Mn behaviour under alkaline pH (~8), which promotes formation of Mn-oxides. Removal of aqueous trace elements such as Zn, Co and Ni by Mn-oxides through adsorption/coprecipitation processes have been documented upon neutralisation of acid mine drainage waters (e.g. Fuller et al., 2000; Kay et al., 2001; Lee et al., 2002). Additionally, the absence of detectable Fe in *non-acid producing* leachates (despite likely pyrite oxidation), and the decreasing aqueous Fe concentrations among some of the other shales, indicate that secondary Fe-phases likely precipitated during the experiments. Orange particulate residue was observed visually in a number of reacted vials, particularly for the Bowland-KM and Cooper Basin shales after 120h of leaching with the SHFF, indicating iron oxyhydroxide formation. Iron precipitates, also well documented in the acid mine drainage literature, can form over a much wider pH range than Mn-oxides, and the solution composition, pH, redox and temperature will have an influence on the mineralogy and chemistry of the secondary Fe-precipitate

(Lee et al., 2002; Lottermoser, 2010). For example, jarosite tends to form at pH <3 and high sulfate concentrations, whereas goethite and ferrihydrite are known to form at circumneutral pH. The secondary Fe have a strong capacity to adsorb or coprecipitate trace metals, in particular Pb, Cu and Zn (Lee et al., 2002; Langmuir et al., 2004).

4.5. What about acid flush?

Hydrochloric acid, at a concentration ranging from 3 to 28% v/v, is typically the first chemical introduced into a newly-drilled well, before hydraulic fracturing. This initial acid flush is mainly done to remove any debris that may block well perforations and dissolve any acid-soluble minerals near the wellbore, facilitating more flow paths for fracturing fluids (Arthur et al. 2009, US EPA, 2016). In addition to the initial flush, acid can also be employed multiple times during hydraulic fracturing as an acid pad, often leading the fluid for each fracturing stage (McCurdy, 2011; Li NY et al., 2016).

In shale formations, acid flush will dissolve carbonates, and may also react with clay minerals. Clays are not truly soluble in HCl, but exposure to this acid can affect the mineral structure; chlorite is particularly susceptible to acid attack (Simon and Anderson, 1990). The extent of acid-mineral reactions will be governed by HCl strength, and bottomhole temperature and pressure conditions (Morsy et al., 2015; Simon and Anderson, 1990). For example, illite is stable in the presence of HCl in concentrations up to 15% and temperatures below 82°C (Simon and Anderson, 1990).

Acid flush results in a short-term shale exposure to HCl, although no information could be found for the exact timescale. Therefore, the leaching experiments with 1M HCl (3%) were only conducted for up to 17h at 80°C. Due to limited amounts of samples, only shales from Cooper Basin were investigated, and consequently, only the effect of HCl on uncertain ABA group was explored.

The concentrations of elements leached into solution by 1M HCl are summarised in

Appendix B (Table B5). Generally, acidification of the shale sample resulted in a much higher overall element mobilisation and much faster element release into solution than either SGW or SHFF.

HCl mobilised at least 77% of the available Ca, Mg, Mn and Fe from the Cooper Basin samples into the solution within 5 hours of leaching (Figure 4.19). The exposure to dilute HCl also caused a greater release of Al into solution, with a relatively rapid release within the first 5 hours of experiment and a subsequent plateau. The maximum amount of Al mobilised into solution was sample dependant, with Epsilon-1 releasing all of its available Al (66 mg/l) and Murteree-1 releasing the least (41%) but recording the highest maximum aqueous Al concentration (175 mg/l). Conversely, HCl caused a considerably lower S yield into solution than SGW (note that no S data was collected for SHFF experiments); however, the concentrations released within the first hour of leaching remained stable throughout the experiment (Figure 4.20).

Majority of trace elements also exhibited a rapid initial release before largely plateauing within 5 h, often at values equivalent to the TRE content (Figure 4.21 – Figure 4.24). HCl released considerably higher amounts of the total available As, Cr, Ba, V, Sr and Pb into solution, often one order of magnitude higher than SHFF. Other trace elements, such as Cd, Co, Cu, Li, Mo, Ni and Zn, were mobilised by HCl to a similar extent as by the SHFF, but the maximum element release occurred much faster.

These results indicate that acid flush can significantly impact element release, even in shales lacking sulfide minerals. The reactions occur in the first 5 hours, and so even a short 17h exposure to dilute HCl mobilised geogenic PTEs into solution typically to a much greater extent than SHFF. Therefore, it is possible that wells where acid flush is employed will exhibit a much higher geogenic contaminant mobilisation and the elements may already be present in solution prior to the introduction of hydraulic fracturing fluids.

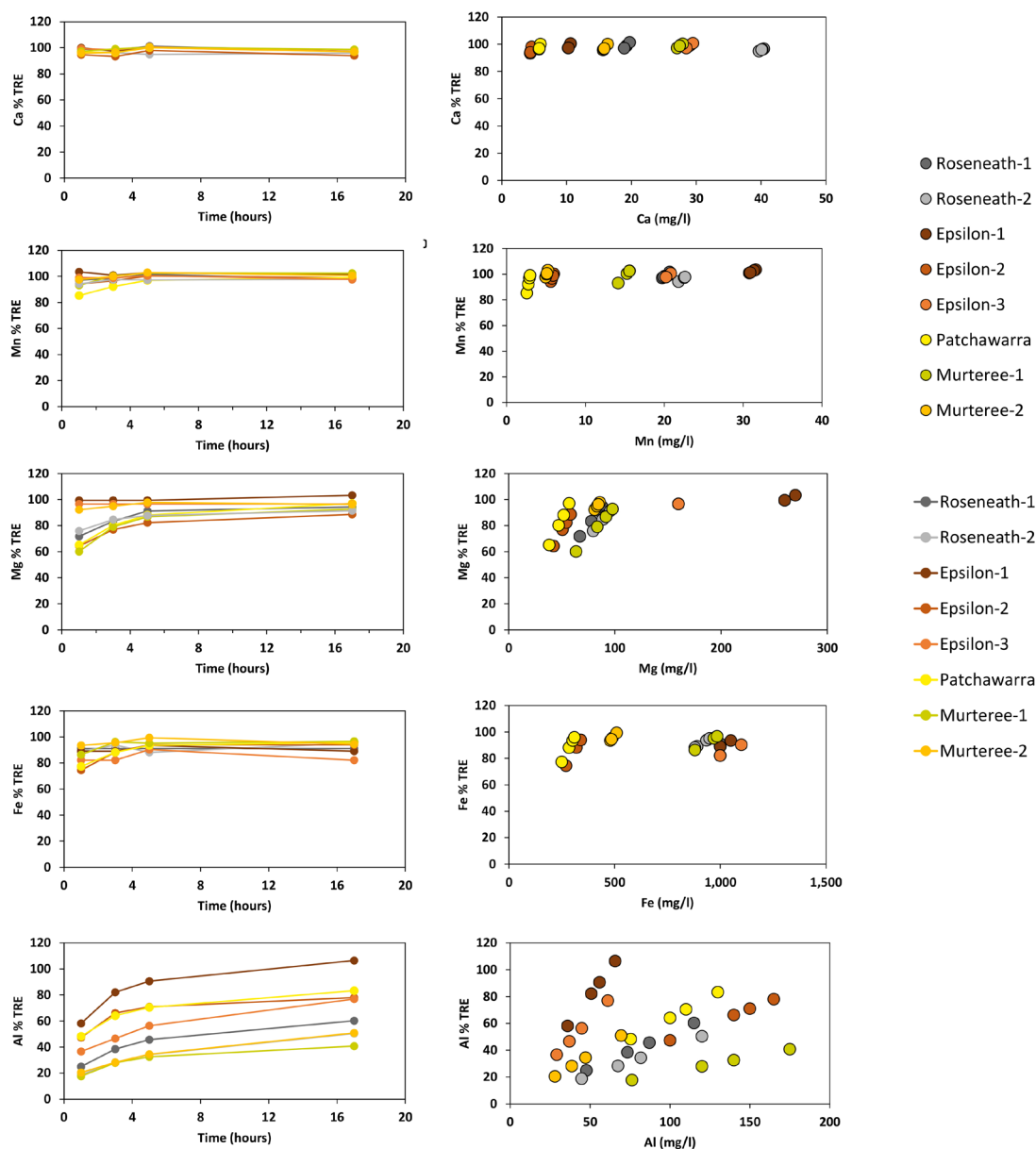


Figure 4.19 Graphs on the left show the amount of total available Ca, Mn, Mg, Fe and Al mobilised over time in the HCl experiments. Graphs on the right show aqueous concentrations of Ca, Mn, Mg, Fe and Al in HCl experiments plotted against the total available content of a given element in the solids.

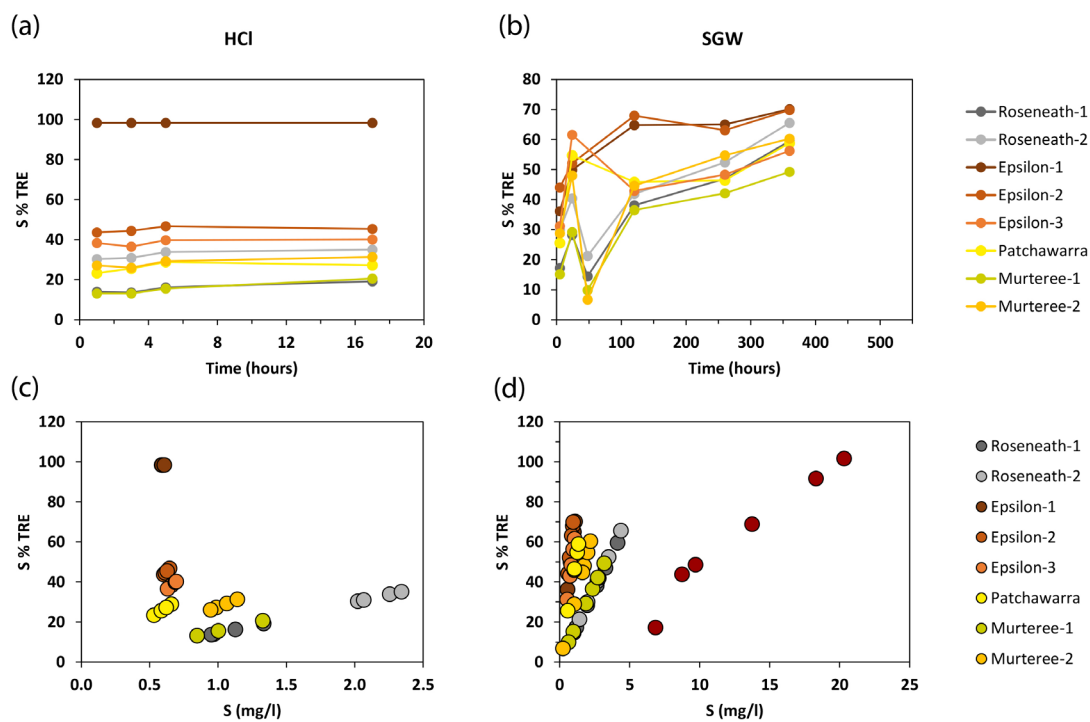


Figure 4.20 Top graphs show the amount of total available S mobilised over time in the (a) HCl and (b) SGW experiments. Bottom graphs show aqueous S concentrations in the (c) HCl and (d) SGW experiments plotted against the total available S content.

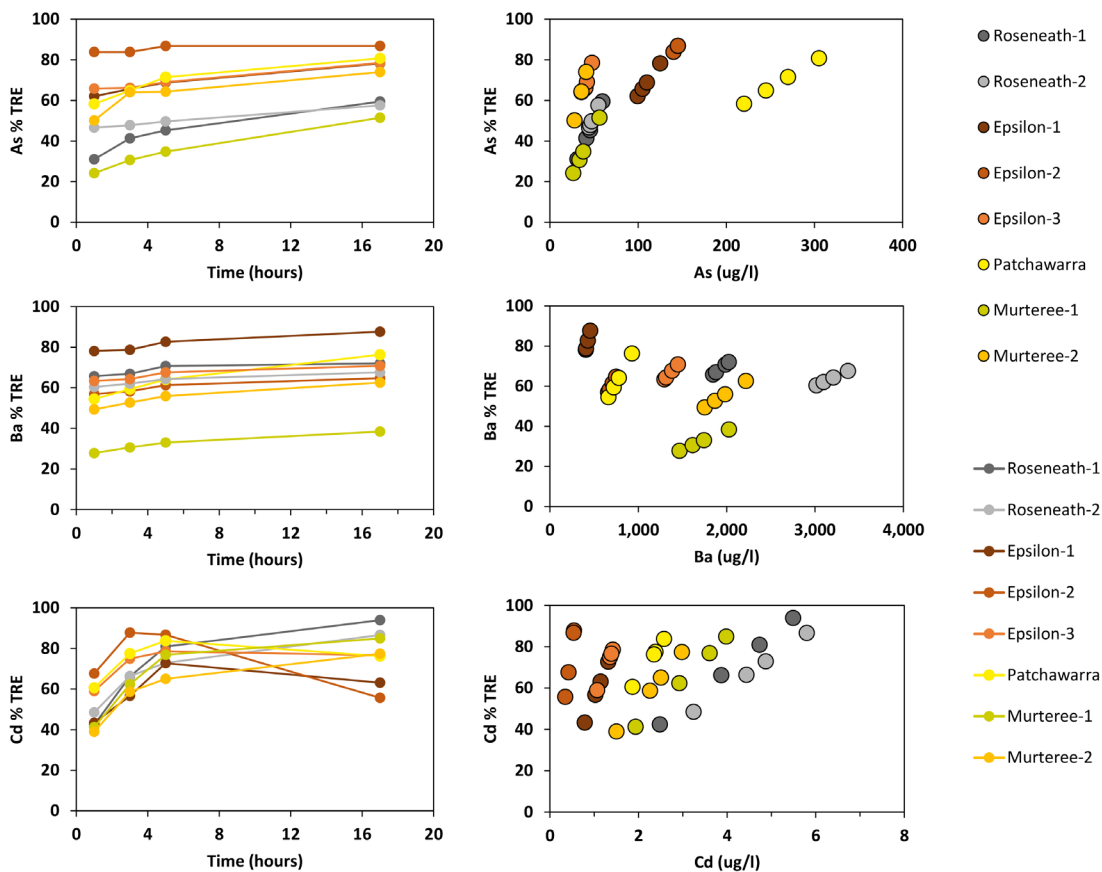


Figure 4.21 Graphs on the left show the amount of total available As, Ba and Cd mobilised over time in the HCl experiments. Graphs on the right show aqueous concentrations of As, Ba and Cd in HCl experiments plotted against the total available content of a given element in the solids.

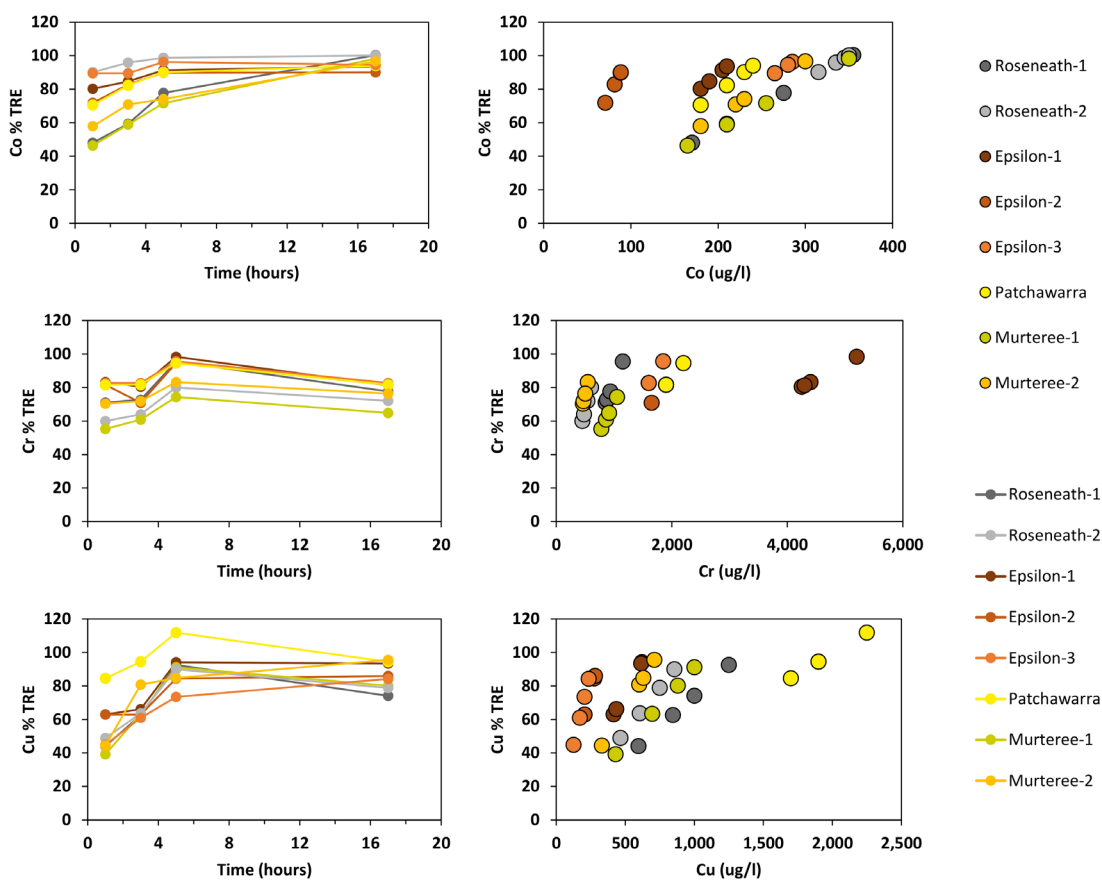


Figure 4.22 Graphs on the left show the amount of total available Co, Cr and Cu mobilised over time in the HCl experiments. Graphs on the right show aqueous concentrations of Co, Cr and Cu in HCl experiments plotted against the total available content of a given element.

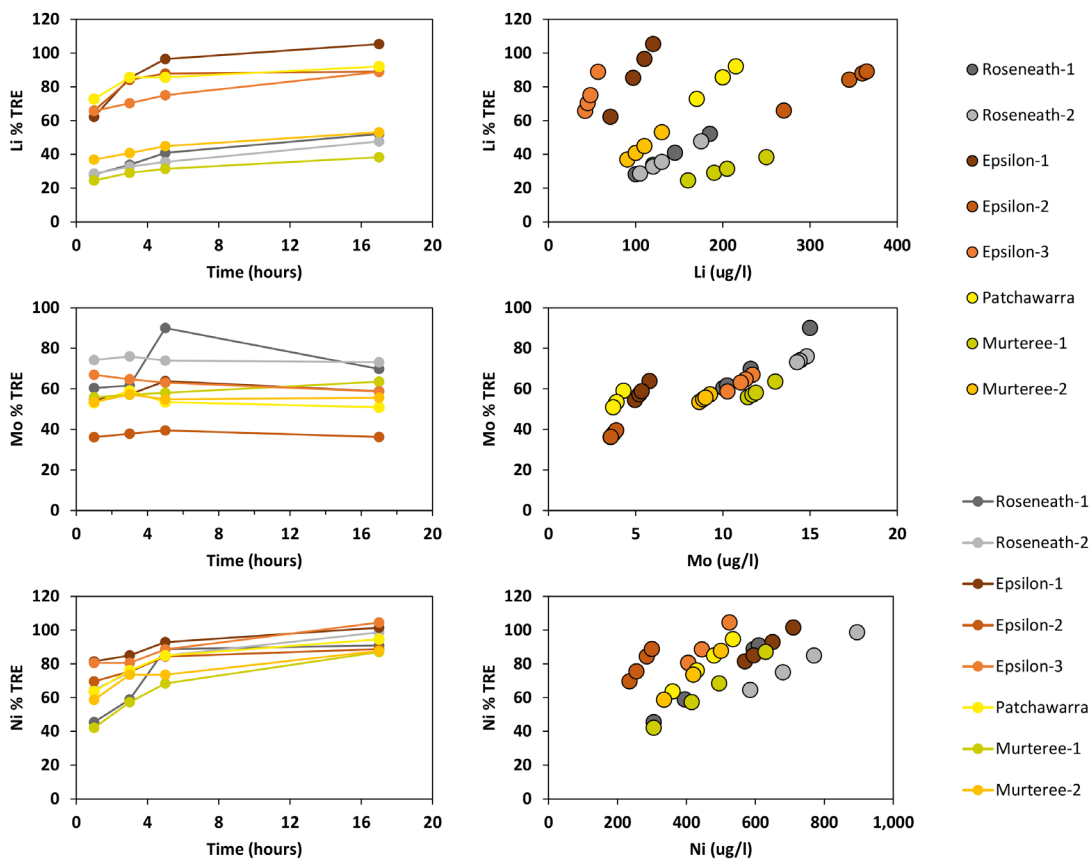


Figure 4.23 Graphs on the left show the amount of total available Li, Mo and Ni mobilised over time in the HCl experiments. Graphs on the right show aqueous concentrations of Li, Mo and Ni in HCl experiments plotted against the total available content of a given element.

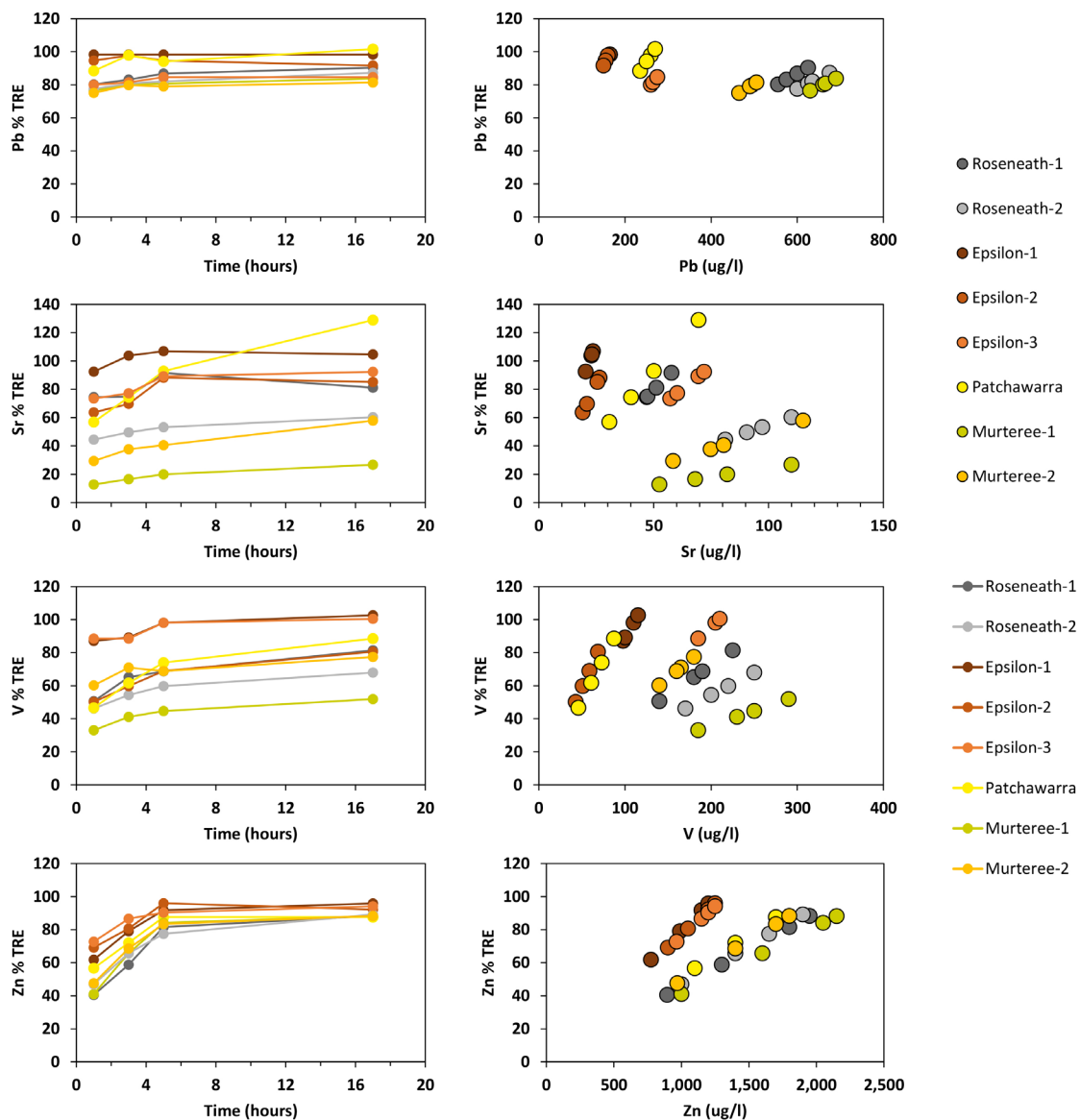


Figure 4.24 Graphs on the left show the amount of total available Pb, Sr, V and Zn mobilised over time in the HCl experiments. Graphs on the right show aqueous concentrations of Pb, Sr, V and Zn in HCl experiments plotted against the total available content of a given element.

4.6. Summary

This part of the study aimed to investigate element release from gas shales during hydraulic fracturing operations in a set of laboratory leaching experiments at reservoir temperature and atmospheric pressure conditions. Three leaching solutions were used: (1) a dilute (1M) HCl, representing acid flush treatment; (2) a synthetic hydraulic fracturing fluid; and (3) synthetic groundwater (SGW), used to establish the concentration of easily leachable elements and as a benchmark for the SHFF experiments.

The aqueous concentrations of most elements were generally much higher in the SHFF than in the SGW experiments, highlighting the role of chemical additives present in SHFF in mobilising trace elements from shale formations.

The shale sample's ability to neutralise acid was revealed to control the pH during the experiments with SHFF, directly impacting element release and mobility in the solution. The *non-acid producing* shales quickly buffered the pH of the SHFF solution from acidic to circumneutral and later alkaline. On the other hand, the pH of the *potentially acid producing* and *uncertain* SHFF leachates remained acidic throughout the experiments. Owing to the acidic pH, higher aqueous concentrations of many elements, particularly Cd, Co, Cu, Ni, and Zn, were observed in the *potentially acid producing* and *uncertain* SHFF leachates than in the *non-acid producing* ones.

In the experiments with SGW, *non-acid neutralising* and *uncertain* samples increased the initial pH (~7.5) to pH 8-9 and subsequently maintained it. Most of the *potentially acid producing* shales deviated from that trend at the 120h time point when the acidity generated from pyrite oxidation began to surpass the buffering capacity of the SGW, decreasing the pH of the leachate to acidic. Aqueous concentrations of several elements, such as Cd, Co, Cu and Ni, increased concurrently with the observed pH drop. This suggests that even when non-aggressive hydraulic fracturing fluids are used in pyrite-rich shales, pyrite oxidation may eventually cause contaminant release and acidification

if the shales lack any neutralisation potential.

Lastly, even a short 17h exposure to 1M HCl mobilised geogenic PTEs into solution typically to a much greater extent than during a much longer equilibration time with SHFF. It is thus likely that when acid flush is employed, geogenic contaminant mobilisation into flowback will be more significant, and the elements may already be present in solution before the introduction of hydraulic fracturing fluids.

CHAPTER 5

EXPERIMENTAL FACTORS AFFECTING ELEMENT MOBILISATION FROM SHALES

5.1. Introduction

The degree of element mobilisation from shale samples and its dependency on one of the three leaching fluids and sample mineralogy has been established in Chapter 4. The aqueous concentrations of elements were generally much higher in SHFF than in the SGW tests, highlighting the role chemical additives present in hydraulic fracturing fluids have in element release. This chapter examines how selected additives and experimental parameters could have influenced the observed mobilisation trends.

The additives examined were EDTA and citric acid, and ammonium persulfate; their effects were not examined systematically, but rather as a single formulation. Their impact was investigated during the development of the SHFF formulation, and these preliminary experiments were performed at a different solid:fluid ratio to the main body of work presented in Chapter 4. Hence, the first section of this chapter describes how the choice of solid:fluid ratio affects element release before discussing the influence of the additives.

The subsequent section examines the impact of different experimental temperatures to account for the range of conditions reported for various shale gas reservoirs (~40-160°C; Haliburton, 2009; McCurdy, 2011).

Lastly, the chapter examines the effect of increased pressure on the rock-fluid interactions. This was done twofold: using powdered Eagle Ford samples and Bowland-BE shale chips. The experiment with shale chips gave insights into how reservoir-representative pressures may affect fracture surface and provided microstructural evidence for some of the dissolution and precipitation reactions inferred from aqueous chemistry in Chapter 4. Samples were scanned before and after treatment to establish the nature and location of the reactions that took place.

The experimental procedures used in this chapter are the same as the ones outlined in Chapter 4.3. unless otherwise specified. Major and trace element analysis of the solid:fluid and fluid additive leachates was carried out using inductively coupled plasma-atomic emission spectrometry (ICP-AES) (Varian 730-ES, Australia).

5.2. Fluid additives and solid:fluid ratio

5.2.1. Solid:fluid ratio

The effects of solid:fluid (S:F) ratio were investigated on Kimmeridge Clay KC-1 sample using synthetic groundwater and 1M HCl, leached for 5 hours at 80°C at four different ratios: 1:100, 1:50, 1:25 and 1:10.

The influence of solid:fluid ratio on mobilisation trends depended on the element as well as the fluid. Diluted HCl promoted higher release of elements than SGW and the element concentrations increased approximately in proportion with the increasing S:F ratio. The only exception was barium, for which the concentrations slightly dropped between 1:25 and 1:10 S:F ratios (Figure 5.1).

Nine out of 22 analysed elements were generally below detection limits in the SGW leachates, including Co, Fe and Zn. Aluminium and Ba showed a decreasing, but not entirely proportional, concentration trend with an increasing S:F ratio (Figure 5.2a).

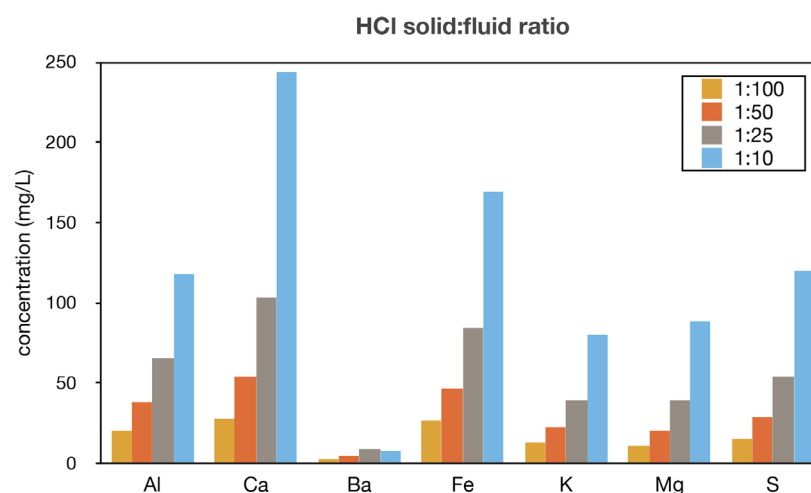


Figure 5.1 Aqueous element concentrations after 5h leaching of KC-1 sample with 1M HCl for different solid:fluid ratios. Data are shown as the averages of duplicates.

Other elements such as Ca and S showed an increase in their concentration with an increasing S:F ratio; however, the trend was not linear (Figure 5.2b). Lastly, the choice of ratio does not seem to significantly affect the mobilisation of As, Pb and V (Figure 5.2c).

The range of ratios was chosen based on previous experimental studies, which utilised powdered shale samples at solid:fluid ratios ranging from 1:12.5 to 1:1000 (Jew et al., 2017; Harrison et al., 2017; Marcon et al., 2017; Tasker et al., 2016; Wilke et al., 2015; Wang et al., 2015; Wang et al., 2016). It is worth noting that the estimated S:F ratio during hydraulic fracturing is at least four orders of magnitude higher (100:1) than the ratios used in this and other studies (Renock et al., 2016). Therefore, laboratory experiments may potentially observe more diluted solutions, at least for some elements, than what could occur during actual hydraulic fracturing operations (Harrison et al., 2017; Paukert Vankeuren et al., 2017).

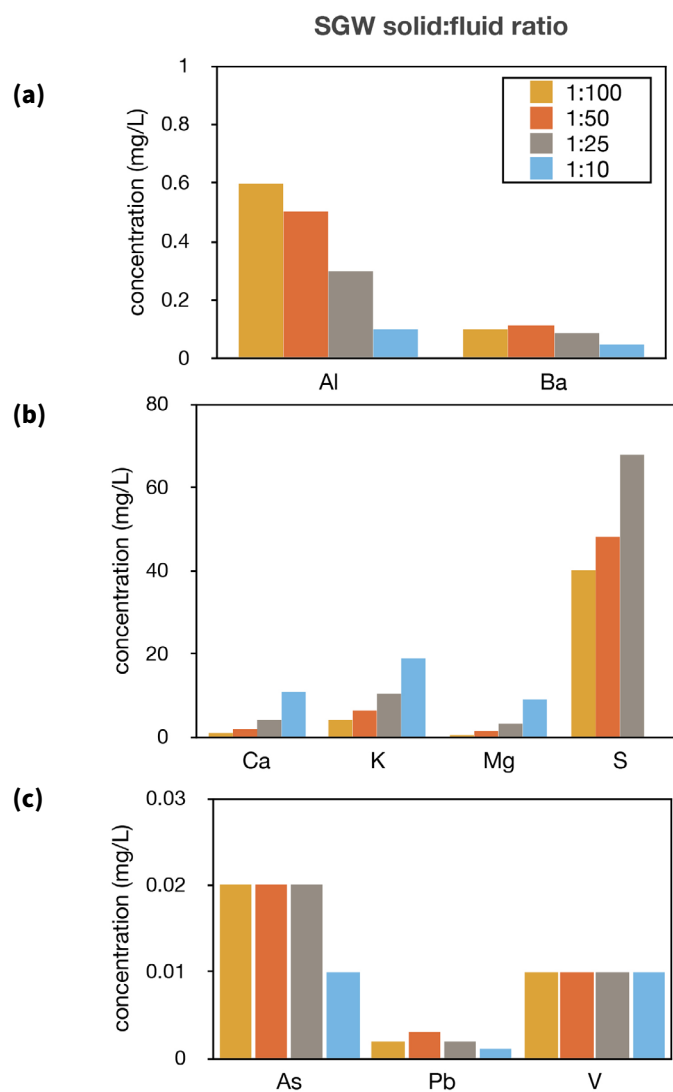


Figure 5.2 Aqueous element concentrations after 5h leaching of KC-1 sample SGW for different solid:fluid ratios. Data are shown as the averages of duplicates. Sulphate concentration for 1:10 ratio exceeded the upper limits of detection on ICP-AES.

5.2.2. EDTA and citric acid concentration

EDTA and citric acid are common additives in hydraulic fracturing fluids, used as iron-chelating agents to prevent Fe(III)-bearing precipitates. However, they can also affect the pH of the solution and cause desorption of metals from their host minerals and the formation of strong complexes. This could lead to increased mobility of several regulated elements (Kourgiantakis et al., 2000; Wang et al., 2016). The strength of these metal chelate complexes depends on the pH of the system, the presence of competing ions and the affinity the chelator has for metals. For example, Ca^{2+} and Mg^{2+} are generally more effectively chelated at high pH, whereas Fe^{3+} and Al^{3+} will most effectively compete for chelating ligands under acidic conditions (Norvell, 1991).

The influence on of EDTA and citric acid on element mobilisation from shales was preliminarily tested on Kimmeridge Clay KC-4 and Cooper Basin's Murteree-2 samples through a 3-hour hot block extraction at 80°C at 1:100 solid:fluid ratio. Three different leaching fluids were used: EDTA and citric acid solution (EDTA+CA), SHFF#4 and SHFF#4 with EDTA+CA (Table 5.1). SHFF#1 was prepared according to the Prud'homme recipe for a synthetic hydraulic fracturing fluid (see 4.2.3.2) with the omission of guar.

Table 5.1 Details on composition of three fluids used in the EDTA and citric acid experiments.

Fluid	Composition
<i>EDTA+CA solution</i>	0.034 g/L EDTA and 0.012 g/L citric acid
<i>SHFF#1</i>	1.2 g/L sodium dictate; 20 g/L potassium chloride; 0.25 ml/L glutaraldehyde solution (25%); 4 ml isopropyl alcohol 9:1 (v/v); SGW (750 mg/L NaCl, 750 mg/L NaHCO_3) to the remaining 1L
<i>SHFF#1 with EDTA+CA</i>	SHFF#1 with 0.034 g/L EDTA and 0.012 g/L citric acid

Aluminium, Co, Cu, Fe, Ni, Pb and Zn were mobilised to a greater extent from both shale samples when EDTA+CA were present. Leaching with the EDTA+CA solution tended to yield higher concentrations of Al, Cd, Fe, Ni, Pb and Zn than with SHFF#1 with EDTA+CA, typically by at least 40% and up to 164% (Figure 5.3 and Figure 5.4).

Conversely, Ca, Mg and S concentrations released into solution were similar for KC-4 for all three fluids (Figure 5.3). For Murteree-2, the presence of EDTA and citric acid in the fluid resulted in lower aqueous Ca and Mg concentrations compared to when no EDTA+CA was added (Figure 5.4). This trend is also visible for Ba for both samples.

5.2.3. Ammonium persulfate concentration

Ammonium persulfate, commonly used as a breaker to decompose gelling agents, was investigated during the development of the final iteration of the synthetic hydraulic fracturing fluid recipe. Given this chemical has strong oxidising properties, it may facilitate element release from sulphide minerals (Marcon et al., 2017; Wang et al., 2016).

Persulfate breakers are activated by heat (50-70°C), ultraviolet light, acidic pH, or through electron transfer from transition metals (e.g. Fe, Co, Mn). Once appropriately activated, the persulfate anion ($S_2O_8^{2-}$) decomposes into strong oxidant intermediates such as sulfate radicals ($SO_4^{\cdot-}$), which ultimately produce sulfate (SO_4^{2-}) as a by-product of oxidation reaction (Johnson et al., 2008; Manz and Carter, 2017; Paukert Vankeuren et al., 2017). The degradation of ammonium persulfate in a blank control SHFF experiments (15 days at 80°C and 175 bar) yielded 3583 mg/l of dissolved SO_4^{2-} . The dissolved sulfate generated from the degradation of the ammonium persulfate breaker has been shown to be a contributing factor to barite scale formation at reservoir conditions (Paukert Vankeuren et al., 2017) and minor anhydrite and gypsum precipitation (Marcon et al., 2017).

Additionally, the heat-activated (55°C) degradation of ammonium persulfate may

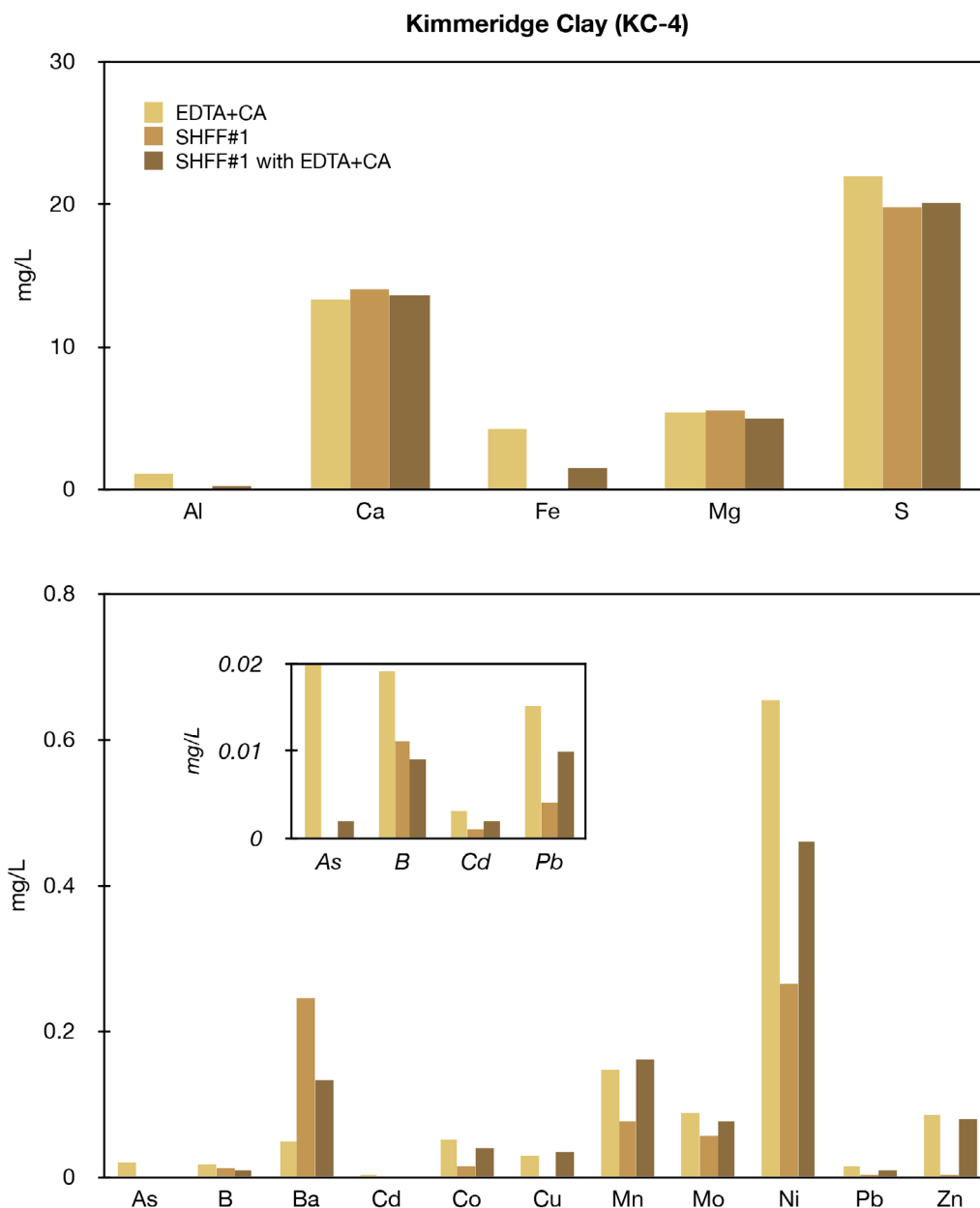


Figure 5.3 Aqueous element concentrations after 3h leaching of KC-4 sample with three fluids: (1) EDTA and citric acid solution; (2) synthetic hydraulic fracturing fluid (SHFF#1 recipe); and (3) SHFF#4 with EDTA and citric acid. Data are shown as the averages of duplicates.

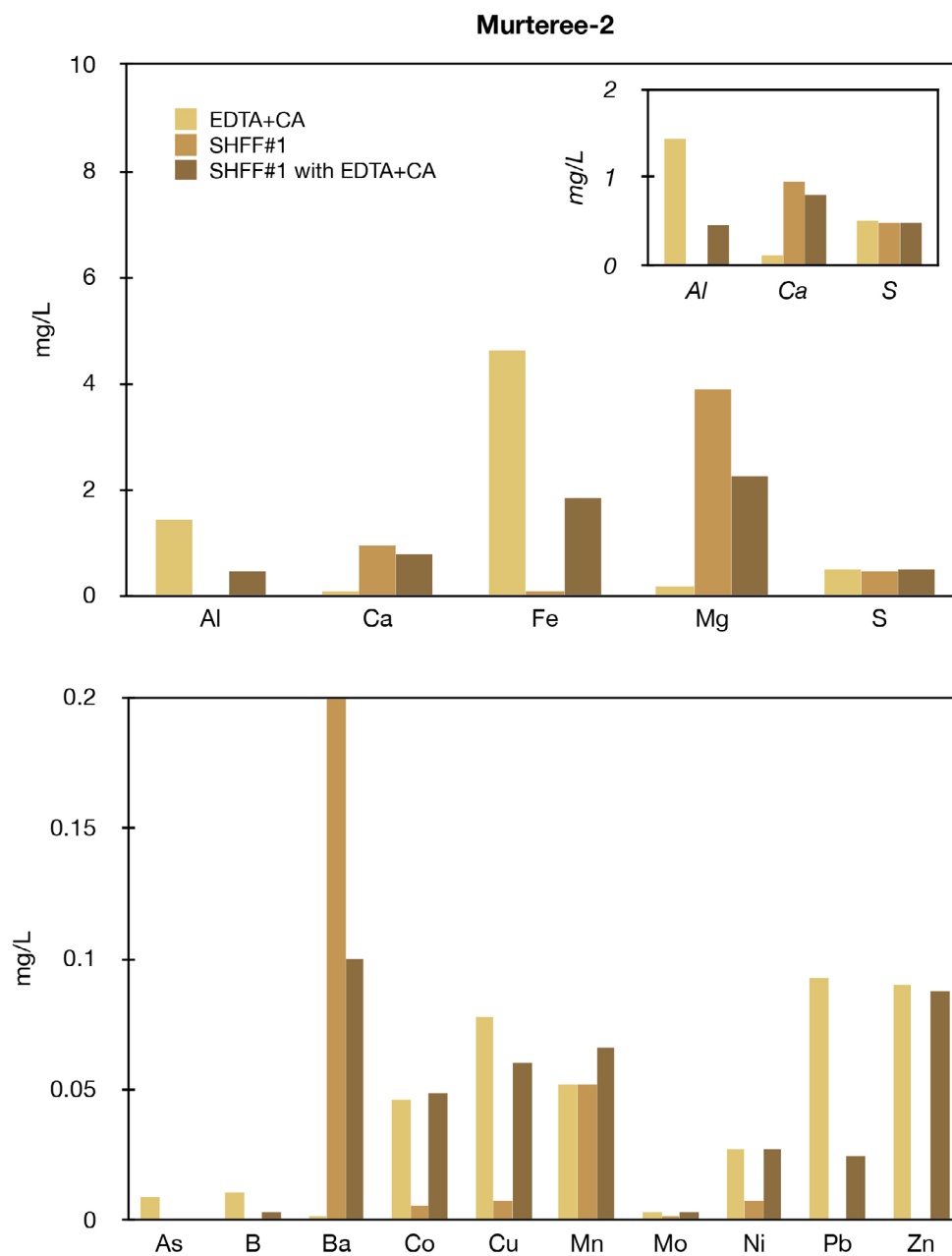


Figure 5.4 Aqueous element concentrations after 3h leaching of Murteree-2 sample with three fluids: (1) EDTA and citric acid solution; (2) synthetic hydraulic fracturing fluid (SHFF#1 recipe); and (3) SHFF#4 with EDTA and citric acid. Data are shown as the average of duplicates

decrease solution pH, especially if the conditions are already acidic (Manz and Carter, 2017). In this study, the addition of ammonium persulfate to the SHFF appeared to control the pH of a blank SHFF control during the 80°C experiments (Figure 5.5). When ammonium persulfate was included in the recipe, the pH of SHFF decreased from 5.1 to 2.5 within 48 minutes of heating (15 min after the fluid reached the target temperature of 80°C). Without ammonium persulfate, the SHFF slowly increases from the initial 5.6 to 6.1 over the 24 hours of heating. Degradation of ammonium persulfate likely contributed to the rapid initial pH drop in the SHFF leaching experiments described in Chapter 4.4.

Several different fluids were used to investigate the impact of ammonium persulfate on element mobilisation as well as to test whether it was a significant contributor to the release of elements in preliminary experiments with Prud'homme recipe for gelled hydraulic fracturing fluid. Although not present in the original recipe, ammonium persulfate was needed as a breaker to reduce fluid viscosity and enable sample recovery and analysis. The working hypothesis was that the high viscosity of the gelled frack

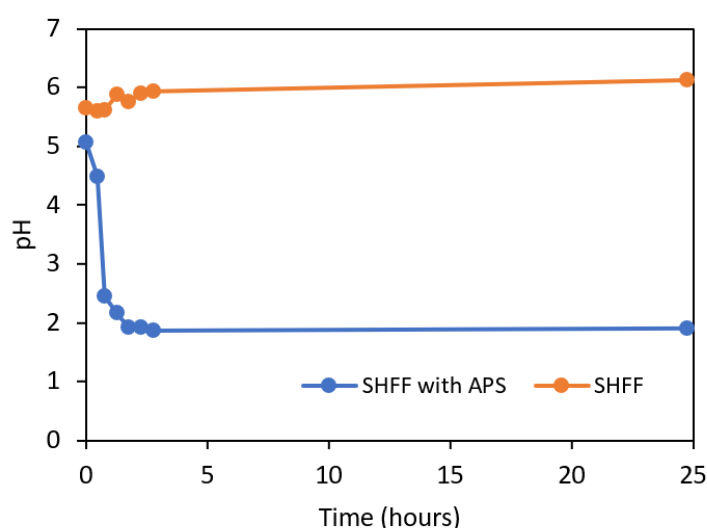


Figure 5.5 pH changes observed during heating of SHFF with and without ammonium persulfate (APS) to 80°C. The initial pH of the SHFF with APS was 5.1 and 5.6 for SHFF without APS. The fluids reached the targeted temperature of 80°C after 47 min of heating.

Table 5.2 Details on composition of fluids used in the ammonium persulfate experiments.

Fluid	Composition
SGW	750 mg/L NaCl, 750 mg/L NaHCO ₃
SGW with APS	SGW with 67 ml/L of 6% m/v ammonium persulfate (APS) solution
SHFF#1	1.2 g/L sodium dictate; 20 g/L potassium chloride; 0.25 ml/L glutaraldehyde solution (25%); 4 ml isopropyl alcohol 9:1 (v/v); SGW to the remaining 1L
SHFF#1 with APS	SHFF#1 with 67 ml/L of 6% m/v ammonium persulfate (APS) solution
Gelled SHFF with APS	SHFF#1 with APS and 4.8 g guar

fluid would retard the rock-fluid interactions and therefore yield small quantities of elements into the solution. However, after 3 hours of leaching with a gelled SHFF, aqueous Ca, Fe, Ni and Pb concentrations were 100-200% higher relative to the SGW results, indicating the possible role of ammonium persulfate in their mobilisation.

The effect of ammonium persulfate was examined using SGW and SHFF#1 with and without 2 ml of the ammonium persulfate solution (Table 5.2), and tested on powdered Kimmeridge Clay KC-4 and Cooper Basin's 1 Murteree-2 samples. The samples were leached for 3 hours at 80°C at 1:100 solid:fluid ratio.

Generally, the addition of ammonium persulfate causes greater mobilisation of most of the elements, but the effects were not constant across both samples (Table 5.3 and Table 5.4). This is likely due to differences in the mineralogy and elemental abundances: KC-4 is *potentially acid producing* with 7 wt% pyrite and no carbonates, whereas Murteree-2 is classified as *uncertain* with neither sulfate nor carbonate minerals present apart from accessory siderite (see CHAPTER 3). Aluminium, As, Cd, Cr, Cu, Fe, Pb and V showed an increase in concentration by at least one order of magnitude for both SGW and SHFF

Table 5.3 Results of the ammonium persulfate experiments for the KC-4 sample. All concentrations are in mg/l.

	<i>SGW</i>	<i>SGW with APS</i>	<i>SHFF</i>	<i>SHFF with APS</i>	<i>Gelled SHFF with APS</i>
Al	0.4	3	0.1	4	1
As	0.01	0.1	<0.003	0.1	0.02
Ba	0.03	0.05	0.6	0.2	0.05
Ca	2	22	19	22	7
Cd	0.0002	0.01	0.003	0.01	0.002
Co	<0.001	0.1	0.1	0.1	0.02
Cr	<0.0003	0.01	0.0002	0.01	0.004
Cu	<0.001	0.12	0.01	0.1	0.02
Fe	0.004	43	0.4	15	3
Mg	1	8	7	7	2
Mn	0.0003	0.3	0.3	0.3	0.1
Mo	0.14	0.12	0.01	0.10	0.02
Ni	0.001	0.8	0.7	0.8	0.2
Pb	<0.001	0.01	0.002	0.05	0.01
Sr	0.03	0.1	0.12	0.11	0.03
V	0.01	0.1	0.0004	0.1	0.02
Zn	<0.0003	0.7	0.12	0.4	0.1

tests with KC-4 when ammonium persulfate was present (Table 5.3). Calcium, Co, Mg, Mn, Ni and Sr appeared to be less affected by the presence of ammonium persulfate in the SHFF, but showed a noticeable increase when the additive was present in the SGW.

For Murteree-2 sample, both SGW and SHFF with added ammonium persulfate mobilised higher concentrations of elements into the solution for all examined solutes apart from As and Mo (Table 5.4). The aqueous Cr, Fe, Mg, Mn, and Ni concentrations were higher by at least an order of magnitude than in the leachates without the breaker.

The results indicate that the addition of ammonium persulfate can increase element mobilisation into the solution, and so the additive was retained in the final fluid formulation, even though the gelling agent was ultimately excluded. The guar gum was

Table 5.4 Results of the ammonium persulfate experiments for the Murteree-2 sample. All concentrations are in mg/l.

	<i>SGW</i>	<i>SGW with APS</i>	<i>SHFF</i>	<i>SHFF with APS</i>	<i>Gelled SHFF with APS</i>
Al	1	7	0.1	6	2
As	0.01	<0.002	<0.003	<0.001	<0.002
Ba	0.01	0.05	0.7	0.2	0.03
Ca	0.2	4	2	4	1
Cd	<0.0001	0.001	0.0002	0.001	<0.001
Co	<0.001	0.11	0.05	0.1	0.03
Cr	<0.0003	0.03	0.0002	0.05	0.02
Cu	<0.001	0.2	0.01	0.1	0.04
Fe	0.002	36	8	69	30
Mg	0.2	21	7	20	6
Mn	0.0001	0.3	0.4	1.5	0.3
Mo	0.003	<0.001	<0.0002	<0.0003	<0.0005
Ni	<0.0004	0.1	0.05	0.1	0.03
Pb	0.005	0.03	0.01	0.1	0.02
Sr	0.001	0.01	0.02	0.01	0.001
V	0.004	0.002	<0.0003	0.01	0.01
Zn	<0.0003	0.6	0.1	0.4	0.11

omitted from the final SHFF recipe to facilitate leachate extraction and alleviate potential analytical problems that may have arisen from elevated carbon concentrations. It was assumed that guar constituents would not mobilise geogenic chemicals from solids.

5.3. The effect of temperature

Element mobilisation during leaching experiments with SHFF and SGW (see Chapter 4.4) was assessed at 80°C, which is representative of the Marcellus reservoir (Harrison et al., 2017 and references therein). However, temperatures within the 38-66°C range have also been reported for this shale gas play (Haliburton, 2009; Paukert Vankeuren

et al., 2017). Bottomhole temperatures for other gas shale reservoirs include 54°C for Fayetteville, 127°C for Eagle Ford and 160°C for Haynesville (McCurdy, 2011).

Temperature can have a substantial effect on the concentration and transport of elements in aqueous solutions. An increase in temperature typically results in an increased reaction rate. Temperature is one of the physiochemical controls on mineral solubility. Generally, the concentration of an element in an aqueous solution is limited by the solubility of the least soluble mineral that contains it (Seward et al., 2014). Solubility of most minerals increases with increasing temperature (prograde solubility), e.g. chloride, oxide, sulfide and silicate minerals. However, carbonates, sulfates and phosphates exhibit retrograde solubility, making them likely to precipitate as temperature rises (Langmuir, 1997; Seward et al., 2014). Other physicochemical factors affecting mineral solubility include pressure, salinity, and fluid pH (Seward et al., 2014).

KC-4 and Amungee-1 samples were leached with SGW and SHFF at 100°C for up to 360 hours and at room temperature for two time-points (140 h and 360 h) to assess how different temperatures affect element release within the experimental framework used in this study. The results were then compared to the time-series results obtained at 80°C. Both samples are classified as *potentially acid producing*, with abundant pyrite and little to no carbonates.

Generally, the increase in temperature from 80 to 100°C had little effect on the release of most elements into the solution for both leaching fluids. The rate and extent of element mobilisation remained similar at both temperatures for most solutes, especially when comparing their concentrations at the last sampling time point (360 h). The only exceptions were Ca and Mg, which observed a substantial decrease in aqueous concentrations between 260 and 360 h in the 100°C experiments with SHFF (Figure 5.6 and 5.7). At 260 h all available Ca and ~80% of TRE Mg content was mobilised, but only 10 and 8 % TRE, respectively, remained in solution at 360h.

The average deviation between the total available trace element content mobilised into

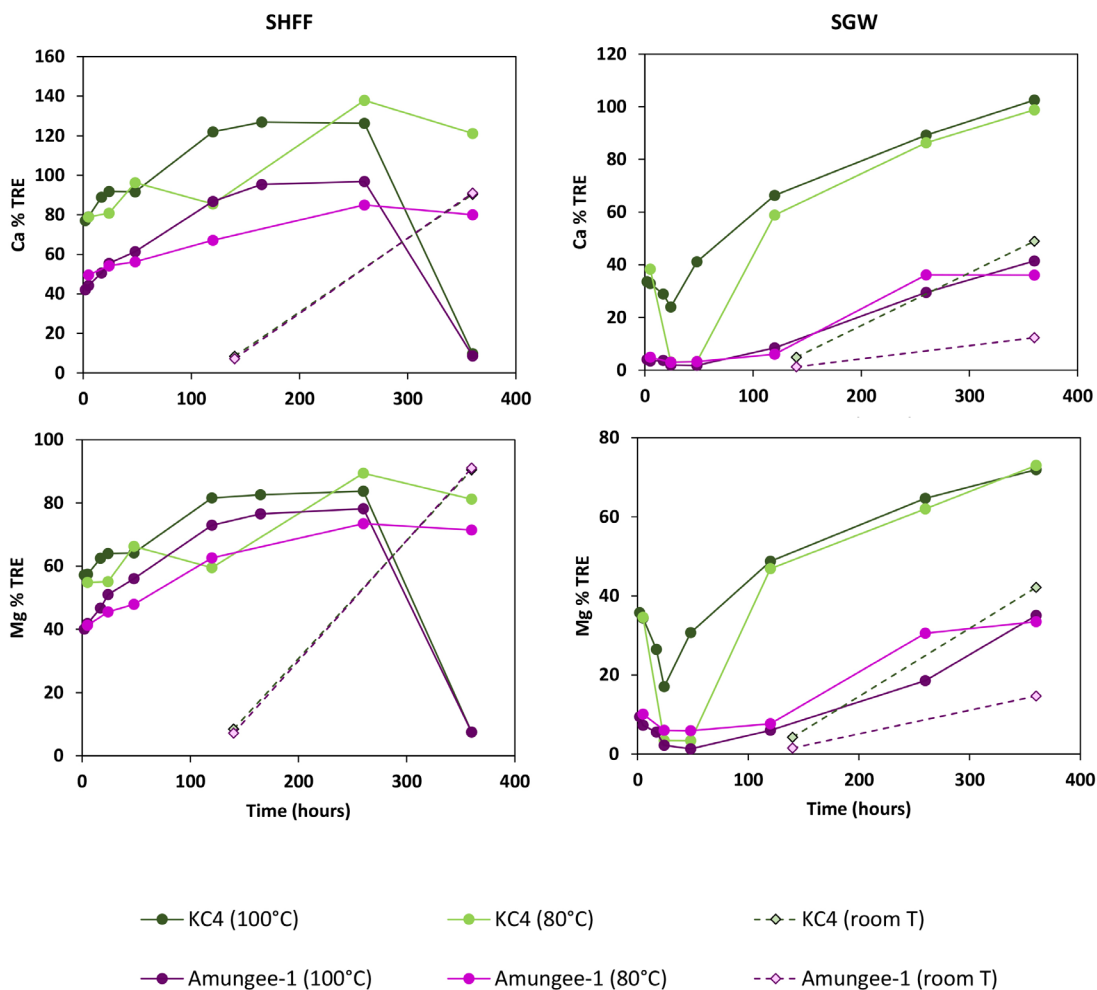


Figure 5.6 Amount of total available element Ca and Mg content mobilised over time in the SGW and SHFF temperature experiments. Note that y axis has different scales among the graphs.

solution during the time series for KC-4 ranged between 1.5 and 15 % TRE for SHFF and 0.1 and 12% TRE for SGW. For Amungee-1, the difference was 1-13 % TRE for SHFF and 0.5-15% TRE for SGW. Neither of the elevated experimental temperatures consistently yielded higher element load into the solution.

The temperature increase between ambient and 80°C had a much more pronounced effect on element mobilisation into solution. Element mobilisation was generally much lower at room temperature, with comparable element concentrations recorded at both 140 and 360 h. Different behaviour was observed for Ca and Mg in the SHFF leachates,

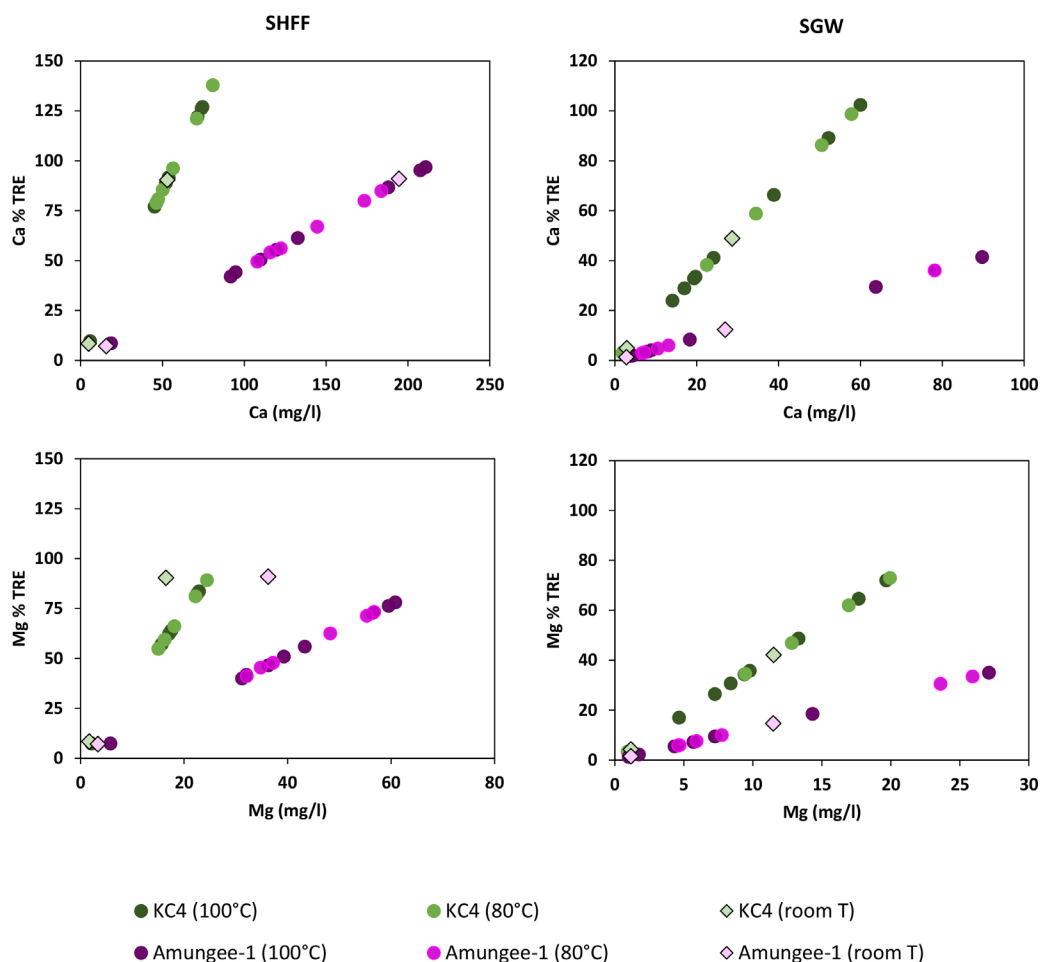


Figure 5.7 Aqueous concentrations of Ca and Mg leached at different temperatures by SHFF and SGW plotted against the total available content of a given element in the solids. Note that graphs have different scales.

which at ambient temperature show a rapid increase in element mobilisation between 140 and 360 h (Figure 5.6 and 5.7). At 360 h they exceed the aqueous concentrations recorded at 100°C for this time point for KC-4 as well as Amungee-1 leachates. The release of Ba into SHFF for both samples also exceeded aqueous concentrations recorded at 80 and 100°C; however, the decreasing Ba mobilisation trend was consistent at all temperatures.

SHFF mobilised less Mo from Amungee-1 at room temperature, but approximately 5% more of the total Mo content was released into the solution at ambient conditions than at elevated temperatures. In SGW leaches, Mo concentrations remained relatively

comparable over 140 and 360 h at room temperature for both samples. However, at 80 and 100°C, Mo showed an initial rapid release followed by a plateau and a fast decrease in dissolved concentrations.

Lastly, the evolution of pH in the SHFF leachates followed the same trend regardless of the temperature conditions (Figure 5.8). However, in the experiments with SGW, the pH progressively decreased for both samples at 80 and 100°C, but remained alkaline at room temperature. The pH drop was likely caused by pyrite oxidation surpassing the buffering capacity of the SGW (see 4.4).

In leaching experiments conducted on powdered Bakken Shale samples, Wang et al. (2016) noted an increase in temperature from 22 to 80°C resulted in increased pyrite oxidation rates, mobilising more S into the solution, but did not affect the release of most of the other elements. This is partially in agreement with the results presented in this section. Based on the pH evolution and aqueous S and Fe concentrations in SGW experiments, elevated temperatures caused greater pyrite oxidation and increased release of these solutes into the leachates. However, the increase in temperature from ambient to 80°C also had a major effect on element release, typically greatly increasing the rate and extent of their mobilisation for both leaching fluids.

5.4. The effect of pressure

The solubility of many carbonate and sulfate minerals is known to increase with pressure, e.g. calcite, anhydrite, gypsum and barite (Seward et al., 2014). However, the effect of a concurrent temperature increase on the solubility of many minerals will typically be much greater than that of pressure (Langmuir, 1997). Nonetheless, higher pressures could increase element mobilisation rates and thermodynamic equilibria (Wilke et al., 2015) and promote greater secondary mineral precipitation during hydraulic fracturing-induced rock-fluid interactions (Pearce et al., 2018). Wilke et al. (2015) observed that

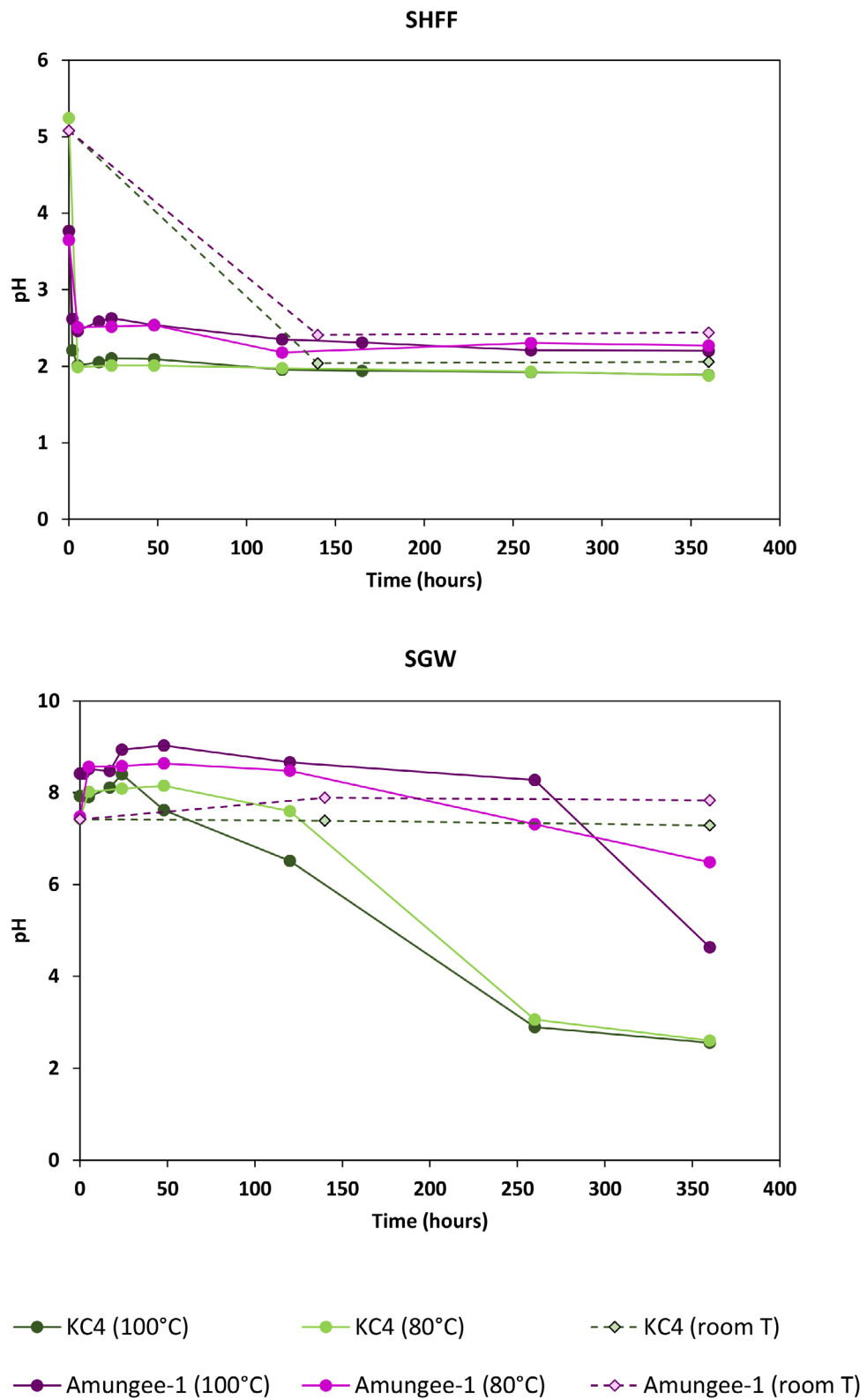


Figure 5.8 Evolution of pH in the temperature experiments with SHFF and SGW.

element mobilisation from their 24-hour experiments under ambient pressure and 100°C was always lower or equal to the element concentrations observed within the first 24 hours of their long-term experiments performed at 100°C and 100 bar. However, Tasker et al. (2016) concluded that elevated pressures and temperatures (83 bar and 80°C) did not impact metal dissolution from their Marcellus sample. They found that the metal concentrations that were released into solution in the experiments at atmospheric and HPHT conditions were comparable (for more details on these studies see CHAPTER 2).

5.4.1. Methods

The exploratory experiments were performed at elevated pressures as well as temperatures to examine how an increase to reservoir-representative pressure impacts element mobilisation trends observed at elevated temperature and atmospheric conditions. The preliminary experiments were conducted on powdered Eagle Ford samples and four Bowland-BE chips (B1 to B4), with SHFF and SGW solutions at 1:50 solid:fluid ratio. Selected chip samples were imaged before and after the leaching tests using JEOL JXA-8530F field-emission electron probe microanalyser (EPMA) with an energy-dispersive X-ray (EDX) detector. The B1 sample was also imaged using low vacuum scanning electron microscope (LVSEM) (JEOL JSM-6490LA) with EDX. Following the experiment, the reacted powders and one chip sample (B1) were vacuum filtered and subsequently put in a desiccator cabinet for a week. The remaining three shale chips were placed in the desiccator immediately after the end of the leaching.

The experiments were performed in a Berghof DB300 pressure reactor equipped with a PTFE reaction chamber of approximately 300 mL capacity. The reactor was heated to 80°C and gas-pressurised with nitrogen, doped with approximately 10 bar of oxygen, to maintain aerobic conditions. The maximum operating pressure was 200 bar. Following the experiment, the samples were vacuum dried and put in a desiccator cabinet for a week.

The pressure rig set up allowed only for one sample to be leached at a time, and accurately pressurising the system to the same pressures each time was challenging. Consequently, the pressure tests were performed without replicates. A blank SHFF control treatment (no solids added) was also included; however, it was not used to perform blank correction.

The pH of all leaching fluids was measured before the pressure experiments, but the final pH of the leachate was only possible to measure for the SHFF HPHT test (B1 chip) owing to sample volume limitations.

5.4.2. Fluid chemistry

Both shales used for the pressure investigations were *non-acid producing* with high carbonate content. As expected, the end pH in all experiments was alkaline for all of the leaching fluids at the temperature and pressure conditions used in the experiments (Table 5.5 and 5.6).

The concentrations of selected major and trace elements leached into solution from the powdered Eagle Ford shale by 80° SHFF and SGW at different pressure conditions are summarised in Tables 5.5 and 5.6, respectively. The results were ranked using a ratio of element concentrations released under elevated pressure compared to under atmospheric pressure.

Increasing the pressure from atmospheric (1 bar) to 173 bar resulted in changes to the concentrations of elements mobilised by SGW into solution. Some elements showed an enhanced release into solution under high pressure, particularly Fe, Cr and Cu. Their aqueous concentrations increased 28, 14 and 9 times, respectively. Other elements were affected more moderately (2-7x increase), e.g. Ni, Pb, U, Tl and Ca. Aluminium, As, and Sb were the only elements where the increase in pressure caused a definite decrease in mobilisation in the SGW leachates.

Table 5.5 Effect of pressure on dissolved element concentrations in SHFF leachates from Eagle Ford powdered samples. HPHT – high pressure and high temperature; HT – high temperature and atmospheric pressure.

		HPHT	HT	Ratio	Trajectory
start pH		4.0	2.3		
final pH		8.0	8.4		
Pressure (bar)		200	atmospheric		
Fe	ug/L	62	28	2	↑
U	ug/L	0.3	0.1	2	↑
V	ug/L	95	55	1.7	↑
B	ug/L	17	14	1.2	↑
Ca	mg/L	828	673	1.2	↑
Mo	ug/L	272	224	1.2	↑
Mg	mg/L	13	11	1.2	→
Sr	mg/L	2.5	2.2	1.1	→
Sb	ug/L	2.1	1.9	1.1	→
Tl	ug/L	70	65	1.1	→
Ba	ug/L	118	113	1.0	→
Li	ug/L	19	19	1.0	→
Hg	ug/L	<0.05	<0.05	1.0	→
Ni	ug/L	268	431	0.6	↓
Pb	ug/L	0.5	1.0	0.5	↓
As	ug/L	2.2	5	0.5	↓
Cd	ug/L	10	36	0.3	↓
Co	ug/L	7	27	0.3	↓
Al	ug/L	9	46	0.2	↓
Cr	ug/L	6	41	0.1	↓
Mn	ug/L	6	54	0.1	↓
Cu	ug/L	26	238	0.1	↓
Zn	ug/L	15	465	0.03	↓

Table 5.6 Effect of pressure on dissolved element concentrations in SGW leachates from Eagle Ford powdered samples. HPHT – high pressure and high temperature; HT – high temperature and atmospheric pressure.

		HPHT	HT	Ratio	Trajectory
start pH		7.7	7.5		
final pH		8.4	8.5		
Pressure (bar)		173	atmospheric		
Fe	ug/L	57	2.0	28	↑
Cr	ug/L	4	<0.3	14	↑
Cu	ug/L	7	<0.8	9	↑
Ni	ug/L	10	<1.4	7	↑
Pb	ug/L	0.5	0.1	3	↑
U	ug/L	0.6	0.2	3	↑
Tl	ug/L	42	14	3	↑
Ca	mg/L	153	77	2	↑
Mg	mg/L	8	4	2	↑
Mn	ug/L	0.4	0.3	1.3	↑
Co	ug/L	0.1	<0.1	1.3	↑
S	mg/L	269	214	1.3	↑
B	ug/L	22	18	1.2	→
Zn	ug/L	2.1	<1.8	1.2	→
Mo	ug/L	317	274	1.2	→
Cd	ug/L	0.2	0.2	1.1	→
Ba	ug/L	61	56	1.1	→
Hg	ug/L	<0.05	0.05	0.9	→
V	ug/L	138	153	0.9	→
Sr	mg/L	0.9	1.0	0.9	→
Li	ug/L	14	17	0.8	→
Al	ug/L	33	46	0.7	↓
As	ug/L	2.3	6	0.4	↓
Sb	ug/L	1.5	4	0.4	↓

In the SHFF experiments, the increase in pressure led to a suppression of elemental release for more solutes than in SGW, particularly Zn, Cu, Mn and Cr. The release of Fe was once again enhanced, albeit only moderately, followed by U, V and Ca.

For the Bowland-BE chips, a similar range of behaviours was observed, but the pressure increase impacted element release more significantly. Leaching with SGW at 150 bar resulted in 264 times higher Ca mobilisation and increased the release of Tl, Mg, and Ni 116, 85 and 30 times, respectively. Only a few elements showed a decrease in their aqueous concentrations with pressure increase, such as As, Mo, V and Sb (Table 5.7).

Conversely, suppression of elemental release with pressure increase was the dominant trend in the SHFF experiments (Table 5.8). Molybdenum, Zn, Mn, Li and Ba were among the elements that showed the highest decrease based on the calculated ratios. Enhanced element release was observed especially for U, Ca and Cu, which increased their aqueous concentration 67, 9 and 7 times.

Additionally, element mobilisation at high temperature and atmospheric pressure was affected by the form of the leached solid. Shale chips exposed to SHFF yielded a higher element load into the solution for most examined elements than powdered samples. Cadmium, Mo, Tl, Ba and Zn, in particular, saw an increase in mobilisation. On the other hand, Ca showed a significantly lower release into solution, recording over 1274 mg/l aqueous concentration in the powdered sample test compared to only 114 mg/l mobilised from the shale chip. Other elements showing a lower release from shale chips included Mg, V and As.

More elements displayed a higher release from the powdered sample in SGW tests compared to SHFF leachates, e.g. Ni and U. The elements that did show a greater mobilisation from the shale chip included Mo, Ba, Fe and Sr.

One would expect that experiments with shale powders would generally yield a higher elemental load into the solution provided mineral solubilities are not exceeded. Powdered samples will have an increased surface area available for reactions and

Table 5.7 Effect of pressure on dissolved element concentrations in SGW leachates from Bowland-BE chips. Results from powdered Bowland-BE leachates given for comparison. HPHT – high pressure and high temperature; HT – high temperature and atmospheric pressure.

		HPHT	HT	HT powder	Ratio	Trajectory
start pH		8.2	8.2	7.5		
final pH		n/a	n/a	9.7		
Pressure (bar)		150	atmospheric	atmospheric		
Ca	mg/L	42	0.2	0.3	264	↑
Tl	ug/L	23	<0.2	0.2	116	↑
Mg	mg/L	3	<0.03	0.1	85	↑
Ni	ug/L	18	0.6	5	30	↑
Cd	ug/L	3	<0.2	0.1	17	↑
S	mg/L	608	41	25	15	↑
Sr	mg/L	3	0.2	0.01	15	↑
Mn	mg/L	0.03	0.002	<0.0003	14	↑
Co	ug/L	1.1	<0.1	<0.1	11	↑
Cu	ug/L	15	1.4	4	10	↑
Zn	ug/L	6	<1.2	11	5	↑
Al	mg/L	<2	0.5	0.4	4	↑
U	ug/L	0.6	0.2	1.3	3	↑
Ba	ug/L	44	19	<0.5	2	↑
B	ug/L	178	86	49	2	↑
Fe	mg/L	0.1	0.1	0.003	1.6	↑
Li	ug/L	32	20	8	1.6	↑
Cr	ug/L	0.8	0.7	0.6	1.1	→
V	ug/L	<0.5	1.9	5	0.3	↓
Sb	ug/L	0.5	5	1.5	0.1	↓
Mo	ug/L	19	260	8	0.1	↓
As	ug/L	0.6	18	8	0.0	↓
Hg	ug/L	<0.06	<0.06	<0.02	n/a	
Pb	ug/L	<0.05	<0.05	0.8	n/a	

Table 5.8 Effect of pressure on dissolved element concentrations in SHFF leachates from Bowland-BE chips. Results from powdered Bowland-BE leachates given for comparison. HPHT – high pressure and high temperature; HT – high temperature and atmospheric pressure. Zn, Cr and Pb were excluded from this table due to high blank values.

		HPHT blank	HPHT	HT	HT powder	Ratio	Trajectory
start pH		5.2	5.3	3.9	5.4		
final pH		1.9	7.6	n/a	8.8		
Pressure (bar)		175	183	atmospheric	atmospheric		
U	ug/L	0.1	0.6	0.01	0.003	67	↑
Ca	mg/L	0.2	1085	114	>1274	9	↑
Cu	ug/L	5	48	6	18	7	↑
Mg	mg/L	0.1	24	4	26	7	↑
Tl	ug/L	0.6	23	14	0.6	2	↑
Sr	mg/L	0.01	6	5	2	1.1	→
Cd	ug/L	0.6	10	11	0.2	0.9	→
Sb	ug/L	0.6	0.6	0.8	<0.2	0.7	↓
Ni	ug/L	13	193	264	93	0.7	↓
Co	ug/L	0.3	19	29	11	0.7	↓
B	ug/L	6	88	144	60	0.6	↓
Ba	ug/L	5	195	336	16	0.6	↓
Li	ug/L	0.2	16	40	9	0.4	↓
Mn	mg/L	0.004	0.1	0.4	0.2	0.4	↓
As	ug/L	<0.2	<0.2	0.6	2	0.3	↓
Fe	mg/L	0.1	0.01	0.04	0.003	0.2	↓
Mo	ug/L	0.1	5	179	6	0.0	↓
Al	mg/L	<0.16	<0.16	<2	0.01	n/a	
Hg	ug/L	<0.05	<0.05	<0.06	<0.14	n/a	
V	ug/L	<0.7	<0.7	<0.5	1.7	n/a	

eliminate any inherent heterogeneities present on the rock chip or fracture surface, allowing the leaching agent concurrent contact with all of the sample. The incongruity in the elemental release from the shale chips and powders of the Bowland-BE shale indicates that the distribution of reactive minerals and texture of a chip surface are likely to influence element mobilisation.

5.4.3. The effects of pressure on the fracture surface

The differences in mineral (and thus element) distribution across the fracture surface

influenced the dissolution and precipitation reactions upon contact with SHFF and SGW was obtained using surface analysis (EPMA with EDX detection). Four shale chips (B1-B4) were imaged before and after the experiments at two scales: (1) a transect across the chip, perpendicular to the apparent lamination; and (2) where possible, an image from the center of each transect. Although care was taken to ensure the pre- and post-leaching images cover the same area, some offset was observed. The transects are approximately 1.3 cm long for B1 samples and 0.6 cm for B2-B4. The offsets range 0.03-0.15 mm horizontally and 0.02 - 0.2 mm vertically and are marked with red arrows on the backscatter images based on recognisable features. The images from the transect centres have a resolution of 125 x 95 μm for B1 and 120 x 90 μm for B2-B4. Consequently, the before and after zoom-ins might not cover exactly the same area.

The unreacted Bowland-BE centimeter-sized chips were fine-grained, black to light grey with parallel laminae. The laminae occurred as planar layers, 1 mm or more in thickness, typically with sharp contacts marked by a colour change. The edge of two of the chips used in the experiments (B1 and B3) included a calcite vein running across the laminae. EPMA and EDX data revealed further that lamina are associated with mineralogy changes, particularly the abundance of carbonates (calcite and dolomite).

5.4.4. SGW

5.4.4.1. Elevated temperature and atmospheric pressure

The unreacted B4 sample displayed textural and mineralogical heterogeneity. From left to right, element distribution highlighted the apparent banding that is clear in Figure 5.9:

1. a silicate-rich zone, approximately 2.5 mm thick, with scattered framboidal

pyrite, and dispersed carbonate clusters and discontinuous wispy carbonate
~0.1 mm laminae;

2. a gradational transition into a carbonate-dominated 2.5 mm thick layer, with little to no pyrite present;
3. a relatively sharp transition into another silicate-rich 0.5 mm lamina with dispersed carbonate clusters and more abundant pyrite;
4. a carbonate-rich ~0.5 mm lamina;
5. and another silicate-rich 0.5 m lamina with less abundant carbonates dispersed in a clay matrix with abundant pyrite.

Following a 360h equilibration with SGW at 80°C, the chip surface became covered in mostly rhombohedral Ca phases, identified as calcite (CaCO_3) (Figure 5.10). The crystals are euhedral and measure approximately 30-50 μm in length. They are larger towards the left and right edge of the chip. The secondary Ca precipitates diminish towards the middle of the chip in size and abundance and appear spherular to subhedral. A distinct line of these less well-developed Ca phases runs from the right edge to the center, likely infilling porosity formed during the leaching. A scatter of acicular Ca crystals, likely aragonite (a CaCO_3 polymorph), formed on the left side of the chip. Their size and abundance similarly decrease towards the center of the sample. The cross-cutting relationship indicates that aragonite needles were formed after calcite precipitates.

The area with scarce new precipitates coincides with the thickest carbonate lamina. The light-grey carbonate features visible in the unreacted backscatter image are also identifiable after leaching, indicating that this part of the chip was subject to the least alteration. Where present, the calcite crystals are small and preferentially formed in pre-existing pore spaces or troughs (dark outlines visible in the backscatter image) at the edges of the carbonate features. A zoom-in, taken in the transect center, shows that the secondary Ca phases in this area are semi-euhedral, measuring 4-20 μm (Figure 5.11).

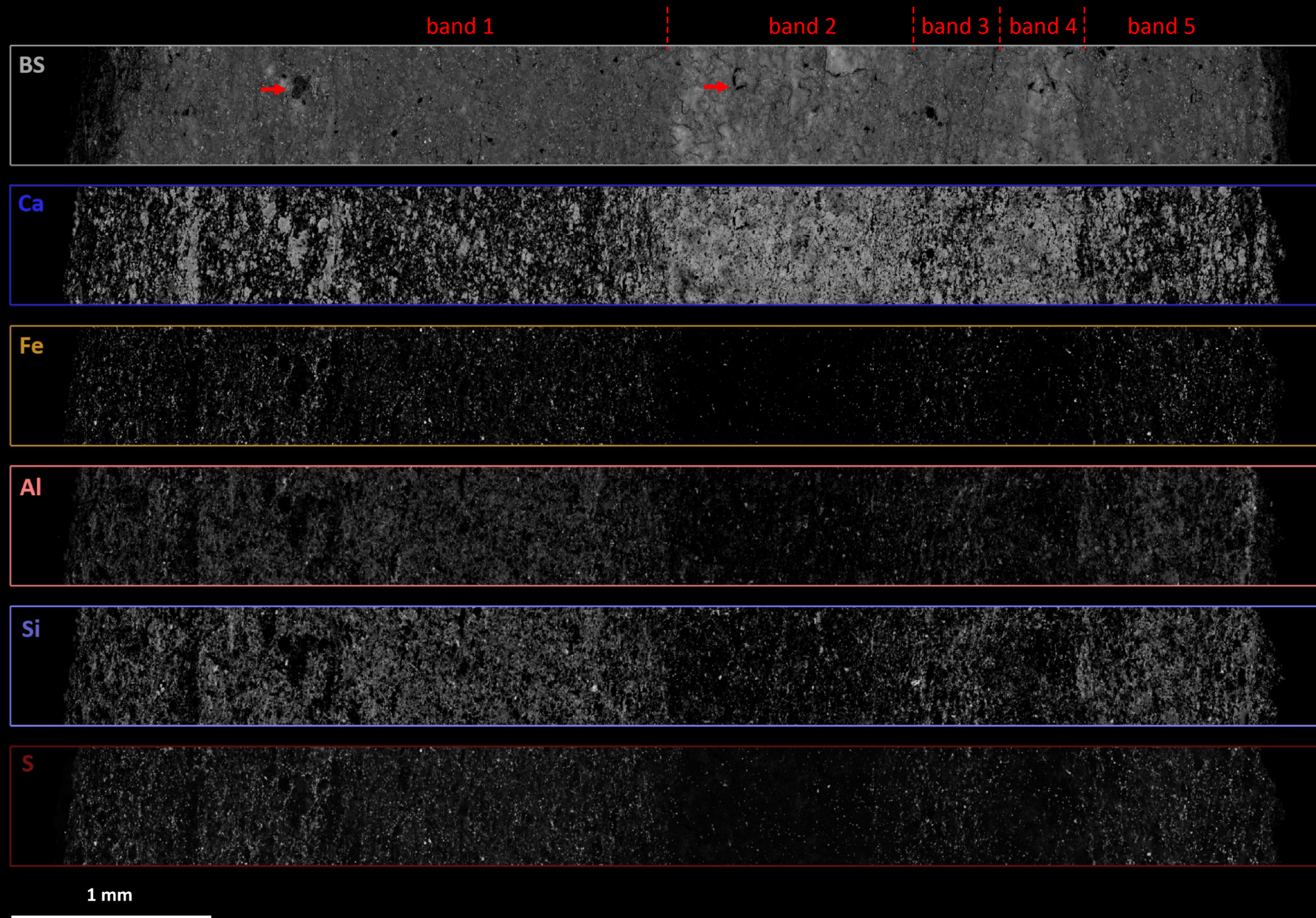


Figure 5.9 EPMA backscatter (BS) image and EDX maps for selected elements of the unreacted B4 chip. Red arrows in the BS image indicate features serving as markers between before and after leaching images. Band 1 - a silicate-rich zone, approximately 2.5 mm thick, with scattered framboidal pyrite, and dispersed carbonate clusters and discontinuous wispy carbonate ~0.1 mm laminae; Band 2 - a gradational transition into a carbonate-dominated 2.5 mm thick layer, with little to no pyrite present; Band 3 - a relatively sharp transition into another silicate-rich 0.5 mm lamina with dispersed carbonate clusters and more abundant pyrite; Band 4 - a carbonate-rich ~0.5 mm lamina; and Band 5 - a silicate-rich 0.5 m lamina with less abundant carbonates dispersed in a clay matrix with abundant pyrite.

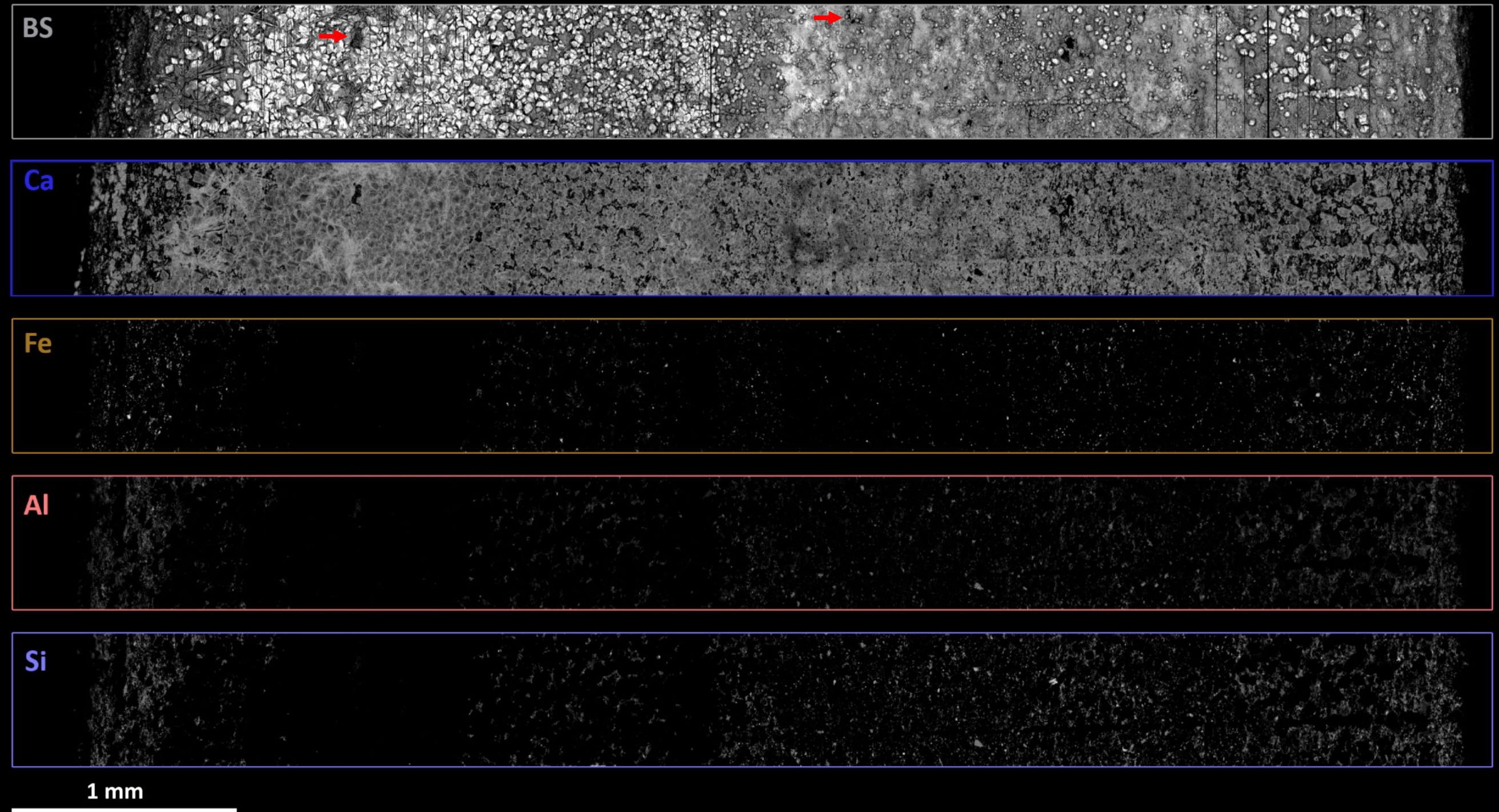


Figure 5.10 EPMA backscatter (BS) image of B4 chip after leaching with SGW at 80°C for 360h and EDX maps for selected elements. No S was detected by EDX after the experiment. The post-leaching images are offset 0.14 mm vertically and 0.12 mm horizontally from the unreacted ones and slightly rotated left. Red arrows in the BS image indicates a feature serving as a marker between before and after leaching images.

The crystals appear to have hexagonal to poorly defined rhombic faces growing on an amorphous Ca substrate. As the crystals do not have the conventional rhombohedral shape of calcite, it is challenging to ascertain which CaCO₃ polymorph they represent without further analysis, e.g. XRD or X-ray photoelectron spectroscopy (XPS) (Ni and Ratner, 2008). The morphology of CaCO₃ polymorphs is influenced by the crystallisation conditions (e.g. temperature and fluid composition) and incorporation of impurities, which may result in unconventional crystal shapes (Chakrabarty and Mahapatra, 1999; Fernandez-Diaz et al., 2006; Ni and Ratner, 2008).

The backscatter zoom-in of the unreacted transect center shows multiple pyrite framboids, their presence further confirmed by overlapping S and Fe EDX maps (Figure 5.11). No pyrite can be easily identified on the backscatter image post-reaction. However, element maps show a coinciding S and Fe hotspot, indicating that some pyrite is likely still present after the experiment. It is possible that pyrite dissolution became inhibited due to precipitation of secondary minerals as surface coatings or exhaustion of the available aqueous O₂, which is necessary for aqueous pyrite dissolution at neutral and alkaline pH.

The EDX maps (Figure 5.11) also show considerable changes in element distribution across the B4 surface following leaching, which appears to be controlled by textural heterogeneity. The silicate-rich layer with carbonate clusters and scattered framboidal pyrite on the left side of the chip was impacted the most: Fe, Al and Si were almost entirely replaced by Ca in that area.

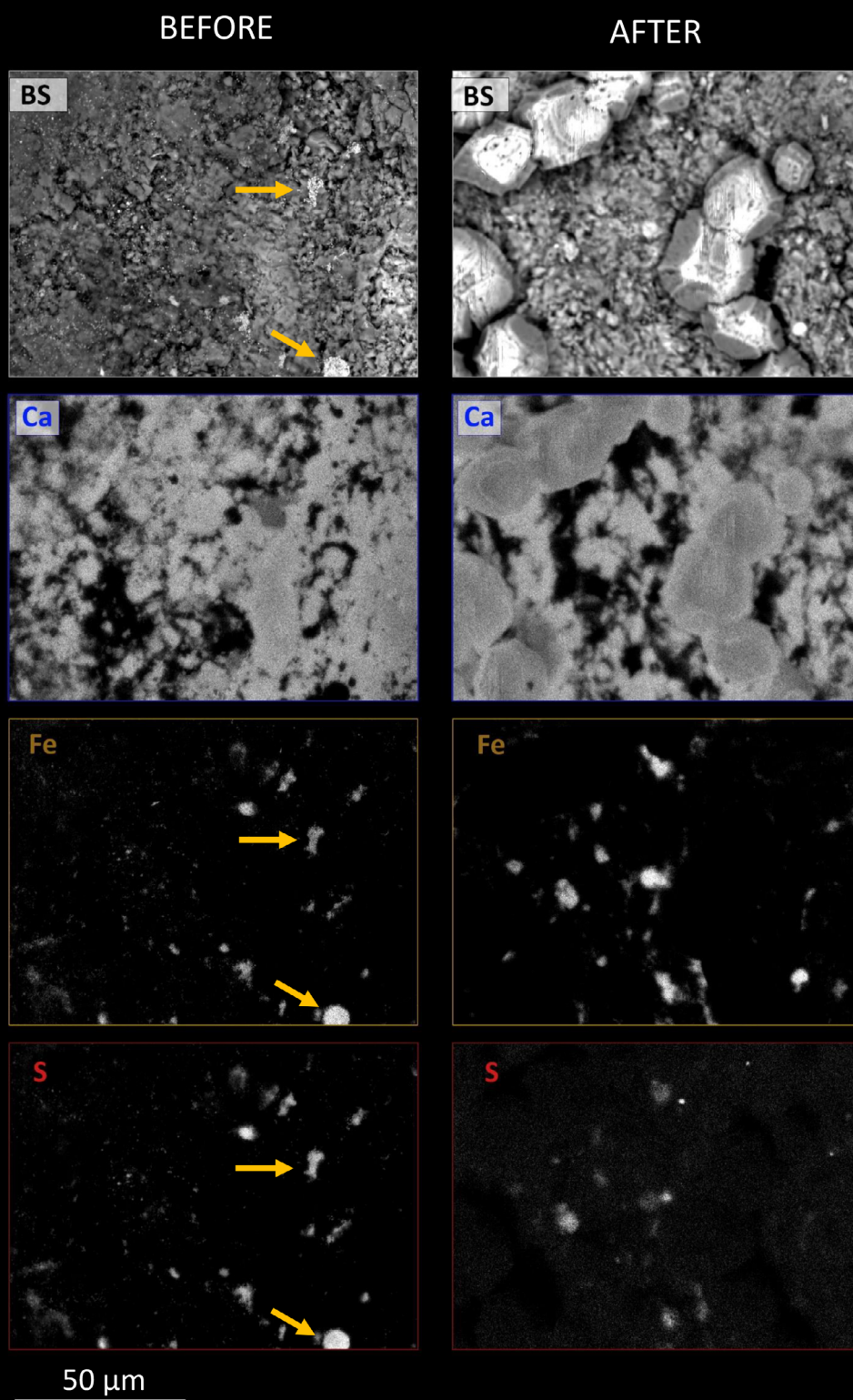


Figure 5.11 EPMA backscatter image of B4 chip zoom in, taken in the middle of the transect, before and after leaching with SGW at 80°C for 360h. Yellow arrows indicate pyrite framboids. Before and after images and maps do not coincide, as the post-leaching transect images are offset 0.14 mm vertically and 0.12 mm horizontally from the unreacted ones.

5.4.4.2. Elevated temperature and pressure

The unreacted B2 chip was fairly homogenous without any visible lamination in the backscatter image or the EDX maps (Figure 5.12). The elements appeared to be relatively uniformly distributed across the chip, with scattered pyrite framboids and carbonate minerals. The surface was rougher than that of the other chips.

Following leaching with SGW at 80°C and 150 bar, the sample's surface was almost uniformly covered with secondary Ca-precipitates, creating almost a crust-like appearance (Figure 5.13). Due to unusually high charging, zoom-in data was impossible to obtain. The Ca phases are relatively small, the largest measuring approximately 25 µm. They appear to be rhombohedral when well developed, closely resembling the CaCO₃ crystals which formed on the B4 chip after exposure to warm SGW at atmospheric pressure.

Large (0.15-0.4 mm) acicular secondary precipitates are also present in the center and on the right side of the chip, seemingly on the surface of the CaCO₃ crust. However, the exact order of precipitation cannot be determined due to the resolution of the transect image. EDX data shows it to be primarily composed of Ca and S, most likely a calcium sulphate mineral.

An increase in pressure to 150 bar resulted in considerably higher aqueous S concentrations (608 mg/l) at the end of experiment compared to the experiment conducted at atmospheric pressure (45 mg/l). The EDX maps show a complete redistribution of Fe and S across the chip surface, and these elements no longer coincide following the experiment. This suggests that the increase in pressure caused greater dissolution of pyrite, potentially by: (1) increasing the rate of pyrite reaction; or (2) by preventing or delaying precipitation of secondary minerals, which could passivate pyrite surfaces, until the pyrite reaction was complete.

The main secondary precipitate observed on the chip's surface post-reaction was a CaCO₃

crust, potentially calcite due to the rhombohedral morphology among the euhedral crystals. The solubility of CaCO_3 minerals decreases with increasing temperature but increases with increasing pressure (Seward et al., 2014), which could account for higher aqueous Ca concentrations under HPHT condition than those observed under HT and atmospheric pressure in this study. Provided the secondary precipitates formed in-situ and not as an artefact following the experiment, the increased solubility would affect the solution's saturation index with respect to CaCO_3 and thus impact when the secondary calcite precipitated.

Aqueous pressure oxidation of pyrite is a well known metallurgical pretreatment process for refractory gold ores, such as pyrite and arsenopyrite (Deng, 1993). Commercially employed since the 1980s, it involves oxidation of powdered sulfides with oxygen at high temperatures (180-210°C) and pressures (11-33 bar) to increase reaction kinetics and ensure complete oxidation of sulfide to sulfate. It can be conducted in alkaline or acidic media (Deng, 1993; Long, 2000 and references therein), and nowadays can also be performed under milder pressure and temperature conditions (SGS, 2021).

It is likely then that doping the pressure reactor with 10 bar of O_2 to maintain aerobic conditions led to a greater pyrite dissolution by increasing the amount of dissolved oxygen in solution, which forced the equilibrium of reaction into the product side of pyrite oxidation. As the Bowland-BE sample is mostly composed of calcite (66.3 wt%) and the starting SGW pH was 8.2, it can be assumed that pyrite oxidation in the HPHT SGW experiment progressed under alkaline conditions. According to Long (2000), alkaline pressure oxidation (in the presence of CaCO_3) will follow reaction and yield a residue of Fe(III)-oxides and calcium sulfate precipitates, which would support the secondary precipitates observed on the B3 sample. However, in the presence of water, the more likely oxidation product would be Fe(III) hydroxides rather than Fe(III) oxides.

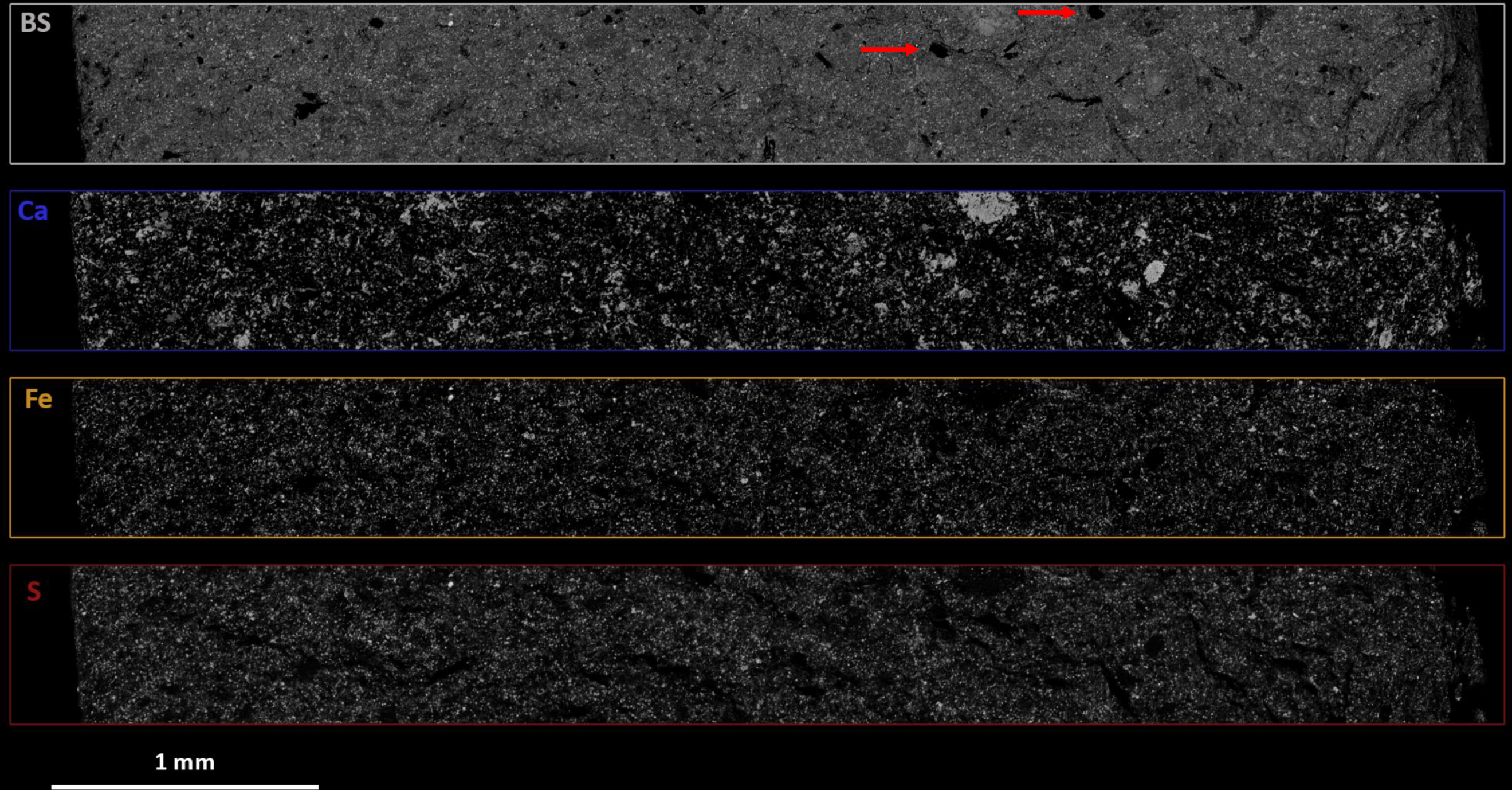


Figure 5.12 EPMA backscatter (BS) image and EDX maps for selected elements of the unreacted B2 chip. Red arrows in the BS image indicate features serving as markers between before and after leaching images.

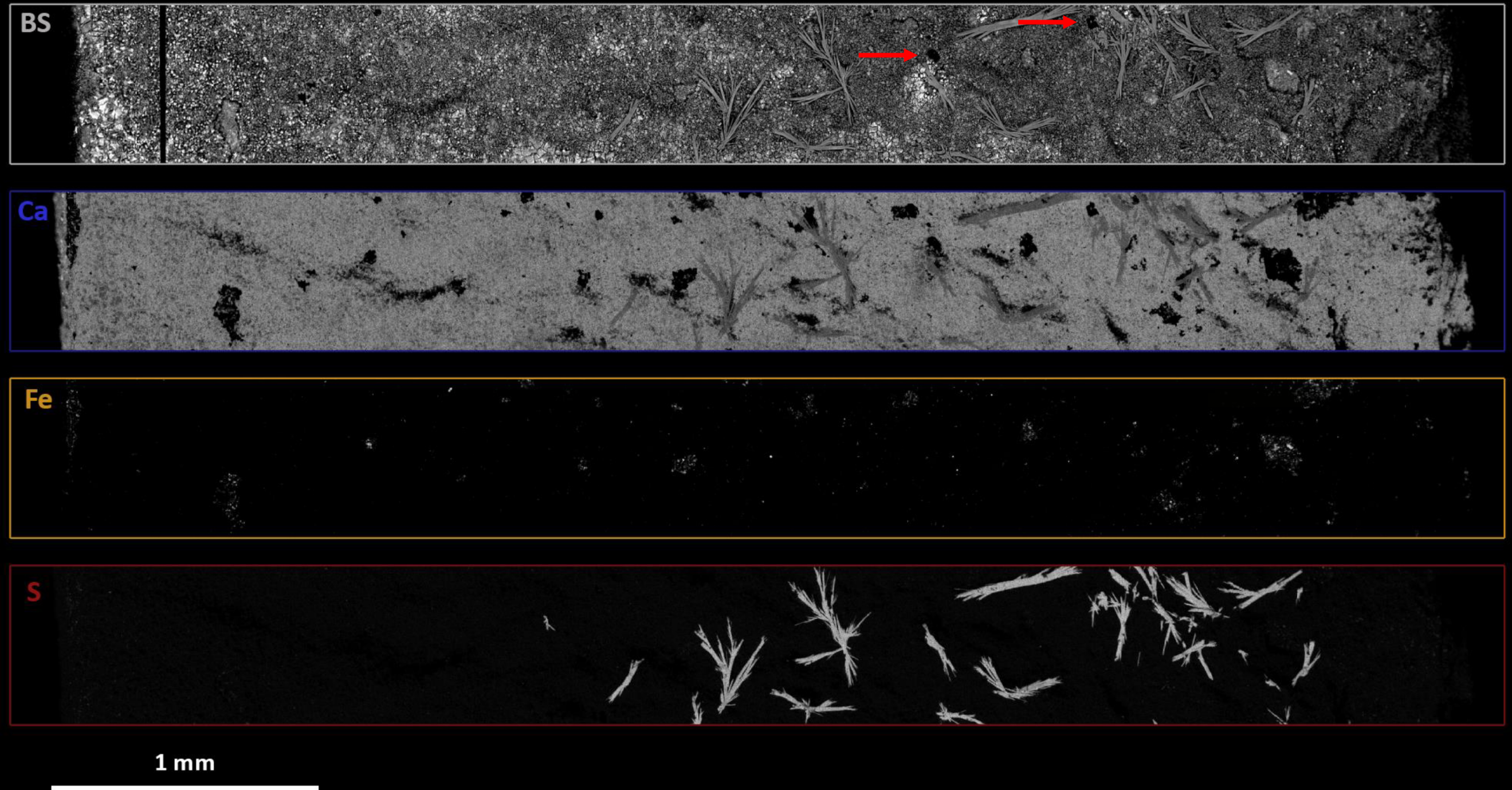


Figure 5.13 EPMA backscatter (BS) image of B2 chip after leaching with SGW at 80°C and 140 bar for 360h and EDX maps for selected elements. The post-leaching images are offset by 0.03 mm both vertically and horizontally from the unreacted ones. Red arrows in the BS image indicate features serving as markers between before and after leaching images.

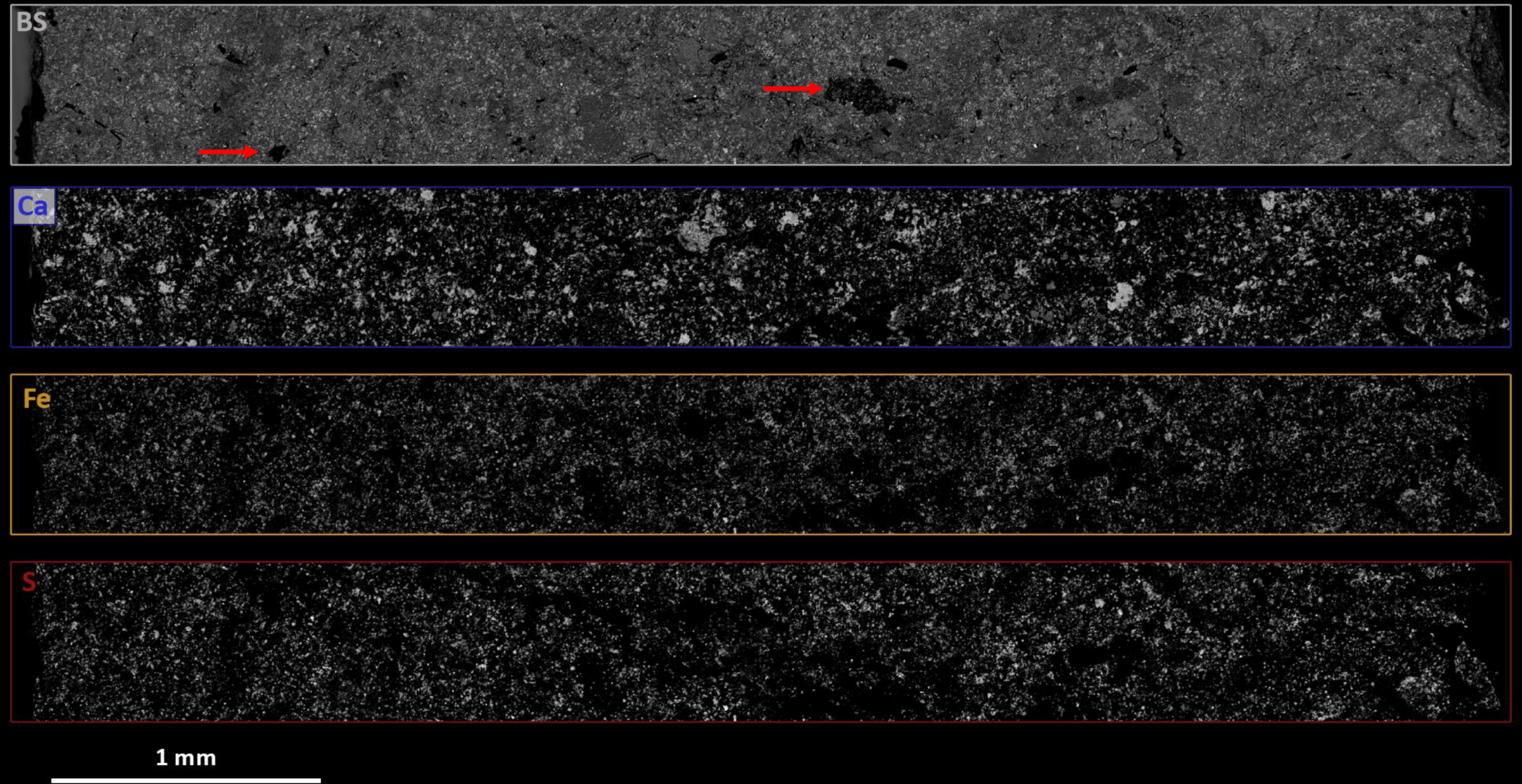


Figure 5.14 EPMA backscatter (BS) image and EDX maps for selected elements of the unreacted B3 chip. Red arrows in the BS image indicate features serving as markers between before and after leaching images.

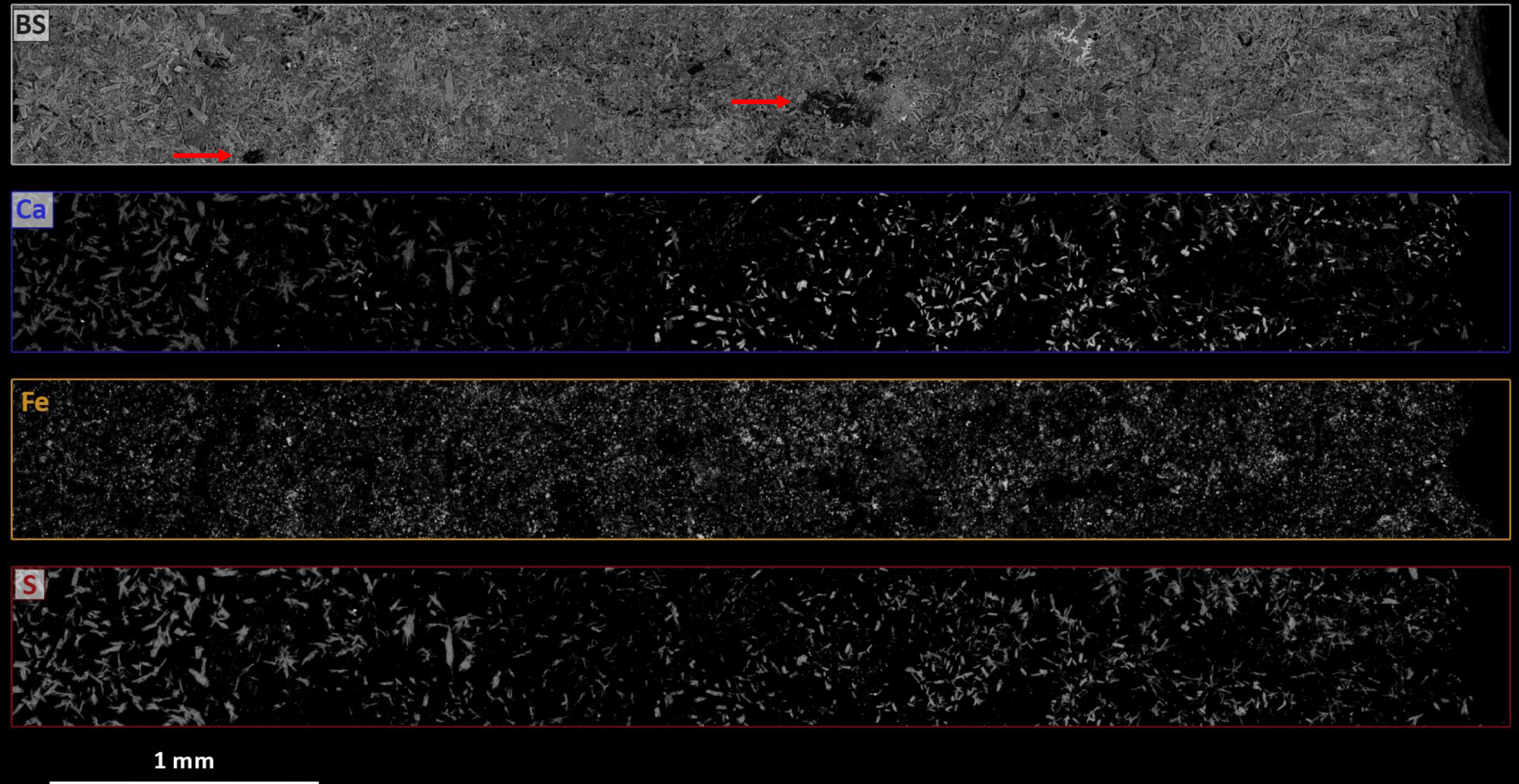


Figure 5.15 EPMA backscatter (BS) image of B3 chip after leaching with SHFF at 80°C for 360h and EDX maps for selected elements. The post-leaching images are offset by 0.01mm vertically and 0.1 mm horizontally from the unreacted ones. Red arrows in the BS image indicate features serving as markers between before and after leaching images.

5.4.5. SHFF

5.4.5.1. Elevated temperature and atmospheric pressure

The unreacted surface of the B3 chip was very similar to that of B2. It was generally homogenous without any visible lamination in both the backscatter image and the EDX maps (Figure 5.14). The element distribution was relatively uniform across the chip, with no readily apparent clusters or banding, and the elements appeared to be relatively uniformly distributed across the chip. Framboidal pyrite and carbonate minerals were dispersed over the whole sample.

Following leaching with warm SHFF, the B3 chip surface was covered in acicular and tabular blade-like CaSO_4 precipitates (Figure 5.15). Acicular phases are particularly abundant towards the left and right edges of the chip but less noticeable in the middle of the transect, which is dominated by the tabular precipitates. The blade-like crystals display a strong cleavage (Figure 5.16) and are present across the whole surface. The precipitate sizes vary across the reacted chip: crystals of both morphologies are considerably larger on the left side of the chip and smallest in the center.

Both morphologies observed are typical of CaSO_4 precipitates, particularly gypsum (Antony et al., 2011). Factors such as supersaturation ratio and crystallisation kinetics can influence CaSO_4 morphology. In other studies, acicular crystals have been observed to form under low supersaturation ratios (<2.27) and governed by surface crystallisation with lengthy induction time before nucleation. The plate-like morphology has been observed at a supersaturation ratio of 10.86, dominated by bulk crystallisation (Antony et al., 2011). Additionally, the ratio of Ca^{2+} to SO_4^{2-} ions at constant supersaturation was shown to influence the rate of growth and morphology of gypsum crystals: SO_4^{2-} rich solutions produced plate-like crystals, whereas needle-like crystals formed in Ca^{2+} rich solutions (Mbogoro et al., 2017). The degree of supersaturation is also known to

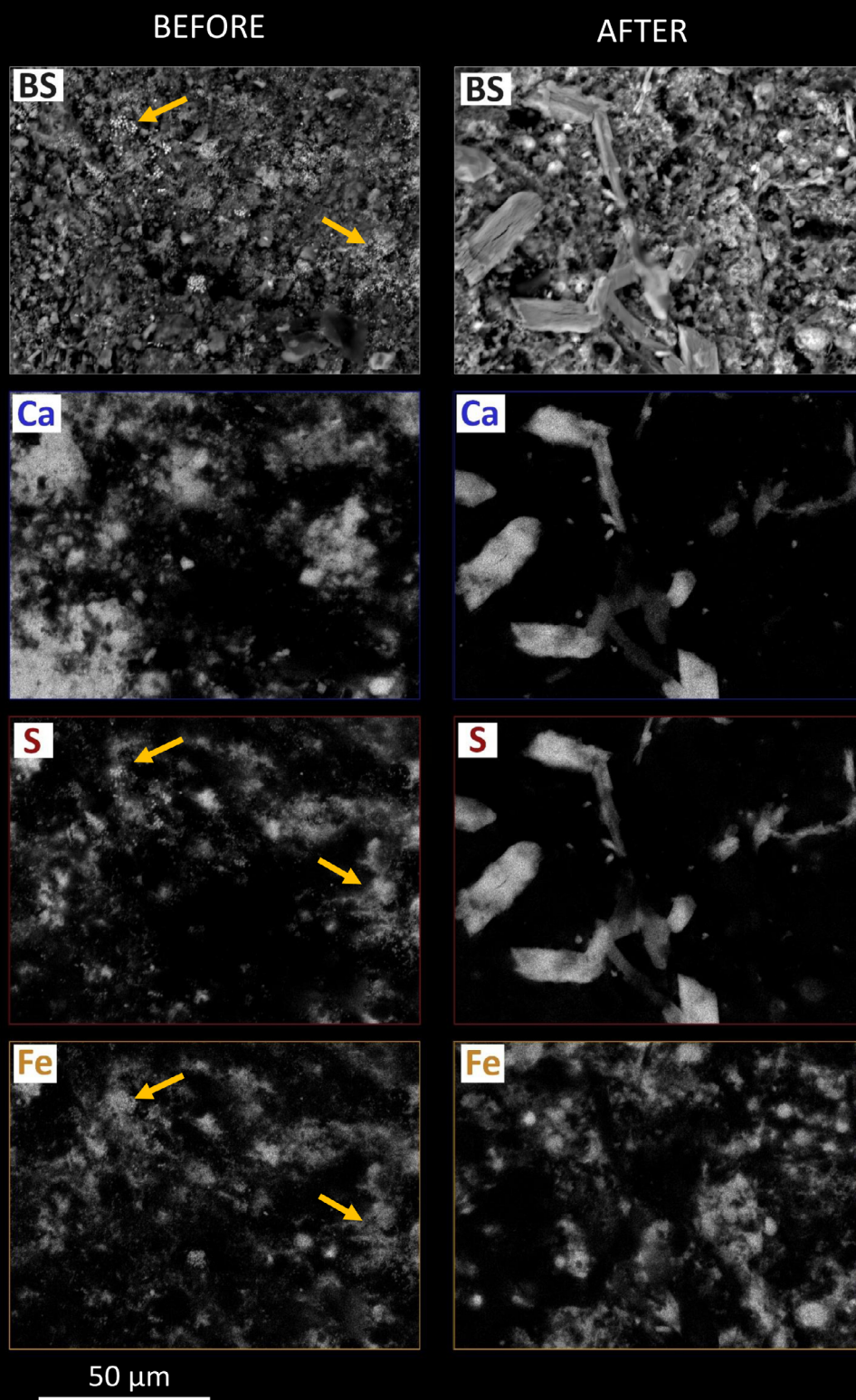


Figure 5.16 EPMA backscatter image of B3 chip zoom in, taken in the middle of the transect, before and after leaching with SHFF at 80°C for 360h. Yellow arrows indicate examples of pyrite framboids. Before and after images and maps do not coincide, as the post-leaching transect images are offset by 0.01 mm vertically and 0.1 mm horizontally from the unreacted ones.

influence the nucleation rate and crystal size. The formation of numerous but small crystals is favoured by high supersaturation conditions, which promote high nucleation rates. At low supersaturation, crystals can grow faster than they nucleate, leading to less numerous but larger crystals (Bard and Bilal, 2011). Consequently, precipitation of the two different habits of CaSO_4 crystals likely reflects the changing chemistry of the leachate.

The EDX maps show a complete redistribution of Ca and S before and after the experiment. Prior to leaching, element maps for S and Fe overlapped and have can be interpreted to represent disseminated pyrite which was identified in the zoom-in backscatter image (Figure 5.16). Following the experiment, the two element maps no longer coincide and Ca and S have been mobilised into the solution and redistributed as the CaSO_4 precipitates. On the other hand, EDX maps for Fe appear similar before and after leaching. No pyrite is visible in the backscatter image after leaching, and its dissolution is further supported by the remobilised S content and the elevated aqueous SO_4^{2-} concentration of 4822 mg/l compared to 3583.4 mg/l recorded in a heated and pressurised blank SHFF. The post-leaching Fe element map likely represents secondary Fe-(oxy)hydroxides, a product of pyrite oxidation reactions (see Chapter 3.3). Under alkaline conditions, secondary Fe-precipitates have been shown to form nearby Fe point sources, primarily framboidal pyrite, due to rapid rates of aqueous Fe(II) oxidation (Harrison et al., 2017; Jew et al., 2017). The in-situ precipitation of Fe-(oxy)hydroxides is supported by the low aqueous Fe concentrations at the end of the chip experiment (see Table 5.8). Given that the main source of Fe in Bowland-BE is pyrite, Fe released during its oxidation must have been released, oxidised and precipitated as solid before the end of the experiment to account for the negligible dissolved Fe concentrations. The new precipitates may directly coat pyrite surfaces, leading to their passivation and severely limiting pyrite oxidation (Chandra and Gerson et al., 2010; Harrison et al., 2017; Jeng et al., 1992).

5.4.5.2. Elevated temperature and pressure

The unreacted B1 chip was the largest reacted with visible parallel lamination highlighted by colour changes. The laminae were less noticeable in the backscatter image. However, the EDX maps showed that the chip could be divided into three zones (Figure 5.17):

1. a ~2 mm silicate-rich layer with disseminated framboidal pyrite, dispersed carbonate clusters and discontinuous wispy carbonate laminae;
2. a ~8 mm thick carbonate-rich zone, with a lesser amount of pyrite; carbonate abundance appears to very gradually decrease towards the right edge;
3. and another ~2mm silicate-rich layer with carbonate clusters and disseminated framboidal pyrite.

Exposure to SHFF at 80°C and 180 bar for 360h caused strong mineral etching and dissolution across the sample's surface. The initial mineral heterogeneity appeared to control the degree of alteration (Figure 5.18). Carbonate dissolution caused a considerable porosity increase, with large channels and voids forming in the silicate-rich zones on the left and right sides of the chip where carbonate lamina or clusters were previously observed. The carbonate-rich zone was not uniformly affected, reflecting the decrease in carbonate abundance towards the right.

The EDX maps further illustrate the high degree of element mobilisation and redistribution as a result of the experiment. Before the experiment, Fe and S distributions coincided and showed an inverse relationship with Ca (Figure 5.19). Afterwards, Ca and S element maps overlap and were inferred to represent secondary CaSO_4 phases, located primarily along the chip's left and right edges. The post-leaching Fe distribution is no longer related to S and again likely represents secondary Fe-(oxy)hydroxides that precipitated nearby or on Fe-point sources (i.e. pyrite framboids).

Pyrite dissolution and precipitation of secondary Fe-phases is supported by the zoom-

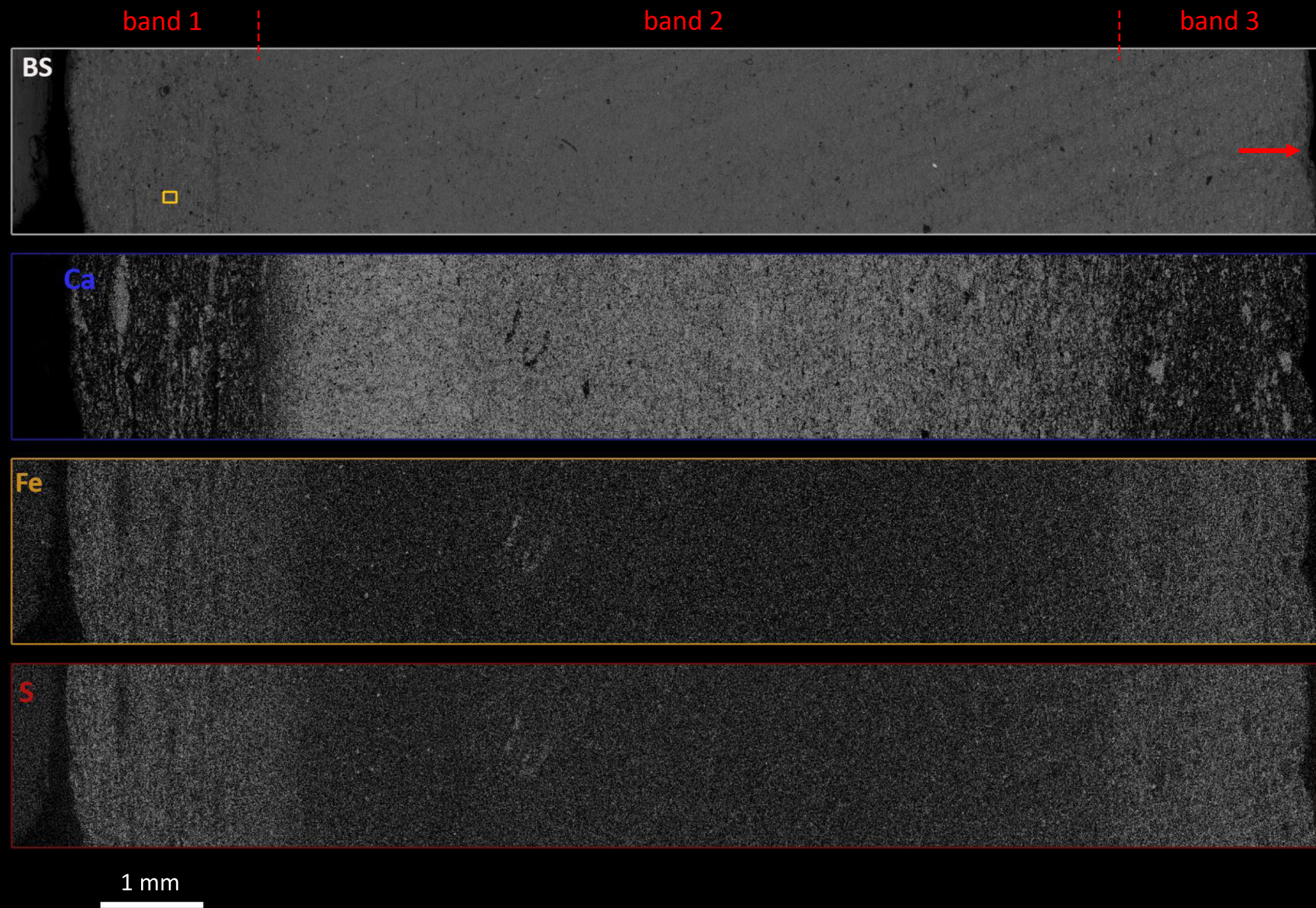


Figure 5.17 LVSEM backscatter (BS) image and EDX maps for selected elements of the unreacted B1 chip. Red arrow in the BS image indicates a feature serving as a marker between before and after leaching images.



Figure 5.18 LVSEM backscatter (BS) image and EDX maps for selected elements of the unreacted B1 chip. Red arrow in the BS image indicates a feature serving as a marker between before and after leaching images.

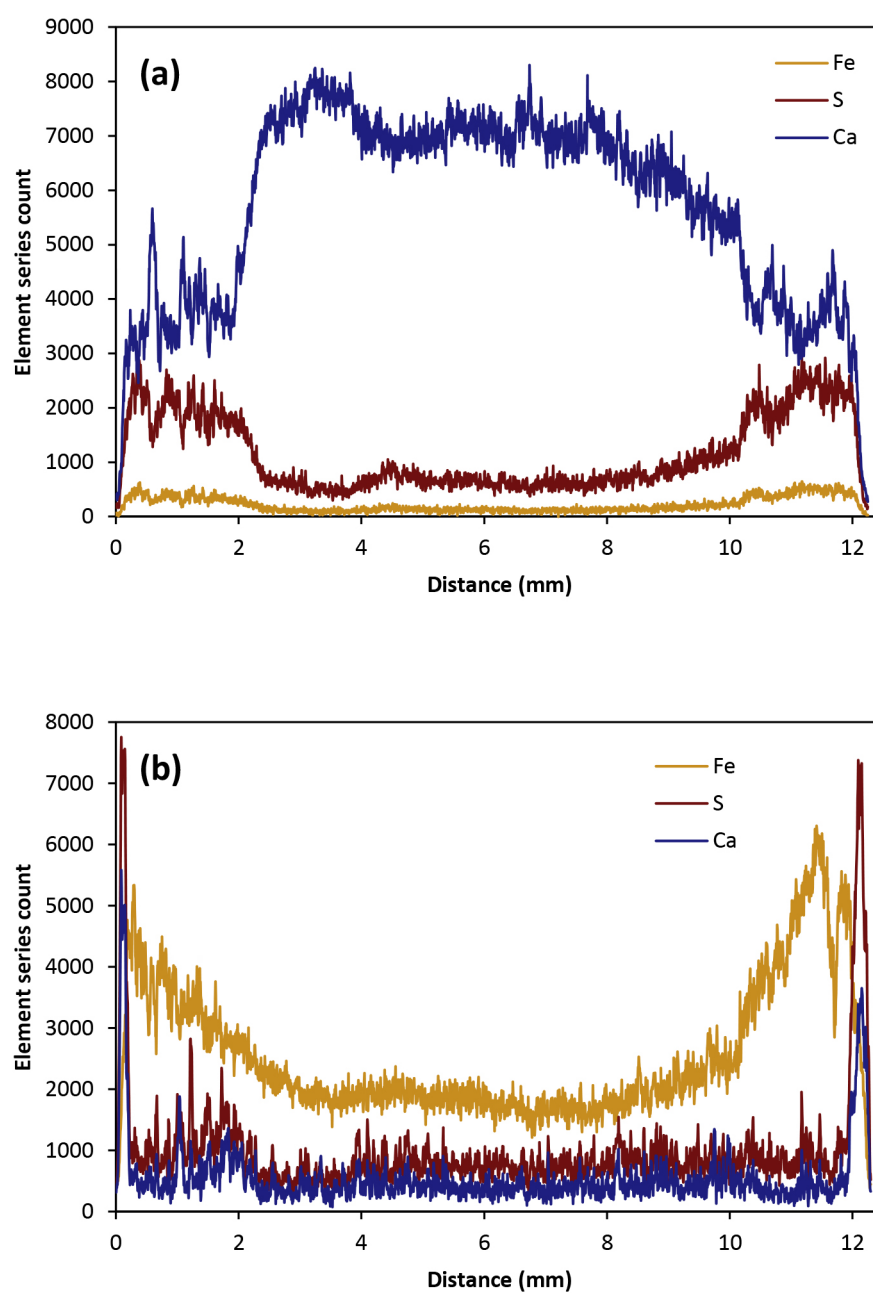


Figure 5.19 Relative abundance of Fe, S and Ca across the length of B1 chip (a) before and (b) after leaching with SHFF at HPHT. Data represent EDX measurements and do not represent actual concentrations.

in backscatter and element maps, taken on the left side of the sample before and after the experiment. Multiple pyrite framboids are visible prior to leaching in the backscatter image and marked by co-located S and Fe hotspots. No pyrite can be easily identified on the backscatter image post-reaction, and S and Fe EDX maps no longer match indicating they are now in independent phases. The zoom-in backscatter image also shows a subhedral precipitate (Figure 5.20); EDX spectra indicated that it was mainly composed of Sr and S.

Since no substantial CaSO_4 precipitation occurred on the chip's surface, an aliquot of warm filtered leachate was taken immediately following the end of experiments and inspected using LVSEM for any precipitates that may occur due to cooling and depressurisation. Two distinct phases formed (Figure 5.21): (1) large tabular crystals strongly associated with K and Cl, appear lighter in the backscatter image, with (2) blade- and rosette-like CaSO_4 crystals growing around them.

5.4.6. Discussion and summary

The experiments with Bowland-BE chips provide insight into how elevated pressures might affect rock-fluid interactions at reservoir temperatures. Mineral dissolution and precipitation were observed under all examined pressure and temperature conditions and for both leaching fluids. However, the extent of precipitation and the type of secondary minerals was controlled by pressure, fluid type, and the original rock chip mineralogy and structure .

In experiments with SGW, CaCO_3 precipitation dominated under both atmospheric and elevated pressures, extensively coating the surfaces of the reacted samples with carbonate crystals. An increase in pressure to 150 bar resulted in greater pyrite dissolution due to pressure oxidation and yielded higher aqueous S concentrations. This, in turn, resulted in the precipitation of large acicular CaSO_4 crystals.

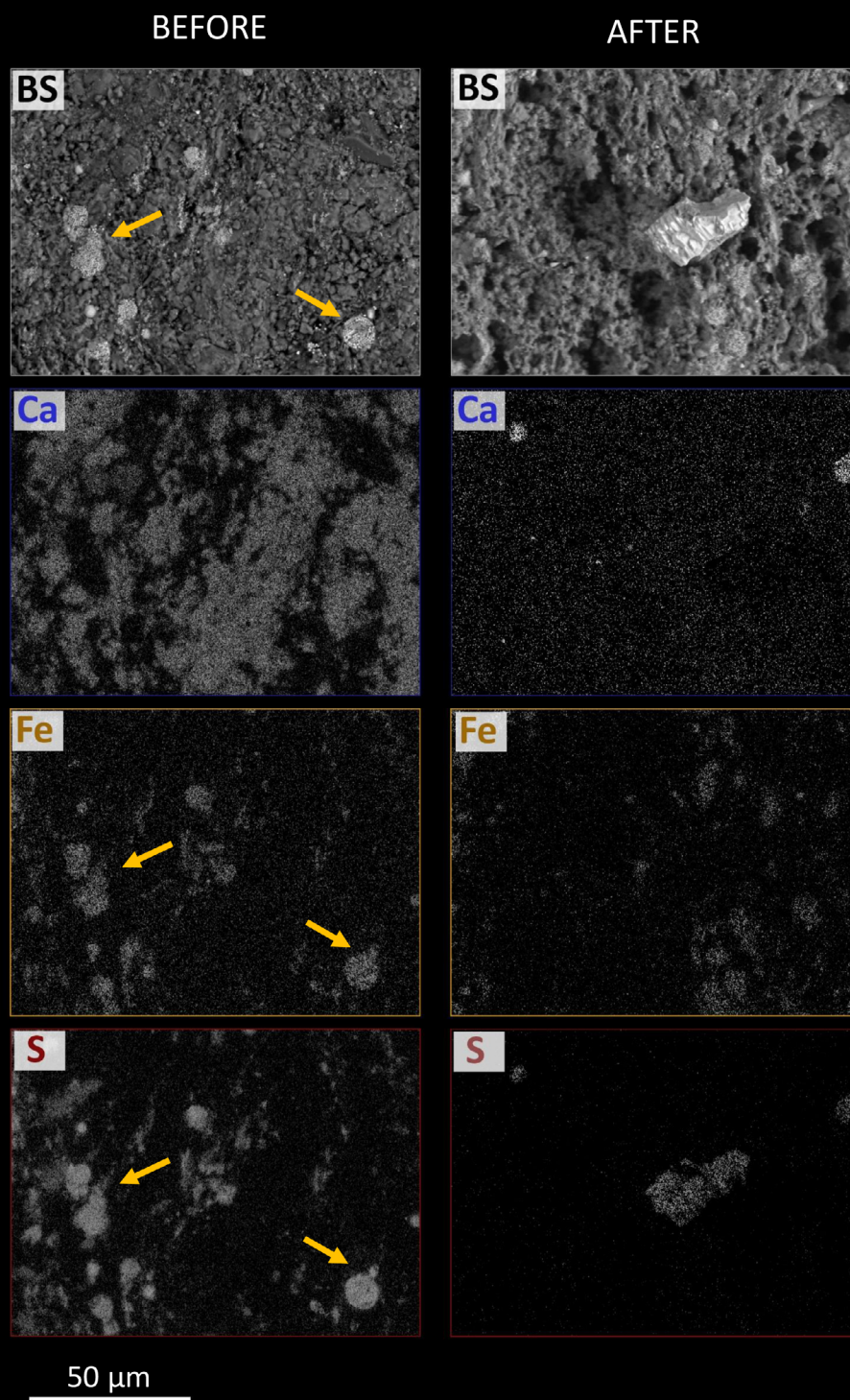


Figure 5.20 LVSEM backscatter image of B1 chip zoom in, taken on the lower left side of the transect, before and after leaching with SHFF at 80°C and 183 bar for 360h. Yellow arrows indicate examples of pyrite framboids. Before and after images and maps do not coincide, as the post-leaching transect images are offset by 0.2 mm vertically and 0.15 mm horizontally from the unreacted ones.

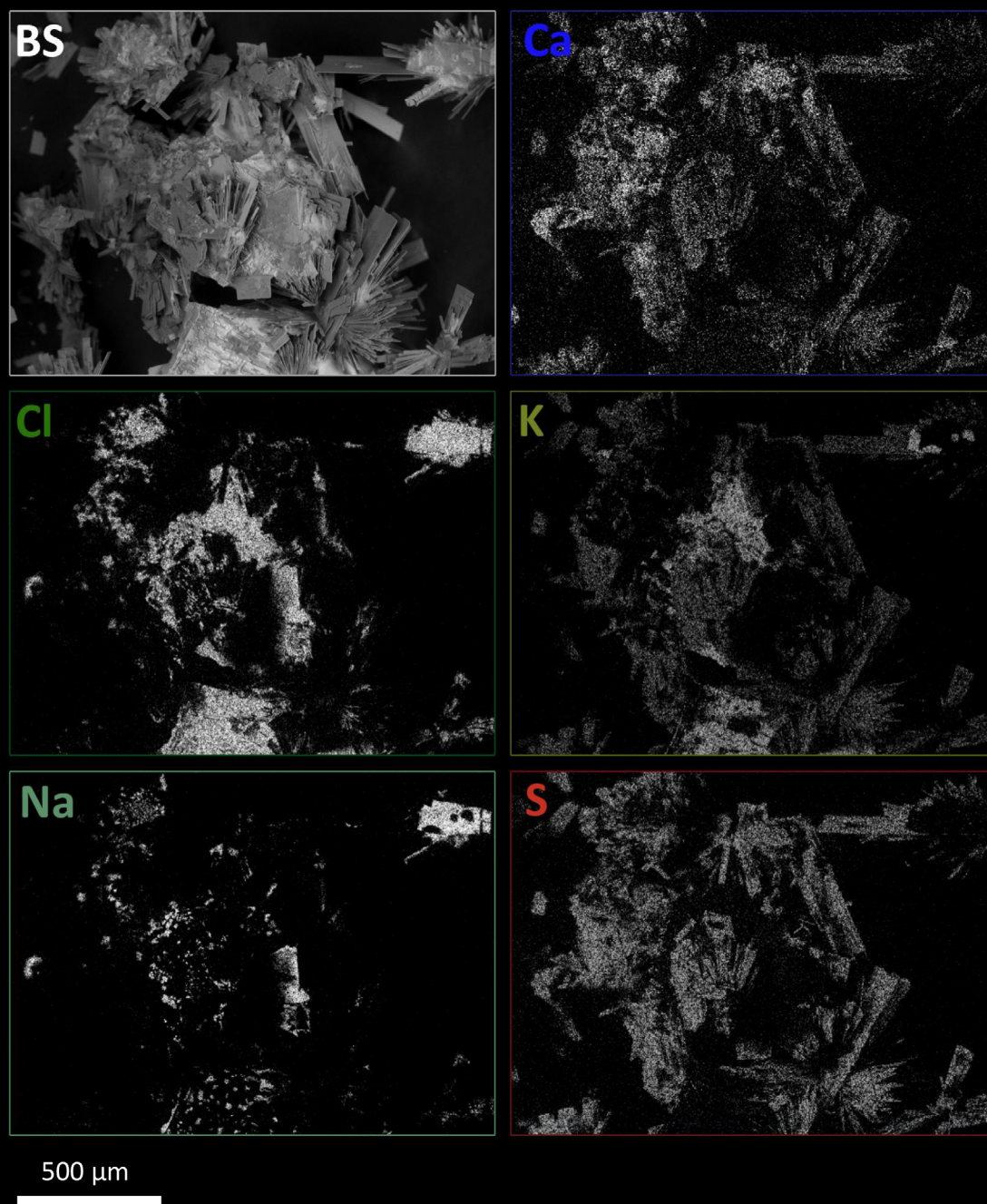


Figure 5.21 LVSEM backscatter image of precipitates formed during cooling of B1 leachate, following a 360h experiment with SHFF at 80°C and 183 bar.

In the experiments with SHFF, thermal activation of ammonium persulfate significantly contributed to the dissolved SO_4^{2-} concentration, and consequently, CaSO_4 phases were preferentially precipitated. The secondary CaSO_4 phases were abundant under elevated temperature and atmospheric pressure, but neither they nor other micrometre-scale precipitates were plentiful under HPHT conditions. Exposure to the SHFF under 80°C and 180 bar caused severe changes to the sample's surface. The porosity was visibly increased due to mineral etching and dissolution across the whole chip but was particularly enhanced in areas where carbonate minerals were previously abundant either as laminae or clusters.

Some of the newly-formed porosity was likely occluded by in-situ precipitation of secondary Fe-(oxy)hydroxides, which were produced due to pyrite oxidation. Due to the alkaline conditions, these should be expected to precipitate rapidly as individual grains or grain clusters close to where pyrite framboids originally were or as coatings on pyrite surfaces. Consequently, these secondary Fe-precipitates are likely to affect porosity (and inhibit gas flow), albeit in a localised manner. Secondary Fe-(oxy)hydroxides were also inferred in the chip experiments with SHFF at elevated temperature and atmospheric pressure and following leaching with SGW at elevated temperature and pressure. These results agree with results from other experimental studies on fluid-rock interactions during hydraulic fracturing, which showed evidence for secondary Fe-precipitates at both ambient and elevated pressure and temperature conditions (Harrison et al., 2017; Jew et al., 2017; Pearce et al., 2018; Wang et al., 2015; Wilke et al., 2015).

Conversely, no significant porosity enhancements were observed during SHFF leaching at 80°C and during both SGW experiments. The surface alteration was not as severe as during HPHT exposure to SHFF, and many distinct surface features remained easily recognisable after the experiment. Additionally, the extensive precipitation of either or both CaCO_3 and CaSO_4 phases likely greatly occluded any secondary porosity that might have formed. However, it is unclear if these precipitates formed *in situ* or due to the decrease in temperature and pressure at the termination of the experiment. Blade-

and rosette-like CaSO_4 crystals precipitated from an aliquot of warm filtered leachate taken immediately following the end of HPHT SHFF experiments. This indicates that some if not all of the micrometer-scale precipitates observed on the remaining chips could have formed as experimental artefacts.

Calcium carbonate and calcium sulfate minerals are common scales in oil and gas wells, geothermal wells, or even on reverse osmosis membranes during desalination and wastewater treatment (Antony et al., 2011; Dai et al., 2017; Kamal et al., 2018; Mackay and Jordan, 2005). These scales can often precipitate in the wellbore when produced water flows to the surface due to temperature and pressure drops (Dai et al., 2017). Generally, scales may precipitate at any point both in the wells or in the reservoir if the system's equilibrium is disturbed and supersaturation is generated. Supersaturation can be achieved due to changes in the pressure and temperature conditions, which affect mineral solubility – CaCO_3 and CaSO_4 solubilities decrease with higher temperature but considerably increase with higher ionic strength and pressure. These scales can also form as a result of chemical interaction between two incompatible fluids, e.g. during mixing of injected seawater with high SO_4^{2-} content and formation brines enriched in Ca, Ba or Sr ions (Mahmoud, 2014; Mackay and Jordan, 2005). Several experimental studies demonstrated an in-situ precipitation of calcium carbonate, gypsum, anhydrite or barite due to the interaction of synthetic fracturing fluids with shale solids (Dieterich et al., 2016; Marcon et al., 2017; Paukert Vankeuren et al., 2017). Paukert Vankeuren et al. (2017) concluded that the most likely timeframe for scale formation during hydraulic fracturing operation is during fluid injection and during the shut-in period. These precipitates could lead to localised reductions in porosity and fracture aperture and inhibit gas flow to the well.

Therefore, further research would be beneficial to investigate whether the observed CaCO_3 and CaSO_4 precipitates formed during the experiments or afterwards, e.g. using a core flow-through experiment combined with real-time imaging by X-ray computer tomography (XCT). Further analysis, e.g. XRD or XPS, could also shed light on which

CaCO_3 and CaSO_4 polymorphs precipitated as EPMA or SEM tend to be inconclusive for distinguishing between them as their morphologies are not unique. The morphology of CaCO_3 polymorphs (calcite, vaterite and aragonite) is easily influenced by the crystallisation conditions (e.g. temperature and fluid composition) and incorporation of impurities, which may result in unconventional crystal shapes (Chakrabarty and Mahapatra, 1999; Fernandez-Diaz et al., 2006; Ni and Ratner, 2008). Calcium sulfate also commonly precipitates from aqueous solutions in three crystalline forms: gypsum (the dihydrate form), bassanite (the hemihydrate form), and anhydrite (the anhydrous form). Bassanite is metastable in aqueous solutions, whereas gypsum is most stable below 40-60°C and anhydrite above 130°C, with no clear indication of which phase is more stable between 40-130°C (Dai et al., 2017). Parameters such as supersaturation level, temperature, pressure and ionic strength will affect which polymorph is formed (Dai et al., 2017).

CHAPTER 6

DISCUSSION

This chapter provides a synthesis of the study's findings and discusses the implications of the results presented in Chapters 3 to 5. First, the rationale behind the main research questions will be summarised before discussing the heterogeneity of shale samples. The next section focuses on the observed trends in element mobilisation by SGW and SHFF and compares them to previous studies. The factors that might affect the observed element release are then discussed. The implications for environmental impacts and future operations in the field are then described, using the leaching data from the Australian powdered samples and powdered Bowland Shale. The chapter concludes by examining how the results obtained in this study can be applied to other systems.

6.1. Rationale and main research questions

Technological advancements in hydraulic fracturing and horizontal drilling have facilitated the economic extraction of hydrocarbons from previously unviable organic-rich shales. This has resulted in an acceleration of natural gas production, especially shale gas, in the USA during the last decade (Vidic et al., 2013) and has transformed the global energy markets. The most productive shale gas plays in the US (the Marcellus and Utica shales in the Appalachian Basin; Eagle Ford and Haynesville shales in the Gulf Coast) increased the amount of gas produced in the USA from less than 20tcf in 2000 to over 25tcf in 2017 (EIA, 2018). Therefore, many other countries began exploring their own shale gas resource potential, but significant environmental and social concerns

have been raised that have culminated in several countries or regions imposing a ban or moratorium on shale gas extraction (Thomas et al., 2017). One of the key concerns regards the composition of the fluids produced from shale gas extraction activities (flowback and produced water) and their potential to contaminate water resources (e.g. Entekin et al., 2011; Rahm and Riha, 2012; Vengosh et al., 2014). For example, wastewater from wells in the Marcellus Shale, US, can have TDS concentrations of up to 345,000 mg/l, which to remove effectively require the use of expensive technologies such as reverse osmosis that may not be easily available (Boschee, 2014; Ferrar et al., 2013; Wilson and VanBriesen, 2012). Final wastewater composition is thought to be a function of the local geology, mineralogy and geochemical conditions, fracturing fluid additives, the quality of the fracturing fluid makeup water (fresh versus recycled), and the length of the contact time between the fluid and the formation (US EPA, 2016).

The large quantities of wastewater produced throughout the lifetime of a well can contain heavy metals and other regulated potentially toxic elements (PTEs), which can arise from: (1) mixing of formation brines with fracturing fluids and (2) rock- fluid interactions, such as dissolution of shale minerals caused by the injection of fracturing fluids into the target formation (Chapman et al., 2012; Haluszczak et al., 2013; Phan et al., 2015; Renock et al., 2016). A few anecdotal studies have potentially connected PTEs from shale gas wastewater spills to animal and human harm (e.g. Bamberger and Oswald, 2012; Papoulias and Velasco, 2013). A review of publicly available literature (CHAPTER 1) revealed that publicly available information on *exact* concentrations of PTEs in shale gas wastewater is limited to a handful of sources - predominantly grey literature reports on the Marcellus Shale wastewater composition (Alley et al., 2011; Rowan et al., 2015; Ziemkiewicz and He, 2015). This lack of publicly available information impedes a detailed evaluation of the potential environmental and human health impacts of shale gas wastewater (mis)management. It also suggests that the current evidence base is not sufficiently robust and extensive enough to support comprehensive risk evaluation, especially in areas where shale gas development is only under consideration.

To date, most studies have tended to focus on salinity (major elements) in the shale gas wastewater and whether it originated from mixing of the injected fluids with the formation brines (e.g. Haluszczak et al., 2013; Rowan et al., 2015). PTEs (including heavy metals such as arsenic, mercury and lead) have so far received little direct research attention although they are one of the areas of public concern (Abualfaraj et al., 2014; Kibble et al., 2013; Ziemkiewicz and He, 2015). The extent to which the rock-fluid interactions during hydraulic fracturing contribute to the wastewater geochemistry or impact the shale formation properties is still an area of active research (e.g. Harrison et al., 2017; Phan et al., 2020; Xiong et al., 2020). Consequently, laboratory studies are needed to characterise geochemical reactions that may occur upon the injection of fracturing fluids into the targeted shale formation and evaluate the potential for PTE mobilisation during the hydraulic fracturing process.

Twelve relatively recent studies (2015-2020), designed chiefly as benchtop or batch reactor experiments, investigated the rock-fluid interactions during hydraulic fracturing operations (see Table 2.1 Summary of experimental parameters used by the different studies discussed in section 2.2). Some of these studies show evidence for calcite dissolution and pyrite oxidation, and precipitation of secondary iron and sulfate phases. These processes appear to control the amount of PTEs mobilised into solution (Harrison et al., 2017; Jew et al., 2017; Marcon et al., 2017; Pearce et al., 2018; Wang et al., 2015; Wang et al., 2016; Wilke et al., 2015; Xiong et al., 2020). Most studies were performed under atmospheric pressures and ambient or elevated temperatures and utilised primarily powdered shale samples exposed to distilled water or water mixed with common hydraulic fracturing additives (e.g. citrate, HCl) for varying lengths of time (24 h to 6 months). Eight studies included experiments at elevated pressures and temperatures (Dieterich et al., 2016; Li et al., 2019b; Marcon et al., 2017; Paukert Vankeuren et al., 2017; Pearce et al., 2018; Tasker et al., 2017; Wilke et al., 2015; Xiong et al., 2020).

Any experimental study will be designed to test a specific hypothesis or recreate a particular set of *in operando* conditions using a specific, tailored set of parameters. Fluid composition, length of experiment, solid:fluid ratio, and the pressure and temperature conditions therefore vary widely among the reviewed studies. Although some general trends in the possible rock-fluid interactions during hydraulic fracturing emerge from the laboratory studies, the differences in the key experimental parameters - especially if their exact control on the observed interactions is not always known – impede cross-study comparisons or extrapolation of the results to field conditions. Additionally, the suite of shale samples used in the studies have been largely limited to American shales, predominantly Marcellus Shale.

The principal aim of this thesis was to systematically explore which PTEs could be mobilised into flowback and produced waters from shale gas formations due to hydraulic fracturing and examine how different mineralogies and experimental parameters can influence the observed rock-fluid interactions.

The key research questions the laboratory work in this study aimed to answer were:

Q1. What are the trace element concentrations of the selected gas shales, and how much do they vary? Which metals and metalloids may be amenable to mobilisation under environmental conditions?

Q2. Do hydraulic fracturing fluids mobilise elements from the shale? Do the considered chemical additives affect element mobilisation? Are the trace element mobilisation patterns consistent among the different shales? If not, why?

Q3. How do experimental conditions (T, P, pH and solid:fluid ratio) affect element mobilisation?

6.2. Not each shale is the same, and it matters

6.2.1. Mineralogy and trace element content

Shale gas formations are typically heterogeneous, with multiple lithologies and lithofacies occurring in cyclical sequences (e.g. Dawson, 2000; Harris et al., 2011; Hemmesch et al., 2014). The formations are often divided into multiple members, each with distinct characteristics. For example, the Eagle Ford Formation is typically divided into lower and upper Eagle Ford (Donovan and Staerker, 2010). The Lower Eagle Ford is an organically rich basal section of predominantly dark and well-laminated shales with minor bioturbation, interpreted as transgressive deposits in low-energy, poorly oxygenated marine environment. An organically leaner but more calcareous overlying Upper Eagle Ford is dominated by thin, high-frequency cycles of shales, limestones and siltstones which were deposited in a high energy, well-oxygenated shallow marine setting (Dawson, 2000; Donovan and Staerker, 2010).

Such lithological heterogeneity and associated mineralogical variations will have implications for a particular shale's mechanical properties as well as its chemical composition, particularly trace element distribution (Harris et al., 2011; Harris et al., 2013; Sano et al., 2013; Toten and Hanan, 2007). Chermak and Schreiber (2014) reviewed published mineralogical and trace element data for nine producing US gas shales, highlighting a wide intergroup and intragroup variance in mineralogy and wide ranges of trace metal concentrations among and within the individual shale formations. As an example, a comparison of trace element data for the five US and two Canadian shale gas formations, collated from published sources and compiled as part of this study, showed that element concentrations within one shale gas formation could range up to four orders of magnitude (Table 6.1).

Unsurprisingly, the mineralogy and elemental composition of the shale samples used in this study was also variable. The shales range from carbonate mudstones (Eagle

Table 6.1 Trace element content of several gas-producing shales from US (Eagle Ford, Marcellus, New Albany, Utica and Woodford) and Canada (Duvernay and Montney).

		Trace elements (ug/g)												
Shale statistics		As	Ba	Co	Cr	Cu	Ni	Pb	Se	Sr	Th	U	V	Zn
Duvernay ^a	<i>n of data</i>	448	448	448	448	448	448	448	448	448	448	448	445	448
	<i>Minimum</i>	0.3	4	0.1	2	1.0	0.1	0.7	0.1	45	0.1	0.2	1.0	0.3
	<i>Median</i>	7	161	9	48	34	41	11	1.1	304	4.1	3.1	50	15
	<i>Maximum</i>	42	16012	29	739	148	189	77	12	5936	17	28	426	1125
Eagle Ford ^b	<i>n of data</i>	10	146	145	146	145	150	145	<i>n/a</i>	150	146	148	148	149
	<i>Minimum</i>	3	19	1.3	4	3	7	0.5	<i>n/a</i>	162	0.7	0.5	13	3
	<i>Median</i>	12	187	8	102	31	48	5	<i>n/a</i>	577	9	5	194	86
	<i>Maximum</i>	24	4902	38	382	232	196	31	<i>n/a</i>	1082	57	30	1018	1345
Marcellus ^c	<i>n of data</i>	676	682	673	729	673	736	669	<i>n/a</i>	658	725	750	733	667
	<i>Minimum</i>	4.9	98	3	0.9	7	5	5	<i>n/a</i>	63	0.2	1.8	16	5
	<i>Median</i>	28	1200	23	80	87	134	26	<i>n/a</i>	142	10	14	350	95
	<i>Maximum</i>	165	10001	77	586	302	939	78	<i>n/a</i>	2610	26	99	5215	10001
Montney ^d	<i>n of data</i>	88	88	88	88	88	88	88	88	88	88	88	88	88
	<i>Minimum</i>	0	7	0.3	2	0.4	1.2	1.1	0.05	16	0.2	0.2	4	4
	<i>Median</i>	6	39	8	18	15	21	7	0.7	38	4	0.7	16	21
	<i>Maximum</i>	53	196	38	147	145	81	34	35	646	9	12	123	302
New Albany ^e	<i>n of data</i>	385	385	385	385	383	385	330	385	385	385	385	383	385
	<i>Minimum</i>	0.5	30	2	7	0.7	4	1.4	0.1	55	0.4	1	19	2
	<i>Median</i>	24	450	20	83	73	76	33	2	94	10	16	180	130
	<i>Maximum</i>	110	6800	59	180	230	290	250	25	1600	62	75	1600	3600
Utica ^f	<i>n of data</i>	51	51	51	51	51	51	51	<i>n/a</i>	51	51	51	51	51
	<i>Minimum</i>	0.1	41	1.5	0.5	4	10	5	<i>n/a</i>	186	4	0.4	11	7
	<i>Median</i>	2.8	314	20	27	20	43	19	<i>n/a</i>	458	11	3	76	52
	<i>Maximum</i>	17	563	42	68	34	120	43	<i>n/a</i>	1804	35	13	151	452
Woodford ^g	<i>n of data</i>	148	148	148	148	148	148	144	144	144	148	148	148	148
	<i>Minimum</i>	2	393	1.8	7	8	17	3	1.4	19	0.7	3	49	8
	<i>Median</i>	26	966	15	48	53	105	12	5	98	6	33	176	104
	<i>Maximum</i>	147	17664	43	164	222	243	30	61	497	11	87	2045	2143

^a compiled from McMillan (2016) and Rokosh et al. (2016)

^b compiled from VanHazebroeck and Borrok (2016), Harbor (2011), and Ratcliffe et al. (2012) (data used in the article was obtained through personal communication with Dr Ratcliffe, 23 June 2016)

^c compiled from Bracht (2010), Leventhal (1980), Leventhal (1981), Chen et al. (2015), and Phan et al. (2015)

^d Rokosh et al. (2016); trace element content of Montney shale in Alberta, Canada only

^e Frost et al. (1985)

^f West Virginia Geological and Economic Survey (no date); data supplied as part of the Geologic Play Book for Utica Shale Appalachian Basin Exploration

^g compiled from Mnich (2009) and Harris et al. (2013); trace element content of Woodford shale in Permian Basin only

Ford, Bowland-LE) to silica-dominated (e.g. Termite Range, Kimmeridge Clay) and clay-rich siliceous mudstones (Epsilon-3, Murteree-2, Roseneath-2) (Figure 6.1). The differences in mineralogic assemblages are also present between samples from the same shale formations. For the shales from the UK's Bowland Basin, Bowland-BE is classified as a carbonate mudstone, but Bowland-LE and Bowland-KM are clay-rich and siliceous. Similarly from Australia's Cooper Basin, Epsilon-3 is clay-dominated, whereas Epsilon-1 and -2 can be categorised as clay-rich siliceous mudstone and a silica-dominated mudstone, respectively.

The total recoverable element (TRE) concentrations for many elements were quite variable and typically ranged over one to two orders of magnitude across the shales. Nearly all of the samples apart from the ones from Australia's Cooper Basin and Mt Isa Superbasin are consistently enriched in Cd, Mo, Sb, Se, and S relative to average upper

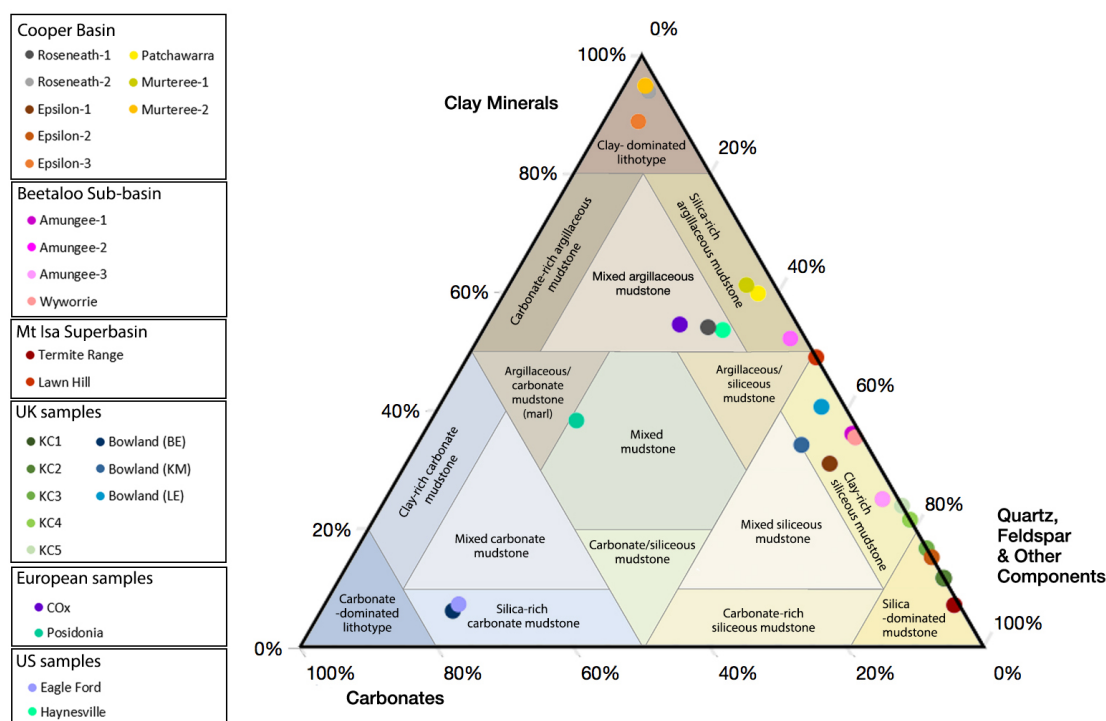


Figure 6.1 Ternary plot of bulk mineralogy of shale samples used in this study, superimposed on the Shlumberger's sCore classification scheme for organic mudstones. sCore scheme layout adapted from Gamero-Diaz et al. (2012), and Linder (2016).

crustal abundance (Rudnick and Gao, 2003) and the average shale values (Turekian and Wedepohl, 1961) (see 3.2.2). The variability also extends to the elemental composition among samples from the same shale formations. Bowland-LE contains 20 $\mu\text{g/g}$ of As compared to 3 $\mu\text{g/g}$ in the other two Bowland shale samples. On the other hand, it contains less Mn than Bowland-KM and Bowland-BE. Similar variability can be seen for Cu, Mn, Ni and Zn among the Beetaloo samples, all belonging to Velkerri Formation, or for Ba, Cr and Mn among the Cooper Basin's Epsilon samples.

A single gas shale formation is likely to exhibit a complex mineralogic and elemental assemblage that will vary spatially and vertically, influencing rock-fluid interactions during hydraulic fracturing. Examples of this site-specificity are that each of the Bowland Shale samples was taken from a different basin, and that the Velkerri and Epsilon Formation samples come from two wells in different parts of the Beetaloo Sub-basin and Cooper Basin, respectively. Therefore, formation characteristics need to be understood on a local scale down to a specific well and horizon to predict geogenic contaminant mobilisation into flowback and produced water and thus identify any potential environmental risks.

6.2.2. Neutralisation capacity

Some of the potential rock-fluid interactions, which may increase or reduce the element load mobilised into solution, can be quantitatively predicted based on the sample's mineralogy using Acid-Base Accounting (ABA). Described in detail in Chapter 3, ABA estimates whether a rock sample will generate an acid, neutral or alkaline environment by establishing its Acid Potential (AP) and Neutralisation Potential (NP). Acid Potential is based on the abundance of acid-producing minerals, primarily sulfides such as pyrite. The Neutralisation Potential is obtained by quantifying acid-neutralising minerals, mainly carbonates, and the moles of protons they can neutralise.

Previous experimental studies (see Chapter 2) highlighted the role of relative abundances of carbonate minerals versus sulphides (particularly pyrite) in the mobilisation of PTEs from shales during hydraulic fracturing (e.g. Harrison et al., 2017; Jew et al., 2017). The injection of oxygenated hydraulic fracturing fluids can result in pyrite oxidation, which causes acidification and releases pyrite-hosted PTEs into solution (e.g. Jamieson et al., 2015; Harrison et al., 2017). The acidity produced by pyrite oxidation can be countered by the dissolution of acid-neutralising minerals, mainly Ca-Mg carbonates (Dold, 2017; Karlsson et al., 2018). Where carbonates are abundant, this is likely to maintain the solution pH at near-neutral levels, leading to the rapid oxidation of Fe(II), released during pyrite oxidation, and subsequent precipitation of Fe(III)-(oxy)hydroxides. These secondary precipitates can sequester trace elements that were initially mobilised into the solution, potentially mitigating contaminant transport but could also occlude porosity and impede gas recovery (Harrison et al., 2017; Jew et al., 2017). This is why citric acid and EDTA, and other iron-scavenging agents, are frequently included in the hydraulic fracturing fluids.

The majority of the shale samples used in this study are *potentially acid-producing*, especially the Kimmeridge Clay and Beetaloo samples. On the other hand, Bowland (BE), Haynesville, COx, Eagle Ford, and Posidonia samples are overall *non-acid producing*. Cooper Basin samples lack any sulfide or acid-neutralising minerals and so were assigned an *uncertain acid generation potential*.

In this study samples of a range of ABA classifications were leached with synthetic hydraulic fracturing fluid (SHFF) and synthetic groundwater (SGW). As expected, the *non-acid producing* samples buffered the solution pH to 8.5 -8.8 during leaching with SHFF and, based on aqueous chemistry, experienced rapid precipitation of secondary Fe(III) phases. The *potentially acid-producing* and *uncertain* samples did not counteract the acidity generated from pyrite dissolution or the acidic pH of the SHFF and generally mobilised higher aqueous concentrations of many trace elements, e.g. Cd, Cu, Ni, Mn, Zn (Chapter 4.4).

The mineralogical ABA performed for this study was relatively simplistic, but proved to be a fast and effective screening tool. Calculation of NP considered only carbonate minerals with definite acid-neutralising potential and intermediately fast-reacting silicates, such as chlorite. Minerals with more complex behaviours, such as siderite, were excluded: depending on the pH conditions, siderite may act as a neutraliser or an acid producer (Dold, 2017) (see 3.3). For more in-depth calculations, it would be beneficial to include minerals such as siderite in the predictions.

It would also be prudent to perform mineralogical ABA for samples from units bounding the target zone. Fractures may unintentionally propagate outwith the shale formations, allowing the fracturing fluids to interact with adjacent lithologies (and potentially introducing formation waters with different chemistry).

6.3. Element mobilisation trends

From the experiments described in this thesis, it is clear that element mobilisation behaviours vary among the different ABA groups and depend on the leaching fluid.

The sample's ability to neutralise acid controls the pH during the experiments with SHFF and so directly impacts element release and mobility in the solution. The *non-acid producing* shales neutralise the acidity generated through pyrite oxidation and degradation of ammonium persulfate, buffering the solution pH to circumneutral or alkaline. Following the initial rapid decrease within the first 24 hours, the pH of the *potentially acid producing* and *uncertain* SHFF leachates remains acidic throughout the experiments (see Figure 4.3 pH evolution with samples divided based on their acid neutralisation potential: (a) SHFF experiments, (b) SGW experiments.).

Acidic conditions generally increase PTE mobility, which explains the higher aqueous concentrations of Cd, Co, Cu, Ni, and Zn observed in the *potentially acid producing* and

uncertain SHFF leachates. These samples also released almost all of their total Ca, Mg and Mn content and relatively high Fe concentrations. The elements were typically released rapidly, often leading to a plateau, except for Ba, Mo and Sb, which decreased following the initial mobilisation within the 48h.

The *non-acid producing* shales released the least of their total Cd, Co, Cr, Cu, Li, Ni, and Zn content among the samples and often recorded some of the lowest maximum aqueous concentrations of these elements. However, they mobilised significantly higher Sr and Ca concentrations than other shales. Little to no Fe was detectable in the *non-acid producing* SHFF leachates, and only low levels of Mn and Mg were in solution. Magnesium increased gradually until 260h and subsequently slightly decreased, whereas Mn showed an overall decreasing trend after the initial release. Cobalt and Cu also showed a decrease towards the end of the leaching.

Similar trends of element mobilisation, and the control of the initial carbonate content, were also observed in the few experiments that exposed shale material to synthetic fracturing fluids (discussed in detail in Chapter 2) (e.g. Jew et al., 2017; Marcon et al., 2017; Wilke et al., 2015). Wilke et al. (2015) and Harrison et al. (2017) noted that carbonate-rich shales or those with higher carbonate/pyrite ratio rapidly buffered fluid pH to circumneutral, regardless of the initial fluid pH. These samples generally exhibited low element loads in solution, likewise observing little to no dissolved Fe. Conversely, element concentrations in solution were higher in experiments with carbonate-poor shales, where fluid pH remained acidic. Additionally, multiple studies have also observed an initial enrichment of certain PTEs (e.g. Co, Cr, Cu, Ni) in the solution before subsequently decreasing in concentration, which was inferred to represent the removal of these elements due to coprecipitation or sorption onto secondary mineral precipitates (Harrison et al., 2017; Marcon et al., 2017; Wilke et al., 2015). The observations of precipitates in chapter 5 suggest this is a plausible mechanism. The studies also associated the mobilisation of many trace elements, e.g. Cr, Co, Ni, Cu, mainly with pyrite dissolution (Harrison et al., 2017; Pearce et al., 2018).

For most shale samples, the concentrations of the majority of the elements in the solution were relatively low throughout the time series for the SGW tests. Many measurements were below the detection limit (<DL), particularly for Cr (65% <DL), Zn (63%), Fe (58%) and Hg (53%) across all samples. The SHFF typically caused greater element mobilisation from all of the shale samples but not for all elements. Molybdenum and Sb, in particular, were more impacted by SGW, which mobilised more of the total Mo and Sb content and yielded higher aqueous concentrations of each element in the SGW leachates than in the SHFF ones.

The influence of acid neutralisation potential is also apparent when the shales are exposed to SGW. The *non-acid producing* and *uncertain* samples typically increase the initial pH (~7.5) within the first 5h to pH 8-9 and subsequently maintain it for the remainder of the experiment. All of the *potentially acid-producing* shales, except for Bowland-KM and -LE samples, deviate from that trend at the 120h time point when the first drop in pH was recorded. The pH proceeds to further decrease for the remainder of the experiment, although the decrease rate varies among the samples. The decrease in pH in the SGW Kimmeridge Clay and Beetaloo Sub-Basin leachates coincides with the rapid mobilisation of Mn, Fe, Cd, Co, Cu, Ni, U and Zn into solution. Based on the aqueous S and Fe concentrations (Chapter 4.4.), it is likely that the observed drop in pH was caused by pyrite oxidation surpassing the buffering capacity of the SGW as the Kimmeridge Clay and Beetaloo sample lack any neutralisation potential themselves. The acidification of the solution, in turn, allowed several trace metals, which could have been mobilised directly from pyrite, to remain in the solution. Although Bowland-KM and -LE did not display this trend within the experiment timeframe, it is likely that this was due to the presence of small quantities of siderite and calcite, which would buffer some of the acidity released from pyrite dissolution.

These results indicate that even when non-aggressive hydraulic fracturing fluids are used, oxygen-driven pyrite oxidation may eventually lead to contaminant release from shales that lack any neutralisation potential but contain sulfide minerals.

The results from this thesis are in agreement with other published work where shales were leached with water (Jeng, 1991; Jeng, 1992; Pearce et al., 2018). In a HPHT experiment (75°C, 200 bar) conducted with MilliQ water and 1 cm³ cube of carbonate-poor Roseneath shale, oxidative dissolution of sulfide minerals decreased the solution pH from 5 to ~3, enhanced the release of multiple elements, including Cd, Co, Cr Ni, Mg and Mn, and precipitation of fine-grained Fe-rich phases (Pearce et al., 2018). Similar trends were observed during water-leaching of powdered Norwegian Alum shales under ambient conditions for 100 days (Jeng, 1991, Jeng, 1992). The calcareous sample maintained the solution pH above 7 during the entire experiment and released only small amounts of acid, Fe, Al and other elements into the solution (Jeng, 1992). On the other hand, the non-calcareous samples developed high acidities and released Cd, Cu, Fe, Mn, Ni and Zn into solution in increasing amounts with time. The elements were released faster from samples where pyrite was present in framboidal form, which is more reactive than massive or concretionary forms (Jeng, 1991).

6.4. Factors affecting element mobilisation

6.4.1. Solid:fluid ratio and additives

Element mobilisation during laboratory experiments will be a function of the experimental parameters, such as solid:fluid ratio and the temperature and pressure conditions. Understanding how the parameters influence element release is vital for cross-study comparisons and the extrapolation of the results to subsurface conditions and management of the resulting wastewater. To this end, several preliminary experiments were performed to assess the influence of solid:fluid (S:F) ratio, temperature, pressure, and selected chemical additives on element mobilisation trends observed within the main experimental framework.

The S:F ratio was tested by leaching KC-1 sample with SGW and 1M HCl for 5 hours at 80°C at four different ratios: 1:100, 1:50, 1:25 and 1:10. Element release generally increased approximately in proportion with the increasing S:F ratio in the dilute HCl tests. In the SGW experiments, the influence of S:F ratio on element release depended on the element, and the relationship was not linear. Some elements (Al, Ba) displayed increasing aqueous concentration with increasing S:F ratio, others (Ca, S) showed the reverse trend, and some appeared to be unaffected (As, Pb, V).

Similar results were observed in two published studies that examined the effect of S:F ratio on element release using 1:100, 1:500 or 1:1000 ratios (Wang et al., 2015; Wang et al., 2016). The impact likewise depended on the element, some non-linearly increasing in concentrations with higher ratios (Mg, U, Ba, S²⁻), but overall other parameters – such as solution pH and redox conditions – had a greater influence on element mobilisation.

The additives examined in this study were EDTA and citric acid (EDTA+CA) and ammonium persulfate, commonly used in hydraulic fracturing fluid formulations. EDTA and citric acid are iron scavenging agents added to prevent the precipitation of Fe oxides. They can, however, form strong complexes with several regulated metals, increasing their mobility (Wang et al., 2016). The enhanced mobility was observed in this study - many elements, including Al, As, Cd, Co, Fe and Pb, were mobilised to a much greater extent with EDTA+CA present and leaching with the pure EDTA+CA solution tended to yield higher concentrations than when EDTA+CA was added to the base SHFF (Chapter 5.2.2).

Despite their purpose, the iron-chelating agents were not completely effective in preventing the precipitation of secondary Fe-oxides. The precipitation of Fe-oxides on Bowland-BE chips reacted with SHFF was inferred from aqueous chemistry and visual investigation of the chips with EPMA. Jew et al. (2017) also noticed that adding a Fe controlling agent (ethylene glycol) to their SHFF was only partially effective in preventing Fe oxidation, and that precipitation of Fe(III)-(oxy)hydroxides was observed in both

carbonate-poor and carbonate-rich shale systems. If secondary phases precipitate in the formation, they can occlude porosity and fracture apertures, negatively impacting gas recovery. However, they can also be environmentally beneficial by removing some of the PTEs and organic contaminants from the solution due to adsorption or coprecipitation (Flynn et al., 2019; Harrison et al., 2017; Jew et al., 2017). Formation of Fe(III)-(oxy)hydroxides has also been observed during cooling of flowback water as it returned to the surface where it became oxygenated again (Flynn et al., 2019). Hence, aeration of flowback and produced water was proposed as a potential treatment technique to reduce the aqueous toxicity of the shale gas wastewater, promoting its reuse and decreasing transportation risks (Flynn et al., 2019).

The second additive examined in this study was ammonium persulfate, a commonly used breaker to decompose gelling agents (Chapter 5.2.3). Its addition to the SHFF formulation enhanced element release for many elements; however, which elements were most affected was sample-dependent. For the *potentially acid producing* KC-4, Al, As, Cd, Cr, Cu, Fe, Pb, and V showed an increase in concentration by at least one order of magnitude when ammonium persulfate was added to both SGW and SHFF. For the *uncertain* Murterree-2 sample, both SGW and SHFF with added ammonium persulfate mobilised higher concentrations of elements into the solution for all examined solutes apart from As and Mo.

The thermal degradation of ammonium persulfate in the SHFF decreased solution pH and significantly contributed to the dissolved SO_4^{2-} concentrations in the leachates. The degradation of ammonium persulfate in a blank control SHFF experiments (15 days at 80°C and 175 bar) yielded 3583 mg/l of dissolved SO_4^{2-} . The dissolved sulfate from the degradation of the ammonium persulfate breaker has been shown to be a contributing factor to barite scale formation at reservoir conditions (Paukert Vankeuren et al., 2017) and minor anhydrite and gypsum precipitation (Marcon et al., 2017). In the shale chip experiment in this study with *non-acid producing* Bowland-BE (see 5.4), the addition of dissolved sulfate from ammonium persulfate decomposition promoted precipitation of

CaSO₄ phases. Whether the phases precipitated *in situ* during the experiments or as an artefact resulting from depressurisation requires further investigation. However, even if the latter was responsible, this highlights the potential for sulfate mineral scaling if ammonium persulfate is used in shale systems with high content of carbonate minerals. Additional experiments with *potentially acid producing* and *uncertain* shale chips within the experimental setup used in this study, as well as thermodynamic modelling, would be beneficial to establish whether sulfate minerals could precipitate in systems with lower aqueous Ca concentrations.

6.4.2. Temperature and pressure

The impact of elevated temperature on element mobilisation was investigated by leaching two *potentially acid producing* samples, KC-4 and Amungee-1, with SHFF and SGW at 100°C, 80°C and room temperature. Overall, the increase in temperature from 80 to 100°C had little effect on the release of most elements into the solution for both leaching fluids. Elements were generally mobilised into the solution at a similar rate and extent at both temperatures, especially when comparing their aqueous concentrations at the final sampling time point (360 h). Calcium and Mg were the only exceptions, showing a decrease in mobilisation between 260 and 360 h in the SHFF experiments at 100°C.

On the other hand, temperature increase from room to 80°C had a far more pronounced effect on element release. Apart from Ca and Mg, element mobilisation was generally much lower at room temperature, with comparable aqueous element concentrations at both sampling timepoints. This emphasises the importance of performing laboratory experiments on rock-fluid interactions during hydraulic fracturing at elevated (reservoir) temperatures. Experiments performed at ambient conditions may provide useful information, e.g., to assess the potential for contaminant mobility relevant to

disposal of drill cuttings, but may underestimate the release of elements from the shale in the subsurface.

The effects of elevated pressure on element release were investigated using powdered Eagle Ford and Bowland-BE shale chips, both shales classified as *non-acid producing*. The experiment with shale chips aimed to examine how reservoir-representative pressures may impact fracture surface morphology, and how fracture surface heterogeneity influences mineral dissolution and precipitation reactions.

The effects of increased pressure on aqueous chemistry depended on the leaching fluid and the solute. For powdered Eagle Ford, leaching with SGW under pressure led to enhanced mobilisation for some elements (e.g. Fe, Cr, Cu) but suppressed the release of others (Al, As, Sb). The mobilisation trends similarly varied in the pressurised SHFF leachates; however, more solutes showed decreased release than in the SGW tests.

A similar range of behaviours was observed when Bowland-BE chips were leached under pressure, but the magnitude of the impact was greater than for Eagle Ford powders. This difference is possibly associated with the form of a leached solid. At atmospheric pressure and 80°C, Bowland-BE chips mobilised higher element concentrations for most solutes into warm SHFF than powdered samples; only Ca showed a significantly lower release. Conversely, in tests with SGW under the same pressure and temperature conditions, more elements displayed a higher release from the powdered sample. The incongruity in the elemental release from the shale chips and powders of the Bowland-BE shale indicates that the distribution of reactive minerals and texture of a chip surface is likely to affect element mobilisation.

The experiments with Bowland-BE chips at elevated temperature illustrated that pressure, fluid type and the unreacted shale chip mineralogy and surface structure controlled the extent of mineral dissolution and precipitation reactions (Chapter 5.4).

In experiments with SGW under both atmospheric and elevated pressures, secondary precipitates were dominated by CaCO₃ polymorphs. Their morphology, abundance

and distribution tended not to be uniform across the reacted samples' surface, and correlated with the lamination-related mineral distribution of elemental concentrations in the unreacted chip. An increase in pressure to 150 bar resulted in higher aqueous S concentrations, which, in turn, resulted in the precipitation of large acicular CaSO_4 crystals. The increase in dissolved S levels was likely due to greater pyrite dissolution due to pressure oxidation.

The influence of pressure on pyrite oxidation rate was also observed by Pearce et al. (2018). They observed that a surface of a carbonate-poor Roseneath shale cube was covered in fine-grained Fe-rich precipitate following a 168 hour equilibration time with MilliQ water at 75°C and 200 bar pressure. Throughout the experiment, the solution pH decreased from 5 to ~3, which was attributed to the oxidative dissolution of sulfide minerals. In a separate experiment at 75°C and ambient pressure, the pH was maintained at ~5 and relatively fewer Fe-rich precipitates formed.

Secondary Fe-(oxy)hydroxides were also inferred in the SHFF experiments at both atmospheric and elevated pressures, based on EDX maps which showed a redistribution of Fe on the chips' surface that no longer matched S spatial distribution and a red-brown colouration of the reacted chips. Other precipitates observed in the SHFF experiments were CaSO_4 phases, which preferentially precipitated due to dissolved SO_4^{2-} contributed by ammonium persulfate degradation. The CaSO_4 precipitates were abundant on the chip reacted at 80°C and ambient pressure but significantly less formed at HPHT conditions.

The highest surface alteration was observed for the Bowland-BE chip exposed to SHFF at 80°C and 180 bar. The porosity was visibly increased due to mineral etching and dissolution across the whole sample, particularly in areas where carbonate minerals were previously abundant either as laminae or clusters. Some of the newly-formed porosity was likely occluded by *in-situ* precipitation of secondary Fe-(oxy)hydroxides, which due to alkaline conditions, formed relatively rapidly, close to where pyrite

framboids were initially present.

Conversely, the surface alteration was not as severe during SHFF leaching at 80°C and ambient pressure, and during both SGW experiments. Considerable porosity enhancement was not observed. It is likely that any newly formed porosity would have been occluded by the extensive precipitation of CaCO_3 and/or CaSO_4 , provided these phases formed *in situ*. Calcium carbonate and CaSO_4 are common scaling minerals in oil and gas wells and often form in a wellbore due to temperature and pressure drops (Dai et al., 2017). However, several other studies observed *in situ* precipitation of calcium carbonate, gypsum, anhydrite or barite have due to the interaction of synthetic fracturing fluids with shale solids (Dieterich et al., 2016; Marcon et al., 2017; Paukert Vankeuren et al., 2017).

Further research is necessary to examine the timing and cause of CaCO_3 and CaSO_4 precipitation and whether they would form in carbonate-poor systems, e.g. using thermodynamic modelling. Experiments with *potentially acid producing* and *uncertain* shale chips are needed to ascertain whether increased pressures under acidic conditions would lead to greater dissolution and alteration of fracture surfaces, and whether secondary precipitates would counteract the porosity. In shales with poor buffering capacity, Jew et al. (2017) suggested that Fe(II) oxidation at low pH can be considerably enhanced by bitumen, facilitating the formation of smaller Fe(III)-oxyhydroxides. However, as the Fe(II) will be slower to oxidise than at circum-neutral pH, it can be transported further from the Fe source prior to oxidising and precipitating more diffusely. These precipitates have the potential to occlude pores, fractures or wellbore piping, and over time reduce hydrocarbon recovery (Jew et al., 2018).

Figure 6.2 summarises the key rock-fluid interaction processes that have been observed in this study.

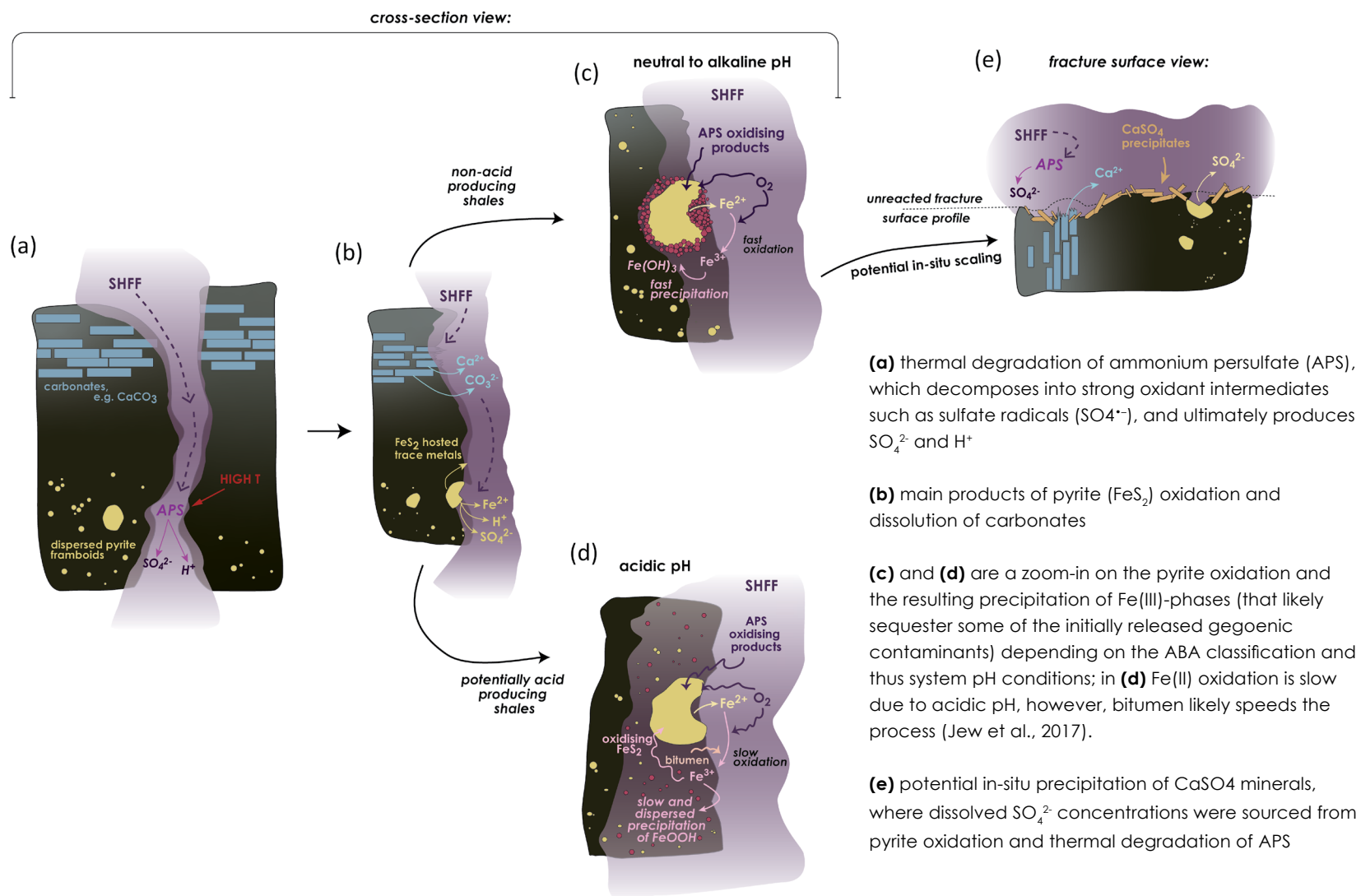


Figure 6.2 Conceptual model of the main rock-fluid interactions observed in the laboratory experiments; (d) adapted from Jew et al. (2017)

6.4.3. Powder to chip to fracture surface

The logic of the experimental approach of using powdered samples was that the increased surface area would produce faster reaction rates than would be expected on natural fracture surfaces. It would also remove any heterogeneities that may be present along a rock surface, allowing the leaching fluid to react with the whole of the sample simultaneously. Thus, the experiments with powders were assumed to simulate upper bound estimates of geogenic release. However, the inconsistency in the element mobilisation trends between Bowland-BE shale chips and powders indicates that it may not always be the case. The mineral distribution and surface heterogeneities along fracture are likely to affect rock-fluid interactions and element mobilisation considerably. It is worth noting that final pH measurements were not taken for all but one chip experiments, and these would have provided a strong line of evidence for what processes might have occurred.

Paukert Vankeuren et al. (2017) performed a core-flooding experiment on shale samples to investigate rock-fluid reactions during hydraulic fracturing. Conducted under slow flow rates that aimed to simulate the shut-in period, the experiments showed that the precipitation-dissolution reactions do not occur uniformly along the fracture surface. The most extensive calcite dissolution was consistently observed at the inlet and tended to cease away from it. It was typically coupled with barite and/or gypsum precipitation. Barite scale formation was also observed by Xiong et al. (2020) in a set of flow-through experiments on two Marcellus Shale cores, which aimed to study rock-fluid interactions during the hydraulic stimulation and shut-in periods. In the stimulation phase of the experiment, the fluid was injected at 0.3 ml/min for 4 days. The injection rate was subsequently lowered to 0.01 mL/min or zero for 21 to mimic the shut-in period. The study showed that using a high-sulfate make-up water and reusing produced water with high Ba²⁺ content for the fracturing fluid can lead to barite scale formation during the early stages of hydraulic fracturing. Additionally, fast flow rate was found to be

critical for barite scaling, where more than 80% of the barite formed inside the cores during the stimulation phase (Xiong et al., 2020).

In the experiments conducted by Paukert Vankeuren et al. (2017), calcite dissolution and barite precipitation were less pronounced where clusters of quartz proppant were present along parts of the fracture than in the unobstructed areas of the fracture. The clusters slowed down fluid flow, forcing it through the more open zones, thus creating a preferential fluid pathway where dissolution occurred faster due to the greater availability of the reactive fluid (Paukert Vankeuren et al., 2017).

The process of calcite dissolution is limited by mass-transfer, and thus, in principle, higher flow velocities should result in faster calcite dissolution rates (Garcia-Rios et al., 2015; Singurindy and Berkowitz, 2003) and increased flux of dissolved calcium into the solution (Noiriel et al., 2007).

However, in a core flow-through experiment, Deng et al. (2016) observed the development of an altered layer along the fracture surface, with its spatial pattern controlled by the influent flow velocity. At a lower flow rate, the effluent's Ca concentrations were high as the altered layer only developed at the inlet, allowing for a relatively fast calcite dissolution further along the fracture towards the outlet. Conversely, at higher flow rates, Ca concentrations in the effluent decreased significantly due to the altered layer covering almost the entire fracture surface. The layer restricted further fluid diffusion into the rock matrix and consequently limited progressive dissolution of calcite.

Hence, it would be invaluable to examine how spatial heterogeneities along a flow path and other reservoir-representative parameters, e.g. fluid flow rate, confining pressures, the degree of fluid uptake into the matrix, influence the reactions and element mobilisation trends observed during powdered batch experiments. This would allow for a more informed extrapolation of experimental results to field-scale operations.

6.5. (Environmental) Implications for future practice

A range of stakeholders, including the public and policymakers, have raised concerns around environmental contamination arising from hydraulic fracturing (Adgate et al., 2014; Boudet et al., 2014; O'Hara et al., 2014). For example, in the UK, these concerns led to an expert-led inquiry into the public health effects of shale gas extraction (Kibble et al., 2013). In the USA, the industry response to public concern around the chemicals used in hydraulic fracturing was to set up FracFocus. In this online portal, shale gas operators disclose all chemical additives used in their operations (<https://fracfocus.org>). In 2017, the Australian government funded a Geological and Bioregional Assessment Program (GBA), which aims to assess the potential impact of shale and tight gas development on water and the environment and identify appropriate mitigation and management approaches (Kirby et al., 2020).

However, there is still uncertainty around the composition of, and the potential hazard posed by, the contaminants in the flowback and produced water generated during hydraulic fracturing for shale gas (e.g. Annevelink et al., 2016; Shrestha et al., 2017; Tasker et al., 2018). Two processes are thought to be responsible for the evolution of shale gas wastewater chemistry in time: (1) mixing of the injected fluids with the formation brines of the target or adjacent formations (Barbot et al., 2013; Rowan et al. 2015); and (2) rock-fluid interactions between the injected fracturing fluids and the target formation (Blauch et al., 2011; Renock et al., 2016; Wang et al., 2016). Some of the contaminants that may be sourced directly from the rock formation include naturally occurring radioactive materials and other potentially toxic elements (PTEs) such as heavy metals (e.g. arsenic, mercury and lead) (e.g. Harrison et al., 2017; Pearce et al., 2018).

The laboratory batch leaching tests with SHFF and SGW identified which inorganic geogenic chemicals can be mobilised into solution during hydraulic fracturing, and the obtained results can be further used to assess which elements may be of potential

environmental importance. To this end, the SHFF and SGW leaching results (Chapter 4.4) for the powdered Australian and Bowland shale samples were compared to relevant regulatory water guideline values.

It is imperative to note that these results reflect only the contaminants that may be mobilised directly from the rock during hydraulic fracturing and do not account for the composition of the formation waters, which will significantly contribute to the chemistry of shale gas wastewater, particularly salinity (e.g. Barbot et al., 2013; Stewart et al., 2015). Their composition is challenging to predict as little to no field data is generally available before hydrocarbon exploration boreholes are drilled, although laboratory methods have been developed to attempt to account for their contribution (Williams et al., 2013). It is worth noting that the formation water in gas shales is very rarely free, and gas shales are highly water-undersaturated, making them act as a dehydrated sponge (Engelder et al., 2014). Some water will be capillary-bound, and the rest will be immobile, captured in the crystalline structure of clays. The mixing of formation water and injected fluids has been proposed to occur due to diffusion and osmotic processes. The contrast in water activity between the relatively low salinity of injected stimulation fluids and high-salinity formation waters creates osmotic pressure differences, driving imbibition of hydraulic fracturing fluids into the shale matrix while simultaneously expelling gas and formation brines (Engelder et al., 2014 and references therein).

Moreover, the shale matrix tends to contain high amounts of water-soluble inorganic cations and anions, and diffusion osmosis forces may transfer them to the fractures and into the waters that end up returning to the surface (Engelder et al., 2014). Other sources of formation brines into flowback and produced water may come from more permeable underlying or overlying strata if fractures penetrate beyond the targeted formation. Consequently, the composition of the formation water component of shale gas wastewater is likely to be highly site-specific.

Comparing the observed PTE concentrations to the regulatory limits effectively assumes

an exposure to undiluted wastewater, which is unlikely to occur in the field. There is a prevalence in the literature of highlighting flowback and produced water constituents as of concern if their concentrations exceed regulatory limits (especially drinking water regulations), often regardless of the magnitude of the exceedance (e.g. Alley et al., 2011; Haluszczak et al., 2013; Shresta et al., 2017). This approach does not consider pollutant pathways - how transport mechanisms and physical processes impact the PTE concentrations after a wastewater spill or leak occurs. Contaminant levels can be naturally attenuated, for example, due to advection, dilution and dispersion downstream from the spill source, or due to (ad)sorption, complexation and precipitation during infiltration through soils (e.g. Rish and Pfau, 2018; Salomons, 1995; US EPA, 2016). The characteristics of the receiving water resource will also significantly influence the severity of the potential impact, for example, by altering the chemistry and hence the bioavailability of PTEs. Therefore, although the observed concentrations of a given element may greatly exceed the water regulations, accidental release of flowback and produced water might not necessarily mean the PTE concentrations will exceed the regulatory limits in the impacted body of water.

This initial comparison with water quality guidelines is only intended as a tier 1 screen that aims to eliminate potential contaminants while highlighting the elements that should be monitored in the field and be subject to further environmental assessments.

6.5.1. Approach and water quality guidelines used

To date, concerns about environmental impacts caused by mismanagement of flowback and produced water have focussed mainly on potential impacts on drinking water (e.g. Entrekin et al., 2011; Vengosh et al., 2013; Vidic et al., 2013). The concentrations of constituents of concern in the flowback and produced water have typically been assessed against the Drinking Water Regulations (e.g. Abualfaraj et al., 2014; Haluszczak et al.,

2013). However, aquatic life, wildlife, livestock and vegetation are also at risk (Adams, 2011; Bamberger and Oswald, 2012; Entekin et al., 2011; Papoulias and Velasco, 2013). Each receptor is likely to have different susceptibility to a given pollutant and may be assigned a unique guideline or regulatory level to protect against short- and long-term exposures. Therefore, in Tables 6.2-6.8 the leached PTE concentrations are also compared to regulations for receptors other than drinking water to enable a more comprehensive assessment of potential contaminants of concern.

Some of the guidelines aim to provide protection against both short-term and long-term exposure, setting maximum allowable concentrations and annual average standards, respectively. In these circumstances, the maximum allowable PTE concentrations should be used since contamination of surface and groundwater with flowback and produced water is more likely to be episodic rather than systematic (Fontenot et al., 2013). For some PTEs, the guidelines for the protection of aquatic life can depend on specific parameters of the receiving surface water (such as hardness) or are relevant to the concentration of bioavailable metal (i.e. the fraction of the dissolved metal that is toxic to aquatic flora and fauna; SEPA, 2015). Metal bioavailability is influenced by water quality parameters such as hardness, pH and dissolved organic carbon, and thus the bioavailable fraction can only be estimated on a site-by-site basis (WFD-UKTAG, 2015). Rather than hypothesise on the quality of the receiving body of water to calculate the bioavailable metal fraction, a conservative approach was taken, and the most stringent limits were used in Table 6.8.

The leached PTEs concentrations for the Australian shales and Bowland Shale samples were compared to Australian and UK regulatory limits, respectively. As human exposure to undiluted flowback and produced water is highly unlikely, comparison with drinking water guidelines was deemed inappropriate. The following regulations and guidelines were used as toxically-derived benchmarks or contamination:

-
- i. *Australia*: Australian and New Zealand Guidelines for Fresh and Marine Water Quality (2000);
 - ii. *United Kingdom*: Environmental Quality Standards (EQS) and Standards for Discharges to Surface Waters (SEPA, 2015);

6.5.2. Environmental and human health implications

The results in Tables 6.2-6.8 are expressed as a ratio between the maximum observed aqueous element concentrations and the corresponding water quality regulations. This ratio value illustrates the magnitude to which the concentrations exceed the guidelines and is indicated by a traffic light colour system. Following the approach of Abualfaraj et al. (2014), ratios of ten or higher (i.e. concentrations exceed the regulatory limit ten-fold or more) are considered to be elements that have the most significant environmental implications, and so are shown in red. However, it is vital to note that this cut off is arbitrary and cannot be used to indicate, e.g. whether an accidental release of flowback water would raise the PTEs concentrations in the impacted water body to problematic levels.

6.5.2.1. Australian samples

Tables 6.2 to 6.4 show the calculated ratios for aquatic toxicants, irrigation and livestock drinking water regulations for the SHFF leachates.

Generally, the maximum detected aqueous concentrations remain below the Water Quality Criteria (WQC) for irrigation and livestock drinking water. In the few instances where the concentrations are elevated, the calculated ratio tends to remain <10. The only

Table 6.2 Ratio of maximum aqueous element concentration mobilised by SHFF from Australian shale samples versus Australian Water Quality Criteria (WQC) for freshwater aquatic toxicants.

Element	WQC (mg/L)	Cooper Basin								Beetaloo Sub-basin				Mt Isa Superbasin	
		R-1	R-2	P	E-1	E-2	E-3	M-1	M-2	A-1	A-2	A-3	W	TR	LH
As	0.013	<1	<1	1	<1	1	<1	<1	<1	8	5	16	7	1	5
Cd	0.0002	30	32	14	6	3	8	22	19	365	355	807	1158	1	113
Co															
Cr	0.001	62	30	323	229	367	113	61	79	51	67	48	41	3043	249
Cu	0.0014	458	337	1199	247	150	114	351	349	1005	1069	926	1993	52	386
Mn	1.9	10	13	1	17	3	11	8	3	1	1	1	<1	4	1
Mo															
Ni	0.011	46	74	48	54	26	53	45	48	417	132	209	275	13	52
Pb	0.0034	22	22	19	8	20	9	35	24	29	94	1	3	11	53
U															
Zn	0.008	266	265	274	120	191	137	287	317	805	485	1630	1718	18	315

Table 6.3 Ratio of maximum aqueous element concentration mobilised by SHFF from Australian shale samples versus Australian Water Quality Criteria (WQC) for irrigation water.

Element	WQC (mg/L)	Cooper Basin								Beetaloo Sub-basin				Mt Isa Superbasin	
		R-1	R-2	P	E-1	E-2	E-3	M-1	M-2	A-1	A-2	A-3	W	TR	LH
As	2	<1	<1	<1	<1	<1	<1	<1	<1	<1	<1	<1	<1	<1	<1
Cd	0.05	<1	<1	<1	<1	<1	<1	<1	<1	1.5	1	3	5	<1	1
Co	0.1	3	3	3	2	1	3	3	3	3	3	3	3	1	4
Cr	1	<1	<1	<1	<1	<1	<1	<1	<1	<1	<1	<1	<1	3	<1
Cu	5	<1	<1	<1	<1	<1	<1	<1	<1	<1	<1	<1	1	<1	<1
Mn	10	2	3	<1	3	1	2	2	1	<1	<1	<1	<1	1	<1
Mo	0.05	<1	<1	<1	<1	<1	<1	<1	<1	8	5	4	4	<1	1
Ni	2	<1	<1	<1	<1	<1	<1	<1	<1	2	1	1	1.5	<1	<1
Pb	5	<1	<1	<1	<1	<1	<1	<1	<1	<1	<1	<1	<1	<1	<1
U	0.1	<1	<1	<1	<1	<1	<1	<1	<1	<1	<1	<1	<1	<1	<1
Zn	5	<1	<1	<1	<1	<1	<1	<1	<1	1	1	3	3	<1	1

Table 6.4 Ratio of maximum aqueous element concentration mobilised by SHFF from Australian shale samples versus Australian Water Quality Criteria (WQC) for livestock drinking water.

Element	WQC (mg/L)	Cooper Basin								Beetaloo Sub-basin				Mt Isa Superbasin	
		R-1	R-2	P	E-1	E-2	E-3	M-1	M-2	A-1	A-2	A-3	W	TR	LH
As	0.5	<1	<1	<1	<1	<1	<1	<1	<1	<1	<1	<1	<1	<1	<1
Cd	0.01	1	1	<1	<1	<1	<1	<1	<1	7	7	16	23	<1	2
Co	1	<1	<1	<1	<1	<1	<1	<1	<1	<1	<1	<1	<1	<1	<1
Cr	1	<1	<1	<1	<1	<1	<1	<1	<1	<1	<1	<1	<1	3	<1
Cu	0.4	2	1	4	1	1	<1	1	1	4	4	3	7	<1	1
Mn															
Mo	0.15	<1	<1	<1	<1	<1	<1	<1	<1	3	2	1	1	<1	<1
Ni	1	1	1	1	1	<1	1	1	1	5	1	2	3	<1	1
Pb	0.1	1	1	1	<1	1	<1	1	1	1	3	<1	<1	<1	2
U	0.2	<1	<1	<1	<1	<1	<1	<1	<1	<1	<1	<1	<1	<1	<1
Zn	20	<1	<1	<1	<1	<1	<1	<1	<1	<1	<1	1	1	<1	<1

exception is Cd in Amungee-3 and Wyworrie samples, which exceeds the irrigation WQC 16 and 23 times, respectively.

For nearly all the Australian shale samples, the maximum recorded concentrations for most examined regulated elements exceeded the WQC for freshwater aquatic toxicants. Cadmium, Cr, Cu, Ni and Zn show extremely high levels of exceedance in some samples, up to three orders of magnitude, especially those from the Beetaloo Sub-basin.

On the other hand, Mn and As concentrations show a variable response among the different shales. Manganese concentrations are typically equal to WQC for Beetaloo and Mt Isa samples but exceed the regulations by a factor of 1.5 to 17 for the Cooper Basin shales. Arsenic levels are typically under the regulatory limits, especially among the Cooper Basin shales. A small exceedance can be observed among the Beetaloo Sub-basin and Mt Isa's Lawn Hill samples.

The concentrations of element mobilised into solution by SGW were compared to the regulations as a benchmark for less aggressive hydraulic fracturing fluids (Tables 6.5 to 6.7). As expected, ratios for the maximum aqueous concentrations versus the guidelines

Table 6.5 Ratio of maximum aqueous element concentration mobilised by SGW from Australian shale samples versus Australian Water Quality Criteria (WQC) for freshwater aquatic toxicants.

Element	WQC (mg/L)	Cooper Basin								Beetaloo Sub-basin				Mt Isa Superbasin	
		R-1	R-2	P	E-1	E-2	E-3	M-1	M-2	A-1	A-2	A-3	W	TR	LH
As	0.013	1	<1	11	1	5	<1	1	1	2	3	2	3	1	5
Cd	0.0002	<1	1	1	1	<1	1	1	<1	38	76	799	889	1	2
Co															
Cr	0.001	2	1	3	1	2	2	1	1	<1	<1	4	1	11	4
Cu	0.0014	16	16	3	16	15	3	2	2	3	22	701	848	<1	<1
Mn	1.9	<1	<1	<1	<1	<1	<1	<1	<1	<1	<1	<1	<1	<1	<1
Mo															
Ni	0.011	<1	1	<1	<1	<1	1	<1	<1	14	7	194	165	<1	<1
Pb	0.0034	<1	<1	<1	<1	<1	<1	<1	<1	<1	<1	<1	<1	<1	<1
U															
Zn	0.008	1	2	2	1	<1	2	1	1	15	25	1444	927	<1	1

Table 6.6 Ratio of maximum aqueous element concentration mobilised by SGW from Australian shale samples versus Australian Water Quality Criteria (WQC) for irrigation water.

Element	WQC (mg/L)	Cooper Basin								Beetaloo Sub-basin				Mt Isa Superbasin	
		R-1	R-2	P	E-1	E-2	E-3	M-1	M-2	A-1	A-2	A-3	W	TR	LH
As	2	<1	<1	<1	<1	<1	<1	<1	<1	<1	<1	<1	<1	<1	<1
Cd	0.05	<1	<1	<1	<1	<1	<1	<1	<1	<1	<1	3	4	<1	<1
Co	0.1	<1	<1	<1	<1	<1	<1	<1	<1	<1	<1	3	1	<1	<1
Cr	1	<1	<1	<1	<1	<1	<1	<1	<1	<1	<1	<1	<1	<1	<1
Cu	5	<1	<1	<1	<1	<1	<1	<1	<1	<1	<1	<1	<1	<1	<1
Mn	10	<1	<1	<1	<1	<1	<1	<1	<1	<1	<1	<1	<1	<1	<1
Mo	0.05	<1	<1	<1	<1	<1	<1	<1	<1	24	19	14	13	<1	5
Ni	2	<1	<1	<1	<1	<1	<1	<1	<1	<1	<1	1	1	<1	<1
Pb	5	<1	<1	<1	<1	<1	<1	<1	<1	<1	<1	<1	<1	<1	<1
U	0.1	<1	<1	<1	<1	<1	<1	<1	<1	<1	<1	<1	<1	<1	<1
Zn	5	<1	<1	<1	<1	<1	<1	<1	<1	<1	<1	2	2	<1	<1

Table 6.7 Ratio of maximum aqueous element concentration mobilised by SGW from Australian shale samples versus Australian Water Quality Criteria (WQC) for livestock drinking water.

Element	WQC (mg/L)	Cooper Basin								Beetaloo Sub-basin				Mt Isa Superbasin	
		R-1	R-2	P	E-1	E-2	E-3	M-1	M-2	A-1	A-2	A-3	W	TR	LH
As	0.5	<1	<1	<1	<1	<1	<1	<1	<1	<1	<1	<1	<1	<1	<1
Cd	0.01	<1	<1	<1	<1	<1	<1	<1	<1	1	2	16	18	<1	<1
Co	1	<1	<1	<1	<1	<1	<1	<1	<1	<1	<1	<1	<1	<1	<1
Cr	1	<1	<1	<1	<1	<1	<1	<1	<1	<1	<1	<1	<1	<1	<1
Cu	0.4	<1	<1	<1	<1	<1	<1	<1	<1	<1	<1	3	3	<1	<1
Mn															
Mo	0.15	<1	<1	<1	<1	<1	<1	<1	<1	8	6	5	4	<1	2
Ni	1	<1	<1	<1	<1	<1	<1	<1	<1	<1	<1	2	2	<1	<1
Pb	0.1	<1	<1	<1	<1	<1	<1	<1	<1	<1	<1	<1	<1	<1	<1
U	0.2	<1	<1	<1	<1	<1	<1	<1	<1	<1	<1	<1	<1	<1	<1
Zn	20	<1	<1	<1	<1	<1	<1	<1	<1	<1	<1	1	<1	<1	<1

are consistently <1 for most of the elements, particularly for livestock drinking water and irrigation WQC. The only exceptions are Mo and Cd among the Beetaloo Sub-basin samples, which show exceedance greater than a factor of 10.

6.5.2.2. Bowland Shale samples (UK)

For all three Bowland Shale samples, the maximum element concentrations mobilised by SGW were generally below or equal to the EQS for freshwater (Table 6.8).

On the other hand, maximum concentrations of elements mobilised into solution by SHFF often exceed the EQS, and this response varies among the samples. Bowland-BE shows the lowest degree of exceedance: only Cu, Mn and Ni are above the EQS but remain below the tenfold threshold.

The SHFF mobilises considerably higher concentrations of most elements from Bowland-KM and -LE samples. The aqueous concentrations of Cu, Mn, Ni and Zn in

Table 6.8 Ratio of maximum aqueous element concentration mobilised by SHFF and SGW from powdered Bowland shale samples versus UK Environmental Quality Standards (EQS) for freshwater.

Element	Guideline value (mg/L)	SHFF			SGW		
		BE	KM	LE	BE	KM	LE
As	0.05	<1	<1	<1	<1	<1	<1
Cd	0.0005	1	2	47	<1	<1	<1
Co	0.1	<1	3	2	<1	<1	<1
Cr	0.0034	<1	2	11	1	<1	<1
Cu	0.0045	6	33	51	2	1	1
Mn	0.123	5	78	11	<1	<1	<1
Ni	0.034	3	12	10	<1	<1	<1
Pb	0.014	<1	4	7	<1	<1	<1
Zn	0.012	1	85	75	3	1	2

the Bowland-KM leachate exceed the EQS up to 85 times, whereas Cd, Cr, Cu, Mn, Ni and Zn levels in the Bowland-LE leachate exceed the EQS by at least a factor of 12 and up to a factor of 85.

6.5.3. Implications for future practice

The results presented in section 6.5.2. highlights that the elements which might be mobilised during hydraulic fracturing at concentrations that may be environmentally concerning are highly site-specific. The potential hazards also depend on the receptors that are used to assess them. Some of the examined contaminants may be released in concentrations that significantly exceed water quality guidelines, particularly the aquatic life ones. Other guidelines, such as WQC for irrigation or livestock drinking water, are likely to only rarely be exceeded. However, it is worth noting that the salt content of flowback and produced water will remain a problem for many water use

applications (e.g. Adams, 2011; Skalak et al., 2014; Tasker et al., 2018).

The Bowland Shale samples represent two members of one shale formation, and each sample originates from a different well in different basins (see Table 3.1). The samples have different mineralogies and different ABA potentials. Most of the elements mobilised by SHFF from the *non-acid producing*, carbonate-dominated, Bowland-LE sample remain below the guidelines or slightly exceed them. On the other hand, the silica- and clay-dominated and *potentially acid producing* Bowland-KM and Bowland-LE samples release higher element concentrations which can considerably exceed the regulations.

Similarly, some Australian samples represent the same formation but may originate from a different well or were taken from a different core depth. There is little variance in exceedance of the guideline values among the multiple Roseneath, Epsilon and Murteree shale samples. Conversely, there is quite a variability in the maximum aqueous element concentrations among the four Beetaloo sub-basin samples, which belong to two members of the Velkerri Formation. Amungee-1 and -2 are core samples from Tanumbirini 1 well, whereas Amungee-3 and Wyworrie originate from Atree-2 well. All of the Beetaloo samples mobilise high levels of Cd, Cu, Ni and Zn that are above the WQC for freshwater toxicants, but the magnitude of the exceedance varies. For example, in Amungee-3 leachate, Cd exceeds the WQC 807 times, but only 365 and 355 times for Amungee-1 and Amungee-2, respectively. Maximum Zn concentration exceeds the regulations by a factor of 485 for Amungee-2, 805 for Amungee-1 and 1630 for Amungee-3. Lead WQC are exceeded 94 times in the Amungee-2 samples and 29 times in the Amungee-1, but in the Amungee-3 and Wyworrie samples, the Pb concentrations are equal to or only slightly exceed the WQC.

Given the mineralogical heterogeneity within a single shale formation and variability in the quantities and types of chemical additives that may be added to fracturing fluids at different wells, it should be expected that the inorganic fraction of wastewater derived

from the rock-fluid interactions will be site-specific.

Therefore, even if some field data were available for a given shale gas play, it may still be challenging to predict wastewater composition and any hazards it may pose for a prospective well that is in a different location. Laboratory leaching tests of shale samples from an exploratory well could provide site-specific empirical evidence to identify inorganic chemicals that may be mobilised into shale gas flowback and produced water at concentrations of *potential concern*. Additionally, laboratory tests are far cheaper than field investigations and allow control of many variables. The results of such tests should then guide future field-based monitoring and could be useful for site-specific quantitative environmental risk assessments. Ideally these data should be placed in the public domain, as in the USA's FracFocus database, that would allow any systematics to be worked out.

Additionally, it would be beneficial to compare laboratory leaching test results against field investigations in order to validate the experimental approach as well as gain insights into contaminant contributions from formation waters. The knowledge gained from the laboratory studies could also aid in the development of appropriate hydraulic fracturing fluids. For example, based on the results from this study, removal of oxidants from the hydraulic fracturing fluid formulations may decrease the geogenic contaminant footprint in the flowback and produced waters. One possibility could involve finding an alternative breaker to ammonium persulfate and including an oxygen scavenger to inhibit pyrite oxidation. A stronger pH buffer could also be added to reduce acidification events, particularly where the shales are pyrite-rich and *potentially acid producing*.

6.6. Applications to other systems

Beyond the direct application to geogenic element mobilisation from shales during the hydraulic fracturing operation, this work carries implications for other geoengineered

and natural systems in which fluid-rock interactions occur. An example of the latter would be the diagenesis of gas shales during episodes of basin inversion and burial, where changes in temperature and pressure and the introduction of new fluids are likely to happen. Similarly, element mobilisation from organic-rich shales as a function of different pressures and temperatures could help predict inorganic contaminant mobilisation during mine-water geothermal operations or coalbed methane production. Coal deposits tend to be interbedded between clastic sediments, including shales, and are known to contain PTEs associated with sulfides and selenides, such as As, Hg, Tl, Se and Pb (Finkelman et al., 2019; Haszeldine, 1989).

Many activities in the geotechnical, hydrocarbon, geothermal and underground storage fields utilise fracture-dominated geological media and typically involve an injection of fluids into the subsurface. The resulting disequilibrium can induce a range of reactions, such as observed in this study mineral dissolution and precipitation, which can alter the permeability, porosity and surface reactivity.

These chemical reactions, coupled with other thermal, hydrological and mechanical (THMC) processes, can significantly impact the connectivity of a fracture network, particularly in fracture-dominated reservoirs, changing its existing hydraulic and transport processes (Lima et al., 2019). Understanding how the fracture properties are affected by the THMC processes following the injection of reactive fluids is crucial to the success of many subsurface engineering operations.

CHAPTER 7

CONCLUSIONS AND FUTURE WORK

7.1. Conclusions

The large quantities of wastewater produced throughout the lifetime of a shale gas well can contain heavy metals and other regulated potentially toxic elements. These can be mobilised from the target formation by some of the additives present in the hydraulic fracturing fluids. High levels of inorganic geogenic chemicals may pose a hazard to the environment through accidental releases such as spills of untreated wastewater. The concentration of mobilised elements and the hazard they pose is uncertain and is likely dependent on the chemical agents used in fracturing fluids, the composition of formation waters and the trace element content of targeted shale gas formation.

This study aimed to: (1) investigate the release of potential inorganic contaminants of concern (e.g. As, Co, Cu, Pb) from shale gas formations from around the world; (2) examine how experimental factors may affect the element release, e.g. temperature and pressure; and (2) identify the key reactions that are most likely to occur upon shale exposure to hydraulic fracturing fluids.

In systematic batch experiments at elevated temperature (80°C) and atmospheric pressure, powdered shale samples were leached for up to 500 hours with synthetic hydraulic fracturing fluid (SHFF), synthetic groundwater (SGW) and dilute (1M) HCl. The key observations were as follow:

1. Elemental concentrations released into the solution were generally much higher in the SHFF leachates than in the SGW treatments, indicating that the chemical additives in the SHFF influenced element mobilisation.
2. The shale sample's ability to neutralise acid controls the pH during the experiments, directly impacting element release and mobility in the solution. This is particularly important for pyrite-rich samples. As demonstrated by this study, mineralogy-based Acid Base Accounting (ABA) can be a cheap, fast and effective tool for predicting pH during leaching and thus constrain some of the potential rock-fluid interactions. The *non-acid producing* samples buffered the solution pH to circumneutral or alkaline during leaching with SHFF and, based on aqueous chemistry, experienced rapid precipitation of secondary Fe(III) phases. The *potentially acid-producing* and *uncertain* samples did not counteract the acidity generated from pyrite dissolution or the acidic pH of the SHFF and generally mobilised higher aqueous concentrations of many trace elements, e.g. Cd, Cu, Ni and Zn.

In the experiments with SGW, *non-acid neutralising* and *uncertain* samples increased the initial pH (~7.5) to alkaline and subsequently maintained it. Most of the *potentially acid producing* shales deviated from that trend at the 120h time point when the acidity generated from pyrite oxidation began to surpass the buffering capacity of the SGW, decreasing the pH of the leachate to acidic. Aqueous concentrations of several elements, such as Cd, Co, Cu and Ni, increased concurrently with the observed pH drop. This suggests that even when non-aggressive hydraulic fracturing fluids are used in pyrite-rich shales, pyrite oxidation may eventually cause contaminant release and acidification if the shales lack any neutralisation potential.

3. Even a dilute acid flush may mobilise geogenic PTEs into the solution to a much greater extent than during more prolonged exposure to SHFF. Therefore, if acid flush is employed during field operations, it may cause a greater contaminant load into the flowback.

Additionally, several preliminary experiments were performed to assess the influence of temperature, pressure, and selected chemical additives (EDTA and citric acid, and ammonium persulfate) on element mobilisation trends observed during the main batch leaching tests. The temperature and additives investigations were performed using powdered shale samples, whereas the effect of elevated pressure was assessed using both powdered Eagle Ford samples and Bowland-BE chips. These experiments showed that:

1. The addition of EDTA and citric acid to SHFF enhanced the mobility of several elements, including Al, Co, Cu, Fe, Ni, Pb and Zn. However, despite their purpose, these iron-chelating agents were not wholly effective in preventing the precipitation of secondary Fe-oxides. The precipitation of Fe-oxides on Bowland-BE chips reacted with SHFF was inferred from aqueous chemistry and visual investigation of the chips with EPMA.
2. The thermal degradation of ammonium persulfate (APS) in the SHFF decreased solution pH and significantly contributed to the dissolved SO_4^{2-} concentrations in the leachates. The addition of APS-derived dissolved SO_4^{2-} promoted precipitation of CaSO_4 phases in the Bowland-BE chip experiments.
3. The increase in temperature from 80 to 100°C overall had little effect on the release of most elements into the SGW or SHFF solutions. However, temperature increase from room to 80°C had a far more pronounced effect on element release. Apart from Ca and Mg, element mobilisation was generally much lower at room temperature.

4. An increase in pressure from atmospheric to reservoir representative resulted in enhanced release of some elements (e.g. Fe, Cr, Cu) but suppressed the release of others (Al, As, Sb) in the SGW leachates. The mobilisation trends similarly varied in the pressurised SHFF leachates; however, more solutes showed decreased release than in the SGW tests. An increase in pressure from atmospheric to 150 bar also resulted in greater pyrite dissolution due to pressure oxidation and yielded higher aqueous S concentrations.
5. The experiments with Bowland-BE chips at elevated temperature showed that pressure, fluid type and the unreacted shale chip mineralogy and surface structure control the extent of mineral dissolution and precipitation reactions. The highest surface alteration was observed when the chip was exposed to SHFF at 80°C and 180 bar. Mineral etching and dissolution were observed across the whole sample, particularly in areas that were carbonate-rich before the experiment. *In-situ* precipitation of secondary Fe-(oxy) hydroxides, which due to alkaline pH formed close to where pyrite framboids were initially present, occluded some of the newly-formed porosity. The surface alteration was not as severe during SHFF leaching at 80°C and ambient pressure, and during SGW experiments, and no considerable porosity enhancement was observed. Following these experiments, the reacted chips' surfaces were extensively covered by CaCO₃ and/or CaSO₄ precipitates.

The element leaching profiles generated in this study assess the possible contribution of fluid-rock interactions to the composition of flowback and produced waters gas shales worldwide. This study shows that additives can enhance the release of geogenic chemicals and that subsequent precipitation within the fracture system could limit their ultimate release to the surface. Monitoring during field operations is recommended to understand the system-specific environmental implications and hazards.

7.1. Future work

The most limiting factor for this study was the sample availability, which prevented many of the experiments to be performed with samples spanning all ABA groups. Further experiments with samples representative of all ABA groups would help ascertain the broader mineralogical influence on element release and rock-fluid interactions during hydraulic fracturing.

For example, the effect of pressure and temperature on a shale chip surface was only examined on a *non-acid producing* sample. Experiments with *potentially acid producing* and *uncertain* shale chips are needed to determine whether increased pressures under acidic conditions would also lead to greater dissolution and alteration of the fracture surface and whether secondary precipitates, particularly Fe(III) phases, would counteract any porosity enhancement.

Additional research is also necessary to examine the timing and cause of CaCO_3 and CaSO_4 precipitation and whether these precipitates would also form in carbonate-poor systems, e.g. using thermodynamic modelling or empirically in a core flow-through experiment combined with real-time imaging by X-ray computer tomography (XCT).

The experiments with Bowland-BE chips demonstrated that the mineral distribution and surface heterogeneities along fractures are likely to affect rock-fluid interactions and element mobilisation considerably. Future experiments should examine how spatial heterogeneities along a flow path and other reservoir-representative parameters, e.g. fluid flow rate, confining pressures, the degree of fluid uptake into the matrix, influence the reactions and element mobilisation trends observed during experiments using powders and chips. This would allow for a more informed extrapolation of experimental results to field-scale operations.

References

- Abanda, P. A. and Hannigan, R. E. (2006), Effect of diagenesis on trace element partitioning in shales. *Chemical Geology*, 230(1–2), p. 42–59.
- Abualfaraj, N., Gurian, P.L. and Olson, M.S. (2014), Characterization of Marcellus shale flowback water. *Environmental Engineering Science*, 31 (9), p. 514-524.
- Adams, M.B. (2011), Land application of hydrofracturing fluids damages a deciduous forest stand in West Virginia. *Journal of Environmental Quality*, 40 (4), p. 1340-1344.
- Adgate, J. L., Goldstein, B. D. and McKenzie, L. M. (2014), Potential public health hazards, exposures and health effects from unconventional natural gas development. *Environmental Science and Technology*, 48(15), p. 8307–8320.
- Akob, D.M., Cozzarelli, I.M., Dunlap, D.S., Rowan, E.L. and Lorah, M.M. (2015), Organic and inorganic composition and microbiology of produced waters from Pennsylvania shale gas wells. *Applied Geochemistry*, 60, p. 116–125.
- Al-Bazali, T., Zhang, J., Chenevert, M.E. and Sharma, M.M. (2008), Factors controlling the compressive strength and acoustic properties of shales when interacting with water-based fluids. *International Journal of Rock Mechanics and Mining Sciences*, 45 (5), p. 729-738.
- Alley, B., Beebe, A., Rodgers Jr, J. and Castle, J.W. (2011), Chemical and physical characterization of produced waters from conventional and unconventional fossil fuel resources. *Chemosphere*, 85 (1), p. 74-82.
- Annevelink, M. P. J. A., Meesters, J. A. J. and Hendriks, A. J. (2016), Environmental contamination due to shale gas development. *Science of The Total Environment*, 550, p. 431–438.
- Antony, A., Low, J. H., Gray, S., Childress, A. E., Le-Clech, P. and Leslie, G. (2011), Scale formation and control in high pressure membrane water treatment systems: A review. *Journal of Membrane Science*, 383(1–2), p. 1–16.
- ANZECC/ARMCANZ (2000), *Australian and New Zealand guidelines for fresh and marine water quality*. Australia and New Zealand Environment and Conservation Council/Agricultural and Resource Management Council of Australia and New Zealand. Canberra, Australia.
- Apte, S.C., Williams, M., Kookana, R.S., Batley, G.E., King, J.J., Jarolimek, C.V. and Jung, R.F. (2017), *Release of geogenic contaminants from Australian coal seams: experimental studies, project report*. Report prepared by the Land & Water, Commonwealth Scientific and Industrial Research Organisation (CSIRO) as part of the National Assessment of Chemicals Associated with Coal Seam Gas Extraction in Australia, Commonwealth of Australia, Canberra
- Armstrong, J.G., Parnell, J., Bullock, L.A., Boyce, A.J., Perez, M. and Feldmann, J. (2019), Mobilisation of arsenic, selenium and uranium from Carboniferous black shales in west Ireland. *Applied Geochemistry*, 109, p.104401.
- Arthur, J.D., Bohm, B.K., Coughlin, B.J., Layne, M.A. and Cornue, D. (2009), *Evaluating the environmental implications of hydraulic fracturing in shale gas reservoirs*. SPE Americas E&P Environmental and Safety Conference (23-25 March), San Antonio, Texas, USA.
- Bamberger, M. and Oswald, R.E. (2012), Impacts of gas drilling on human and animal health. *New Solutions: A Journal of Environmental and Occupational Health Policy*, 22 (1), p. 51–77.
- Barati, R. and Liang, J.T. (2014), A review of fracturing fluid systems used for hydraulic fracturing of oil and gas wells. *Journal of Applied Polymer Science*, 131(16).

- Barbot, E., Vidic, N.S., Gregory, K.B. and Vidic, R.D. (2013), Spatial and temporal correlation of water quality parameters of produced waters from Devonian-Age Shale following hydraulic fracturing. *Environmental Science & Technology*, 47 (6), p. 2562–2569.
- Bard, F. and Bilal, E. (2011), Semi-batch precipitation of calcium sulfate dihydrate from calcite and sulfuric acid. *Carpathian Journal of Earth and Environmental Sciences*, 6(1), p. 241–250.
- Bazilian, M., Brandt, A.R., Billman, L., Heath, G., Logan, J., Mann, M., Melaina, M., Statwick, P., Arent, D. and Benson, S.M. (2014), Ensuring benefits from North American shale gas development: Towards a research agenda. *Journal of Unconventional Oil and Gas Resources*, 7, p. 71–74.
- Bertoncello, A., Wallace, J., Blyton, C., Honarpour, M. M., and Kabir, S. (2014), Imbibition and water blockage in unconventional reservoirs: Well-management implications during flowback and early production. *SPE Reservoir Evaluation & Engineering*, 17(4), p. 497–506.
- Bibby, K.J., Brantley, S.L., Reible, D.D., Linden, K.G., Mouser, P.J., Gregory, K.B., Ellis, B.R. and Vidic, R.D. (2013), Suggested reporting parameters for investigations of wastewater from unconventional Shale gas extraction. *Environmental Science & Technology*, 47 (23), p. 13220–13221.
- Blauch, M.E., Myers, R.R., Moore, T.R., Lipinski, B.A. and Houston, N.A. (2009), *Marcellus Shale Post-Frac Flowback Waters- Where is All the Salt Coming From and What are the Implications?*. Society of Petroleum Engineers, Eastern Regional Meeting: Charleston, WV, September 23–25, 2009. Paper SPE 125740.
- Blewett, T. A., Delompré, P. L. M., He, Y., Folkerts, E. J., Flynn, S. L., Alessi, D. S., and Goss, G. G. (2017), Sublethal and Reproductive Effects of Acute and Chronic Exposure to Flowback and Produced Water from Hydraulic Fracturing on the Water Flea *Daphnia magna*. *Environmental Science and Technology*, 51(5), p. 3032–3039.
- Blondes, M.S., Gans, K.D., Rowan, E.L., Thordsen, J.J., Reidy, M.E., Engle, M.A., Kharaka, Y.K. and Thomas, B. (2016), *US Geological Survey National Produced Waters Geochemical Database v2. 2 (PROVISIONAL) Documentation*.
- Bodin, S., Godet, A., Matera, V., Steinmann, P., Vermeulen, J., Gardin, S., Adatte, T., Coccioni, R., and Föllmi, K.B. (2007), Enrichment of redox-sensitive trace metals (U, V, Mo, As) associated with the late Hauterivian Faraoni oceanic anoxic event. *International Journal of Earth Sciences*, 96 (2), p. 327–341.
- Boggs, S., Jr. (2006), *Principles of Sedimentology and Stratigraphy*. 4th ed. Upper Saddle River, NJ: Pearson Education Inc.
- BOGM (Bureau of Oil and Gas Management) (no date), *Frac and flowback water analytical data, inorganics, spreadsheet*. Available on request from Pennsylvania Department of Environmental Protection.
- Boschee, P. (2014), Produced and Flowback Water Recycling and Reuse Economics, Limitations, and Technology. *Oil and Gas Facilities*, February (1), p. 17–21.
- Boudet, H., Clarke, C., Bugden, D., Maibach, E., Roser-Renouf, C. and Leiserowitz, A. (2014), “Fracking” controversy and communication: using national survey data to understand public perceptions of hydraulic fracturing. *Energy Policy*, 65, p.57-67.
- Bouzahzah, H., Benzaazoua, M., Bussiere, B. and Plante, B. (2014), Prediction of acid mine drainage: importance of mineralogy and the test protocols for static and kinetic tests. *Mine Water and the Environment*, 33(1), p.54-65.
- Boyer, C., Kieschnick, J., Suarez-Rivera, R., Lewis, R.E. and Waters, G. (2006), Producing gas from its source. *Oilfields Review*, 18 (3), p. 36–49.
- Bracht, R., (2010), *Geochemistry and Depositional Environment of the Union Springs Member of the Marcellus Shale in Pennsylvania*. Unpublished M.Sc. thesis, the Pennsylvania State University.
- Brittingham, M.C., Maloney, K.O., Farag, A.M., Harper, D.D. and Bowen, Z.H. (2014), Ecological risks of Shale oil and gas development to wildlife, aquatic resources and their habitats. *Environmental Science & Technology*, 48 (19), p. 11034–11047.

- Burgos, W.D., Castillo-Meza, L., Tasker, T.L., Geeza, T.J., Drohan, P.J., Liu, X., Landis, J.D., Blotevogel, J., McLaughlin, M., Borch, T. and Warner, N.R. (2017), Watershed-scale impacts from surface water disposal of oil and gas wastewater in Western Pennsylvania. *Environmental Science and Technology*, 51 (15), p.8851-8860.
- Butkovskiy, A., Bruning, H., Kools, S. A. E., Rijnaarts, H. H. M., & Van Wezel, A. P. (2017), Organic Pollutants in Shale Gas Flowback and Produced Waters: Identification, Potential Ecological Impact, and Implications for Treatment Strategies. *Environmental Science and Technology*, 51(9), p. 4740–4754.
- Capo, R.C., Stewart, B.W., Rowan, E.L., Kohl, C.A.K., Wall, A.J., Chapman, E.C., Hammack, R.W. and Schroeder, K.T. (2014), The strontium isotopic evolution of Marcellus Formation produced waters, southwestern Pennsylvania. *International Journal of Coal Geology*, 126, p. 57-63.
- Cappuyns, V., Claes, H., Geris, P., Maquil, R., & Swennen, R. (2019), Mineralogical and geochemical characterization of Mo-rich black shales in the Grand Duchy of Luxembourg. *Journal of Geochemical Exploration*, 206(August), p. 106351.
- Chakrabarty, D., & Mahapatra, S. (1999), Aragonite crystals with unconventional morphologies. *Journal of Materials Chemistry*, 9(11), p. 2953–2957.
- Chandra, A.P. and Gerson, A.R. (2010), The mechanisms of pyrite oxidation and leaching: a fundamental perspective. *Surface Science Reports*, 65(9), p. 293-315.
- Chapman, E.C., Capo, R.C., Stewart, B.W., Kirby, C.S., Hammack, R.W., Schroeder, K.T. and Edenborn, H.M. (2012), Geochemical and Strontium Isotope characterization of produced waters from Marcellus Shale natural gas extraction. *Environmental Science and Technology*, 46 (6), p. 3545– 3553.
- Chariag, B. (2007), Maximize Reservoir Contact. *E&P Magazine*, 1, p. 11–12.
- Chen, R., Sharma, S., Bank, T., Soeder, D., and Eastman, H. (2015), Comparison of isotopic and geochemical characteristics of sediments from a gas- and liquids-prone wells in Marcellus Shale from Appalachian basin, west Virginia. *Applied Geochemistry*, 60, p. 59–71.
- Chermak, J.A. and Schreiber, M.E. (2014), Mineralogy and trace element geochemistry of gas shales in the United States: Environmental implications. *International Journal of Coal Geology*, 126, p. 32–44.
- Clark, C.E. and Veil, J.A. (2009), *Produced water volumes and management practices in the United States (No. ANL/EVS/R-09-1)*. Report prepared by Argonne National Lab. (ANL), Argonne, IL (United States).
- Clarke, H., Bustin, M. and Turner, P. (2014), *Unlocking the resource potential of the Bowland basin, NW England. SPE 167776*. Paper prepared for presentation at the SPE/EAGE European Unconventional Conference and Exhibition held in Vienna, Austria, 25–27 February 2014.
- Colborn, T., Kwiatkowski, C., Schultz, K. and Bachran, M. (2011), Natural gas operations from a public health perspective. *Human and Ecological Risk Assessment: An International Journal*, 17 (5), p. 1039–1056.
- Cook, P., Beck, V., Brereton, D., Clark, R., Fisher, B., Kentish, S., Toomey, J., Williams, J. (2013), *Engineering energy unconventional gas production: a study of shale gas in Australia*. Australian Council of Learned Academies (ACOLA), Melbourne.
- Cozzarelli, I.M., Skalak, K.J., Kent, D.B., Engle, M.A., Benthem, A., Mumford, A.C., Haase, K., Farag, A., Harper, D., Nagel, S.C. and Iwanowicz, L.R. (2017), Environmental signatures and effects of an oil and gas wastewater spill in the Williston Basin, North Dakota. *Science of The Total Environment*, 579, p. 1781-1793
- Crafton, J. W. and Gunderson, D. (2007), Stimulation flowback management: Keeping a good completion good. *Proceedings - SPE Annual Technical Conference and Exhibition*, 6(8), p. 3939–3949.
- Crafton, J. W. and Noe, S. (2013), *Factors Affecting Early Well Productivity in Six Shale Plays*. Society of Petroleum Engineers, SPE Annual Technical Conference and Exhibition: New Orleans, LA, 30 September-2 October, 2013. Paper SPE 166101.

- Dai, Z., Kan, A. T., Shi, W., Zhang, N., Zhang, F., Yan, F., Bhandari, N., Zhang, Z., Liu, Y., Ruan, G. and Tomson, M. B. (2017), Solubility Measurements and Predictions of Gypsum, Anhydrite, and Calcite Over Wide Ranges of Temperature, Pressure, and Ionic Strength with Mixed Electrolytes. *Rock Mechanics and Rock Engineering*, 50(2), p. 327–339.
- Dawson, W. C. (2000), Shale Microfacies: Eagle Ford Group (Cenomanian-Turonian) North-Central Texas Outcrops and Subsurface Equivalents. *Gulf Coast Association of Geological Societies Transactions*, 50, p. 607-621.
- Deng, H., Molins, S., Steefel, C., DePaolo, D., Voltolini, M., Yang, L. and Ajo-Franklin, J., (2016). A 2.5 D reactive transport model for fracture alteration simulation. *Environmental Science and Technology*, 50 (14), p. 7564-7571.
- Deng, T. (1993), Aqueous Pressure Oxidation of Minerals - A Salient Development in Hydrometallurgy. *Mineral Processing and Extractive Metallurgy Review*, 12 (2–4), p. 185-222.
- Dewhurst, D.N., Raven, M.D. and Dautriat, J. (2015), *Composition and Microstructure of REM Shales from Encounter-1*. CSIRO Report Number EP152386.
- Dieterich, M., Kutchko, B. and Goodman, A. (2016), Characterization of Marcellus Shale and Huntersville Chert before and after exposure to hydraulic fracturing fluid via feature relocation using field-emission scanning electron microscopy. *Fuel*, 182, p. 227–235.
- Dold, B. (2010), Basic Concepts in Environmental Geochemistry of Sulfidic Mine-Waste Management. In: Kumar, S. (ed.), *Waste Management*. Rijeka: IntechOpen.
- Dold, B. (2017), Acid rock drainage prediction: A critical review. *Journal of Geochemical Exploration*, 172, p. 120-132.
- “Donovan, A. D., and Staerker, T. S. (2010), Sequence stratigraphy of the Eagle Ford (Boquillas) Formation in the subsurface of South Texas and outcrops of West Texas. *Gulf Coast Association of Geological Societies Transactions*, 60, p. 861-899.”
- EA (2011), *Shale Gas: North West – Monitoring of Flowback water*. Report by UK Environment Agency.
- EIA (US Energy Information Administration) (2020), *Natural gas imports and exports*. Available at: <https://www.eia.gov/energyexplained/natural-gas/imports-and-exports.php> (Accessed: 12 March 2021).
- EIA (US Energy Information Administration) (2021b), *What is U.S. electricity generation by energy source?* <https://www.eia.gov/tools/faqs/faq.php?id=427&t=8> (Accessed: 12 March 2021).
- EIA (US Energy Information Administration) (2016), *Hydraulically fractured wells provide two-thirds of U.S. natural gas production*. Available at: <https://www.eia.gov/energyexplained/natural-gas/imports-and-exports.php> (Accessed: 28 January 2021).
- EIA (US Energy Information Administration)(EIA) (1993), *Drilling Sideways - A review of Horizontal Well Technology and Its Domestic Application*. DOE/EIA-TR-0565. Available at: http://www.eia.gov/pub/oil_gas/natural_gas/analysis_publications/drilling_sideways_well_technology/pdf/tr0565.pdf (Accessed: 9 June 2016).
- EIA (US Energy Information Administration) (2018), *Annual Energy Outlook 2018 with projections to 2050*. Available at: <https://www.eia.gov/outlooks/archive/aeo18/pdf/AEO2018.pdf> (Accessed: 2nd January 2019).
- EIA (US Energy Information Administration) (2021a), *Where our natural gas comes from*. Available at: <https://www.eia.gov/energyexplained/natural-gas/where-our-natural-gas-comes-from.php> (Accessed: 12 March 2021).
- Elsner, M. and Hoelzer, K. (2016), Quantitative survey and structural classification of hydraulic fracturing chemicals reported in unconventional gas production. *Environmental Science and Technology*, 50 (7), p. 3290-3314.
- Engelder, T., Cathles, L.M. and Bryndzia, L.T. (2014), The fate of residual treatment water in gas shale. *Journal of Unconventional Oil and Gas Resources*, 7, p. 33-48.

- Engle, M. A. and Rowan, E. L. (2014), Geochemical evolution of produced waters from hydraulic fracturing of the Marcellus Shale, northern Appalachian Basin: A multivariate compositional data analysis approach. *International Journal of Coal Geology*, 126, p. 45–56.
- Entrekin, S., Evans-White, M., Johnson, B. and Hagenbuch, E. (2011), Rapid expansion of natural gas development poses a threat to surface waters. *Frontiers in Ecology and the Environment*, 9 (9), p. 503–511.
- Eshlman, K.N. and Elmore, A. (2013), *Recommended Best Management Practices for Marcellus Shale Gas Development in Maryland*. Report submitted to: Maryland Department of the Environment Baltimore, MD.
- Estrada, J.M. and Bhamidimarri, R. (2016), A review of the issues and treatment options for wastewater from shale gas extraction by hydraulic fracturing. *Fuel*, 182, p. 292-303.
- Evangelou, V. P., & Zhang, Y. L. (1995), Critical Reviews in Environmental Science and Technology A review: Pyrite oxidation mechanisms and acid mine drainage prevention A Review: Pyrite Oxidation Mechanisms and Acid Mine Drainage Prevention. *Critical Reviews in Environmental Science and Technology*, 25(252), p. 37–41.
- Farag, A.M. and Harper, D.D. (2014), A review of environmental impacts of salts from produced waters on aquatic resources. *International Journal of Coal Geology*, 126, p.157-161.
- Fernández-Díaz, L., Astilleros, J. M. and Pina, C. M. (2006), The morphology of calcite crystals grown in a porous medium doped with divalent cations. *Chemical Geology*, 225(3–4), p. 314–321.
- Ferrar, K.J., Michanowicz, D.R., Christen, C.L., Mulcahy, N., Malone, S.L. and Sharma, R.K. (2013), Assessment of effluent contaminants from three facilities discharging Marcellus Shale wastewater to surface waters in Pennsylvania. *Environmental Science & Technology*, 47 (7), p. 3472-3481
- Ferrer, I. and Thurman, E.M. (2015), Chemical constituents and analytical approaches for hydraulic fracturing waters. *Trends in Environmental Analytical Chemistry*, 5, p. 18–25.
- Finkelman, R. B., Dai, S. and French, D. (2019), The importance of minerals in coal as the hosts of chemical elements: A review. *International Journal of Coal Geology*, 212 (August), 103251.
- Flewelling, S. A., & Sharma, M. (2014), Constraints on upward migration of hydraulic fracturing fluid and brine. *Groundwater*, 52(1), p. 9–19.
- Flewelling, S.A., Tymchak, M.P. and Warpinski, N. (2013), Hydraulic fracture height limits and fault interactions in tight oil and gas formations. *Geophysical Research Letters*, 40 (14), p. 3602-3606.
- Flynn, S. L., Von Gunten, K., Warchola, T., Snihur, K., Forbes, T. Z., Goss, G. G., Gingras, M. K., Konhauser, K. O. and Alessi, D. S. (2019), Characterization and implications of solids associated with hydraulic fracturing flowback and produced water from the Duvernay Formation, Alberta, Canada. *Environmental Science: Processes and Impacts*, 21(2), p. 242–255.
- Fontenot, B.E., Hunt, L.R., Hildenbrand, Z.L., Carlton Jr., D.D., Oka, H., Walton, J.L., Hopkins, D., Osorio, A., Bjorndal, B., Hu, Q.H. and Schug, K.A. (2013), An evaluation of water quality in private drinking water wells near natural gas extraction sites in the Barnett Shale formation. *Environmental Science & Technology*, 47 (17), p. 10032–10040.
- Frost, J.K., Zierath, D.L., Shimp, N.F., and Bergstrom, R.E. (1985). *Chemical composition and geochemistry of the New Albany shale group (Devonian–Mississippian) in Illinois*. IGS Contract/Grant Report 1985-4, Illinois State Geological Survey.
- Fuller, C. C. and Harvey, J. W. (2000), Reactive uptake of trace metals in the hyporheic zone of a mining-contaminated stream, Pinal Creek, Arizona. *Environmental Science and Technology*, 34(7), p. 1150–1155.
- Gamero Diaz, H., Miller, C., Lewis, R., and Contreras Fuentes, C. (2013). *Evaluating the Impact of Mineralogy on Reservoir Quality and Completion Quality of Organic Shale Plays*. Search and Discovery Article #41221. Available at: http://www.searchanddiscovery.com/pdfz/documents/2013/41221diaz/ndx_diaz.pdf.html (Accessed: 7 July 2016)

- Garcia-Rios, M., Luquot, L., Soler, J.M. and Cama, J., (2015), Influence of the flow rate on dissolution and precipitation features during percolation of CO₂-rich sulfate solutions through fractured limestone samples. *Chemical Geology*, 414, p. 95-108.
- Gregory, K.B., Vidic, R.D. and Dzombak, D.A. (2011), Water management challenges associated with the production of Shale gas by hydraulic fracturing. *Elements*, 7 (3), p. 181–186.
- Gregory, D.D., Large, R.R., Halpin, J.A., Baturina, E.L., Lyons, T.W., Wu, S., Danyushevsky, L., Sack, P.J., Chappaz, A., Maslennikov, V.V. and Bull, S.W. (2015), Trace element content of sedimentary pyrite in black shales. *Economic Geology*, 110 (6), p. 1389–1410.
- Grieser, W.V., Wheaton, W.E., Magness, W.D., Blauch, M.E. and Loghry, R. (2007), *Surface reactive fluid's effect on shale*. SPE Production and Operations Symposium (31 March - 3 April), Oklahoma City, Oklahoma, USA.
- Gross, D., Sachsenhofer, R. F., Bechtel, A., Pytlak, L., Rupprecht, B. and Wegerer, E. (2015), Organic geochemistry of Mississippian shales (Bowland Shale Formation) in central Britain: Implications for depositional environment, source rock and gas shale potential. *Marine and Petroleum Geology*, 59, p. 1–21.
- Gu, X., Heaney, P.J., Reis, F.D.A. and Brantley, S.L., (2020), Deep abiotic weathering of pyrite. *Science*, 370(6515).
- Gulbis, J. and Hodge, R.M. (2000), Fracturing fluid chemistry and proppants. In: Economides, M.J. and Nolte, K.G. (eds.), *Reservoir stimulation (3rd edition)*. Englewood Cliffs, NJ: Prentice Hall. Reservoir Stimulation, p. 7-1 to 7-23. Chichester, West Sussex: John Wiley & Sons, LTD.
- Ground Water Protection Council (GWPC) and ALL Consulting (2009), *Modern shale gas development in the United States—A primer*. Prepared for U.S. Department of Energy Office of Fossil Energy and National Energy Technology Laboratory.
- Halliburton (2009), *Meeting the Challenges of the Marcellus Shale Through Technology*. Available online at: <http://www.gaselectricpartnership.com/BBHalliburton%20Marcellus.pdf> (Accessed: 26th February 2021)
- Hall, L.S., Wang, L., Bailey, A.H.E., Orr, M.L., Owens, R., Jarrett, A.J.M., Lech, M.E., Skeers, N., Reese, B. and Woods, M. (2020), *Petroleum prospectivity of the Beetaloo Sub-basin. Technical appendix for the Geological and Bioregional Assessment Program: Stage 2*. Department of the Environment and Energy, Bureau of Meteorology, CSIRO and Geoscience Australia, Australia.
- Haluszczak, L.O., Rose, A.W. and Kump, L.R. (2013), Geochemical evaluation of flowback brine from Marcellus gas wells in Pennsylvania, USA. *Applied Geochemistry*, 28, p. 55–61.
- Haney, E. B., Haney, R. L., Hossner, L. R., and White, G. N. (2006), Neutralization Potential Determination of Siderite (FeCO₃) Using Selected Oxidants. *Journal of Environmental Quality*, 35(3), p. 871–879.
- Harbor, R.L. (2011), *Facies Characterization and Stratigraphic Architecture of Organic-Rich Mudrocks, Upper Cretaceous Eagle Ford Formation, South Texas*. Unpublished M.Sc. thesis, University of Texas, Austin.
- Harkness, J.S., Dwyer, G.S., Warner, N.R., Parker, K.M., Mitch, W.A. and Vengosh, A. (2015), Iodide, Bromide, and ammonium in hydraulic fracturing and oil and gas Wastewaters: Environmental implications. *Environmental Science & Technology*, 49 (3), p. 1955–1963.
- Harris, N.B., Mnich, C.A., Selby, D., and Korn, D. (2013), Minor and trace element and Re–Os chemistry of the upper Devonian Woodford Shale, Permian basin, west Texas: Insights into metal abundance and basin processes. *Chemical Geology*, 356, p. 76–93.
- Harris, N.B., Miskimins, J.L., and Mnich, C.A. (2011), Mechanical anisotropy in the Woodford Shale, Permian Basin: Origin, magnitude, and scale. *The Leading Edge*, 30 (3), 284–291.
- Harris, N.B., Mnich, C.A., Selby, D., and Korn, D. (2013), Minor and trace element and Re–Os chemistry of the upper Devonian Woodford Shale, Permian basin, west Texas: Insights into metal abundance and basin processes. *Chemical Geology*, 356, p. 76–93.
- Harrison, A.L., Jew, A.D., Dustin, M.K., Thomas, D.L., Joe-Wong, C.M., Bargar, J.R., Johnson, N., Brown, G.E. and Maher, K. (2017), Element release and reaction-induced porosity alteration during shale- hydraulic fracturing fluid interactions. *Applied Geochemistry*, 82, p. 47–62.

- Haszeldine, R. S. (1989), Coal reviewed: Depositional controls, modern analogues and ancient climates. *Geological Society Special Publication*, 41, p. 289–308.
- Hayes, T. (2009), *Sampling and Analysis of Water Streams Associated with the Development of Marcellus Shale Gas*. Report prepared for Marcellus Shale Coalition.
- He, Y., Flynn, S. L., Folkerts, E. J., Zhang, Y., Ruan, D., Alessi, D. S., Martin, J. W. and Goss, G. G. (2017), Chemical and toxicological characterizations of hydraulic fracturing flowback and produced water. *Water Research*, 114, p. 78–87.
- Hemmesch, N.T., Harris, N.B., Mnich, C.A., and Selby, D. (2014), A sequence-stratigraphic framework for the upper Devonian Woodford Shale, Permian basin, west Texas. *AAPG Bulletin*, 98 (1), p. 23–47.
- Hill, A.J. and Mauger, A.J. (2016), HyLogging unconventional petroleum core from the Cooper Basin, South Australia. *Australian Journal of Earth Sciences*, 63(8), p.1087-1097.
- Holditch, S. A., Prerry, K. and Lee, J. (2007), *Unconventional Gas Reservoirs - Tight Gas, Coal Seams, and Shales. Working Document of the National Petroleum Council on Global Oil and Gas Study*. Available at: http://www.npc.org/study_topic_papers/29-ttg-unconventional-gas.pdf (Accessed: 8 June 2016).
- Jackson, R.E., Gorody, A.W., Mayer, B., Roy, J.W., Ryan, M.C. and Van Stempvoort, D.R. (2013), Groundwater protection and unconventional gas extraction: The critical need for field-based Hydrogeological research. *Groundwater*, 51 (4), p. 488–510.
- Jackson, R.B., Vengosh, A., Carey, J.W., Davies, R.J., Darrah, T.H., O'sullivan, F. and Pétron, G. (2014), The environmental costs and benefits of fracking. *Annual review of Environment and Resources*, 39, p. 327–362
- Jamieson, H. E., Walker, S. R. and Parsons, M. B. (2015), Mineralogical characterization of mine waste. *Applied Geochemistry*, 57, 85–105.
- Jarrett, A.J.M., Hall, L.S., Carr, L., Anderson, J., Orr, M., Bradshaw, B., Henson, P. and Gorton, J. 2019. *Source rock geochemistry of the Isa Superbasin and South Nicholson Basin, Northern Australia: Baseline regional hydrocarbon prospectivity*. Record 2018/38.
- Geoscience Australia, Canberra. Jeng, A.S. (1991), Weathering of some Norwegian alum shales: I. Laboratory simulations to study acid generation and the release of sulphate and metal cations (Ca, Mg & K). *Acta Agriculturae Scandinavica*, 41 (1), p. 13-35.
- Jeng, A.S. (1992), Weathering of some Norwegian alum shales, II. Laboratory simulations to study the influence of aging, acidification and liming on heavy metal release. *Acta Agriculturae Scandinavica B-Plant Soil Sciences*, 42 (2), p. 76-87
- Jenner, S. and Lamadrid, A.J. (2013), Shale gas vs. coal: Policy implications from environmental impact comparisons of shale gas, conventional gas, and coal on air, water, and land in the United States. *Energy Policy*, 53, p. 442-453.
- Jew, A.D., Dustin, M.K., Harrison, A.L., Joe-Wong, C.M., Thomas, D.L., Maher, K., Brown Jr, G.E. and Bargar, J.R. (2017), Impact of organics and carbonates on the oxidation and precipitation of iron during hydraulic fracturing of shale. *Energy & Fuels*, 31(4), p. 3643-3658.
- Jew, A.D., Besançon, C.J., Roycroft, S.J., Noel, V.S., Bargar, J.R. and Brown Jr, G.E. (2020), Chemical Speciation and Stability of Uranium in Unconventional Shales: Impact of Hydraulic Fracture Fluid. *Environmental science & technology*, 54(12), p. 7320-7329.
- Johnson, R. L., Tratnyek, P. G. and Johnson, R. O. B. (2008), Persulfate persistence under thermal activation conditions. *Environmental Science and Technology*, 42(24), p. 9350–9356.
- Jones, A.M., Griffin, P.J. and Waite, T.D. (2015), Ferrous iron oxidation by molecular oxygen under acidic conditions: The effect of citrate, EDTA and fulvic acid. *Geochimica et Cosmochimica Acta*, 160, p. 117-131.
- Kamal, M.S., Hussein, I., Mahmoud, M., Sultan, A.S. and Saad, M.A. (2018), Oilfield scale formation and chemical removal: A review. *Journal of petroleum science and engineering*, 171, p. 127-139.

- Karlsson, T., Räisänen, M.L., Lehtonen, M. and Alakangas, L. (2018), Comparison of static and mineralogical ARD prediction methods in the Nordic environment. *Environmental monitoring and assessment*, 190(12), p. 1-29.
- Kassotis, C.D., Tillitt, D.E., Davis, J.W., Hormann, A.M. and Nagel, S.C. (2014), Estrogen and Androgen receptor activities of hydraulic fracturing chemicals and surface and ground water in a drilling-dense region. *Endocrinology*, 155 (3), p. 897–907.
- Kay, J. T., Conklin, M. H., Fuller, C. C. and O'Day, P. A. (2001), Processes of nickel and cobalt uptake by a manganese oxide forming sediment in Pinal Creek, Globe mining district, Arizona. *Environmental Science and Technology*, 35(24), p. 4719–4725.
- Kesavan, S. and Prud'Homme, R.K. (1992), Rheology of guar and (hydroxypropyl) guar crosslinked by borate, *Macromolecules*, 25(7), p. 2026-2032.
- Kibble, A., Cabianca, T., & Daraktchieva, Z. (2013), *Review of the Potential Public Health Impacts of Exposures to Chemical and Radioactive Pollutants as a Result of Shale Gas Extraction Process*. Centre for Radiation, Chemical and Environmental Hazards, Public Health England.
- Kim, S., Omur-Ozbek, P., Dhanasekar, A., Prior, A. and Carlson, K. (2016), Temporal analysis of flowback and produced water composition from shale oil and gas operations: Impact of frac fluid characteristics. *Journal of Petroleum Science and Engineering*, 147, p. 202-210.
- King, G. E. (2012), *Hydraulic Fracturing 101: What Every Representative, Environmentalist, Regulator, Reporter, Investor, University Researcher, Neighbor and Engineer Should Know About Estimating Frac Risk and Improving Frac Performance in Unconventional Gas and Oil Wells*. SPE Hydraulic Fracturing Technology Conference: The Woodlands, Texas, USA, Society of Petroleum Engineers, p. 80.
- Kirby, J.K., Golding, L., Williams, M., Apte, S., Mallants, D., King, J., Otalega, I. and Kookana, R. (2020), *Qualitative (screening) environmental risk assessment of drilling and hydraulic fracturing chemicals for the Beetaloo GBA region. Technical appendix for the Geological and Bioregional Assessment: Stage 2*. Department of the Environment and Energy, Bureau of Meteorology, CSIRO and Geoscience Australia, Australia.
- Kondash, A. and Vengosh, A. (2015), Water footprint of hydraulic fracturing. *Environmental Science & Technology Letters*, 2 (10), p. 276-280.
- Kondash, A.J., Albright, E. and Vengosh, A. (2017), Quantity of flowback and produced waters from unconventional oil and gas exploration. *Science of the Total Environment*, 574, p. 314-321.
- Kourgiantakis, M., Matzapetakis, M., Raptopoulou, C.P., Terzis, A. and Salifoglou, A. (2000), Lead–citrate chemistry. Synthesis, spectroscopic and structural studies of a novel lead (II)–citrate aqueous complex. *Inorganica Chimica Acta*, 297(1), p. 134-138.
- Kramer, J., Prud'homme, R.K., Norman, L.R. and Sandy, J.M. (1987), *Characteristics of Metal-Polymer Interactions in Fracturing Fluid Systems*. 62nd Annual Technical Conference and Exhibition of the Society of Petroleum Engineers (27-30 September), Dallas, Texas, USA.
- Langmuir, D., Chrostowski, B.V. and Chaney, R. (2004), *Issue paper on the environmental chemistry of metals*. US Environmental Protection Agency.
- Langmuir, D. (1997), *Aqueous Environmental Geochemistry*. Upper Saddle River, New Jersey: Prentice-Hall.
- Lauer, N.E., Harkness, J.S. and Vengosh, A. (2016), Brine spills associated with unconventional oil development in North Dakota. *Environmental Science & Technology*, 50 (10), p. 5389-5397.
- Lee, G., Bigham, J. M. and Faure, G. (2002), Removal of trace metals by coprecipitation with Fe, Al and Mn from natural waters contaminated with acid mine drainage in the Ducktown Mining District, Tennessee. *Applied Geochemistry*, 17(5), p. 569–581.
- Leventhal, J.S. (1980), Comparative geochemistry of Devonian shale cores from the Appalachian Basin, Mason, Monongalia, and Upshur Counties, West Virginia; Illinois Basin, Tazwell County, Illinois; Clark County, Indiana; and Michigan Basin, Sanilac County, Michigan. Open File Report 80-938. U.S. Geological Survey.

- Leventhal, J.S., Crock, J.G., and Malcolm, M.J. (1981), *Geochemistry of trace elements and uranium in Devonian shales of the Appalachian Basin*. Open File Report 81-778. U.S. Geological Survey.
- Leventhal J. (1993), Metals in Black Shales. In: Engel M.H., Macko S.A. (eds.), *Organic Geochemistry: Principles and Applications*, p. 581-607. Boston, MA: Springer.
- Li, S., Lei, Q., Wang, X., Cai, B., Liu, G. and Wang, L. (2019a), Permeability regain and aqueous phase migration during hydraulic fracturing shut-ins. *Scientific Reports*, 9(1), p. 1–10.
- Li, Q., Jew, A.D., Kohli, A., Maher, K., Brown Jr, G.E. and Bargar, J.R. (2019b), Thicknesses of chemically altered zones in shale matrices resulting from interactions with hydraulic fracturing fluid. *Energy & Fuels*, 33 (8), p. 6878-6889.
- Li NY., Dai, J., Li, J., Bai, F., Liu, P. and Luo, Z. (2016), Application status and research progress of shale reservoirs acid treatment technology. *Natural Gas Industry B*, 3(2), p. 165-172.
- Lima, M.G., Vogler, D., Querci, L., Madonna, C., Hattendorf, B., Saar, M.O. and Kong, X.Z. (2019), Thermally driven fracture aperture variation in naturally fractured granites. *Geothermal Energy*, 7(1), p. 1-28.
- Lindner, E. (2016), *Review of the Effects of CO₂ on Very-Fine-Grained Sedimentary Rock/Shale - Part I: Problem Definition*. NETL-TRS-1-2016, NETL Technical Report Series. Morgantown: U.S. Department of Energy, National Energy Technology Laboratory. Available at: <https://edx.netl.doe.gov/dataset/review-of-the-effects-of-co2-on-very-fine-grained-sedimentary-rockshale-part-i-problem-definition> (Accessed: 7 July 2016).
- Llewellyn, G.T., Dorman, F., Westland, J.L., Yoxheimer, D., Grieve, P., Sowers, T., Humston-Fulmer, E. and Brantley, S.L. (2015), Evaluating a groundwater supply contamination incident attributed to Marcellus Shale gas development. *Proceedings of the National Academy of Sciences*, p. 6325-6330.
- Long, H (2000), *A fundamental study of the acidic pressure oxidation of orpiment and pyrite and high temperature*. Unpublished PhD thesis, Department of Metals and Material Engineering, University of British Columbia, Vancouver.
- Lottermoser, B. G. (2010), *Mine Wastes: Characterization, treatment and environmental impacts, third edition*. Berlin Heidelberg: Springer-Verlag.
- Lutz, B. D., Lewis, A. N. and Doyle, M. W. (2013), Generation, transport, and disposal of wastewater associated with Marcellus Shale gas development. *Water Resources Research*, 49(2), p. 647–656.
- Mackay, E. J. and Jordan, M. M. (2005), Impact of Brine Flow and Mixing in the Reservoir on Scale Control Risk Assessment and Subsurface Treatment Options: Case Histories. *Journal of Energy Resources Technology*, 127(3), p. 201–213.
- Mahmoud, M.A. (2014), Evaluating the damage caused by calcium sulfate scale precipitation during low-and high-salinity-water injection. *Journal of Canadian Petroleum Technology*, 53(03), p. 141-150.
- Maloney, K.O., Baruch-Mordo, S., Patterson, L.A., Nicot, J.P., Entekin, S.A., Fargione, J.E., Kiesecker, J.M., Konschnik, K.E., Ryan, J.N., Trainor, A.M. and Saiers, J.E. (2017), Unconventional oil and gas spills: Materials, volumes, and risks to surface waters in four states of the US. *Science of the Total Environment*, 581, p. 369-377.
- Manz, K. E. and Carter, K. E. (2017), Investigating the effects of heat activated persulfate on the degradation of furfural, a component of hydraulic fracturing fluid chemical additives. *Chemical Engineering Journal*, 327, p. 1021–1032.
- Marcon, V., Joseph, C., Carter, K.E., Hedges, S.W., Lopano, C.L., Guthrie, G.D. and Hakala, J.A. (2017), Experimental insights into geochemical changes in hydraulically fractured Marcellus Shale. *Applied Geochemistry*, 76, p. 36-50.
- Matamoros-Veloza, A., Newton, R.J. and Benning, L.G. (2011), What controls selenium release during shale weathering? *Applied geochemistry*, 26, p. S222-S226.

- Maule, A. L., Makey, C. M., Benson, E. B., Burrows, I. J. and Scammell, M. K. (2013), Disclosure of hydraulic fracturing fluid chemical additives: analysis of regulations. *New solutions: a journal of environmental and occupational health policy*, 23(1), p. 167–187.
- McCready, S., Birch, G.F. and Taylor, S.E. (2003), Extraction of heavy metals in Sydney Harbour sediments using 1M HCl and 0.05M EDTA and implications for sediment-quality guidelines. *Australian Journal of Earth Sciences*, 50, p. 249-255
- McCurdy, R. (2011), High Rate Hydraulic Fracturing Additives in Non-Marcellus Unconventional Shales. In: U.S. EPA (U.S. Environmental Protection Agency), *Proceedings of the Technical Workshops for the Hydraulic Fracturing Study: Water Resources Management* (EPA 600/R-11/048).
- McMillan, J.M. (2016), *Expression of Major and Trace Element Signatures of the Frasnian Duvernay Formation within a Sea Level Context: insights into the processes that control mudstone composition, paleoredox conditions and organic matter enrichment*. Unpublished M.Sc. thesis, University of Alberta, Edmonton.
- Mnich, C. A. (2009), *Geochemical signatures of stratigraphic sequences and sea-level change in the Woodford Shale, Permian Basin*. Unpublished M.Sc. thesis, Colorado School of Mines.
- Moniz, E. J., Jacoby, H.D. and Meggs, J. M. (study co-chairs) (2011), *The Future of Natural Gas, an interdisciplinary MIT Study*. Available at: http://mitei.mit.edu/system/files/NaturalGas_Report.pdf (Accessed: 6 June 2016).
- Montgomery, C. (2013), Fracturing Fluid Components. In: Bungler, A.P., McLennan, J. and Jeffrey, R. (eds.), *Effective and Sustainable Hydraulic Fracturing*. IntechOpen.
- Morgan, B. and Lahav, O. (2007), The effect of pH on the kinetics of spontaneous Fe (II) oxidation by O₂ in aqueous solution—basic principles and a simple heuristic description. *Chemosphere*, 68 (11), p. 2080-2084.
- Morsy, S., Hetherington, C.J. and Sheng, J.J. (2015), Effect of low-concentration HCl on the mineralogy, physical and mechanical properties, and recovery factors of some shales. *Journal of Unconventional Oil and Gas Resources*, 9, p. 94-102.
- Moses, C.O. and Herman, J.S. (1991), Pyrite oxidation at circumneutral pH. *Geochimica et Cosmochimica Acta*, 55(2), p.471-482.
- Myers, K. J., Colledge, I., & Paul, B. (1987). Understanding Jurassic Organic-rich Mudrocks—New Concepts using Gamma-ray Spectrometry and Palaeoecology : Examples from the Kimmeridge Clay of Dorset and the Jet Rock of Yorkshire. *Marine Clastic Sedimentology*, p. 172–189.
- Myers, T. (2012), Potential Contaminant pathways from hydraulically fractured Shale to aquifers. *Groundwater*, 50 (6), p. 872–882.
- Ni, M. and Ratner, B.D. (2008), Differentiating calcium carbonate polymorphs by surface analysis techniques—an XPS and TOF-SIMS study. *Surface and Interface Analysis*, 40(10), p.1356-1361.
- Noiriel, C., Madé, B. and Gouze, P. (2007), Impact of coating development on the hydraulic and transport properties in argillaceous limestone fracture. *Water resources research*, 43(9).
- Núñez, O., Fernández-Navarro, P., Martín-Méndez, I., Bel-Lan, A., Locutura, J. F. and López-Abente, G. (2016), Arsenic and chromium topsoil levels and cancer mortality in Spain. *Environmental Science and Pollution Research*, 23(17), p. 17664–17675.
- Núñez, O., Fernández-Navarro, P., Martín-Méndez, I., Bel-Lan, A., Locutura, J. F. and López-Abente, G. (2017), Association between heavy metal and metalloid levels in topsoil and cancer mortality in Spain. *Environmental Science and Pollution Research*, 24(8), p. 7413–7421.
- O'Hara, S., Humphrey, M., Andersson, J., Jaspal, R., Nerlich, B., and Knight, W. (2014) *Public perception of shale gas extraction in the UK: Has Balcombe bottomed out?* September 2014 Report. University of Nottingham.
- Orr, M.L., Bradshaw, B.E., Bernardel, G., Palu, T.J., Hall, L.S., Bailey, A.H.E., Skeers, N., Dehelean, A., Reese, B. and Woods, M. (2020), *Geology of the Isa GBA region. Technical appendix for the Geological and Bioregional Assessment: Stage 2*. Department of the Environment and Energy, Bureau of Meteorology, CSIRO and Geoscience Australia, Australia.

- Owens, R., Hall, L., Smith, M., Orr, M., Lech, M., Evans, T., Skeers, N., Woods, M. and Inskeep, C. (2020), *Geology of the Cooper GBA region. Technical appendix for the Geological and Bioregional Assessment: Stage 2*. Department of the Environment and Energy, Bureau of Meteorology, CSIRO and Geoscience Australia, Australia.
- Paikaray, S. (2012), Environmental hazards of arsenic associated with black shales: A review on geochemistry, enrichment and leaching mechanism. *Reviews in Environmental Science and Biotechnology*, 11(3), p. 289–303.
- Palisch, T.T., Vincent, M. and Handren, P.J. (2010), Slickwater fracturing: food for thought. *SPE Production & Operations*, 25 (03), p. 327-344.
- Papoulias, D. M. and Velasco, A. L. (2013), Histopathological analysis of fish from Acorn Fork Creek, Kentucky exposed to hydraulic fracturing fluid releases. *Southeastern Naturalist*, 12, p. 90–111.
- Parviainen, A. and Loukola-Ruskeeniemi, K. (2019), Environmental impact of mineralised black shales. *Earth-science reviews*, 192, p. 65-90.
- Parbhakar-Fox, A. and Lottermoser, B. G. (2015), A critical review of acid rock drainage prediction methods and practices. *Minerals Engineering*, 82, p. 107–124.
- Parnell, J., Brolly, C., Spinks, S. and Bowden, S. (2016), Selenium enrichment in Carboniferous Shales, Britain and Ireland: Problem or opportunity for shale gas extraction? *Applied Geochemistry*, 66, p. 82–87.
- Paukert Vankeuren, A.N., Hakala, J.A., Jarvis, K. and Moore, J.E. (2017), Mineral reactions in shale gas reservoirs: Barite scale formation from reusing produced water as hydraulic fracturing fluid. *Environmental science & technology*, 51(16), p. 9391-9402.
- Pearce, J.K., Turner, L. and Pandey, D. (2018), Experimental and predicted geochemical shale-water reactions: Roseneath and Murteree shales of the Cooper Basin. *International Journal of Coal Geology*, 187, p. 30-44.
- Phan, T. T., Paukert Vankeuren, A. N. and Hakala, J. A. (2018), Role of water–rock interaction in the geochemical evolution of Marcellus Shale produced waters. *International Journal of Coal Geology*, 191, p. 95–111.
- Phan, T.T., Capo, R.C., Stewart, B.W., Graney, J.R., Johnson, J.D., Sharma, S. and Toro, J. (2015), Trace metal distribution and mobility in drill cuttings and produced waters from Marcellus Shale gas extraction: Uranium, arsenic, barium. *Applied Geochemistry*, 60, p. 89–103.
- Phan, T.T., Capo, R.C., Stewart, B.W., Macpherson, G.L., Rowan, E.L. and Hammack, R.W. (2016), Factors controlling Li concentration and isotopic composition in formation waters and host rocks of Marcellus Shale, Appalachian basin. *Chemical Geology*, 420, p. 162–179.
- Phan, T.T., Hakala, J.A. and Sharma, S. (2020), Application of isotopic and geochemical signals in unconventional oil and gas reservoir produced waters toward characterizing in situ geochemical fluid-shale reactions. *Science of The Total Environment*, 714, p.136867.
- Priestley, S. (2020), *Shale gas and fracking*. Briefing Paper Number CBP 6073, 31 March 2020. House of Commons Library.
- Prud'homme, R.K., Chu, A., and Kramer, J. (1984), *Rheological Characterization Of Fracturing Fluids*. Annual Meeting Papers, Division of Production (1-4 April), New Orleans, Louisiana, USA.
- Prud'homme, R.K., Ellis, S., Constien, V.G. and Knoll, S. (1988), *Reproducible Rheological Measurements on Crosslinked Fracturing Fluids*. 63rd Annual Technical Conference and Exhibition of the Society of Petroleum Engineers (2-5 October), Houston, Texas, USA.
- Rahm, B.G. and Riha, S.J. (2012), Toward strategic management of shale gas development: Regional, collective impacts on water resources. *Environmental Science & Policy*, 17, p. 12–23.
- Ratcliffe, K., Wright, A. M. and Schmidt, K. (2012), *Application of Inorganic Whole-Rock Inside: From the Eagle Ford Shale Formation, Texas*. 3rd EAGE Shale Workshop: Shale Physics and Shale Chemistry. 53.
- Renock, D., Landis, J.D. and Sharma, M. (2016), Reductive weathering of black shale and release of barium during hydraulic fracturing. *Applied Geochemistry*, 65, p. 73-86.

- Revie, D., Normington, V.J. and Jarrett, A.J.M. (2021) *Shale resource data from the greater McArthur Basin*. Northern Territory Geological Survey, Digital Information Package DIP 014.
- Rish, W.R. and Pfau, E.J. (2018), Bounding Analysis of Drinking Water Health Risks from a Spill of Hydraulic Fracturing Flowback Water. *Risk Analysis*, 38(4), p. 724-754.
- Roh, T., Lynch, C.F., Weyer, P., Wang, K., Kelly, K.M. and Ludewig, G. (2017), Low-level arsenic exposure from drinking water is associated with prostate cancer in Iowa. *Environmental research*, 159, p.338-343.
- Rokosh, C.D., Anderson, S.D.A. and Pawlowicz, J.G. (2016), *QEMSCAN analysis of various lithologies from tight- and shale-gas plays in Alberta*. Alberta Energy Regulator: AER/AGS Special Report, 99.
- Rowan, E.L., Engle, M.A., Kirby, C.S., and Kraemer, T.F. (2011), *Radium content of oil- and gas-eld produced waters in the northern Appalachian Basin (USA)—Summary and discussion of data*. U.S. Geological Survey Scientific Investigations Report 2011–5135. Reston, Virginia: U.S. Geological Survey.
- Rowan, E.L., Engle, M.A., Kraemer, T.F., Schroeder, K.T., Hammack, R.W. and Doughten, M.W. (2015), Geochemical and isotopic evolution of water produced from middle Devonian Marcellus shale gas wells, Appalachian basin, Pennsylvania. *AAPG Bulletin*, 99 (02), p. 181–206.
- Rozell, D.J. and Reaven, S.J. (2012), Water pollution risk associated with natural gas extraction from the Marcellus Shale. *Risk Analysis*, 32 (8), p. 1382–1393.
- Rudnick, R.L. and Gao, S. (2003), The composition of the continental crust. In: Rudnick, R.L. (ed.), *The crust*, vol 3, p. 1-64. Amsterdam: Elsevier.
- Salomons, W. (1995), Environmental impact of metals derived from mining activities: processes, predictions, prevention. *Journal of Geochemical exploration*, 52 (1-2), p.5-23
- Sano, J.L., Ratcliffe, K.T., and Spain, D.R. (2013), Chemostratigraphy of the Haynesville Shale. In: Hammes, U. and Gale, J. (eds.), *Geology of the Haynesville Gas Shale in East Texas and West Louisiana*, U.S.A, p. 137-154. AAPG Memoir 105.
- Schieber J. (1978), Black shales. In: *Sedimentology. Encyclopedia of Earth Science*. Berlin, Heidelberg: Springer.
- Schmidt, C. W. (2013), Estimating wastewater impacts from fracking. *Environmental Health Perspectives*, 121(4), A117.
- Seemann T., Bertier P., Krooss B.M. & Stanjek H. (2017). Water vapour sorption on mudrocks. In: Rutter E.H., Mecklenburgh J. & Taylor K.G. (eds.), *Geomechanical and Petrophysical Properties of Mudrocks*. Geological Society, London, Special Publications, 454, p. 201-233.
- SEPA (Scottish Environment Protection Agency) (2015), *Supporting Guidance (WAT-SG-53), Environment Quality Standards and Standards for Discharges to Surface Waters*.
- Seward, T.M., Williams-Jones, A.E. and Migdisov, A.A., (2014), The chemistry of metal transport and deposition by ore-forming hydrothermal fluids. In: Holland, H.D. and Turekian, K.K (eds.), *Treatise on geochemistry*, 2nd ed., 13, p.29-57.
- SGS (2011), *Pressure Oxidation*. <https://www.sgs.co.uk/en-gb/mining/metallurgy-and-process-design/unit-operations-and-metallurgical-services/pressure-and-ambient-leaching/pressure-oxidation> (Accessed: 19 March 2021).
- Shrestha, N., Chilkoor, G., Wilder, J., Gadhamshetty, V. and Stone, J.J. (2017), Potential water resource impacts of hydraulic fracturing from unconventional oil production in the Bakken shale. *Water research*, 108, p. 1-24.
- Simon, D. E. and Anderson, M. S. (1990). Stability of clay minerals in acid. *Proceedings of the Western Regional Meeting*, p. 7–18.
- Singurindy, O. and Berkowitz, B. (2003), Evolution of hydraulic conductivity by precipitation and dissolution in carbonate rock. *Water Resources Research*, 39 (1).

- Sinha, S. and Marfurt, K. J. (2017), *Effect of frequent well shut-in's on well productivity: Marcellus shale case study*. SPE Eastern Regional Meeting, Lexington, Kentucky, USA, 4-6 October.
- Skalak, K. J., Engle, M. A., Rowan, E. L., Jolly, G. D., Conko, K. M., Benthem, A. J. and Kraemer, T. F. (2014), Surface disposal of produced waters in western and southwestern Pennsylvania: Potential for accumulation of alkali-earth elements in sediments. *International Journal of Coal Geology*, 126, p. 162–170.
- Skousen, J. (2017), A methodology for geologic testing for land disturbance: Acid-Base Accounting for surface mines. *Geoderma*, 308, p. 302–311.
- Soeder, W.M. and Kappel, D. J. (2009), *Water Resources and Natural Gas Production from the Marcellus Shale*. Reston, Virginia: US Department of the Interior, US Geological Survey.
- Sovacool, B.K. (2014), Cornucopia or curse? Reviewing the costs and benefits of shale gas hydraulic fracturing (fracking). *Renewable and Sustainable Energy Reviews*, 37, p. 249–264.
- Stepan, D.J., Shockey, R.E., Kurz, B.A., Kalenze, N.S., Cowan, R.M., Ziman, J.J. and Harju, J.A. (2010), *Bakken water opportunities assessment-Phase 1*. University of North Dakota Energy and Environmental Research Center for North Dakota Industrial Commission Oil and Gas Research Council. Available at: <http://www.undeerc.org/bakken/pdfs/FracWaterPhaseIreport.pdf> (accessed 9th September 2019).
- Stephenson, M.H. (2015), Shale gas in North America and Europe. *Energy Science & Engineering*, 4 (1), p. 4-13.
- Stewart, B.W., Chapman, E.C., Capo, R.C., Johnson, J.D., Graney, J.R., Kirby, C.S. and Schroeder, K.T. (2015), Origin of brines, salts and carbonate from shales of the Marcellus Formation: Evidence from geochemical and Sr isotope study of sequentially extracted fluids. *Applied Geochemistry*, 60, p. 78-88.
- Stringfellow, W. T., Domen, J. K., Kay, M., Sandelin, W. L. and Borglin, S. (2014), Physical, chemical, and biological characteristics of compounds used in hydraulic fracturing. *Journal of Hazardous Materials*, 275, p. 37–54.
- Strong, L. C., Gould, T., Kasinkas, L., Sadowsky, M. J., Aksan, A. and Wackett, L. P. (2014), Biodegradation in Waters from Hydraulic Fracturing: Chemistry, Microbiology, and Engineering. *Journal of Environmental Engineering*, 140(5), p. 1–15.
- Sun, Y., Wang, D., Tsang, D.C., Wang, L., Ok, Y.S. and Feng, Y. (2019), A critical review of risks, characteristics, and treatment strategies for potentially toxic elements in wastewater from shale gas extraction. *Environment international*, 125, p. 452-469.
- Tasker, T. L., Burgos, W. D., Piotrowski, P., Castillo-Meza, L., Blewett, T. A., Ganow, K. B., Stallworth, A., Delompré, P. L. M., Goss, G. G., Fowler, L. B., Vanden Heuvel, J. P., Dorman, F. and Warner, N. R. (2018), Environmental and Human Health Impacts of Spreading Oil and Gas Wastewater on Roads. *Environmental Science and Technology*, 52(12), p. 7081–7091.
- Tasker, T.L., Piotrowski, P.K., Dorman, F.L. and Burgos, W.D. (2016), Metal associations in Marcellus shale and fate of synthetic hydraulic fracturing fluids reacted at high pressure and temperature. *Environmental Engineering Science*, 33(10), p. 753-765.
- Tasker, T. L., Burgos, W. D., Piotrowski, P., Castillo-Meza, L., Blewett, T. A., Ganow, K. B., Stallworth, A., Delompré, P. L. M., Goss, G. G., Fowler, L. B., Vanden Heuvel, J. P., Dorman, F. and Warner, N. R. (2018), Environmental and Human Health Impacts of Spreading Oil and Gas Wastewater on Roads. *Environmental Science and Technology*, 52(12), p. 7081–7091.
- Tawonezvi, J. (2017), The legal and regulatory framework for the EU' shale gas exploration and production regulating public health and environmental impacts. *Energy, Ecology and Environment*, 2(1), p. 1–28.
- Tayong A, R., Alhubail, M. M., Maulianda, B. and Barati, R. (2019), Simulating yield stress variation along hydraulic fracture face enhances polymer cleanup modeling in tight gas reservoirs. *Journal of Natural Gas Science and Engineering*, 65, p. 32–44.
- Thomas, M., Pidgeon, N., Evensen, D., Partridge, T., Hasell, A., Enders, C., Herr Harthorn, B. and Bradshaw, M. (2017), Public perceptions of hydraulic fracturing for shale gas and oil in the United States and Canada. *Wiley Interdisciplinary Reviews: Climate Change*, 8 (3), p. e450.

- Thorogood, J.L. and Younger, P.L. (2015), Discussion of "Oil and gas wells and their integrity: Implications for shale and unconventional resource exploitation" by RJ Davies, S. Almond, RS, Ward, RB Jackson, C. Adams, F. Worrall, LG Herringshaw, JG Gluyas and MA Whitehead. (Marine and Petroleum Geology 2014). *Marine and Petroleum Geology*, 59, p. 671-673.
- Totten, M.W., and Hanan, M.A. (1998), The Accessory-Mineral Fraction of Mudrocks and its Significance for Whole-rock Trace-element Geochemistry. In: Schieber, J., Zimmerle, W., and Sethi, P. (eds.), *Mudstones and Shales, vol. II, Petrography, Petrophysics, Geochemistry, and Economic Geology*, p. 35-53. Stuttgart: Schweizerbart'sche Verlagsbuchhandlung.
- Totten, M.W., and Hanan, M.A. (2007), Heavy minerals in Shales. In: Mange, M.A. and Wright, D.T. (eds.), *Heavy minerals in use (Developments in Sedimentology 58)*, p. 323-341. Edinburgh, United Kingdom: Elsevier Science.
- Tourtelot, H. (1964), Minor-element composition and organic carbon content of marine and non marine shales of Late Cretaceous age in the western interior of the United States. *Geochimica et Cosmochimica Acta*, 28, p. 1579-1604.
- Tourtelot, H. (1979), Black shale - its deposition and diagenesis. *Clays and Clay Minerals*, 27 (5), p. 313-321.
- Tribovillard, N., Algeo, T.J., Lyons, T. and Riboulleau, A. (2006), Trace metals as paleoredox and paleoproductivity proxies: An update. *Chemical Geology*, 232 (1-2), p. 12-32.
- Turekian, K. K. and Wedepohl, K. H. (1961), Distribution of the elements in some major units of the earth's crust. *Bulletin of the Geological Society of America*, 72(2), p. 175-192.
- Tuttle, M. L. W., Fahy, J. W., Elliott, J. G., Grauch, R. I. and Stillings, L. L. (2014), Contaminants from Cretaceous black shale: I. Natural weathering processes controlling contaminant cycling in Mancos Shale, southwestern United States, with emphasis on salinity and selenium. *Applied Geochemistry*, 46, p. 57-71.
- Tuttle, M. L. W., Fahy, J. W., Elliott, J. G., Grauch, R. I. and Stillings, L. L. (2014), Contaminants from Cretaceous black shale: II. Effect of geology, weathering, climate, and land use on salinity and selenium cycling, Mancos Shale landscapes, southwestern United States. *Applied Geochemistry*, 46, 72-84.
- UNCTAD (United Nations Conference on Trade and Development) (2018), *Commodities at a Glance: Special Issue on Shale Gas*, N°9, UNCTAD/SUC/2017/10. Available at: <https://unctad.org/en/pages/Publication-Webflyer.aspx?publicationid=2116>
- URS Corporation (2011), *Water-related issues associated with gas production in the Marcellus Shale: Additives use, flowback quality and quantities, regulations, on-site treatment, green technologies, alternate water sources, water well-testing*. Contract PO No. 10666, URS Corporation, Fort Washington, Pennsylvania.
- U.S. EPA (U.S. Environmental Protection Agency) (2011), *Proceedings of the Technical Workshops for the Hydraulic Fracturing Study: Water Resources Management* (EPA 600/R-11/048).
- U.S. EPA (U.S. Environmental Protection Agency) (2015), *Analysis of Hydraulic Fracturing Fluid Data from the FracFocus Chemical Disclosure Registry 1.0*. Office of Research and Development, Washington, DC. EPA/A/601/R-14/003.
- U.S. EPA (U.S. Environmental Protection Agency) (2016), *Hydraulic Fracturing for Oil and Gas: Impacts from the Hydraulic Fracturing Water Cycle on Drinking Water Resources in the United States*. Office of Research and Development, Washington, DC. EPA/600/R-16/236Fa.
- U.S. Geological Survey (USGS) (2013), *Map of Assessed Shale Gas in the United States, 2012. Digital Data Series DDS - 69 - Z*. Available at: http://pubs.usgs.gov/dds/dds-069/dds-069-z/DDS-69-Z_pamphlet.pdf (Accessed: 20 March 2016).
- VanHazebroeck, E. and Borrok, D.M. (2016), A new method for the inorganic geochemical evaluation of unconventional resources: An example from the Eagle Ford Shale. *Journal of Natural Gas Science and Engineering*, 33, p. 1233-1243.
- Vengosh, A., Jackson, R.B., Warner, N., Darrah, T.H. and Kondash, A. (2014), A critical review of the risks to water resources from unconventional Shale gas development and hydraulic fracturing in the United States. *Environmental Science & Technology*, 48 (15), p. 8334-8348.

- Vidic, R.D., Brantley, S.L., Vandenbossche, J.M., Yoxtheimer, D. and Abad, J.D. (2013), Impact of Shale gas development on regional water quality. *Science*, 340 (6134), p. 1235009.
- Vine, J.D., and Tourtelot, E.B. (1970), Geochemistry of Black Shale Deposits - A Summary Report. *Economic Geology*, 65, p.253-272.
- Wang, L., Fortner, J.D. and Giammar, D.E. (2015), Impact of water chemistry on element mobilization from Eagle Ford Shale. *Environmental Engineering Science*, 32 (4), p. 310-320.
- Wang, L., Burns, S., Giammar, D.E. and Fortner, J.D. (2016), Element mobilization from Bakken shales as a function of water chemistry. *Chemosphere*, 149, p. 286-293.
- Warner, N. R., Jackson, R. B., Darrah, T. H., Osborn, S. G., Down, A. and Zhao, K. (2012), Geochemical evidence for possible natural migration of Marcellus Formation brine to shallow aquifers in Pennsylvania. *Proceedings of the National Academy of Sciences*, 109(30), p. 11961–11966.
- Warner, N.R., Christie, C.A., Jackson, R.B. and Vengosh, A. (2013a), Impacts of Shale gas wastewater disposal on water quality in western Pennsylvania. *Environmental Science & Technology*, 47(20), p. 11849–11857.
- Warner, N.R., Kresse, T.M., Hays, P.D., Down, A., Karr, J.D., Jackson, R.B. and Vengosh, A., (2013b), Geochemical and isotopic variations in shallow groundwater in areas of the Fayetteville Shale development, north-central Arkansas. *Applied Geochemistry*, 35, p.207-220.
- Wattenberg, E.V., Bielicki, J.M., Suchomel, A.E., Sweet, J.T., Vold, E.M. and Ramachandran, G. (2015), Assessment of the acute and chronic health hazards of hydraulic fracturing fluids. *Journal of Occupational and Environmental Hygiene*, 12 (9), p. 611–624.
- Weltman-Fahs, M. and Taylor, J.M. (2013), Hydraulic fracturing and Brook Trout habitat in the Marcellus Shale region: Potential impacts and research needs. *Fisheries*, 38 (1), p. 4–15.
- Werner, A.K., Vink, S., Watt, K. and Jagals, P. (2015), Environmental health impacts of unconventional natural gas development: A review of the current strength of evidence. *Science of The Total Environment*, 505, p. 1127–1141.
- The Water Framework Directive (Standards and Classification) Directions (England and Wales) (WFD-UK-TAG) (2015).
- Wilke, F.D., Vieth-Hillebrand, A., Naumann, R., Erzinger, J. and Horsfield, B. (2015), Induced mobility of inorganic and organic solutes from black shales using water extraction: Implications for shale gas exploitation. *Applied Geochemistry*, 63, p. 158-168.
- Williams, R. D., Mortensen, D. C., Willberg, D. M., Fay, M. and Spivakovskaya, D. (2013), *Innovative method for connate water determination in core material identifies formation heterogeneity and potential damage mechanisms*. Society of Petroleum Engineers - SPE Canadian Unconventional Resources Conference 2013 - Unconventional Becoming Conventional: Lessons Learned and New Innovations, 2, p. 1432–1445.
- Wilson, J.M. and VanBriesen, J.M. (2012), Oil and gas produced water management and surface drinking water sources in Pennsylvania. *Environmental Practice*, 14 (4), p. 288-300.
- Wollin, K. M., Damm, G., Foth, H., Freyberger, A., Gebel, T., Mangerich, A., Gundert-Remy, U., Partosch, F., Röhl, C., Schupp, T. and Hengstler, J. G. (2020), Critical evaluation of human health risks due to hydraulic fracturing in natural gas and petroleum production. *Archives of toxicology*, 94(4), p. 967–1016.
- Worley Parsons (2010), *Spatial Analysis of Coal Seam Water Chemistry*. Report for Department of Environment and Resource Management (DERM), Queensland.
- Xiong, W., Gill, M., Moore, J., Crandall, D., Hakala, J.A. and Lopano, C. (2020), Influence of reactive flow conditions on barite scaling in marcellus shale during stimulation and shut-in periods of hydraulic fracturing. *Energy & Fuels*, 34 (11), p. 13625-13635.
- Yan, Q., Lemanski, C., Karpyn, Z. T. and Ayala, L. F. (2015), Experimental investigation of shale gas production impairment due to fracturing fluid migration during shut-in time. *Journal of Natural Gas Science and Engineering*, 24, p. 99–105.

- Yost, E.E., Stanek, J., DeWoskin, R.S. and Burgoon, L.D. (2016), Overview of chronic oral toxicity values for chemicals present in hydraulic fracturing fluids, Flowback, and produced waters. *Environmental Science & Technology*, 50 (9), p. 4788–4797.
- Ziemkiewicz, P.F. and He, Y.T. (2015), Evolution of water chemistry during Marcellus Shale gas development: A case study in West Virginia. *Chemosphere*, 134, p. 224-231.
- Zolfaghari, A., Dehghanpour, H., Noel, M. and Bearinger, D. (2016), Laboratory and field analysis of flowback water from gas shales. *Journal of Unconventional Oil and Gas Resources*, 14, p. 113-127.

APPENDIX A

See attached spreadsheet named Appendix A. It contains total recoverable element concentrations (TRE sheet) and acid extractable element concentrations (AEE sheet) for approximately 65 elements for all the shale samples used in this study. The element concentrations are reported as an average of duplicates.

Appendix A is available through the University of Strathclyde's Knowledgebase portal under the following DOI: <https://doi.org/10.15129/523764a3-e528-4fda-a7d0-02d9a553f67a>

APPENDIX B

See attached spreadsheet named Appendix B. It contains five sheets as follows:

Table B1 SHFF: Summary results of leaching tests with synthetic hydraulic fracturing fluid (SHFF) for elements of interest.

- **Table B2 SGW:** Summary results of leaching tests with synthetic groundwater (SGW) for elements of interest.
- **Table B3 % SHFF TRE:** SHFF leaching results for elements of interest, normalised to the element content of each sample (TRE) and expressed as a %. Numbers in red are % calculated based on the detection limit.
- **Table B4 % TRE SGW:** SGW leaching results for elements of interest, normalised to the element content of each sample (TRE) and expressed as a %. Numbers in red are % calculated based on the detection limit.
- **Table B5 1M HCl:** results of the preliminary 1M HCl leaching tests. % TRE represents element concentrations normalised to a given element total recoverable content of each sample. Numbers in red are % calculated based on the detection limit.

The element concentrations are reported as an average of duplicates.

Appendix B is available through the University of Strathclyde's Knowledgebase portal under the following DOI: <https://doi.org/10.15129/523764a3-e528-4fda-a7d0-02d9a553f67a>

APPENDIX C

See attached spreadsheet named Appendix C.

It is a full dataset of the synthetic hydraulic fracturing fluid (SHFF, 54 elements) and synthetic groundwater (SGW, 54 elements) leaching results presented in Chapter 4.4. The element concentrations are reported as an average of duplicates.

Appendix C is available through the University of Strathclyde's Knowledgebase portal under the following DOI: <https://doi.org/10.15129/523764a3-e528-4fda-a7d0-02d9a553f67a>